Investigating Mechanisms of Cognitive Resilience to Aging and Brain Disease

Thesis

for the degree of

doctor rerum naturalium (Dr. rer. nat.)

approved by the Faculty of Natural Sciences of Otto von Guericke University Magdeburg

by M.Sc. Niklas Vockert

born on 11.06.1993 in Köln

Examiners: Prof. Dr. Anne Maass
Prof. Dr. Michael Ewers

submitted on: 11.09.2024
defended on: 28.05.2025

Abstract

A general decline in cognitive function across the later decades of life is considered near-inevitable, with hippocampus-dependent functions such as episodic memory being among the first to decline. Neurodegenerative and cerebrovascular diseases severely accelerate the journey to cognitive impairment and potentially dementia. Yet, some individuals exhibit astounding resilience of their cognitive abilities to aging and disease. Recently, in living humans the vascularization pattern of the hippocampus (HVP), a brain region which is particularly vulnerable to ischemia due to its sparse vascular network, has been classified into an augmented supply through both the posterior cerebral artery (PCA) and anterior choroidal artery (AChA) as opposed to a basic supply via the PCA alone. An association of an augmented supply with better cognitive performance and hippocampal volumes in older adults has indicated a role of the HVP in resilience to cognitive decline, possibly via structural correlates. In the first study of this thesis, we aimed to gain a deeper understanding of the link between the HVP and brain structural integrity in old age. Within the medial temporal lobe (MTL), an augmented supply was specifically associated with greater volumes in the anterior portion, matching the perfusion territory of the AChA. Furthermore, structural benefits of an additional AChA supply reached beyond the ipsilateral MTL to the contralateral entorhinal cortex and associations of the HVP with gray matter volumes throughout the whole brain were established as the mediator of better cognitive performance in augmented supply-individuals. This provides evidence that an augmented vascular supply fosters brain reserve, i.e. the build-up of neurobiological resources (e.g. synapses, neurons) in early life, or brain maintenance, denominating a preservation of the neurobiological capital across the lifespan. Additionally, mean hippocampal vessel distances were found to be involved in cognitive resilience to cerebrovascular disease. In the second study, ultra-high field MRI was utilized for a more thorough characterization of structural and functional aspects of the hippocampal vasculature in young adults, which deepened the understanding of the hippocampal vasculature as assessed via MR angiography. The lack of associations between hippocampal vascular properties and brain structure as well as cognition in young adults points towards brain maintenance as the more plausible mode of action of an augmented supply as opposed to brain reserve. In the third study, resilience was investigated in the form of cognitive reserve, i.e. the adaptability of cognitive processes that allows to maintain cognitive performance despite brain aging or pathology. The use of an fMRI paradigm of successful memory encoding in a large sample of almost 500 older adults on the continuum from cognitively normal through at-risk stages for Alzheimer's disease (AD) to AD dementia allowed for the investigation of the neural basis of cognitive reserve. Cognitive reserve was mainly associated with a more pronounced expression of the task-related network, including deactivation of the default mode network and activation of inferior temporal regions including fusiform gyrus. Higher levels of (de)activation in these regions during memory encoding attenuated the effect of AD pathology on cognitive decline over time. This indicates that individual brain activity levels of those regions during memory encoding have prognostic value for future cognitive decline and represent a potential target for interventions.

Zusammenfassung

Ein allgemeiner Rückgang der kognitiven Fähigkeiten im höheren Alter ist nahezu unvermeidlich, wobei das vom Hippocampus abhängige episodische Gedächtnis als eine der ersten kognitiven Funktionen nachlässt. Neurodegenerative und zerebrovaskuläre Erkrankungen verkürzen den Weg zur kognitiven Beeinträchtigung und schließlich zur potenziellen Demenz erheblich. Dennoch zeigen einige Menschen eine erstaunliche Widerstandsfähigkeit ihrer kognitiven Fähigkeiten gegenüber Alterung und Krankheit. Kürzlich wurde beim lebenden Menschen das Vaskularisierungsmuster des Hippocampus (HVP), der aufgrund seines vergleichsweise spärlichen Gefäßnetzes besonders anfällig für Ischämie ist, in eine verstärkte Versorgung sowohl durch die arteria posterior cerebri (PCA) als auch durch die arteria chroidea anterior (AChA) im Gegensatz zu einer grundlegenden Versorgung durch die PCA allein eingeteilt. Eine Assoziation der verstärkten Versorgung mit besseren kognitiven Leistungen und grösseren hippocampalen Volumina bei älteren Erwachsenen deutet auf eine Rolle des HVP für die Resilienz gegenüber kognitivem Verfall hin, möglicherweise über strukturelle Korrelate. Das Ziel der ersten Studie dieser Arbeit war, ein tieferes Verständnis der Verbindung zwischen dem HVP und der strukturellen Integrität des Gehirns im Alter zu erlangen. Eine verstärkte Versorgung wurde speziell mit grösseren Volumina des vorderen Teils des medialen Temporallappens (MTL) in Verbindung gebracht, welcher sich im Perfusionsgebiet der AChA befindet. Darüber hinaus reichten die strukturellen Vorteile der zusätzlichen AChA-Versorgung über den ipsilateralen MTL hinaus bis in den kontralateralen entorhinalen Kortex. Ausserdem wurden Assoziationen zwischen dem HVP und dem Volumen an grauer Substanz im gesamten Gehirn als Mediator besserer kognitiver Leistungen bei Individuen mit zusätzlicher Versorgung durch die AChA identifiziert. Dies liefert einen Hinweis darauf, dass eine verstärkte Versorgung die Gehirnreserve, d. h. den Aufbau neurobiologischer Ressourcen (z. B. Synapsen, Neuronen) im frühen Leben, oder die Gehirnerhaltung, d. h. die Aufrechterhaltung des neurobiologischen Kapitals über die gesamte Lebensspanne, fördert. Zusätzlich wurde festgestellt, dass der durchschnittliche Abstand der hippocampalen Arterien mit der kognitiven Resilienz gegenüber zerebrovaskulären Erkrankungen in Zusammenhang steht. In der zweiten Studie wurde ebenfalls Ultrahochfeld-MRT eingesetzt, um eine gründlichere Charakterisierung der strukturellen und funktionellen Aspekte der Hippocampus-Gefäße bei jungen Erwachsenen zu erreichen. Dies trug zu einer Vertiefung des Verständnisses der hippocampalen Gefäße bei, wie sie mittels MR-Angiographie beurteilt werden. Fehlende Zusammenhänge zwischen den vaskulären Eigenschaften des Hippocampus und der Hirnstruktur sowie Kognition deuten darauf hin, dass die Gehirnerhaltung gegenüber der Gehirnreserve der plausiblere Wirkungsmechanismus einer verstärkten Versorgung ist. In der dritten Studie wurde Resilienz in Form von kognitiver Reserve untersucht, d. h. der Anpassungsfähigkeit kognitiver Prozesse, die es ermöglicht, die kognitive Leistung trotz Hirnalterung oder Pathologie aufrechtzuerhalten. Die Verwendung eines fMRT-Paradigmas zur erfolgreichen Gedächtniskodierung in einer großen Stichprobe von fast 500 älteren Erwachsenen auf dem Kontinuum von normaler Kognition über Risikostufen für die Alzheimer-Krankheit bis hin zur Alzheimer-Demenz ermöglichte die Untersuchung der neuronalen Grundlage der kognitiven Reserve. Kogni-

tive Reserve war hauptsächlich mit einer stärkeren Ausprägung des während der erfolgreichen Gedächtniskodierung aktiven Netzwerks verbunden und war besonders durch die Deaktivierung des Standardmodus-Netzwerks und die Aktivierung von inferioren temporalen Regionen einschließlich des gyrus fusiformis gekennzeichnet. Höhere Hirnaktivität in diesen Regionen während der Gedächtniskodierung hing mit einer Dämpfung der Auswirkungen der Alzheimer-Pathologie auf den kognitiven Abbau im Laufe der Zeit zusammen. Dies deutet darauf hin, dass die individuelle Hirnaktivität während der Gedächtniskodierung in diesen Regionen einen hohen Vorhersagewert für künftigen kognitiven Abbau hat und ein potenzielles Ziel für Interventionen darstellt.

Abbreviations

Aβ amyloid-beta

AChA anterior choroidal artery

aHC anterior hippocampus

ACC anterior cingulate cortex

AD Alzheimer's disease

ADAS-cog Alzheimer's disease Assessment Scale - Cognitive Subscale

ADD Alzheimer's disease dementia

ADR AD patient first-degree relatives

aMCI amnestic mild cognitive impairment

ASHS Automatic Segmentation of Hippocampal Subfields

BOLD blood oxygen level dependent

BR brain reserve

CA Cornu Ammonis

CAA cerebral amyloid angiopathy

CBF cerebral blood flow

CI cognitively impaired

CMB cerebral microbleeds

CN cognitively normal

CoMD center of mass distance

CoW Circle of Willis

CR cognitive reserve

cSS cortical superficial siderosis

CSF cerebrospinal fluid

CSVD cerebral small vessel disease

CT computer tomography

CU cognitively unimpaired

CVLT Californian Verbal Learning Test

CVR cerebrovascular reactivity

DMN default mode network

DS Digit Span

DPA deep perforator arteriopathy

ERC entorhinal cortex

$EtCO_2$ end-tidal CO_2 partial pressure

FA flip angle

FDR false discovery rate

fMRI functional magnetic resonance imaging

FTP fetal-type PCA

FWE family-wise error

FWHM full width at half maximum

GM gray matter

GLM general linear model

gVD global vessel distance

HC hippocampus

HVP hippocampal vascularization pattern

ICA internal carotid artery

ICH intracerebral haemorrhage

IQR interquartile range

LM Logical Memory

LME linear mixed effects model

LRT likelihood ratio test

MoCA Montreal Cognitive Assessment

MMSE Mini-Mental State Examination

MRA magnetic resonance angiography

MRI magnetic resonance imaging

MTL medial temporal lobe

OLT object location task

PACC5 Preclinical Alzheimer's Cognitive Composite 5

$PaCO_2$ CO_2 arterial partial pressure

PC principal component

PCA posterior cerebral artery

PCC posterior cingulate cortex

PComA posterior communicating artery

PFC prefrontal cortex

PL pathological load

pHC posterior hippocampus

PHC parahippocampal cortex

PRC perirhinal cortex

PVS perivascular spaces

RBW receiver bandwidth

ROCFT Rey-Osterrieth Complex Figure Test

ROI region of interest

RRF respiratory response function

RSFA resting state fluctuation amplitude

RVT respiration volume per time

SCD subjective cognitive decline

std standard deviation

SDMT Symbol Digit Modalities Test

SM subsequent memory

SNR signal-to-noise ratio

SOP standard operating procedure

T Tesla

TE echo time

TI tortuosity index

TIV total intracranial volume

TMT Trail Making Test

ToF time-of-flight

TR repetition time

t-SNE t-distributed stochastic neighbor embedding

tSNR temporal signal-to-noise ratio

VaD vascular dementia

VCI vascular cognitive impairment

VDM vessel distance mapping

vsVD vessel-specific vessel distance

wHC whole hippocampus

WM white matter

WMH white matter hyperintensities

Contents

1 General introduction

The general aim of this thesis was to examine factors that enable some individuals to retain their cognitive abilities despite age- and disease-related changes of the brain. For this purpose the general introduction starts by introducing the hippocampus and medial temporal lobe as the central hubs of memory functioning and describes the most prominent pathological conditions that lead to a deterioration of memory and other cognitive functions. Next, a few essential theoretical concepts in the realm of successful cognitive aging are defined. Subsequently, different aspects of the cerebral vasculature are introduced due to their importance for cognitive functioning. This includes a short explanation of neurovascular coupling, which is crucial for the measurement of brain activity via MRI. How brain activity patterns during successful encoding of new information contribute to maintenance of cognitive performance is a central question addressed in this thesis. After the broader introduction to cerebral vascularization, the introduction specifically focuses on the vascular features of the hippocampus, whose involvement in resilience of cognitive abilities against age- and pathology-related decline is the other central topic of this thesis. Last, alterations of the cerebral vasculature in aging and disease are covered, highlighting their potential importance for cognitive resilience. The introduction concludes with a presentation of the specific aims and the outline of the remaining thesis.

1.1 The hippocampus and memory functions

The hippocampus is part of the medial temporal lobe (MTL), where it is located superiorly to the entorhinal cortex (ERC), perirhinal cortex (PRC) and parahippocampal cortex (PHC) (see Fig. 1.1A). It consists of the subiculum, Cornu Ammonis (CA) and dentate gyrus. Together with its adjacent structures it plays a crucial role for learning and memory [Squire et al., 2004]. Memory in this context refers to conscious memory about facts (semantic memory) and experienced events (episodic memory), termed declarative memory [Manns et al., 2003, Squire, 2004]. Although other (non-declarative/unconscious) forms of long-term memory exist, e.g. procedural memory for execution of cognitive and motor skills or priming, it is primarily declarative memory that has been linked to the functional integrity of the MTL [Martin and Barense, 2023]. Among other processes, the hippocampus with its surrounding structures is involved in two memory-related processes termed pattern separation and pattern completion [Kirwan and Stark, 2007, Lee et al., 2020, Yassa and Stark, 2011], introduced by Marr et al. [1991]. Pattern separation enables the hippocampus to create non-overlapping memory representations to distinguish similar memories. Pattern completion, on the other hand, supports the retrieval of memories from incomplete or degraded memory representations through facilitation by previously stored representations. However, the traditional view

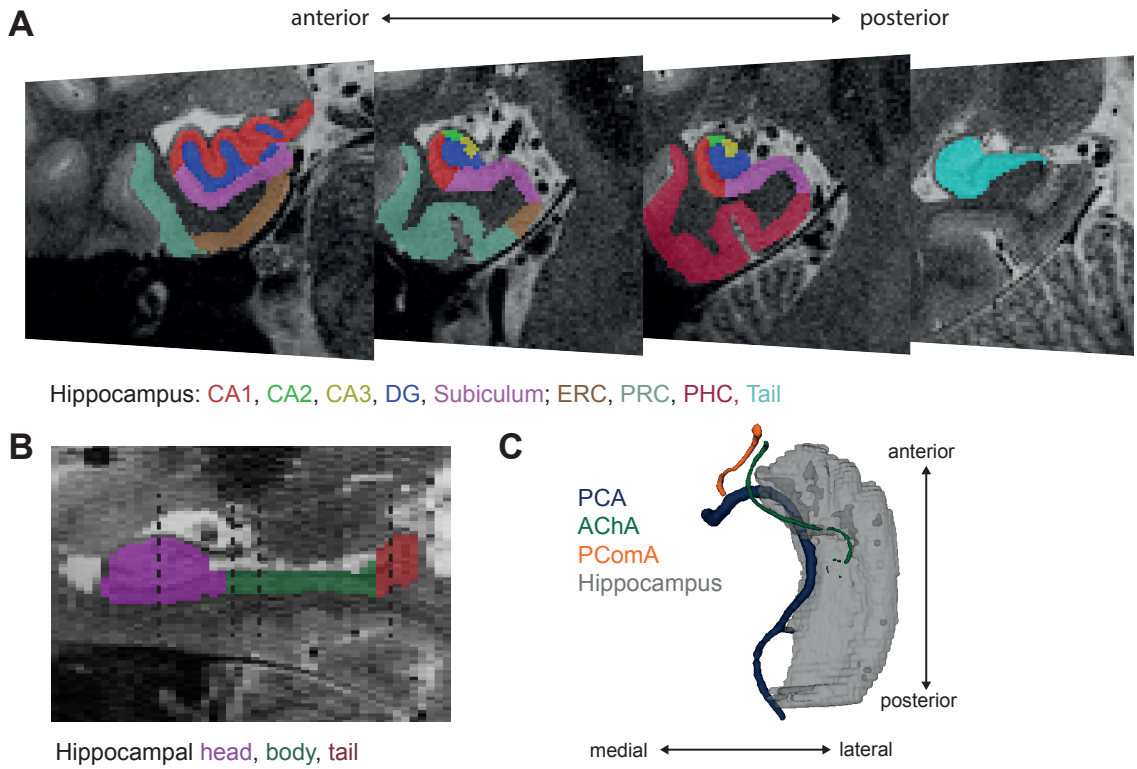

Figure 1.1: **Medial temporal lobe.** (A) Zoomed-in coronal view of the left MTL on four slices of a high-resolution T2-weighted MRI scan including MTL subregions and hippocampal subfields. (B) Zoomed-in sagittal view of the same hippocampus, divided into head, body and tail (other MTL subregions not shown). The dashed lines indicate the positions of the coronal slices shown in panel A. Please note that the orientation of the hippocampus within the brain is usually slightly tilted, but is displayed as straight, since MRI acquisition was parallel to the hippocampal long axis. (C) Roughly axial 3D view of the right hippocampus and the main trunks of its surrounding vessels segmented on a ToF MRA image (see section 1.4 for more information).

of a unitary memory system [Cohen and Squire, 1980], which proposes an involvement of the MTL in declarative memory exclusively, appears obsolete considering the amount of evidence for an involvement of the MTL in other cognitive processes. Apart from remembering past events, the MTL also seems to be important for imagining or simulating future events [Maguire and Hassabis, 2011, Schacter et al., 2012] and supporting spatial navigation [Aguirre et al., 1996, Ekstrom et al., 2003], e.g. in the form of place cells in the hippocampus [O'Keefe and Dostrovsky, 1971] and grid cells in the ERC [Hafting et al., 2005]. The MTL has also been implicated in higher-order perception, with the PRC and anterior hippocampus, i.e. anterior MTL structures, more involved in perception of object stimuli and the posterior hippocampus and PHC, i.e. posterior MTL structures, more involved in perception of scene stimuli [Lee et al., 2012, Martin and Barense, 2023].

Along its length of ca. 4-4.5cm, the hippocampus can be split into three subregions

from anterior to posterior: the hippocampal head, body and tail [Duvernoy et al., 2013] (see Fig. 1.1B). Often times a simplified distinction into two instead of three subregions is made, in which body and tail are summarized as posterior hippocampus (pHC) and contrasted with the hippocampal head as anterior hippocampus (aHC). These subregions might exhibit a functional specialization, as indicated above. In rodents, support for a functional separation of the hippocampus into ventral (anterior), dorsal (posterior) and intermediate hippocampus comes from behavioral, anatomical and gene expression studies (reviewed in Fanselow and Dong [2010]). According to this view, the dorsal hippocampus is primarily implicated in cognitive functions, whereas the ventral hippocampus is more involved in stress, emotion and affect [Fanselow and Dong, 2010]. Many human studies have also attributed specific functions to the anterior and posterior hippocampus, respectively, but evidence regarding functional specialization has been conflicting (see e.g. Poppenk et al. [2013], Strange et al. [2014] for a comprehensive discussion about the evidence). For instance, the anterior part may be more strongly involved in the encoding of new memory episodes, whereas memory retrieval might rely more on the posterior hippocampus, also suggested by multiple meta-analyses [Kim, 2015, Lepage et al., 1998, Spaniol et al., 2009]. This contradicts another view on memory processes, which posits that the same neural network activated during encoding is re-activated during retrieval [Paulsen and Moser, 1998]. Another distinction might be that aHC is activated when only the gist of the memory trace is recalled, whereas detailed memory representations are rather dependent on the pHC [Poppenk et al., 2013]. In alignment with the rodent data, modulation of memory by emotion and motivation might be localized to the aHC, whereas spatial memory and navigation have been attributed to the pHC rather than the aHC [Poppenk et al., 2013]. Other studies have pointed towards gradual anterior-posterior differences in spatial representations, with global presentations getting more locally specific towards the posterior end [Kjelstrup et al., 2008].

Based on previous studies, Poppenk et al. [2013] posed the idea that the aHC might be biased towards pattern completion, facilitated by connectivity with other cortical and subcortical regions that are better suited for global (coarse-grained) information processing. In contrast, the pHC might be biased towards pattern separation, benefiting from connectivity to regions with more fine-grained (local) information processing [Poppenk et al., 2013]. In an attempt to reconcile human and animal findings Strange et al. [2014] suggested that discrete functional differences along the longitudinal hippocampal axis are overlaid with a functional gradient. This hypothesis of a functional gradient received support from a meta-analysis of human fMRI studies, which failed to demonstrate a clear-cut separation of functional processes between the anterior and posterior hippocampus, but instead showed preferential engagement of the subregions with specific cognitive processes [Grady, 2020]. The meta-analysis provides more support for encoding- and novelty-related activation in the aHC versus retrieval- and spatial memory- or navigation-related activity being located more posteriorly. Overall, the evidence for a functional segregation of the human hippocampus along its longitudinal axis is vast, although the exact organization remains a matter of debate. The functional segregation suggests that damage to specific parts of the hippocampus might affect some

cognitive processes more than others. As we shall see in section 1.4, the vascular organisation of the hippocampus also suggests differential susceptibility between the anterior and posterior parts.

1.1.1 Memory function in aging and disease

While cognition usually declines with older age, not all cognitive functions are affected equally [Nyberg et al., 2003, Rönnlund et al., 2005, Salthouse, 2004, Small et al., 2011]. Perceptual speed and memory have been shown to be affected stronger by aging than general cognition [Salthouse, 2004]. In fact, episodic memory is one of the earliest cognitive functions to deteriorate, with evidence pointing towards a gradual decline from around age 60 [Nyberg et al., 2003, Rönnlund et al., 2005]. In contrast, semantic memory has been proposed to actually improve into older adulthood and might only start to deteriorate around age 70 to levels below those of younger adulthood [Nyberg et al., 2003, Rönnlund et al., 2005]. One caveat is that the tests of semantic memory evaluate the participants' factual knowledge about the world and the meaning of words, hence only probing the retrieval of previously acquired knowledge without encoding of new information unlike in the episodic memory tasks.

Furthermore, cognitive functions and their trajectories over time show considerable inter-individual variability [Habib et al., 2007, Josefsson et al., 2012, Yaffe et al., 2009]. The variability itself has been shown to increase with age, demonstrating greater difference in cognitive scores between individuals with higher age [De Frias et al., 2006]. Previous approaches have classified individuals into three groups based on the change of their cognitive or memory abilities over time [Josefsson et al., 2012, Yaffe et al., 2009]. In a large longitudinal study, Yaffe et al. [2009] categorized 2509 participants into maintainers (30%), individuals with minor cognitive decline (53%) and individuals with major cognitive decline (16%). Josefsson et al. [2012] grouped 1558 participants into maintainers (18%), decliners (13%) and individuals with age-typical average memory change (68%). In concordance with these studies, one could consider three trajectories of cognitive aging: (a) normal aging, representing the average (minor) decline of memory functions experienced with aging, (b) pathological aging with accelerated rates of cognitive decline due to underlying pathology and (c) successful aging or "superaging" that is characterized by unusually stable memory performances above average resembling those of adults in their fifties and sixties or even of young adults (see e.g. Rogalski et al. [2013], Rowe and Kahn [1987]). The latter group might be characterized by a strong expression of brain reserve, brain maintenance and/or cognitive reserve, which are explained in section 1.2.

Alongside the cognitive deficits, the brain also exhibits structural changes during normal aging. As revealed by a review on longitudinal MRI studies, already after age 35 a slow and steady loss of whole brain volume sets in, which further accelerates with older age (about 0.5% whole brain volume loss per year with age 60) [Hedman et al., 2012]. Evidence regarding specific gray and white matter volume loss identified by the review was sparser, but gray matter (GM) loss was suggested to start as early as after childhood, whereas white matter (WM) volumes increased until age 45, by which their

steady decline set in [Hedman et al., 2012]. Another study with a stunning amount of more than 120000 MRI scans of participants 155 days post conception to 100 years of age reported even earlier initial decline of GM and WM volumes, at the ages of 5.9 years and 28.7 years, respectively [Bethlehem et al., 2022]. Again in line with the age-related decline in cognitive functions, regional volume loss with age is not uniform. The fastest age-related volume loss occurs in the frontal lobes and hippocampus [Jernigan et al., 2001, Raz et al., 2005]. The hippocampus, together with some other subcortical structures, seems to show even a non-linear, accelerated decline with age [Fjell et al., 2013, Fraser et al., 2015, Raz et al., 2005, Walhovd et al., 2011, Ziegler et al., 2012]. Apart from atrophy in normal aging, the hippocampus and medial temporal lobe are also implicated in pathological aging underlying many dementias. Hippocampal and MTL atrophy represent a central feature of Alzheimer's Disease [Yang et al., 2012], where hippocampal atrophy rates exceed those of healthy controls by about 2.5 times [Jack et al., 1998].

1.1.2 Dementia

Dementia is the most prevalent condition in the realm of pathological cognitive aging. Dementia does not represent a single disease, but a syndrome, i.e. a group of symptoms, which is characterized by the loss of memory and other cognitive functions to an extent that impairs daily functioning [WHO, 2021]. Memory is usually the first affected cognitive faculty in dementia, but as the disease progresses other cognitive functions decline. Eventually, neurodegeneration spreads into the brainstem, which houses vital autonomic functions like the control of heart rate, breathing and swallowing. This can lead to 'silent' aspiration of food and drinks unbeknownst to the patient, which can cause aspiration pneumonia [Suh et al., 2009]. Consequently, the end stage of dementia is death, most frequently through devastating conditions of the circulatory and respiratory system [Attems et al., 2005, Brunnström and Englund, 2009]. As such, dementia is the seventh leading cause of death [WHO, 2023]. It is also one of the major causes of disability and dependency [WHO, 2023]. As age is a primary risk factor [Braak and Braak, 1997] and the worldwide population is aging [WHO, 2022], dementia prevalence is expected to rise in the future, making it one of the top health priorities in the coming decades. Estimates from 2021 number dementia prevalence at around 50 million cases worldwide, which is predicted to almost triple by 2050 [WHO, 2021]. The associated global health care burden is estimated at the tremendous cost of about 2.8 trillion US dollars annually already in 2030 [Long et al., 2023]. While prevention might be considered better than a cure, in the absence of a cure for dementia, prevention is also the only strategy. According to the Lancet report on dementia prevention, 45% of the dementia cases might be preventable by addressing 14 risk factors, including low education, hypertension, diabetes, obesity, high LDL cholesterol, physical inactivity, smoking, excessive alcohol consumption, air pollution, hearing loss, vision loss, depression, low social contact and traumatic brain injury [Livingston et al., 2024].

The most common individual causes of dementia include Alzheimer's disease (AD), Vascular Dementia, Lewy Body Dementia, Frontotemporal Dementia and Parkinson's

Disease, Yet, mixed dementia of more than one etiology is the most common type of dementia [Kapasi et al., 2017, Schneider et al., 2007] and is especially prevalent in people aged 90 years or older [Livingston et al., 2020].

1.1.3 Alzheimer's Disease

Alzheimer's Disease is the most common single cause of dementia and accounts for about 60-75% of all dementia cases [Qiu et al., 2009, WHO, 2023]. It was first described by Alois Alzheimer, who presented the first case at a congress in 1906 [Möller and Graeber, 1998]. Abnormal aggregates of two proteins represent the key feature of AD: extracellular plaques of misfolded amyloid-beta (Aβ) peptides and intraneuronal (neurofibrillary) tangles of hyperphosphorylated tau. According to the amyloid cascade hypothesis Aβ is the causative agent leading to tau phosphorylation and neuronal damage [Hardy and Higgins, 1992]. Support for this hypothesis also comes from rare genetic forms of ("familial") AD. In all known forms of autosomal dominant AD, one of three genes involved in Aβ cleavage is mutated, namely the gene for the amyloid precursor protein (APP) itself or for the catalytic subunits of the gamma-secretase that cuts the amyloid precursor protein (PSEN1 or PSEN2), leading to abnormal production or reduced clearance of Aβ [Blennow et al., 2006, Jack et al., 2010]. While about 90% of AD cases occur after age 65, these genetic mutations almost always lead to an earlier development of AD dementia [Ryman et al., 2014], called early onset Alzheimer's disease. In contrast, late onset Alzheimer's disease comprises many cases of sporadic AD, which has no specific family link, but is a consequence of a complex interaction of genetics, environment and lifestyle [Bird, 2018, Eid et al., 2019].

Yet, other genes have been associated with an increased risk for the development of late onset AD. The most significant genetic risk factor is the type $\varepsilon 4$ allele of the APOE gene (APOE $\varepsilon 4$) [Saunders et al., 1993]. The risk for development of AD for APOE $\varepsilon 4$ carriers seems to depend on ethnicity, but is always higher compared to non-carriers [Farrer et al., 1997]. In Caucasians, the most studied ethnicity, one copy of APOE $\varepsilon 4$ increases the risk for AD 3- to 4-fold in comparison to the common $\varepsilon 3$ variant, two copies even 9- to 15-fold [Farrer et al., 1997, Neu et al., 2017]. In contrast, the $\varepsilon 2$ variant exerts a protective effect against AD, decreasing the risk by about 40% [Farrer et al., 1997]. APOE $\varepsilon 4$ risk seems to be mediated via inhibition of Aβ clearance and promotion of Aβ accumulation (see Yamazaki et al. [2019] for an overview).

Accumulation of Aβ might occur as early as two decades before the emergence of clinical symptoms [Jack et al., 2009], in the so-called preclinical phase. In the prodromal phase individuals develop mild cognitive impairment (MCI), most commonly characterized by initial deficits in episodic memory [Petersen, 2004]. Biologically, the prodromal phase is characterized by abnormal tau levels and mild neurodegeneration, which are a consequence of the preceding Aβ accumulation [Jack et al., 2010]. In the clinical phase of AD, individuals show more severe neurodegeneration accompanied by the clinical symptoms of dementia.

Multiple biomarkers have been developed to assess the neuropathological features of AD in vivo. The A/T/N framework divides seven major AD biomarkers into three bi-

nary categories in alignment with the biological definition of Alzheimer's disease [Jack et al., 2016, 2018]. "A" represents aggregated Aβ and positivity can be assessed by CSF measures (low $A\beta_{42}$ or $A\beta_{42}$ to $A\beta_{40}$ ratio) or amyloid PET. "T" represents aggregated tau (neurofibrillary tangles) and can be measured as elevated CSF phosphorylated tau (p-tau) or with tau PET. The "N" category represents neurodegeneration or neuronal injury, which can be assessed by atrophy on anatomical MRI images, FDG-PET hypometabolism or via CSF total tau (t-tau). Importantly, neurodegeneration or neuronal injury can result from many causes unrelated to AD. However, it provides important pathologic staging information, as in combination with A^+T^+ it is a much more powerful predictor of future cognitive decline than amyloid positivity alone [Jack et al., 2018]. In recent years, there has been much progress in the development of AD biomarkers in blood plasma, which have the advantage of being less invasive, cheaper and less time-consuming than lumbar punctures or PET scans [Hansson et al., 2023, Salvadó et al., 2023]. In an ongoing revision of the 2016/2018 AD biomarker framework, blood plasma biomarkers are being integrated as an alternative to CSF biomarkers [AlzForum Foundation Inc., 2023]. In summary, AD can nowadays be assessed from a biological standpoint in vivo in a multitude of ways. It is notable, however, that a patient could have biologically defined AD without a clinical diagnosis of AD dementia due to absence of cognitive impairment.

Although an ultimate cure for AD does not yet exist, treatment options for AD recently showed notable advances. Three anti-amyloid antibodies have been approved in the US in the last three years, which were able to clear Aβ from the brain and slow down cognitive decline [Cummings et al., 2021, Riederer, 2021]. In June 2021, Aduhelm (Aducanumab) by Biogen received accelerated approval [Dhillon, 2021], paving the way for the new class of drugs. Leqembi (Lecanemab) by Eisai/Biogen gained fast-track approval in January 2023 [Hoy, 2023] and traditional approval in July 2023 [Biogen Inc., 2023]. In consequence, Biogen announced on January 31st 2024 to discontinue Aduhelm in order to "reprioritize resources allocated to Aduhelm [...] to advance Leqembi" [Biogen Inc., 2024]. Eli Lilly recently gained approval for their anti-amyloid antibody Donanemab (Kisunla) [AlzForum Foundation Inc., 2024] after demonstrating good efficacy in removing Aβ from the brain and decreasing cognitive decline rates compared to placebo [Sims et al., 2023]. In contrast, amyloid immunotherapy is yet to be awaited in Europe after a withdrawn application for Aduhelm [European Medicines Agency, 2024a], refusal of marketing authorization for Leqembi [European Medicines Agency, 2024b] and Donanemab's marketing authorization application in process [Alzheimer Forschung Initiative e.V., 2024].

1.1.4 Vascular contributions to dementia

Cognitive impairment of vascular etiology is the second most common cause of dementia, and might even be the most prominent one in East Asia [Iadecola et al., 2019]. In vascular dementia, cognitive impairment is attributable to a heterogeneous group of cerebrovascular pathologies. According to the Vascular Impairment of Cognition Classification Consensus Study four subtypes can be distinguished: post-stroke dementia

(development of dementia up to 6 months post-stroke), subcortical ischemic dementia, multi-infarct (cortical) dementia and mixed dementias [Skrobot et al., 2018]. As the names imply, vascular dementia (VaD) and its precursor vascular cognitive impairment (VCI) require clinically significant deficits in at least one cognitive domain (attention, memory, executive function, language or visuospatial function). Memory is not necessarily the first affected cognitive faculty and a memory deficit is not required for the diagnosis of VaD or VCI [Gorelick et al., 2011]. Often times vascular brain lesions produce impairments in executive function and processing speed [Iadecola et al., 2019, Peters et al., 2005].

As these vascular lesions are most often a consequence of a condition called cerebral small vessel disease (CSVD), which is an umbrella term for alterations of the cortical and subcortical/deep cerebral microvasculature, CSVD is responsible for most vascular dementias. CSVD is very common in aging, such that almost all individuals aged 90 and about 80% of the 65-year-olds exhibit clinical or radiological manifestations of CSVD [Haffner et al., 2016]. The neuroimaging markers of CSVD are manifold: recent small sucortical infarcts, lacunes (of presumed vascular origin), white matter hyperintensities (WMH), enlarged perivascular spaces (PVS), cerebral microbleeds, cortical superficial siderosis and cortical cerebral microinfarcts [Duering et al., 2023]. Brain atrophy is also considered a neuroimaging marker of CSVD and VaD, but it is unspecific, as neurodegeneration is a hallmark of most dementias. Notably, while WMH are often considered vascular lesions exclusively, an alternative hypothesis states that WMH can be secondary to AD-related processes, e.g. neurodegeneration and inflammation [Garnier-Crussard et al., 2023].

The most common forms of CSVD are cerebral amyloid angiopathy (CAA) and deep perforator arteriopathy (DPA), also called hypertensive angiopathy or non-amyloid CSVD [Schreiber et al., 2016]. They share similarities in their representations, such that pure DPA or CAA are hypothesized to be rare extremes on a continuum of age-related small vessel pathologies [Schreiber et al., 2016]. Like in AD the Aβ peptide plays an integral role in CAA. Specifically, CAA is characterized by deposition of Aβ_{40} (to a lesser extent Aβ_{42}) in the walls of capillaries or non-capillary blood vessels like arterioles, small to medium sized parenchymal and leptomeningeal arteries and rarely veins. The most common diagnostic criteria for CAA are the modified Boston criteria. DPA on the other side is characterized by arteriolosclerosis, fibrinoid necrosis and lipohyalinosis and affects mainly small arteries, veins, arterioles, venules and capillaries originating from deep perforating vessels from large vessels. DPA is related to vascular risk factors like arterial hypertension. In order to quantify CSVD globally, semi-quantitative summary scores have been developed [Charidimou et al., 2016, Staals et al., 2015]. The score by Staals et al. [2015] is more specific to DPA, which has been particularly related to deep lacunes, deep/mixed cerebral microbleeds (CMB) and (visible) PVS in the basal ganglia. Charidimou et al. [2016] developed a score more specific to CAA, which has been more related to CMB, cortical superficial siderosis (cSS) and PVS in the centrum semiovale.

As mentioned before, cerebrovascular pathology can co-occur with neurodegenerative pathology to create mixed forms of dementia. For example, in the presence of additional cerebrovascular pathology, less AD pathology is required to evoke clinical symptoms

[Petrovitch et al., 2005, Snowdon, 1997]. Hence, it can be difficult to attribute the clinical symptoms to a single cause [Gorelick et al., 2011].

1.2 Reserve, resilience and resistance

Already decades ago researchers had identified that some individuals remained non-demented until death despite substantial amounts of AD pathology in their brains [Katzman et al., 1988]. Such discrepancies between the expected cognitive status given disease- and age-related brain changes and the actual cognitive status led to the formulation of the reserve hypothesis [Katzman, 1993, Satz, 1993]. In its original form, reserve was viewed primarily in terms of a threshold model in which age- or disease-related burden, e.g. lesions or AD pathology, would accumulate up to a certain threshold at which clinical symptoms became apparent [Satz, 1993]. The reserve capacity of an individual would determine how much of this burden it can withstand before passing the cutoff to functional impairment. As the field of reserve progressed, the concept expanded and simultaneously the terminology diverged, raising questions about establishing a better consensus of basic concepts and assumptions underlying reserve research. According to the newest consensus definitions of the Collaboratory on Research Definitions for Reserve and Resilience in Cognitive Aging and Dementia (`https://reserveandresilience.com/`), the aforementioned purely passive account of reserve would be called brain reserve (BR) [Stern et al., 2023]. It refers to the neurobiological capital of an individual, e.g. the amount of neurons or synapses. Individuals with more BR would simply have more to lose in face of brain aging and pathology before clinical symptoms emerge. Proxies used for brain reserve include anatomical measures such as head circumference, brain size, synaptic count or dendritic branching [Mortimer et al., 2005, Stern, 2002].

Brain maintenance as a complimentary concept is defined as the relative absence of changes in neurobiological resources or neuropathology [Stern et al., 2023]. In contrast to brain reserve, brain maintenance is not concerned with the initial amount of neurobiological resources, but focuses on the change of these over time [Stern et al., 2023]. Individuals with greater brain maintenance would exhibit fewer structural brain changes and hence fewer cognitive changes than individuals with low brain maintenance. Such change-change relationships have particularly been observed for the hippocampus and episodic memory [Gorbach et al., 2017, Persson et al., 2012]. However, brain maintenance is conceptually somewhat linked to BR, which offers snapshots of neurobiological capital at certain points in time, since higher brain maintenance would translate into a slower depletion of BR [Alvares Pereira et al., 2022, Stern et al., 2023].

Cognitive reserve (CR) on the other hand has been postulated as an active form of reserve [Stern, 2002]. In contrast to the threshold model of brain reserve, CR does not assume a fixed threshold at which functional impairment would occur, but rather considers individual thresholds that depend on how flexible and efficient an individual is in using the remaining neural substrate [Stern, 2002]. According to the recent consensus definitions [Stern et al., 2023], CR "refers to the adaptability (i.e., efficiency, capacity, flexibility) of cognitive processes that helps to explain differential susceptibility of

cognitive abilities or day-to-day function to brain aging, pathology, or insult". Instead of brain structure, CR emphasizes brain function [Arenaza-Urquijo et al., 2015]. Since brain function must, however, have a biological basis with underlying molecular/cellular mechanisms, a complete distinction between BR and CR is not possible. Instead, contemporary definitions refer to qualitatively different levels because it is currently not possible to directly map a cognitive process onto defined biological phenomena [Stern et al., 2020]. In concordance with the definition, CR is operationalized as a moderator variable that moderates the relationship between an individual's brain pathology burden and the level of cognitive performance (due to cognitive and functional brain mechanisms).

As a theoretical construct with ongoing debate about its operationalization, CR is often approximated by sociobehavioral indices identified in epidemiologic research (see Meng and D'Arcy [2012] or Valenzuela and Sachdev [2006] for a review). The most prominent ones are education, occupation, IQ and mentally stimulating leisure activities. While there is striking evidence that these indices are correlated with decreased dementia risk, they are rather indirect assessments of CR. Furthermore, education and occupation can become static measures at a certain point in life. Even though early-life exposure does seem to have strong impact on outcomes in late life [Deary et al., 2004], CR has been conceptualized as a dynamic quantity that can vary over time [Bettcher et al., 2019, Lenehan et al., 2016]. There is an increasing effort to create more comprehensive sociobehavioral CR indices that span multiple sociobehavioral domains including both static and dynamic quantities (see Nogueira et al. [2022] for a review), e.g. by employing extensive questionnaires.

Another approach for assessment of CR builds on residual methods which predict individual measures of cognitive performance based on demographic and brain variables and treat the residual variance as a measure of CR. Although the residual approach (e.g. Reed et al. [2010], Zahodne et al. [2013]; or voxel-wise as in van Loenhoud et al. [2017]) is closer to the functional brain processes underlying CR and might offer a more direct quantification of CR, it relies on an accurate and complete specification of brain measures that account for individual differences in cognitive performance. Misspecification of predictive models might result in systematic estimation biases of CR. For instance, the CR residual will be strongly correlated with the cognitive performance measure unless the amount of unexplained variation in the residual model is quite low [Elman et al., 2022]. The most comprehensive set of predictors in a residual model of CR in the context of AD to date to our knowledge comes from Lee et al. [2019], who estimated cognitive performance with a model including demographic (age + sex) and genetic factors (APOE4 status), brain structural features (total intracranial volume (TIV) and mean cortical thickness) and PET measures of both amyloid and tau burden. Their CR marker (=residual) modified the relationship between brain pathology and memory function across the AD spectrum. The CR marker was significantly correlated with network measures of the right middle-temporal pole.

In contrast to CR proxies and residual approaches, functional imaging approaches like fMRI allow the characterization and measurement of functional brain processes. As such, they might offer the unique opportunity to capture some aspects of the neural

implementation of CR and represent its closest direct measure to date. Many functional neuroimaging studies on CR have been conducted using a wide range of methods applied to both resting-state and task fMRI data. However, most of these studies have identified regions or networks contributing to CR by correlating their expression (activity/connectivity) with a CR proxy like education or IQ instead of investigating their ability to moderate the relationship between aging- or pathology-related brain changes and cognitive performance.

Taking a slightly different viewpoint, the principles of brain reserve and cognitive reserve could be summarized under the term resilience, which can be contrasted with resistance [Arenaza-Urquijo and Vemuri, 2018]. Resilience denotes coping with pathology, i.e. remaining phenotypically normal in spite of pathological changes (in comparison to demographically matched peers) [Arenaza-Urquijo and Vemuri, 2018]. The concept of resistance in contrast describes the process of avoiding pathology in the first place, i.e. exhibiting no major (or less than expected) pathological measures, like Aβ/p-tau or WMH. In that sense resistance is similar to brain maintenance, which can, however, also capture aspects of resilience, as neurobiological capital could be maintained in the presence of neuropathology.

Hippocampal vascularization might be a factor underlying resilience or resistance against age- and pathology-related alterations of the brain that has not been studied extensively in this context. Hence, cerebral vascularization and particularly hippocampal blood supply are reviewed in the following sections.

1.3 Brain vasculature and metabolism

Unlike other organs, the brain, despite having the greatest energy demand (accounting for about 25% of total body glucose consumption and 20% of total body oxygen consumption [Allaman and Magistretti, 2012]), has no energy reserves and is unable to utilize fat for fuel, but relies primarily on glucose. Exceptions are ketone bodies and monocarboxylates like pyruvate and lactate. Lactate is estimated to account for about 8-10% of the brain's energy demands. Under supraphysiological lactate concentrations, e.g. during physical exercise, it might even be utilized in greater amounts and cover up to 20-25% of the brain's energy requirements. Ketone bodies on the other hand are only used as energy source in the adult brain in conditions of inadequate glucose availability like starvation and diabetes [Allaman and Magistretti, 2012].

Due to the lack of energy storage, increased metabolic demands of neural tissue in the form of glucose and oxygen have to be met on the fly in the form of functional hyperemia. Hence, neural activity is spatially and temporally tightly linked to cerebral blood flow (CBF) via a mechanism called neurovascular coupling [Iadecola, 2017]. The resulting increase in CBF overcompensates for the need of tissue oxygen, leading to a relative surplus in local blood oxygen [Raichle and Mintun, 2006]. However, the vascular response occurs on a slower time scale than the neural activity, which may last only a few milliseconds. After an initial short dip in local blood oxygen concentrations, the vascular response reaches its maximum after about 5 seconds, followed by a prolonged

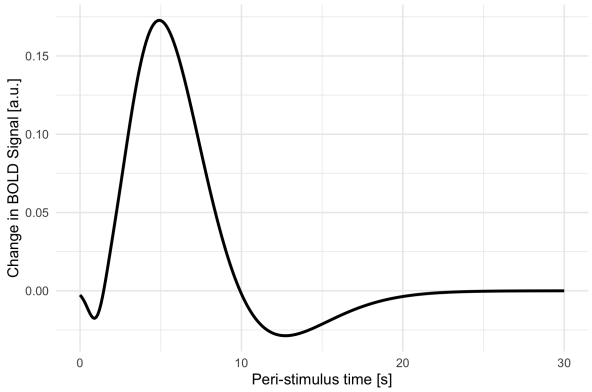

Figure 1.2: **Approximate form of the hemodynamic response function.** After an initial dip the BOLD signal reaches its peak after a few seconds, followed by a post-stimulus undershoot prior to a return to baseline.

post-stimulus undershoot [Hu and Yacoub, 2012, Poldrack et al., 2011] (see Fig. 1.2). The knowledge of the hemodynamic response as a consequence of neurovascular coupling allows the indirect assessment of local neural activity with the use of functional magnetic resonance imaging (fMRI) via the measurement of the associated vascular response. As the name implies, BOLD fMRI (blood oxygen level dependent fMRI) assesses the blood oxygenation level, which is enabled by the distinct magnetic properties of oxygenated (diamagnetic) versus deoxygenated hemoglobin (paramagnetic) [Heeger and Ress, 2002]. An adequate blood supply to the neuronal tissue is absolutely essential, such that an inadequate supply of blood glucose and oxygen to a brain region can lead to neuronal or glial injury or death [Attwell et al., 2010]. Besides a supply in metabolic substrates, cerebral blood flow could also be increased during neural activity in order to aid the removal of metabolic waste-products or for temperature regulation [Yablonskiy et al., 2000, Zhu et al., 2006].

1.3.1 Gross anatomy of the cerebral vasculature

All cerebral arteries arise from the internal carotid arteries (ICAs) or the basilar artery [Schünke et al., 2009]. The latter one is formed from a confluence of the two vertebral arteries at the base of the skull. It supplies the cerebellum and terminates in the posterior cerebral artery (PCA), which supplies the posterior part of the brain (posterior circulation) including some temporal regions. The ICA divides into the anterior cerebral artery and middle cerebral artery. It supplies the anterior and middle part of the brain (anterior circulation). The anterior and posterior circulation are connected via the Circle of Willis (CoW), an arterial circle at the base of the brain (see Fig. 1.3). The purpose of the CoW is to provide collateral flow in the arterial system in order to protect the brain from the consequences of narrowed or blocked arteries. In a complete CoW the posterior communicating artery (PComA) connects the ICA to the PCA and the anterior communicating artery connects both anterior cerebral arteries. However, variations in the CoW are common, some of which are discussed in section 1.4.

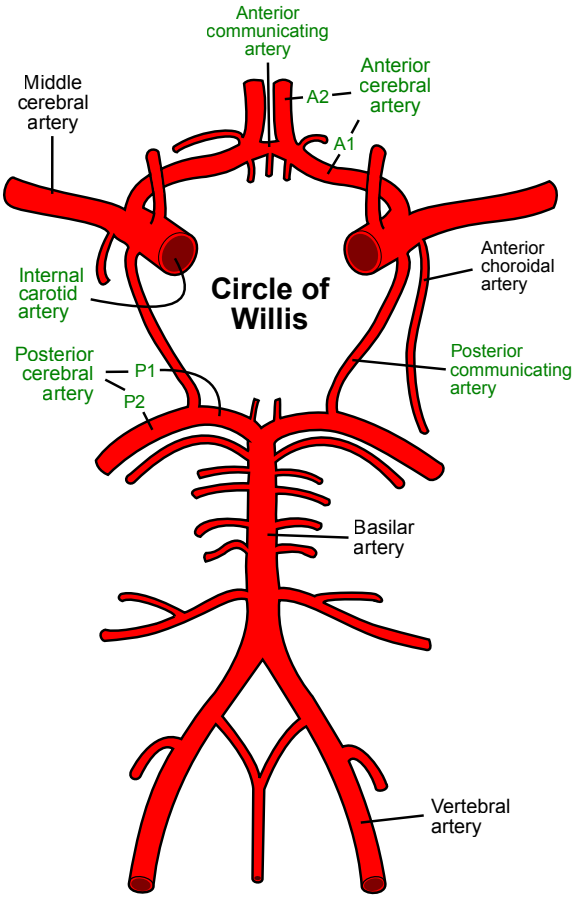

Figure 1.3: **Circle of Willis.** In a complete CoW the posterior communicating artery connects the ICA to the PCA and the anterior communicating artery connects both anterior cerebral arteries. Arteries printed in green ink compose the Circle of Willis. Illustration adapted from `https://commons.wikimedia.org/w/index.php?curid=1597012` with permission.

1.3.2 Tortuosity

Tortuosity comprises one of the morphological features of a blood vessel. Normally, blood vessels are relatively straight pipes that provide perfusion to distant tissues [Han, 2012], but alterations of the vasculature can cause vessels to become serpentine. While sometimes curving, kinking/angulation, looping and spiral twisting are all summarized under the umbrella term of tortuosity [Han, 2012], many authors reserve the term tortuosity more specifically for morphological variations of curving and elongation. This goes back to the definition by Weibel and Fields [1965], who defined tortuosity as "any S- or C-shaped elongation or undulation of the course of the [vessel]". Assessment of tortuosity is carried out via different diagnostic modalities including Doppler sonography and angiographic images from computer tomography (CT) or MRI. The ICA has frequently been subjected to studies on tortuosity (see e.g. Del Corso et al. [1998], Martins et al. [2018], Togay-Isikay et al. [2005]). Prevalence of ICA tortuosity in its wider sense

is rather frequent, but has varied substantially between studies, ranging from 13-58% [Del Corso et al., 1998, Martins et al., 2018, Saba et al., 2015, Togay-Isikay et al., 2005, Weibel and Fields, 1965]. This variability is likely due to subjective assessment of tortuosity, different diagnostic methodology and characteristics of the cohort (demographics and health status). Multiple studies, including a study with almost 20000 patients, have found a higher prevalence of ICA tortuosity for women overall [Del Corso et al., 1998, Martins et al., 2018, Pellegrino et al., 1998] or at least for women above the age of 60 [Togay-Isikay et al., 2005]. Although some authors make the case that tortuosity exclusively originates in embryonic development [Beigelman et al., 2010], others show an increasing prevalence and severity with age [Huang et al., 2024, Martins et al., 2018, Sun et al., 2022], indicating that tortuosity is probably congenital in some cases, but acquired in the greater majority. On top of that, cerebral vessel tortuosity in women might be more age-dependent than in men [Sun et al., 2022]. Some studies have also found more cases of tortuosity on the left side compared to the right [Martins et al., 2018, Pellegrino et al., 1998, Saba et al., 2015].

Qualitatively, tortuosity is often described by the criteria introduced by Metz et al. [1961] (kinking) and Weibel and Fields [1965] (tortuosity). Quantitatively, a couple of different approaches have been developed in order to assess the extent of tortuosity and enable automatic quantification on three-dimensional medial images [Bullitt et al., 2003], three of which are shortly presented in order of increasing sensitivity towards local tortuosity and coils. In the simplest metric (tortuosity index (TI) or distance metric), vessel length is divided by the shortest distance between the start and end of the vessel [Bullitt et al., 2003, Ciurică et al., 2019]. TI has been utilized to examine tortuosity and its relationship with cognitive performance in chapter 3. In the inflection count metric, TI is multiplied by the number of inflection points plus 1 [Bullitt et al., 2003]. The sum of angle metric sums the angles between consecutive triplets of points divided by total vessel length [Bullitt et al., 2003]. Apart from these straightforward approaches, more complex ones have also been developed (see e.g. Johnson and Dougherty [2007]).

1.3.3 Cerebrovascular reactivity

Neurovascular coupling affects the vasculature via a multitude of signaling molecules that cause vasodilation and vasoconstriction in a highly orchestrated manner [Allaman and Magistretti, 2012, Attwell et al., 2010, Iadecola, 2017]. Synaptic signaling induces vasodilation via glutamate-dependent production of nitric oxide and prostaglandins in neurons and astrocytes, respectively (see Attwell et al. [2010] for an extensive overview of molecules regulating blood flow). Vasodilation and -constriction are primarily achieved by relaxation and constriction of smooth muscle cells around arteries and arterioles [Attwell et al., 2010, Welsh and Segal, 1998]. Capillaries are surrounded by pericytes instead of smooth muscle cells [Iadecola, 2017]. Evidence regarding the contractility of pericytes and their involvement in flow regulation is conflicting. Some studies have shown that pericytes are able to affect capillary diameter and modify blood flow [Fernández-Klett et al., 2010, Hall et al., 2014, Mishra et al., 2016, Peppiatt et al., 2006], whereas other have found no involvement of pericytes in flow regulation [Hill et al., 2015, Wei

et al., 2016]. Independent of the role of pericytes in blood flow, however, capillaries also exhibit functional hyperemia [Wei et al., 2016].

The ability of the (cerebral) blood vessels to constrict and dilate in response to a vasoactive stimulus is called cerebrovascular reactivity (CVR) [Zimmerman et al., 2021]. Apart from its essential role in neurovascular coupling, CVR is also important for autoregulation of cerebral blood flow, i.e. ensuring a relatively stable rate of perfusion across a wide range of arterial blood pressures (ca. 60-150mm Hg) [Novak, 2012]. The vasomotor response can also be evoked via exogenous stimuli, enabling the study of CVR in vivo by observing the hemodynamic response to a vasoactive stimulus. A frequently used stimulus is hypercapnia-inducing inhalation of CO_2-enriched gas because of its vasodilatory potency, rapid onset and cessation of the effect [Liu et al., 2019]. Additionally, while the CO_2 arterial partial pressure ($PaCO_2$) cannot be measured directly, hypercapnia can be monitored using the end tidal CO_2 ($EtCO_2$), the level of CO_2 at the end of the breath [Richardson et al., 2016], as a surrogate for $PaCO_2$ [Sleight et al., 2021]. In contrast to injection of acetazolamide, a carbonic anhydrase inhibitor that induces vasodilation via acidosis [Vagal et al., 2009], CO_2 inhalation is also less invasive.

CVR is assessed via measurement of cerebral blood flow, cerebral blood volume or both. The most prominent method in this context nowadays is MRI due to its large coverage (potentially whole brain instead of single large arteries in Transcranial Doppler ultrasound), good spatial resolution (allowing for mapping CVR in microvessels), better temporal resolution (compared to PET and SPECT)[Lin and Alessio, 2009] and non-invasiveness including the absence of ionising radiation [Sleight et al., 2021]. Many different MRI sequences have been utilized for measuring CVR. These include measures of blood flow like arterial spin labeling (ASL) [Nöth et al., 2006] and phase contrast MRI [Valdueza et al., 1997], measures of blood volume like vascular space occupancy [Donahue et al., 2009] and measures of both like dynamic-susceptibility contrast MRI [Taneja et al., 2019]. However, the most frequently used MRI sequence in CVR research is BOLD fMRI, with two thirds of the CVR studies until 2020 being conducted with BOLD fMRI [Sleight et al., 2021]. BOLD fMRI appears favorable because of its wide availability and higher signal-to-noise ratio (SNR) in comparison to perfusion measurements like ASL [Liu et al., 2017].

CVR studies with CO_2 inhalation as vasoactive stimulus have demonstrated good reproducibility [Liu et al., 2019]. Yet, the required gas delivery system comes with additional challenges in the MRI setting, such as necessary MRI-compatibility of all components, space issues of the breathing apparatus within small space of the MRI and head coil, and a need for adjustability of the gas concentration during scanning [Liu et al., 2019]. In addition, cost and demands in time and expertise limit its practical application, especially in the clinical setting [Liu et al., 2017]. Due to these obvious downsides, alternative approaches have been developed, which rely on voluntary alterations in breathing. One technique uses repeated breath holds of 10-36s alternated with periods of normal breathing (in some cases guided) in order to cause hypercapnia without an external stimulus [Bright and Murphy, 2013, Kastrup et al., 2001, Murphy et al., 2010]. CVR results based on breath holds have shown good concordance with CO_2 inhalation [Bright and Murphy, 2013, Murphy et al., 2010]. Similarly, hyperventilation paradigms

are supposed to evoke hypocapnia and cause vessel constriction [Naganawa et al., 2002]. Both approaches have the disadvantage of increasing the likelihood of subject motion [Liu et al., 2019] and requiring patient compliance [Jahanian et al., 2017], which might be especially difficult for elderly participants and patients. To circumvent compliance issues and enable CVR measurements even in patients with stroke, the intrinsic variability of the BOLD signal in resting-state fMRI (rs-fMRI) without any stimulus can be used [Liu et al., 2019, Tsvetanov et al., 2021a]. This approach relies on the change in CO_2 levels due to spontaneous alterations in the breathing pattern [Liu et al., 2019]. One potential issue is that the CO_2 stimulus provided by natural variation in breathing might be too small to evoke meaningful vasomotor responses [Pinto et al., 2021]. Furthermore, the BOLD signal is confounded with other physiological signals, making adequate filtering and data analysis essential [Liu et al., 2019]. Regarding the latter, methods quantifying the variation in filtered signal, like RSFA (resting state fluctuation amplitude) [Kannurpatti and Biswal, 2008] and ALFF (amplitude of low frequency fluctuations) [Di and Biswal, 2012, Kazan et al., 2016] can be distinguished from signal regression methods as used in Liu et al. [2017]. Liu et al. [2020] recently presented another approach utilizing a paced breathing paradigm, in which 12s periods of paced breathing were alternated with free breathing. During paced breathing the natural breathing rate of about 3-5s per breath was reduced to 6 or 12s, in order to enhance changes in breathing patterns observed during pure resting-state scans. Paced breathing has been shown to provide better sensitivity than resting-state measurements, while retaining low issue rates with compliance [Liu et al., 2020]. Hence, a paced breathing task was also utilized in this thesis for investigation of CVR (see chapter 3).

The extent of cerebrovascular reactivity differs among major vascular territories and regions. CVR is higher in parietal and occipital regions as compared to frontal and temporal regions or the insular cortex [Novak, 2012]. Hypoperfusion or chronic hypoxia might particularly affect regions with lower vasoreactivity [Novak, 2012]. Additionally, CVR in gray matter might be two to three times greater than in white matter [Rostrup et al., 2000, Zande et al., 2005].

1.4 Hippocampal vascularization

Anatomical knowledge about the vascularization of the hippocampus stems from neurosurgical autopsy studies [Erdem et al., 1993, Marinković et al., 1992]. Despite the vast variability in hippocampal blood supply, on a coarse level all hippocampal arteries originate directly or indirectly from two arteries: the PCA and the anterior choroidal artery (AChA) (see Figs. 1.1C and 1.3). Most of the hippocampus is supplied via hippocampal arteries arising from the main trunk of the PCA (P2 or P3 segment; see Fig. 1.4) or its inferior temporal, lateral posterior choroidal and splenial branches [Erdem et al., 1993]. Isolan et al. [2020] additionally described a rare case in which the parieto-occipital and calcarine branch of the PCA were involved in hippocampal vascularization. While hippocampal blood supply always depends on the PCA, the AChA has been found to additionally contribute in ca. 50-60% of the examined hemispheres

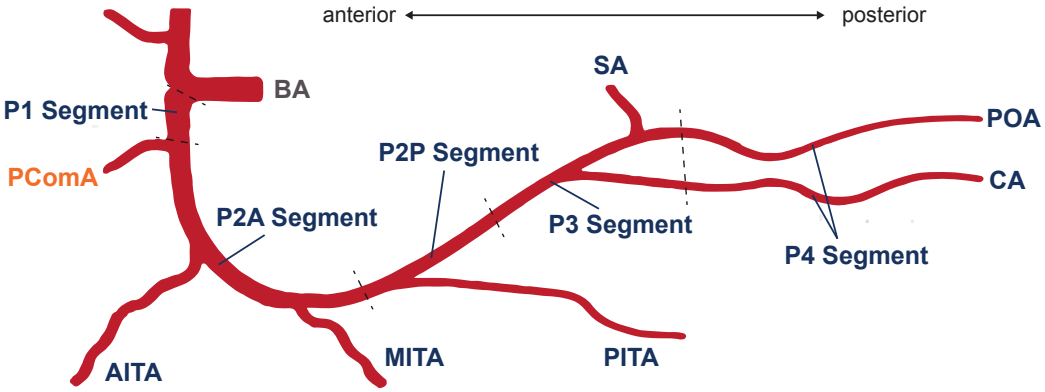

Figure 1.4: **Segments and branches of the posterior cerebral artery.** Provided is a rough outline, as there is still no consensus about the exact segmentation of the PCA, and anatomical variability regarding which segment the branches originate from exists [Cilliers and Page, 2019, Kawashima et al., 2005, Rose et al., 2001, Uz, 2019]. The P1 (pre-communicating) segment of the PCA originates in the termination of the basilar artery (BA) and ends where the posterior communicating artery (PComA) connects the ICA and PCA. The following (post-communicating) P2 segment courses through the crural cistern (anterior subsegment P2A) and the ambient cistern (posterior subsegment P2B) and terminates upon entering the quadrigeminal cistern. The anterior, middle and posterior inferior temporal arteries (AITA/MITA/PITA) most often originate from the P2 segment. The (quadrigeminal) P3 segment runs through the quadrigeminal cistern until it becomes the (calcarine/cortical) P4 segment in the calcarine fissure. The PCA usually divides into the calcarine artery (CA) and parieto-occipital artery (POA) in the P3 segment. The splenial artery (SA) arises from the PCA itself or from the POA. Illustration adapted from Cilliers and Page [2019] with permission.

[Erdem et al., 1993, Isolan et al., 2020, Spallazzi et al., 2019]. Hippocampal blood supply via the AChA is almost exclusive to the hippocampal head [Erdem et al., 1993, Isolan et al., 2020, Marinković et al., 1992]. Once again it was Isolan et al. [2020] who reported a single special case in which the AChA supplied the body and tail of the hippocampus instead of the head.

From a phylogenetic viewpoint, the combined blood supply via the AChA and PCA presents a peculiarity [Raz et al., 2004]. In humans, the AChA originates from the ICA and is hence part of the anterior circulation, whereas the PCA is part of the posterior circulation as terminal branch of the (vertebro)basilar arterial system [Javed et al., 2023]. Evolutionary speaking, the involvement of the vertebrobasilar system in brain blood supply is a relatively recent phenomenon, only observed in higher mammals. In contrast, in fish, which represent some of the most ancient vertebrates, the entire intracranial CNS is supplied by the carotid arteries. An increasing brain size throughout the history of vertebrates came along with elevated demands for blood flow, leading to gradual alteration of the original vascular system in the form of greater vessel size, sprouting of new arteries and formation of anastomoses. Since evolution itself is a rather gradual phenomenon, formation of new vessels is rare as opposed to more common utilization of

already existing structures and pathways [Shapiro and Raz, 2014].

Following evolution up until birds, brain vascularization still depended merely on branches of the carotid system. In those, the AChA was still the primary source of parieto-occipital (posterior) blood supply. However, the phylogenetic precursor of the PCA began to extend its coverage and to form anastomoses with the anterior choroidal system, announcing its future annexation of this territory. Further increases in flow demands seemingly brought the carotid system to its functional limit in higher mammals. Hence, the vertebrobasilar system progressively took over the brainstem and cerebellar territory. A reversal of craniopetal to craniofugal blood flow was the consequence of annexation of further basilar territory by the vertebral artery and is observed in monkeys, apes and humans. Participation of the vertebral system to brain blood supply is maximized in humans where the PCA was functionally acquired by the posterior circulation (although still belonging to the carotid developmentally) and took over previous AChA perfusion territories, probably as a consequence of overwhelming flow demands to the carotid due to the humans' increased frontal lobes [Shapiro and Raz, 2014].

A contribution of the AChA to hippocampal blood supply thus not only constitutes the addition of an artery, but also decreases the dependence of the hippocampus on the posterior circulation. In absence of the AChA-dependent hippocampal branches, a contribution of the anterior circulation to hippocampal blood supply is only indirectly possible via the PComA, which serves as an anastomosis between the ICA and the PCA (see Figs. 1.3 and 1.4). In a complete CoW (depicted in Fig. 1.3) this would be the case, making the PCA less dependent on the basilar artery alone. However, many variations of the CoW exist (see e.g. Krabbe-Hartkamp et al. [1998] for an overview). For instance, the PComA is the most commonly absent or hypoplastic artery in the brain [Gutierrez et al., 2013], weakening the connection between anterior and posterior circulation in many individuals. Especially in hemispheres with an absent PComA the sole contribution of the PCA to hippocampal blood supply could have dramatic consequences, since it would represent a vascular dependence of the hippocampus on the posterior circulation alone. Mice without posterior communicating ateries or an incomplete Circle of Willis are more susceptible to ischemia following an occlusion of the middle cerebral artery or the carotid artery [Barone et al., 1993, Gürsoy Özdemir et al., 1999, Kitagawa et al., 1998]. The contribution of the AChA represents an additional involvement of the anterior circulation and could thus imply qualitative differences beyond the quantitative aspect (two vessels are better than one) and might thus constitute a factor for resilience or resistance against age-related pathology.

With the use of a high-resolution 7T time-of-flight (ToF) magnetic resonance angiography (MRA), the small cerebral arteries in the MTL can now also be visualized in vivo at an unprecedented resolution, allowing an assessment of the anatomical variants of hippocampal vascularization [Spallazzi et al., 2019]. Perosa et al. [2020] utilized this sequence for a binary classification of the hippocampal vascularization pattern (HVP) into a single supply by the PCA alone as contrasted with a mixed supply by both the PCA and AChA in a cohort of older adults with and without CSVD. They discovered that a combined supply by the PCA and AChA was linked to better cognition and overall hippocampal structural integrity using a voxel-based analysis. An additionally

observed interaction between the HVP and CSVD indicated that the HVP potentially confers resilience against CSVD [Perosa et al., 2020].

In another anatomical variation of the Circle of Willis, the PCA remains in its phylogenetically and ontogenetically original stage, in which its parental vessel is the ICA. The P1 segment of a so-called fetal-type PCA (FTP) is hypoplastic or completely absent, whereas the PComA is hyperplastic and takes over the role of the PCA from its P2 segment onwards. As a consequence, hippocampal supply is clearly dominated by the anterior circulation. The prevalence of FTPs in the general population lies approximately between 10 and 30% [Arvind Gunnal et al., 2018, Gutierrez, 2020, Kapoor et al., 2008, van Raamt et al., 2006]. FTPs have also been linked to greater cognitive deficits in the presence of ICA occlusion. After revascularization in patients with an ICA stenosis, patients with an ipsilateral FTP showed faster decline 6 months post operation than patients with an adult configuration of the PCA [Altinbas et al., 2014]. Additionally, adverse interventional procedures on the ICA in hemispheres with an FTP have been shown to impair memory function [Zijlmans et al., 2012]. In summary, hippocampal vascularization and the CoW exhibit a lot of variation with potential implications for memory function and resilience.

In rodents the microvasculature of the hippocampus has been mapped with incredible detail. On the microstructural level the hippocampal vasculature forms a rake-like pattern with continuously spaced alternating arcs of arterioles and venules [Kirst et al., 2020]. The main vessel runs in parallel to the longitudinal hippocampal axis and sends off perpendicular branches deep into the hippocampus [Kirst et al., 2020, Zhang et al., 2019]. Compared to the robust microvascular network of the neocortex, the microvascular network of the hippocampus is quite sparse [Ji et al., 2021, Kirst et al., 2020, Shaw et al., 2021, Zhang et al., 2019]. In fact, Ji et al. [2021] found the hippocampus to have the lowest vascular density out of all examined gray matter regions. The CA1 region has been shown to have particularly low capillary density in mice, whereas CA3 had similar density as frontal or parietal cortex [Cavaglia et al., 2001]. As a consequence, resting blood flow and oxygenation are lower in the hippocampus than in visual cortex [Shaw et al., 2021]. Despite the low vascular density, the metabolic demands of the hippocampus are matched under non-pathological conditions [Ji et al., 2021]. This is likely because the local energy demand is less than in cortex, as fewer cells are simultaneously active [Johnson, 2023]. Hippocampal processes like pattern separation promote such sparse neural coding schemes. Likewise, place cells of the hippocampus, which unlike orientation cells in the visual cortex do not show a structured anatomical organization, employ sparse neural coding [Ekstrom et al., 2003]. However, the hippocampus and particularly the CA1 region exhibits an increased vulnerability towards pathological conditions and shortcomings in blood supply due to its scant capillary network [Nikonenko et al., 2009, Scharrer, 1940, Spielmeyer, 1925, Uchimura, 1928].

1.5 Cerebrovascular alterations in aging and disease

1.5.1 Tortuosity

Morphologically, blood vessels change over the lifetime and have an increased tendency to deviate from their normally rather straight path, causing vessels to become tortuous [Martins et al., 2018, Sahni et al., 2007, Sun et al., 2022, Thore et al., 2007]. Tortuosity of the ICA and other cerebral arteries have been related to multiple risk factors for cardiovascular and metabolic disease including hypertension [Ciurică et al., 2019, Del Corso et al., 1998, Han, 2012, Huang et al., 2024, Martins et al., 2018], atherosclerosis [Del Corso et al., 1998, Eun et al., 2024, Han, 2012], hyperlipidemia [Del Corso et al., 1998, Martins et al., 2018], BMI [Wang et al., 2017] and smoking [Del Corso et al., 1998]. The directionality of these relationships is unclear, but the risk factors might drive tortuosity by directly or indirectly causing damage to the vessel wall and compromising its integrity, leading to repair and vascular remodeling. One prominent mechanical change in tortuous vessels is a weakening of the arterial wall through degradation of elastin, which is considered a cause of vessel lengthening [Han, 2012]. At the same time the artery becomes stiffer as elastin is replaced mainly by collagen [Zimmerman et al., 2021]. Disruption of elastic fiber is also a key feature of artery tortuosity syndrome, a rare autosomal recessive disease characterized by elongation, tortuosity and aneurysm formation in major arteries [Han, 2012]. Hence, elastin degradation might be one mechanism connecting the aforementioned risk factors to arterial tortuosity and stiffness. For hypertension and atherosclerosis the association might be bidirectional, leading to a vicious cycle. Resistance to blood flow is increased in tortuous vessels [Schep et al., 2002], requiring a compensation by higher blood pressure to match flow demands, which in turn causes increased shear stress and more damage to the vessel wall. The shape of the vessels might promote formation of atherosclerotic plaques at inflection points, compromising blood flow further. Considering the increased shear stress and attenuated blood flow at inflection sites, observed associations of tortuosity with artery dissection [Saba et al., 2015], ischemic stroke [Cartwright et al., 2006, Shang et al., 2022] and heart disease [Del Corso et al., 1998, Martins et al., 2018] appear comprehensible.

Due to the compromised blood flow/supply one might suspect an association of cerebral artery tortuosity with cognitive performance. Such a relationship has not been well studied and the results do not all align. Yin et al. [2024] did find that lower TI and other tortuosity metrics of the extracranial ICA and vertebral artery were related to better Montreal Cognitive Assessment (MoCA) scores of cognitive performance. Outside of the brain, a combined measure of retinal amyloid and retinal venous TI was able to discriminate patients with normal and impaired cognition [Dumitrascu et al., 2021]. Yet, Chen et al. [2022b] found a negative association between average (whole-brain) artery tortuosity and MoCA scores to be statistically non-significant. In contrast, they observed a significant positive relationship of both artery length and the number of arterial branches (=arterial density) of the whole brain and MoCA scores [Chen et al., 2022b]. While especially the ICA has been a common subject of investigation, tortuosity of many other arteries has not been specifically examined. For instance the relationship between cog-

nitive performance and arteries potentially implicated in hippocampal supply like the PCA and AChA or with a vital role in the CoW like the PComA is unknown.

1.5.2 Microvascular density

Another vascular change frequently associated with aging in rodents and humans is cerebromicrovascular rarefaction, although some studies reported opposite findings (see Brown and Thore [2011] or Riddle et al. [2003] for an overview). Microvascular density in the hippocampus and ERC have also shown age-related decreases, which were driven by attenuated capillary density, whereas the number of arterioles was higher for old than young adults, especially in subiculum [Bell and Ball, 1981]. Such microvascular rarefaction in the hippocampus and throughout the whole brain has been related to cognitive deficits in the absence of other gross pathology or neurodegeneration [Brown et al., 2007, Troen et al., 2008]. Cognitive impairment has also been observed in obese aged mice with a significant reduction in microvascular density in hippocampus and cortex [Tucsek et al., 2014]. Multiple considerations illustrate the importance of capillary density to its surrounding tissue [Ingraham et al., 2008] and could link microvascular rarefaction to cognitive impairment. First, capillary density indirectly represents the capacity of blood that can be delivered to the brain parenchyma. It further dictates the vascular surface area available for exchange of oxygen and nutrients. Third, it influences the distance between adjacent capillaries, which determines how far oxygen and nutrients will have to diffuse in order to reach neurons and glia. On top of that, vasculature might exert a trophic effect on surrounding tissue by secreting neural growth factors like BDNF and IGF-1 [Ingraham et al., 2008]. Hence, increased capillary density might provide more potential for neuroplasticity, whereas decreased capillary density could limit nutrient supply and neuroplasticity.

Although local hypoxia is one of the core issues of microvascular rarefaction it appears to be an insufficient stimulus to trigger angiogenesis [Warrington et al., 2011]. In contrast, systemic hypoxia induces angiogenesis via vascular endothelial growth factor, leading to a richer microvascular network [Boero et al., 1999, Chavez et al., 2000]. Cognitive deficits in mice subjected to whole brain radiation therapy that substantially reduced their cerebromicrovascular density recovered from both the cognitive impairment and the vessel rarefaction within one month under hypoxic conditions [Warrington et al., 2011, 2012], underlining the importance of the cerebromicrovascular network.

In summary, the microvascular network of the brain exhibits age-related rarefaction that has been related to cognitive impairment in a few studies. It remains unclear, however, if higher microvascular density of the hippocampus is related to better cognitive performance.

1.5.3 Cerebrovascular reactivity

In terms of age-related changes in vascular functionality, a meta-analysis revealed a large effect size for decreases in cerebrovascular reactivity with older age [Wang et al., 2023]. Wang et al. [2023] caution, however, that the underlying studies were significantly

heterogeneous, which might render the effect size estimate unreliable. Interestingly, one longitudinal study demonstrated decline in CVR over four years that was greater in middle-aged individuals (40-60 years) than in older participants (> 60 years). As the cerebrovascular reactivity differs between brain regions [Novak, 2012], age-related CVR changes might also display a pattern of regional specificity. Indeed, some studies report age-related CVR changes only in specific regions, for example the temporal lobe [Catchlove et al., 2018a], cingulum [Catchlove et al., 2018a] and occipital cortices [Hund-Georgiadis et al., 2003]. Longitudinal decreases in CVR were found to be highest in the temporal lobe [Peng et al., 2018].

Furthermore, a plethora of studies has reported lower CVR values in patients with stroke or cerebrovascular disease compared to controls [Wang et al., 2023]. PVS have also been associated with lower values of hypercapnia-induced CVR [Kapoor et al., 2022]. Elahi et al. [2023] even suggest attenuation of regional CVR to be one of three potential key mechanisms in CSVD (in addition to decreased CBF and alterations of the blood-brain-barrier). This suggestion is based on findings from a longitudinal study in which reduced CVR was observed in white matter areas that developed WMH by the time of a one-year follow-up compared to the non-converting contralateral side [Sam et al., 2016a,b]. Additionally, attenuated CVR in white matter was associated with higher WMH and higher PVS in basal ganglia cross-sectionally [Blair et al., 2020]. Given the interrelation between different vascular factors, the involvement of CVR in CSVD and other vascular diseases may not be surprising. However, there is also some evidence for CVR impairment in AD as a disease that is not primarily vascular [Beaudin et al., 2022, Cantin et al., 2011, Meel-van den Abeelen et al., 2014, Yezhuvath et al., 2012], even though etiologic evidence is lacking [Sweeney et al., 2018]. Two studies have observed CVR deficits in APOE $\varepsilon 4$ carriers, i.e. individuals at increased risk for developing AD [Rasmussen et al., 2019, Suri et al., 2015], indicating that impaired CVR might be a very early representation in the development of AD.

Expectedly, cognitive deficits can also be observed in association with attenuated CVR (see Catchlove et al. [2018b] for a review). Yet, Sur et al. [2020] showed that CVR is related to cognitive performance independent of the previously mentioned AD risk. In alignment with the role of the MTL in memory, lower CVR in the temporal lobe has been reported to be associated with worse memory performance across a sample comprised of both older and young adults [Catchlove et al., 2018a]. In the subset of older adults specifically, hippocampal CVR also predicted memory scores. This was not the case in the younger adults.

Overall, the brain's vascular system undergoes a lot of structural and functional changes over the lifetime, which contribute to the decline in cognitive functions often observed in aging and might render individuals more susceptible to disease, not only of purely vascular origin.

1.6 Specific aims and outline

The amount of heterogeneity in cognitive trajectories over the lifetime is astonishing. While some people develop dementia that impairs their ability to carry out basic activities of daily living, let alone their cognitive abilities to perform complex tasks, others can keep up cognitively with individuals many years younger. Mechanistically, this could be conceptualized in different frameworks introduced previously. First, there is the concept of resistance and resilience, distinguishing the ability to withstand pathology from the ability to cope with pathology. On another level, the maintenance of cognitive performance into old age could be seen from a structural or (mainly) functional perspective, employing the concepts of brain reserve/maintenance and cognitive reserve.

The aim of this thesis was to achieve a better understanding of the mechanisms involved in successful cognitive aging, primarily from a vascular perspective. In the following three chapters data will be presented and discussed focusing on resistance against cerebrovascular disease and particularly resilience via brain reserve and cognitive reserve.

In the first study (chapter 2), ultra-high field MRI at 7T was employed (originally acquired by Perosa et al. [2020]) to characterize hippocampal vascularization in a cohort of older adults with and without CSVD [Vockert et al., 2021]. The ability of the hippocampal vascularization pattern to convey resistance against CSVD pathology on the local and global level was examined. Further, associations with local and global brain structure were closely assessed in order to elucidate a potential involvement of the HVP in brain reserve or brain maintenance. Moreover, a new approach termed vessel distance mapping (VDM) was utilized to obtain the mean hippocampal distance from its surrounding arteries, roughly reflecting arterial densities, and examine its relationship with cognitive performance [Garcia-Garcia et al., 2023].

In the second study (chapter 3), hippocampal vascularization was thoroughly characterized including both structural and functional aspects in a cohort of young adults with the use of different MRI sequences at 7T. The study was conducted as part of the CRC1436. Considering the findings of study 1 and the previously elucidated importance of the brain's vasculature for brain health and cognitive functioning, relationships between hippocampal vascularization and brain structural measures were examined to determine if hippocampal vascularization could enable a build-up of neural resources in early life to convey brain reserve. Additionally, the potential cognitive benefits of better hippocampal vascularization in young adults were studied.

The third study (chapter 4) took a different perspective on successful cognitive aging with focus on at-risk stages of Alzheimer's disease by considering functional brain processes instead of morphological aspects [Vockert et al., 2024]. This study was based on a large multicenter cohort of the DZNE that underwent 3T fMRI and longitudinal cognitive assessments. The goal here was to investigate how cognitive reserve is implemented on the neural level utilizing a multivariate moderation approach to an fMRI paradigm of successful memory encoding.

In the last chapter, the results of the three studies are summarized in concert and their implications and limitations are discussed. The dissertation concludes with an outlook on future efforts in the research of hippocampal vascularization and cognitive reserve.

2 Hippocampal vascularization affects brain structure and cognitive performance in older adults

Substantial parts of this chapter have been published in
"**Vockert, N.**, Perosa, V., Ziegler, G., Schreiber, F., Priester, A., Spallazzi, M., ... & Maass, A. (2021). Hippocampal vascularization patterns exert local and distant effects on brain structure but not vascular pathology in old age. Brain Communications, 3(3), fcab127.".

Other brief parts of this chapter have been published in
"Garcia-Garcia, B., Mattern, H., **Vockert, N.**, Yakupov, R., Schreiber, F., Spallazzi, M., ... & Schreiber, S. (2023). Vessel distance mapping: A novel methodology for assessing vascular-induced cognitive resilience. NeuroImage, 274, 120094.".

2.1 Introduction

The MTL is a brain region especially vulnerable to both normal and pathological aging, matching the general observation of episodic memory decline over adult lifetime [Hedden and Gabrieli, 2004]. As mentioned in the general introduction, the vascular network of the hippocampus is very sparse [Cavaglia et al., 2001, Ji et al., 2021, Uchimura, 1928] and promotes hypoxia and ischemia in the hippocampus, especially in the form of vulnerability towards various pathological conditions [Nikonenko et al., 2009, Scharrer, 1940, Spielmeyer, 1925, Uchimura, 1928]. Although CSVD does not act specifically on the hippocampus, it has been associated with hippocampal microinfarcts [Hecht et al., 2018] as well as with hippocampal atrophy and neuronal loss [Kril et al., 2002]. CSVD is related to decline in memory function and various other cognitive domains [Gorelick et al., 2011, Wardlaw et al., 2013a]. An improved vascular supply of the hippocampus could be an important factor that promotes maintenance of cognitive abilities in the context of aging and/or vascular disease. Indeed, Perosa et al. [2020] discovered that a hippocampal vascularization pattern (HVP) with a combined hippocampal vascular supply of the PCA and AChA was linked to better cognition and overall hippocampal structural integrity (voxel-based analysis) in old adults with and without CSVD by utilizing a recently established high-resolution 7T ToF MRA sequence [Spallazzi et al., 2019].

Yet, the specific local and global associations between the HVP and structural brain integrity as well as vascular disease burden are still unknown. More specifically, it is unclear whether higher structural integrity related to a combined hippocampal vascular supply is only seen in hippocampus or extends to adjacent cortical regions such as the entorhinal cortex. This would have implications for aging and AD, where the entorhinal cortex shows earliest neurodegeneration [Du et al., 2004]. Moreover, it is still unresolved whether structural differences or differences in vascular disease burden underlie the benefits in cognition seen in face of a combined hippocampal vascular supply. Furthermore, it remains elusive whether the HVP confers resilience or resistance to vascular disease. However, understanding their potential interplay could help to shape preventive and therapeutic strategies for CSVD.

In addition to the binary HVP classification, a novel approach termed vessel distance mapping (VDM) [Mattern and Speck, 2020] has been recently developed that allows to characterize hippocampal vascularization with continuous metrics that capture further vascular aspects. Like previous approaches [Bernier et al., 2018, Haast et al., 2021, Huck et al., 2019], it sets the structural vasculature into relation to its surrounding anatomy by using distances. Vessel distances have been shown to be inversely related to vascular density [Ji et al., 2021]. Hence, the employed vessel distance metrics are hypothesized to represent different degrees of a gradual mixture between vessel densities and the vascular pattern (see section 2.2.3). The interpolation of the sparse vascular information present in an MRA image via VDM has two big advantages in terms of accuracy compared to traditional metric such as vessel density. First, vessel density estimates in a ROI are more susceptible to inaccuracies in the placement of the ROI compared to VDM. Second, the non-linear transformation to a standard space that would be required in voxel-based

studies is less accurate for a vessel segmentation with only discrete values than for a VDM with continuous values that can effectively interpolated.

Here, we aim to provide comprehensive insight into the relationship between the HVP and brain structure by investigating multiple unattended levels of detail, thereby advancing significantly on previous studies. First, we examine regional associations of the HVP with the volumes of distinct MTL subregions. Second, we assess the specificity of these associations at the hemisphere-level. Third, we examine global effects of the HVP on total grey matter volumes and whether these explain the better cognitive performance observed previously in augmented-supply individuals [Perosa et al., 2020]. Furthermore, we assess markers of vascular disease burden including hippocampal microinfarcts and whole brain white matter lesions as well as a semi-quantitative measure for overall CSVD severity in order to investigate the potential role of HVP in resistance and resilience to vascular disease. Last, we examine the association of the newly introduced vessel distance metrics with cognitive performance and determine whether they provide cognitive resilience to vascular disease.

2.2 Methods

2.2.1 Participants

This cross-sectional study was conducted using the same cohort as the study of Perosa et al. [2020]. The cohort comprised 47 older adults (70.96±8.22 years, 44% female), 20 of which showed neuroimaging markers of CSVD. The demographics of the participants can be found in Tab. 2.1. Exclusion criteria were depression as assessed by the Geriatric depression scale [Brink et al., 1982] and contraindications for scanning at 7T according to the recommendations of the German Ultrahigh Field Imaging (GUFI; `https://mr-gufi.de`) network. All participants provided written informed consent according to the declaration of Helsinki and were compensated for travel costs. The study was approved by the local Ethics Committee (93/17; 28/16).

Presence of CSVD was assessed on a 3T MRI by a specialized neurologist (S.S., 10 years experience) according to the standards for reporting vascular changes on neuroimaging (STRIVE) criteria [Wardlaw et al., 2013b]. CSVD neuroimaging markers comprised non-haemorrhagic (WMH, lacunes, enlarged PVS) and haemorrhagic markers (CMB, cSS). Out of the 20 CSVD patients one fulfilled the modified Boston criteria for a possible CAA and seven the criteria for probable CAA [Linn et al., 2010]. The other 12 participants did not fulfill these criteria.

For the majority of CAA patients, CSF biomarkers for Alzheimer's disease were available. The CSF amyloid β_{1-42} ($A\beta_{42}$) and amyloid β_{1-40} ($A\beta_{40}$) values of the six CAA cases which had CSF measures available were distributed reasonably along the values of a large CAA cohort, and can therefore be considered rather representative for (probable) CAA diagnosis (Fig. S1). Based on the ATN classification scheme [Jack et al., 2016], an Alzheimer's disease pathology profile could be established. Amyloid positivity ('A') was assessed with CSF $A\beta_{42}$ levels, tau positivity ('T') with CSF phosphorylated tau (p-tau) levels and neurodegeneration ('N') with CSF total tau (t-tau) levels. Using

locally established thresholds, only one CAA patient was classified as A^+. However, none of the patients scored T^+ or N^+. One other (non-CAA) patient was also classified $A^+T^-N^-$. Thus, two patients exhibited an Alzheimer's pathological change along the Alzheimer's continuum [Jack et al., 2018].

All participants underwent a series of neuropsychological tests comprising the Mini-Mental State Examination (MMSE) [Folstein et al., 1975], Montreal Cognitive Assessment (MoCA) [Nasreddine et al., 2005], Alzheimer's disease Assessment Scale - Cognitive Subscale (ADAS-cog) [Rosen et al., 1984], Clinical Dementia Rating (CDR) [Hughes et al., 1982] and the German version of the California Verbal Learning Test II (CVLT-II) [Delis et al., 2000].

According to the CDR and MMSE, the CSVD cohort included 10 cognitively normal subjects (CDR = 0, MMSE > 26). Nine cases fulfilled the criteria for mild cognitive impairment ($0 < \text{CDR} \leq 1$, $22 < \text{MMSE} \leq 26$), one participant fulfilled the criteria for mild dementia (CDR = 0.5, MMSE = 18). There was no participant with severe dementia (CDR > 1, MMSE ≤ 18). All control subjects were cognitively normal.

More information regarding the recruitment of the participants can be found in Perosa et al. [2020].

Table 2.1: **Demographics and vascular risk factors** of the cohort with 20 CSVD patients and 27 controls. Mean values ± std are indicated.

	CSVD patients	Controls
Age [years]	70.7±8.5	71.1±8.2
Sex [% female]	35.0	44.4
Education [years]	14.3±4.1	16.0±2.5
MMSE	25.6±2.6	28.6±1.3
Arterial hypertension [%]	90.0	51.9
Diabetes mellitus [%]	25.0	11.1
Hyperlipidemia [%]	60.0	44.4

2.2.2 MRI Acquisition

The scanning protocol was already published in Perosa et al. [2020], but is included in the following for reasons of completeness.

The 7T ultrahigh-field MRI scans were obtained from a Siemens MAGNETOM 7T scanner equipped with a Nova Medical 32-channel head-coil. The protocol included a ToF-angiography for visualization of the cerebral arteries and a T1-weighted sequence as structural reference. The T1-weighted sequence included a 3D magnetization-prepared rapid gradient echo (3D-MPRAGE; 1mm^3 isotropic resolution). The acquisition parameters were the following: repetition time (TR) 2250ms, echo time (TE) 2.8ms, inversion time 1050ms, flip angle (FA) 5°, receiver bandwidth (RBW) 130 Hz/pixel, echo spacing

8.3ms, 3D matrix dimensions 256x256x176. GRAPPA (generalized autocalibrating partial parallel acquisition) was enabled with an acceleration factor of 2 and 32 reference lines. The ToF sequence was acquired with an isotropic voxel size of 0.28x0.28x0.28mm^3 and the following parameters: TR 22ms, TE 4.59ms, FA 23°, RBW 130 Hz/pixel; GRAPPA factor 3, 32 reference lines. Acquisition time was minimized by restricting the ToF to a small part of the brain: the origin of the slab was set at the bottom of the hippocampus and extended 5cm in the dorsal direction, allowing depiction of the Circle of Willis and the hippocampal arteries. To stay within specific absorption rate limits, venous saturation was applied every seventh TR [Mattern et al., 2018]. More sequences were included in the 7T protocol, but did not play a role in this study. Scanning time summed up to 50 min. Thin pillows were placed at the sides of the participant's head to minimize head motion.

To diagnose or exclude CSVD, all participants underwent a 3T MRI scan prior to 7T (mean inter-scan interval 62±23 days). Measurements were performed in a Siemens Verio scanner with a Siemens 32-channel array coil. The protocol included a T2-weighted fluid-attenuated inversion recovery (FLAIR) sequence (1x1x1mm^3 isotropic resolution, TR 5000ms, TE 395ms, FA 120°, RBW 781 Hz/pixel; GRAPPA factor 2, 24 reference lines), to localize lacunes and evaluate WMH [Fazekas et al., 1987]. A T2-weighted sequence permitted the identification of PVS (voxel size 0.5x0.5x0.5mm^3 isotropic, TR 6500ms, TE 63ms, FA 120°, RBW 222 Hz/pixel; GRAPPA with factor 2, 24 reference lines) [Potter et al., 2015]. A susceptibility-weighted 3D gradient-echo pulse sequence (1x1x2mm^3 annisotropic resolution, TR 20ms, TE 28ms, FA 17°, RBW 100 Hz/pixel; GRAPPA with factor 2, 24 reference lines) was used to rate CMB and cSS. An MPRAGE sequence served as an anatomical reference (voxel size 1x1x1 mm^3 isotropic, TR 2500ms, TE 4.37ms, inversion time 1100ms, FA 7°, GRAPPA with factor 2, 24 reference lines). Additionally, a diffusion-weighted imaging sequence (voxel size 1.8x1.8x5.0mm^3, TR 8800ms, TE 72ms, FA 120°, GRAPPA with factor 2, 38 reference lines) allowed the exclusion of recent small subcortical infarcts in all participants at the time of the 3T MRI. Total 3T scanning time amounted to ca. 45 min.

2.2.3 Image Processing

An overview over the image processing and the extracted features can be found in Fig. 2.1.

Analysis of brain structure

For brain structural analyses, the SPM12 segmentation routine was employed to segment the 7T T1 images into gray matter (GM), WM and CSF. In order to account for the higher image inhomogeneities of 7T images, biasfwhm was set to 30 mm and samp (sampling distance) was set to 2. GM and WM volumes for every patient were calculated by summing up the voxel values of the corresponding individual tissue probability maps. Summing up all three corresponding tissue probability maps, TIV were obtained.

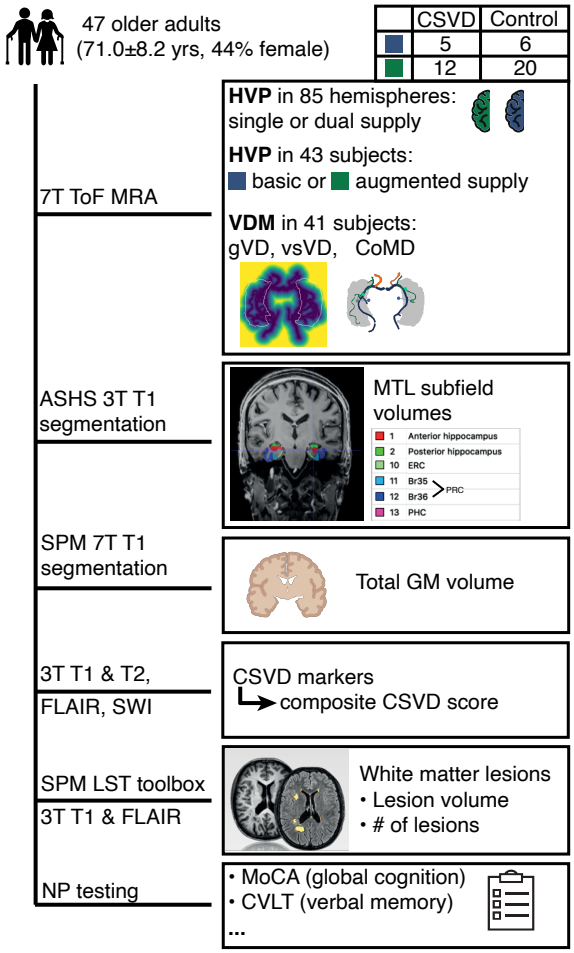

Figure 2.1: **Overview of the extracted features.** Please note that the 43 subjects or 85 hemispheres with classifiable hemispheres were used in subsequent analyses instead of the initial sample of 47 subjects. FLAIR = fluid-attenuated inversion recovery, LST = lesion segmentation toolbox, NP testing = neuropsychological testing, SWI = susceptibility-weighted imaging.

Moreover, volumes of MTL substructures were determined. An automatic segmentation was performed with the ASHS (Automatic Segmentation of Hippocampal Subfields; ashs-fastashs v2.0.0, `https://www.nitrc.org/frs/?group_id=370&release_id=3852`) algorithm. Due to the lack of a high-resolution hippocampal T2-weighted image, the ASHS 3T Pennsylvania Memory Center atlas [Xie et al., 2019], which only requires a T1-weighted image, was used. As the atlas was developed with 3T images, 3T (instead of the also available 7T) T1 images were utilized for MTL subfield segmentation. However, there was no disadvantage in terms of voxel size, as the 3T and 7T MPRAGE had the same resolution. Output of the segmentation were the anterior hippocampus (hippocampal head), posterior hippocampus (hippocampal body and tail), ERC, PRC divided into Brodmann areas 35 and 36 (BA35 and BA36) and PHC (see Fig. 2.2). The segmentations of the atlas were mostly based on the Harmonized Protocol [Boccardi

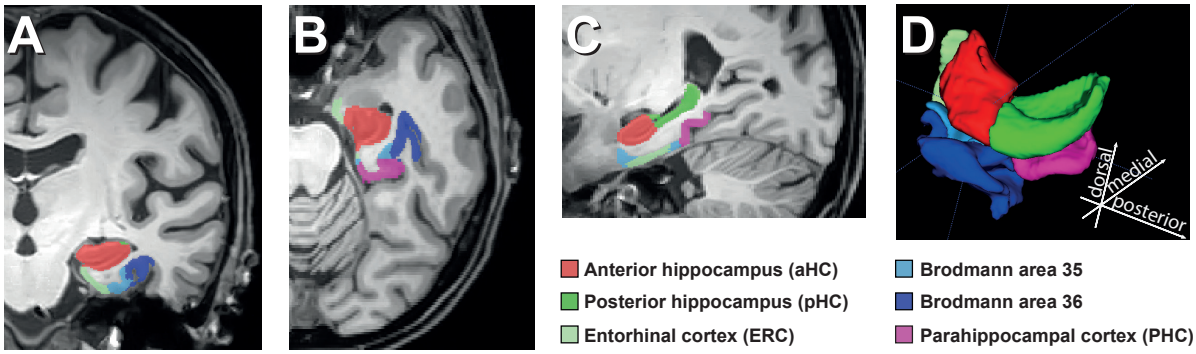

Figure 2.2: **Manually curated ASHS segmentation of one participant.** Only the left hemisphere is shown. (A) Coronal, (B) axial, (C) sagittal and (D) 3D view of the segmented MTL substructures. Image taken from Vockert et al. [2021] with permission.

et al., 2015] for manual hippocampal segmentation on T1-weighted MR scans [Xie et al., 2019]. Since according to the Harmonized Protocol the alveus and fimbria are included as part of the hippocampus [Frisoni et al., 2015], they were also included in the automatic segmentation.
The automatic segmentations were quality-controlled visually. Manual curation was done in absence of any subject information and focused on the correction of the three common errors mentioned in the supplementary of Xie et al. [2019], namely: 1. under-segmentation of the lateral hippocampus border, 2. segmentation of the choroid plexus as the hippocampus and 3. over-segmentation of the MTL cortices. The correction of the segmentation borders was aided by the original segmentation protocol of the ASHS-T2-pipeline [Xie et al., 2017, Yushkevich et al., 2015]. Notably, some information like the exact border between the ERC and dura is not available in the T1-weighted image alone [Xie et al., 2019]. Furthermore, adjustments of the hippocampal border were aided by the Harmonized Protocol [Boccardi et al., 2015], which the automatic segmentations were also based on. Subsequently, the volumes were extracted from the regions of interest (ROIs). The following ROIs were considered for further analyses: aHC, ERC, PRC as sum of BA35 and BA36, pHC and PHC. The segmentation of these substructures is shown exemplary for the left hemisphere of one participant in Fig. 2.2. Segmentations of the whole, anterior and posterior hippocampus have also been used as masks for calculation of vessel distance metrics.

Assessment of CSVD severity

The lesion growth algorithm (LGA) Schmidt [2017] as implemented in the LST toolbox version 3.0.0 (www.statistical-modelling.de/lst.html) for SPM was utilized for quantification of WM lesions from the 3T T2 FLAIR and the 3T T1 images with default parameters ($\kappa = 0.3$, threshold for binary lesion maps $= 0.5$). Total lesion volume as well as number of lesions were obtained and subsequently analyzed as quantitative proxies for CSVD severity throughout the whole brain.
Additionally, a semi-quantitative measure for overall CSVD severity was introduced

based on two previously established scores [Charidimou et al., 2016, Staals et al., 2015]. According to a review by Schreiber et al. [2019], DPA has been particularly related to deep lacunes, deep/mixed CMB and PVS in the basal ganglia. CAA in contrast has been associated with strictly lobar CMB, cSS, WMH and centrum semiovale PVS. As such, the score applied by Staals et al. [2015] is more specific to DPA. It assigns 1 point for one or more CMB in cerebellum, brain stem, basal ganglia, white matter, or cortico-subcortical junction, 1 point for presence of at least one lacune, and 1 point for grade 2-4 PVS in the basal ganglia. In contrast, Charidimou et al. [2016] developed a score more specific to CAA. It accounts for lobar CMB (1 point for 2-4 CMB, 2 points for 5 or more), cSS (1 point if focal, 2 if disseminated) and 1 point for grade 3 or 4 centrum semiovale PVS. Both scores attributed 1 point to WMH when confluent deep WMH (Fazekas score 2 or 3) and/or irregular periventricular WMH extending into the deep white matter (Fazekas score 3) were present. Combining the features from both scores, an overarching CSVD score for both subtypes was obtained, ranging from 0 to 9 points. Furthermore, the number of hippocampal microinfarcts served as a local proxy for CSVD severity.

Classification of the HVP

The classification of the HVP occurred according to a binary scheme. For the purpose of clarity, the following terminology for the HVP at different levels is illustrated in Fig. 2.3. Hemispheres with a hippocampal blood supply encompassing both the AChA and the PCA are termed *dual supply* hemispheres. In contrast, hemispheres without a contribution of the AChA to hippocampal vascularization are referred to as *single supply* hemispheres. On the level of an individual, *basic supply* indicates two single-supply hemispheres, as opposed to an *augmented supply* which implies the presence of at least one hemisphere with dual supply. Thus, an augmented supply could further be subdivided into a *once augmented* and a *twice augmented supply*.

In order to determine the HVP, the method described by Spallazzi et al. [2019] was adopted. For this purpose, the 7T T1-weighted images were bias corrected with SPM12 (Statistical Parametric Mapping; Wellcome Trust Centre for Neuroimaging, London, UK) in MATLAB_2018a after conversion from DICOM to NIfTI. The bias-corrected images were automatically segmented with the subcortical segmentation pipeline of FreeSurfer 6.0. Visual inspection ensured the validity of the hippocampal segmentations. Using Advanced Normalization Tools (ANTs, `http://stnava.github.io/ANTs/`), the hippocampal masks were co-registered (affine transformation) to the 7T ToF MRA images containing the angiographic information. An overlay of the ToF images with the hippocampal masks was visually inspected in MRIcron and MeVisLab to evaluate the contribution of the AChA to the hippocampal blood supply. If the uncal branch originating from the AchA was identified and seen penetrating the hippocampal region, the HVP of the hemisphere was classified as dual supply. However, in nine of the 94 inspected brain hemispheres, the presence of the uncal branch originating from the AchA, and thus its participation to the hippocampal vascular supply, was doubtful (e.g. because the small vessels of the choroideal plexus and its anastomoses could not be differentiated

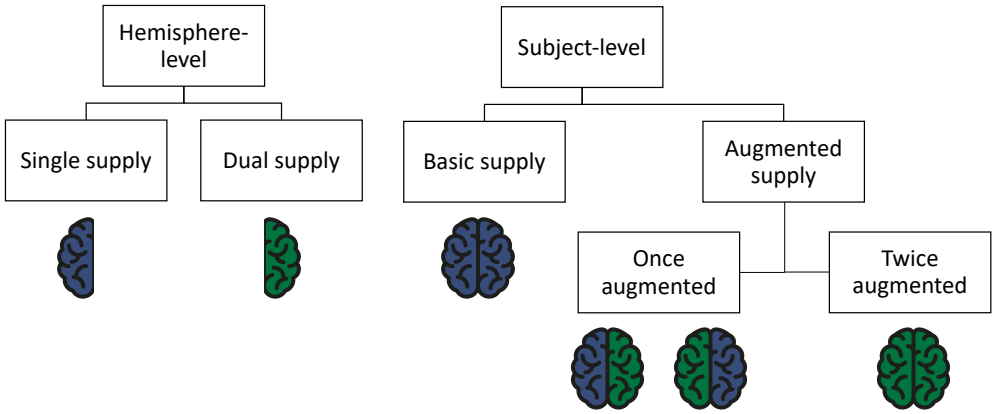

Figure 2.3: **HVP terminology.** Terminology differs on the level of a single hemisphere versus the level of an individual (whole brain). Green color denotes a hemisphere with contribution of both the PCA and AChA to hippocampal blood supply. Blue-colored hemispheres denote no involvement of the AChA in hippocampal blood supply.

from the AchA or due to movement artifacts). Hence, 85 of the 94 hemispheres could be characterized in terms of their dichotomized HVP. This included 41 fully classified subjects and three partially classified subjects. Two of those three patients had a dual-supply hemisphere and thus could be counted towards the augmented-supply group, whereas the third had a single-supply hemisphere, making it impossible to characterize its HVP on a subject-level without the knowledge about the HVP in the other brain hemisphere. The joint distribution of the HVP to the clinical groups is displayed in Fig. 2.1.

The classification was performed by a trained medical student (A.P., 2 years experience) and repeated several times in random order. 42 hemispheres of 21 subjects were additionally rated by a trained neurologist (V.P., 5 years experience) to ensure inter-rater reliability (intraclass correlation coefficient (ICC) = 0.83). The classification of the remaining hemispheres was verified by V.P. and consensus was reached when opinions diverged.

Vessel distance mapping

The Multi-Image Analysis GUI software Mango (`http://ric.uthscsa.edu/mango/`) was used to overlay the individuals' hippocampal masks onto the ToF-images, and the arteries were manually segmented. If depicted in the images, the following four arteries were delineated and labeled individually in each hemisphere: AChA, PCA, PComA (see

Figs. 1.1C and 1.3) and AChA-independent uncal branches. The PCA was segmented from its origin as the terminal branch of the basilar artery, and included the main trunk in its course from basilar towards occiput, as well as all its branches supplying the temporal lobe. Segmentation was performed along P1 (pre-communicating segment), P2 (post-communicating segment), and P3 (quadrigeminal segment) until P4 (cortical segment), at the division of the medial occipital artery into the occipito-temporal and calcarine branches.

Based on the manual artery segmentations, the VDM approach calculates the distance of each voxel to the closest vessel using a Euclidian distance transform. Hence, the binary, sparse vessel segmentation is effectively interpolated, providing a local estimate of the distance to the next surrounding vessel. In contrast, the similar measure of conventional vessel density is computed as the ratio of segmented vessel volume within a ROI to the ROI volume itself. Thus, the regional vascular information is compressed into a single number that only considers the relative vessel volume, not the vascular pattern. In VDM, patterns are approximated by vessel distances. Please note that while it would be more precise to use the term arterial distance in this study because only arteries were considered, the term vessel distance is used on the basis of the VDM approach, which is applicable to vessel data in general.

Three vessel distance metrics were assessed in this study. Global vessel distance (gVD) (see Fig. 3.3) represents the distance to the closest vessel, regardless of its identity (i.e. AChA/PCA). Therefore, gVD is mainly a proxy for vessel density but also considers vascular spatial patterns. Vessel-specific vessel distance (vsVD) computes VD separately for the AChA and PCA and combines them in a root-mean-square per voxel in order to penalize farther distances stronger than a simple average. vsVD provides more sensitivity with regards to vascular patterns as compared to gVD, as distance maps regarding AChA and PCA are computed individually. Thus, instead of a binary classification of the HVP, vsVD summarizes the closeness and density of both supplying vessels with respect to the hippocampus into a single, real-valued number. Voxelwise VD measures were averaged for the hippocampus.

As a third measure, center of mass distance (CoMD) (see Fig. 3.3) was calculated based on the centers of mass of the PCA, AChA and Hippocampus. Thus, the position of each structure is described by a single point in 3D space, defined by each structure's center of mass, which in this study is equivalent to the center of volume (homogeneous density). To obtain a single number, the distances between the centers of mass of the AChA and hippocampus ($d_{AChA-Hipp}$) as well as the centers of mass of the PCA and hippocampus ($d_{PCA-Hipp}$) were combined in a root-mean-square:

$$CoMD = \sqrt{\frac{d^2_{AChA-Hipp} + d^2_{PCA-Hipp}}{2}} \tag{2.1}$$

CoMD represents the computed distances between the hippocampus and the AChA's and PCA's respective main trunks. To reduce an excessive sensitivity towards small vessels, the PCA segmentation was pruned before computing the CoMD, to permit that the computed number represents the position of PCA's main trunk, since most of

the PCAs were much more highly branched compared to AChA. As a consequence of pruning, sensitivity to vascular density is attenuated, and CoMD estimates the proximity of AChA and PCA to the hippocampus.

It is important to note that there were some subjects, in which VD could be calculated, but a reliable classification of the HVP had not been possible due to aforementioned reasons. Nevertheless, the main trunk of the AChA as well as the PCA and its branching was visible, which allowed their segmentation and hence determination of VD. However, other participants were excluded because they had FTPs, PCA aplasia or their superior cerebellar artery was in the ROI, leaving a sample of 41 participants with VD metrics, 37 of which also had an HVP classification.

2.2.4 Statistical Analysis

All statistical analyses were performed in R version 3.6.1 if not stated otherwise. Most analyses were performed on the between-subject level rather than the level of single brain hemispheres. Therefore, subjects were split into two groups: Subjects in the basic-supply group had a single supply in both hemispheres, whereas the augmented-supply group contained individuals with a dual supply in at least one hemisphere (illustrated in Fig. 2.3). This split allowed to preserve more statistical power than a split into three groups, although a more detailed division would certainly be interesting to investigate.

In order to test whether an augmented supply is associated with local benefits in GM volume of the bilateral MTL structures compared to a basic supply, a MANCOVA was performed. To further test whether the HVP confers resilience against CSVD on a structural level (higher than expected volume at same level of pathology), we additionally assessed the relation of the presence of CSVD to those measures and included an interaction term between the factors CSVD and HVP. Separate MANCOVAs were performed for anterior and posterior MTL structures. Anterior MTL structures included anterior hippocampus, ERC and PRC (=BA35+BA36), whereas the posterior hippocampus and PHC were examined as posterior structures. Age, sex and TIV served as covariates. Diabetes, hypertension and hyperlipidemia showed no association with GM volumes and were thus not included as covariates. Univariate ANCOVAs with the same factors and covariates were performed as post-hoc tests.

Differences in GM and WM volumes were assessed with ANCOVAs, again using the same factors and covariates. Same is true for the (M)ANCOVAs on CSVD measures. Permutation tests for the ANCOVAs were applied where deemed appropriate due to potential outliers in the small subgroups. Permutation tests were performed with the *permuco* package (method "manly", 10000 repetitions) [Frossard and Renaud, 2021].

Linear mixed effects models (LMEs; implemented with the *lme4* package [Bates et al., 2015]) served as a tool to explore the directness of the hypothesized unilateral HVP effects on ipsilateral MTL structures. To account for the dependence of measurements for different hemispheres of the same individual, the LME modeled a different intercept for every subject. The covariates age and TIV were scaled (z normalized) to fall into similar ranges as the other variables. In the LME, both the HVP of the ipsilateral hemisphere and of the contralateral hemisphere were accounted for. Interaction terms

between CSVD and the HVP were also included for both the ipsilateral HVP and the contralateral HVP. For example, the LME (full model) for the ERC looked the following: ERC ∼ age + sex + TIV + CSVDgroup*HVP_ipsi + CSVDgroup*HVP_contra + (1 | id).
Inference on the LME results was made with the use of confidence intervals. The use of p values from t and F tests has been discouraged by Bates et al. [2015], as sampling distributions of non-null estimates are not t distributed for finite sample sizes, nor are the corresponding null distributions of differences in scaled deviances F distributed. However, although confidence intervals and hypothesis tests are two sides of the same coin and confidence intervals are sufficient to guide inference, one might argue that p values provide some complementary information [Bates, 2011, Du Prel et al., 2009]. Hence, p values calculated from likelihood ratio tests (LRTs) are additionally provided.

A mediation analysis was performed to test the hypothesis that total GM (TGM) volumes are responsible for the observed better global cognition in augmented-supply individuals, as assessed by the MoCA score. To compare memory and global cognition in this context, a composite memory score was constructed from different tasks of the CVLT. It was calculated as the sum of the z normalized scores for the sum of all five learning trials, the free short-delay task, the free long-delay task and a corrected hit rate (corrected for false alarm rate) from the recognition task.

The mediation analysis employed formal significance testing of the indirect path with a bootstrapping approach (50000 iterations) as suggested by Preacher and Hayes [2004, 2008]. The *mediation* package supplied the required utility [Tingley et al., 2014]. Prior to testing of the indirect path, associations between the independent variable (HVP) and the mediator variables (total GM volumes or ROI GM volumes) as well as the dependent variables (cognition or verbal memory) were tested for significance. As inclusion of TIV did not seem appropriate in every model, GM volumes were corrected for TIV after Raz et al. [2015] for every subject i:

$$Vol_{cor_i} = Vol_{raw_i} - b(TIV_i - TIV_{mean}) \tag{2.2}$$

where b is the slope of the ROI volume regressed on TIV. Consequently, TIV was ommitted as a covariate from the mediation models.

The hypothesized relationship between the VD metrics (bilaterally averaged) and cognitive performance (measured by MoCA and ADAS-cog scores) was assessed with linear regression models. Sex, binary CSVD status, age and years of education (the latter two centered) were included as covariates in the model. One extreme outlier in ADAS-cog scores, gVD and vsVD was removed, respectively.

2.3 Results

2.3.1 HVP is associated with bigger anterior but not posterior MTL GM volumes

The relation between the HVP and brain structure was examined on a regional level by comparing bilateral MTL subvolumes between HVP groups in two MANCOVAs. We

hypothesized the MTL to exhibit an association with the HVP rather in its anterior than posterior parts because of the specificity of the AChA's irrigation to the anterior part of the hippocampus. The first MANCOVA revealed significantly greater anterior MTL volumes (aHC, ERC, PRC) in augmented-supply individuals over individuals with a basic supply while accounting for age, sex and TIV ($F(3,34) = 3.613$, $p = 0.023$). Neither a main effect of CSVD ($F = 0.680$, $p = 0.564$) nor an interaction between CSVD and the HVP ($F = 0.689$, $p = 0.566$) was found for anterior MTL volumes.

Post-hoc univariate ANCOVAs for the different subregions of the anterior MTL identified the effect of the augmented supply to be especially driven by the ERC ($F(1,36)$

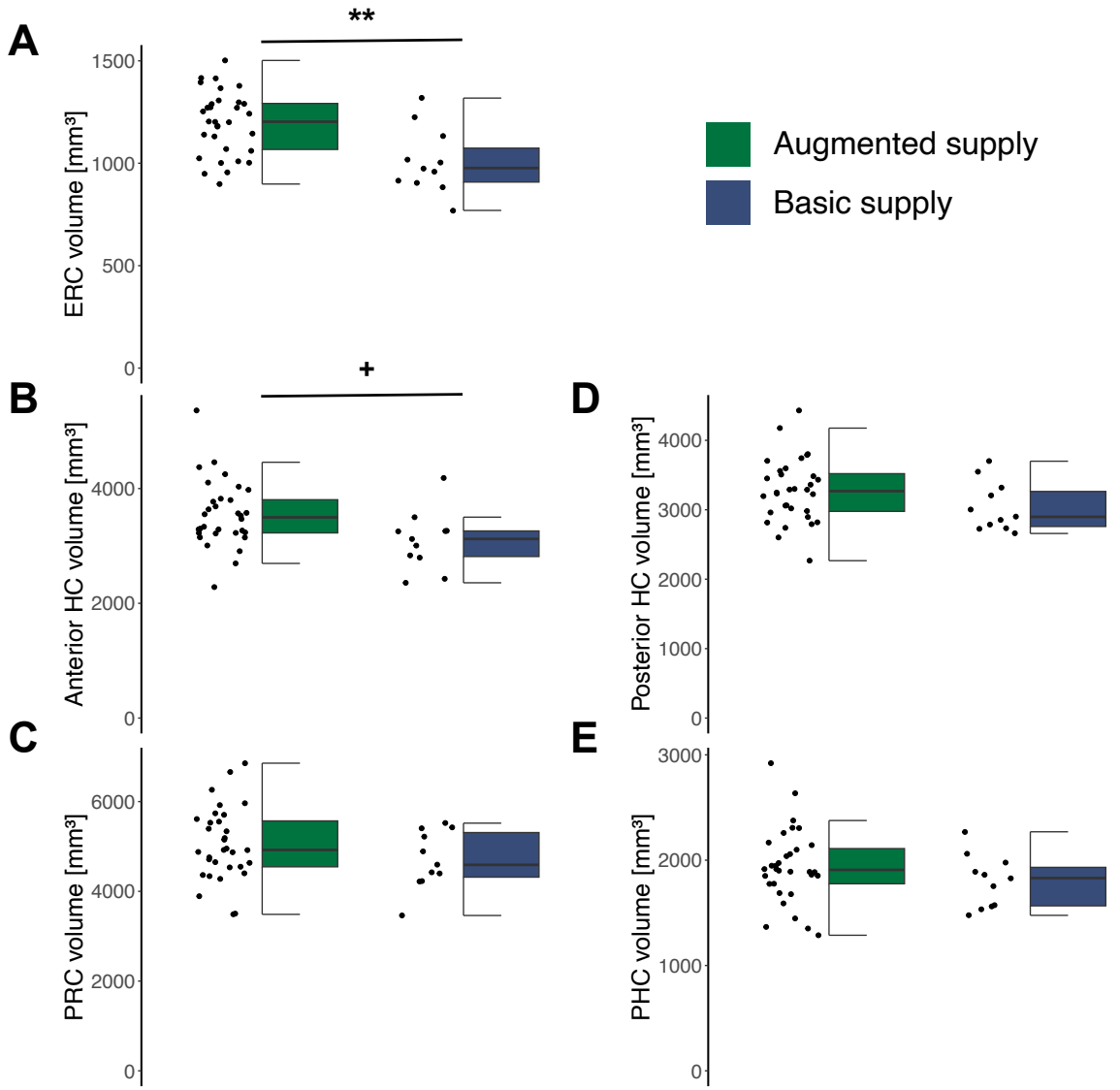

Figure 2.4: **Boxplot of bilateral MTL substructure volumes by subject-level HVP**. ROI volumes were obtained via segmentation of the desired substructures. '+' denotes $p < 0.1$,'**' indicates $p < 0.01$ from post-hoc ANCOVAs. All y axes start at 0 for better comparison.

= 11.259, p = 0.002, $\eta^2 = 0.167$, $\eta_p^2 = 0.238$). The aHC showed a strong trend (F = 4.030, p = 0.053, $\eta^2 = 0.071$, $\eta_p^2 = 0.101$), whereas there was no effect observed for the PRC (F = 0.777, p = 0.384, $\eta^2 = 0.014$, $\eta_p^2 = 0.021$). Permutation ANCOVAs obtained roughly the same results (see Tab. S1).

In contrast to the anterior MTL volumes, the posterior MTL volumes (pHC, PHC) were not associated with differences in the HVP as indicated by MANCOVA (F(2, 35) = 0.685, p = 0.511). Again, no main effect of CSVD (F = 0.531, p = 0.592) nor interaction (F = 0.915, p = 0.410) was present. Fig. 2.4 illustrates the differences in regional GM volume between basic- and augmented-supply individuals for the selected MTL ROIs. In summary, individuals with an augmented HVP generally exhibited higher volumes in the anterior hippocampus and ERC, whereas controls did not (compared to CSVD patients).

2.3.2 Associations between HVP and GM volumes are more pronounced ipsilaterally than contralaterally

To take a differentiated look at the directness of the observed associations between GM volumes and the HVP, the analysis was extended from a subject- to a hemisphere-level. In an LME that accounted for the dependence of both hemispheres of the same individual, the contributions of the ipsilateral versus contralateral HVP were sought to be disentangled. If vascularization affects structural integrity, one might speculate that nearby GM regions are affected stronger by a lack/surplus of supply when compared to more distant (contralateral) brain areas.

As Tab. 2.2 demonstrates, a dual supply in a given hemisphere was associated with greater aHC volumes in both the ipsilateral and contralateral hemisphere when compared to a single supply, on average amounting to 147.37 mm^3 and 84.54 mm^3, respectively. However, of all examined variables, only the ipsilateral HVP showed a significant effect,

Table 2.2: **Estimated effects of CSVD and the ipsi- and contralateral HVP on aHC and ERC volumes**. GM volumes of other substructures were not examined, since there was no relation between the HVP and those in the subject-level model. The estimates come from an LME (separate for aHC and ERC) and can be interpreted as the average effect of the factor (e.g. presence of CSVD or an ipsi-/contralateral dual supply) on the given MTL volume in mm^3. 95% confidence intervals are indicated in square brackets (p values can be found in Tab. S2). Significant results shown in bold. ':' symbolises an interaction between two factors.

	ΔaHC [mm^3]	ΔERC [mm^3]
CSVD	-88.79 [-331.21,153.62]	-1.18 [-70.93,68.57]
$Dual_{ipsi}$	**147.37 [8.91,285.83]**	**54.18 [11.42,96.95]**
$Dual_{contra}$	84.54 [-53.92,222.99]	**50.22 [7.46,92.99]**
CSVD:$Dual_{ipsi}$	-117.09 [-335.45,101.26]	-23.42 [-92.55,45,70]
CSVD:$Dual_{contra}$	75.19 [-143.17,293.54]	-20.47 [-89.59,48.66]

as indicated by the 95% confidence intervals, which do not contain 0. This means that the anterior part of the hippocampus is bigger in hemispheres with a dual supply compared to single-supply hemispheres.

In terms of ERC volumes, this significant association was not only observed for an ipsilateral but also a contralateral dual supply (Tab. 2.2), although the estimations differed slightly in their extent (54.18 mm^3 for the ipsilateral compared to 50.22 mm^3 for the contralateral hemisphere).

CSVD status and both interactions of CSVD with the HVPs were neither associated with regional differences in aHC nor ERC volumes. CSVD does not seem to be related to GM volume in MTL subregions specifically, confirming the findings of the previous (subject-level) analysis. Moreover, in alignment with the subject-level analysis, this hemisphere-level analysis indicated a stronger relation of the HVP to ERC volume than to the anterior hippocampus, as can be assessed by the (relatively) closer proximity of the confidence intervals to 0.

2.3.3 Greater TGM volumes in augmented supply and controls

Using ANCOVAs, we tested the hypotheses that total gray matter and total white matter volumes differ based on the HVP. In terms of TGM volumes, the analysis revealed a strong association between CSVD status and GM volume ($F(1,36) = 8.099$, $p = 0.007$, $\eta^2 = 0.086$, $\eta_p^2 = 0.184$), i.e. CSVD patients had significantly reduced GM volume relative to controls (see Fig. 2.5A). The relation between the HVP and TGM volume was also significant ($F = 6.992$, $p = 0.012$, $\eta^2 = 0.074$, $\eta_p^2 = 0.163$). In this case, augmented-supply individuals had significantly greater total GM volume when compared to basic-supply individuals. When accounting for the anterior MTL volumes by subtracting them from the TGM volumes, the results remained unchanged (CSVD: $p = 0.007$; HVP: $p = 0.013$).

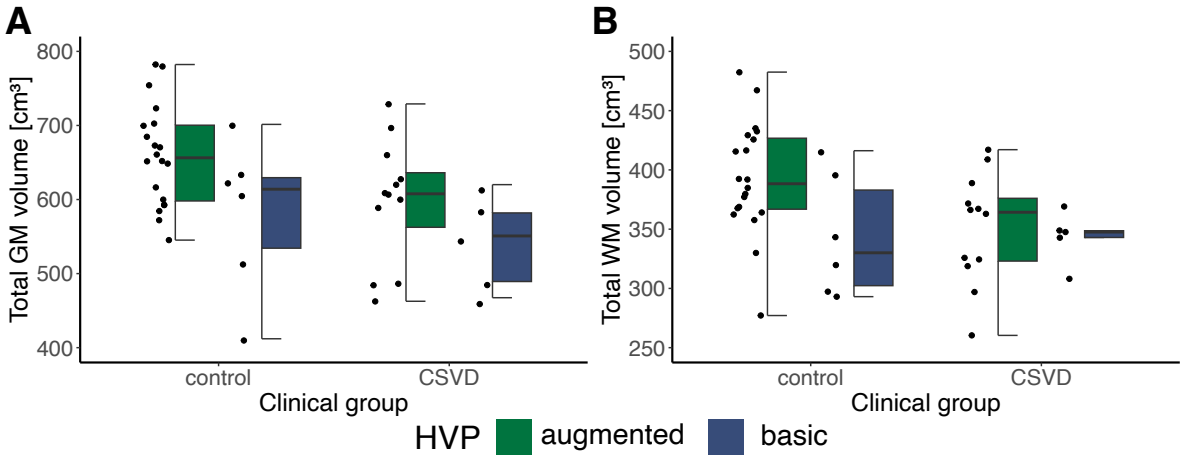

Figure 2.5: **Boxplot of total GM and WM volume by (subject-level) HVP group and CSVD status.** For gray matter, a main effect of both CSVD status and the HVP was found. For white matter, the main effect of the clinical group prevailed. No interaction effects were observed. Significance was tested in an ANCOVA.

To ensure robustness, a permutation test for ANCOVA was executed that presented a weaker association with CSVD (p = 0.024), but similar results for the HVP (see Tab. S1). A VBM-analysis indicated that regions with greater local GM volumes in the augmented-supply groups were located in the temporal lobe or in close proximity to it (see Fig. S2). The interaction between HVP and CSVD status was not statistically significant (F = 0.185, p = 0.670, $\eta^2 = 0.002$, $\eta_p^2 = 0.005$).

ANCOVA with permutation revealed no significant associations between total WM volume (boxplots for HVP-CSVD pairs shown in Fig. 2.5B) and the HVP (F = 2.366, p = 0.134, $\eta^2 = 0.037$, $\eta_p^2 = 0.062$) or CSVD (F = 2.442, p = 0.131, $\eta^2 = 0.038$, $\eta_p^2 = 0.064$). A statistically significant interaction was also not observed (F = 1.316, p = 0.254, $\eta^2 = 0.020$, $\eta_p^2 = 0.035$).

In summary, while greater TGM volumes were seen in the presence of an augmented vascular supply across all individuals, our models do not reveal evidence for resilience towards CSVD-related GM loss specifically (no interaction effect).

2.3.4 TGM volume is a mediator between the HVP and cognition

The relation between the (subject-level) HVP and global cognition as observed by Perosa et al. [2020] in combination with the relation between the HVP and total GM volume gave rise to the hypothesis that the cognitive performance differences might be grounded in the global structural differences). A mediation analysis was employed to support the hypothesis that the differences in global cognition between augmented- and basic-supply individuals are caused by the TGM differences. The mediation analysis confirmed a significant total effect (path c in Fig. 2.6) of the hippocampal vascularization pattern on global cognition represented by the MoCA score (p = 0.017). The average direct effect

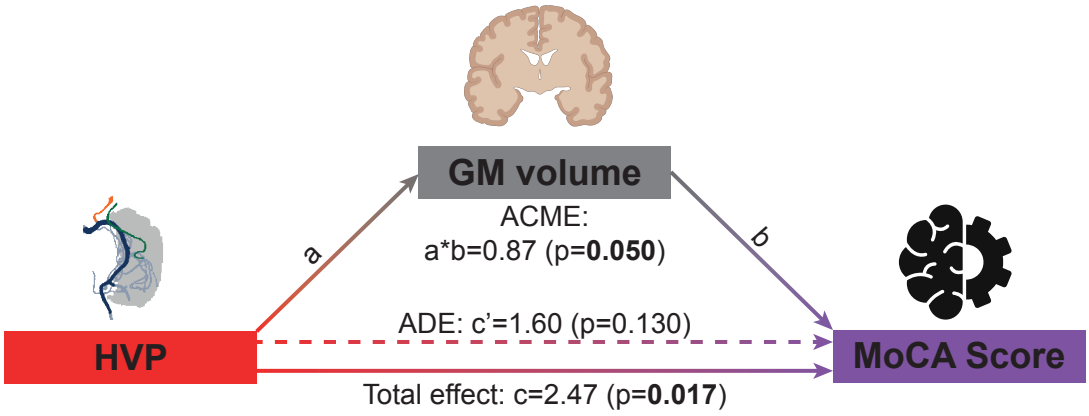

Figure 2.6: **TGM mediates the association between the HVP and MoCA score.** Mediation scheme after Preacher and Hayes [2008], shown for the relation between HVP, total GM volume and MoCA Score. Together, the average direct effect (ADE; here non-significant) and the average causal mediation effect (ACME; here significant) amount to the total effect (c = c' + ab).

Table 2.3: **P values from ANCOVAs between different variables and cognition/memory scores.** These relationships were tested as a prerequisite for the mediation analysis. Each combination of row and column represents a distinct model. Significant results are printed in bold.

	MoCA score	CVLT composite score
HVP	**0.017**	**0.039**
TGM vol	**0.011**	0.449
ERC vol	0.440	0.254
aHC vol	0.660	0.349

(ADE; path c' in Fig. 2.6) was not statistically significant (p = 0.130). In contrast, the average causal mediation effect (ACME; path a*b in Fig. 2.6), which is the difference between the total and average direct effect (a*b = c - c‘), was statistically significant (p = 0.050). These findings are compatible with the hypothesis that better global cognition in augmented-supply individuals is caused by HVP-related differences in total GM volume.

To rule out the possibility that these effects were only driven by higher GM volumes in the MTL, relationships between HVP, MoCA score and anterior MTL volumes were investigated additionally (see Tab. 2.3). As previously shown, an augmented supply was associated with bigger anterior hippocampal and entorhinal GM volumes. However, greater GM volumes in the anterior MTL were not related to better performance on the MoCA score. Thus, they cannot mediate the effect of the HVP on global cognition.

Moreover, Perosa et al. [2020] established a connection between the HVP and verbal memory scores. Since memory is a key function of the hippocampus and MTL, we hypothesized that aHC or ERC volumes mediate the relationship between the HVP and memory functions. A composite CVLT measure served as a combined memory score, which was positively correlated with the HVP (see Tab. 2.3). Yet, neither the examined MTL volumes nor total GM volume were significantly related to the composite CVLT score.

In summary, the mediation analysis indicated that greater TGM volumes are responsible for better cognition in the augmented-supply group, not greater anterior MTL volumes. In contrast, better (verbal) memory in individuals with an augmented supply could be explained neither by global differences in GM nor anterior MTL volumes alone.

2.3.5 No evidence for resistance nor resilience against CSVD

We hypothesized that the HVP confers resilience against CSVD on a structural level, i.e. that individuals with an augmented supply show higher than expected TGM volume given their pathology. This would be represented by an interaction of the presence of CSVD with the HVP. However, no such interaction was observed in any of the models, as stated in the previous results sections.

Assuming that pathological markers of CSVD are similarly distributed among the

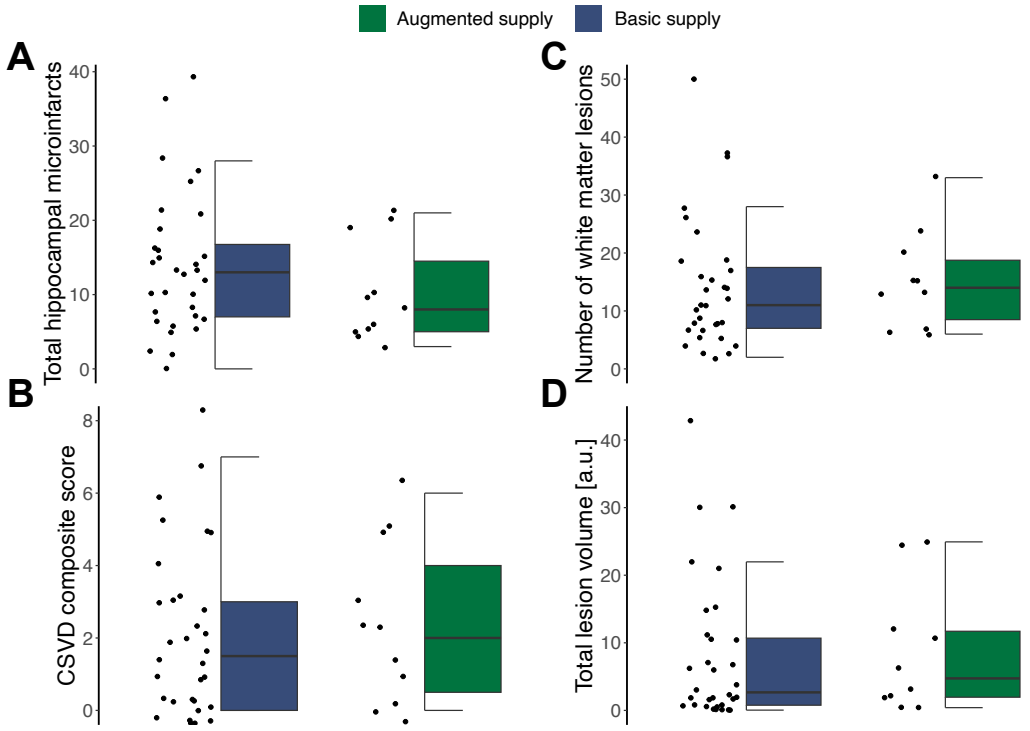

Figure 2.7: **Boxplots of local (A) and global measures (B-D) of CSVD by subject-level HVP.** ANCOVAs revealed no differences between the augmented- and basic-supply group. The number of white matter lesions and the lesion volume were obtained by the LPA algorithm of the LST toolbox.

population (accounting for age, sex and TIV), we further hypothesized that resistance against CSVD would imply lower levels of pathological markers in individuals with an augmented supply. Resistance was examined at multiple levels, namely in the local context of the hippocampus and the global context of the whole brain. The number of hippocampal microinfarcts as a local pathology measure did not reveal any differences between the two HVP groups ($F(1,38) = 0.9141$, $p = 0.345$).

To allow a better evaluation of resistance with regard to the whole brain, CSVD was not considered solely as present or absent, but examined in a more quantitative way by converting it to a novel semi-quantitative score in the previously described manner. However, an augmented supply was not related to a lower whole-brain CSVD score either ($F(1,38) = 0.3263$, $p = 0.571$). A MANCOVA on total lesion volume and the number of lesions as identified by WMH showed the same result ($F(2,35) = 0.2123$, $p = 0.810$). Boxplots of the measures for the different groups are shown in Fig. 2.7. The lack of differences in pathological measures of CSVD between the HVP groups represents a lack of evidence for resistance against CSVD in both a local and a global brain context.

Using Fisher's exact test, we further found no statistical difference in clinical group contingency ($p = 0.25$).

2.3.6 Vessel distances are differently associated with cognitive performance in CSVD patients versus controls

Using linear regression, the relationship between vessel distance metrics and cognitive performance represented by ADAS-cog and MoCA scores was examined. All three vessel metrics showed a statistically significant interaction effect with CSVD status on MoCA scores (gVD: t(33) = -2.678, p = 0.011, standardized regression coefficient β = -0.665; vsVD: t(33) = -3.129, p = 0.004, β = -0.468; CoMD: t(34) = -2.665, p = 0.012, β = -0.495). Hence, participants with CSVD exhibited a different relationship between vessel distances and cognitive performance as compared to control participants. As seen in Fig. 2.8, CSVD patients whose hippocampus is farther away from the surrounding

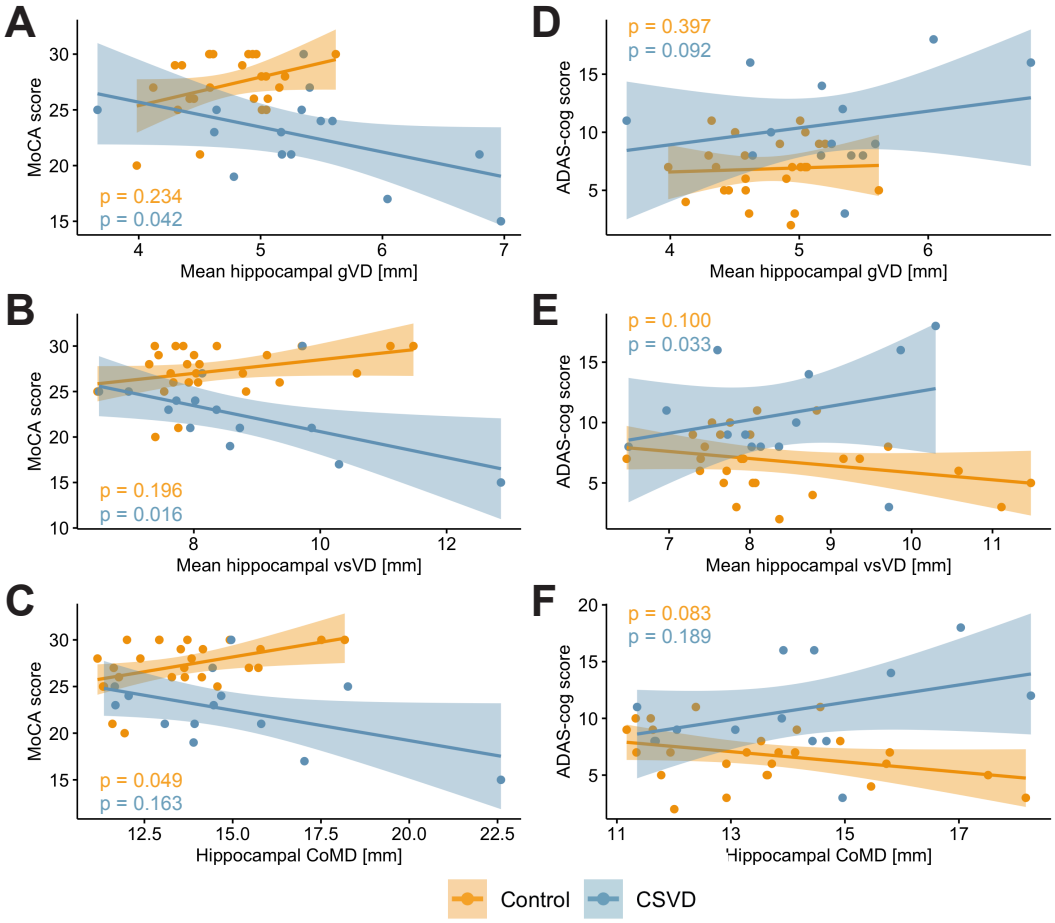

Figure 2.8: **Relationship between VD measures and cognitive performance**. Cognitive performance is represented by the MoCA score in panels A-C and the ADAS-cog score (higher scores = more errors) in panels D-F. Please note that one individual with an extreme outlier in their ADAS-cog score has been excluded in panels D-F. Shaded areas denote 95% confidence intervals. Additional p values from models with only CSVD patients or control participants, respectively, are provided (color-coded correspondingly). They refer to the association between the VD metric (x axis) and cognitive metric (y axis).

arteries have worse cognitive performance. In contrast, controls almost seem to have better cognitive performance when the hippocampus is farther away from its surrounding vessels, as indicated by the positive main effects. These even showed a trend towards statistical significance in gVD (t = 1.807, p = 0.080, $\beta = 0.469$) and CoMD (t = 2.030, p = 0.050, $\beta = 0.362$), but not vsVD (t = 1.596, p = 0.120, $\beta = 0.238$). When only considering the controls, the relationship between CoMD (but not gVD or vsVD) and MoCA is indeed positive (see p values in Figs. 2.8A-C).

When using ADAS-cog as measure of cognitive performance, the interaction was also statistically significant for vsVD (t(32) = 3.536, p = 0.001, $\beta = 0.357$) and CoMD (t(33) = 2.100, p = 0.043, $\beta = 0.236$), where higher distances between the hippocampus and the surrounding vessels were related to higher scores (i.e. more errors). This was not the case for gVD (t(32) = 1.316, p = 0.197, $\beta = 0.183$). None of the vessel distance metrics had a significant main effect on ADAS-cog scores (t = 0.598, p = 0.554, gVD: $\beta = 0.088$; vsVD: t = 0.672, p = 0.506, $\beta = 0.068$; CoMD: t = -0.359, p = 0.722, $\beta =$ -0.039).

2.4 Discussion

Recent advances in ultra-high resolution ToF MRA enabled us to classify the hippocampal vascularization pattern of 85 brain hemispheres in vivo. We examined cross-sectional associations of the HVP with brain structure on a scope far beyond that of previous studies, considering the laterality and vicinity (regional versus global) of those associations. We further investigated the structural underpinnings that might underlie the positive association between an augmented hippocampal vascular supply and cognition. We also examined whether an augmented vascularization was related to reduced vascular pathology burden (resistance against pathology) or preserved gray matter integrity in the face of vascular burden (resilience to pathology), thus making the connection of established and novel structural markers to these two core concepts in aging and disease. Last, we established additional continuous measures of hippocampal vascularization which capture aspects of vessel density and the hippocampal vascularization pattern, and assessed their relationship with cognitive performance.

A comparison between individuals with a basic supply and individuals with an augmented supply, i.e. at least one hemisphere in which anterior circulation directly contributes to hippocampal blood supply via the AChA, revealed bigger anterior but not posterior MTL volumes. This matches the specificity of AChA perfusion to the hippocampal head and the anterior part of the parahippocampal gyrus [Erdem et al., 1993, Fernández-Miranda et al., 2010, Kiernan, 2012]. Such a specific benefit in anterior integrity could have implications for memory function, as a functional gradient along the longitudinal axis of the hippocampus has been proposed [Strange et al., 2014]. Notably, the aHC shows an age-related decrease in functional connectivity that may contribute significantly to memory decline in older adults [Stark et al., 2020]. The hypothesis that brain structures benefit more from a direct effect of vascularization than indirect is supported by our observation that the volume gains for aHC and ERC were stronger for

ipsilateral than contralateral dual supply.

There are likely several mechanisms through which an augmented supply and GM volumes are related to each other. First, dual vascularization could be associated with better blood supply with nutrients and oxygen as well as better clearance of harmful substances and metabolic endproducts. This may promote demand-driven plasticity, including synaptogenesis and neurogenesis, which is known to be coupled with angiogenesis (for a review see Düzel et al. [2016]). Hippocampal neuronal plasticity, in turn, is known to be associated with plasticity of intra- and extra-hippocampal connectivity. In consequence, a local increase of hippocampal plasticity-potential by improved vascularization may have spill-over effects to hippocampal networks, which could also extend to contralateral homotopic regions, as previously shown [Mechelli et al., 2005] and observed for the ERC in this study. While the ERC has been shown to be irrigated by arteries originating from the AChA [Huther et al., 1998], it remains unclear why the hypothesized effect of AChA supply is stronger for the ERC than the hippocampus.

Strikingly, an augmented supply of the hippocampal region was also associated with greater GM volume beyond the MTL. Our data does not provide any mechanistic explanation for these remote, global associations. One interpretation is that cerebral vascularization in other areas covaries with hippocampal vascularization, e.g. in the anterior circulation. As such, the HVP might represent a proxy for blood supply in multiple brain regions. Another interpretation is that an increased potential for hippocampal plasticity has a long-term, maybe even developmental, impact on cortical and sub-cortical networks. Such widespread structural covariance has been reported in chronic conditions affecting the hippocampus such as epilepsy due to medial temporal sclerosis [Cormack et al., 2005, Düzel et al., 2006]. Of note, greater anterior MTL volumes were not able to numerically account for the observed positive association between an augmented supply and greater whole-brain volume. A VBM analysis revealed volumetric gains for augmented over basic supply in extra-hippocampal regions (Fig. S2), especially those in relative proximity to the MTL.

Our hypothesis that whole-brain differences in GM are responsible for the HVP-related better global cognition was supported by the significant mediation effect of TGM. Yet, there might be more direct mediators, e.g. blood perfusion or differences in whole-brain vascularization (covarying with the HVP) that were not measured here. Surprisingly, the composite CVLT score which was used as a proxy for memory was not significantly correlated with anterior MTL volumes. This indicates that the positive association of the HVP with (verbal) memory is grounded in more widespread structural covariance in the memory network, perfusion or patterns of neural activity. Of note, no non-verbal memory modalities were acquired in the current study to assess memory in a broader way.

In patients with CSVD, total GM volumes were significantly smaller compared to controls. This is in correspondence with other studies that reported neurodegeneration in sporadic CSVD [Peres et al., 2016, Samuraki et al., 2015]. There were no volumetric differences between CSVD patients and controls in MTL substructures. This is in line with the lack of specificity of CSVD to certain brain regions [Li et al., 2018].

Our data did not reveal any cross-sectional evidence to support the hypothesis that

the HVP conveys resilience against vascular pathology specifically, since there was no interaction effect between CSVD and the HVP on GM volumes, meaning that the HVP was not associated with greater than expected brain structures in the presence of vascular pathology above and beyond its effect in controls. Certainly, resilience ultimately needs to be assessed in a longitudinal design that allows for HVP-dependent trajectories. Furthermore, our analyses did not indicate that an augmented supply protects individuals from vascular pathology. Yet, CSVD is a whole-brain disease with a very complex etiology (e.g. age, vascular risk, genetics, lifestyle), which makes it unlikely to observe HVP-conveyed resistance against CSVD on the whole-brain level. However, there was also no evidence for hippocampus-specific resistance against vascular pathology when examining the sole measure of hippocampal microinfarcts.

Notably, the current investigations were restricted to downstream MRI measures of CSVD and do not provide insight about other diseases like Alzheimer's disease, in which resistance and resilience conferred by the HVP are imaginable and could be assessed in relation to p-tau or Aβ load. Here, our finding of a potential structural protection of the ERC by an augmented vascular supply is of particular importance, since the ERC is highly vulnerable to tau pathology [Braak and Braak, 1995, Maass et al., 2018] and early atrophy in aging and Alzheimer's disease [Killiany et al., 2002].

While the HVP might also play a distinct role for hippocampal subfield integrity, we believe that subfields could not be faithfully segmented because the stratum radiatum lacunosum moleculare as a necessary landmark is not clearly identifiable in our images due to the lack of a high-resolution T2 hippocampal scan (see Wisse et al. [2021] regarding limitations for segmentation of hippocampal subfields). As the utilized classification is agnostic to the location of small hippocampal arteries, which are beyond the resolution limit of the ToF, it is hard to make predictions about the potential impact of the HVP on hippocampal subfield integrity. However, the subiculum or CA1 might be more likely to benefit from contribution by the AChA, as they extend more anterior compared to other subfields [de Flores et al., 2020]. Moreover, previous studies reported a selective vulnerability of the CA1 region to conditions like hypoxia, ischemia and vascular pathology [Li et al., 2016, Schmidt-Kastner and Freund, 1991, Sugawara et al., 2002] providing further indications for an important role of the HVP for CA1, which should be addressed in future studies.

The newly established vessel distance metrics reflect additional aspects of the brain's vasculature relevant to the hippocampus. Interestingly, smaller mean hippocampal vessel distances and center of mass distances were not related to better cognitive performance across the whole sample. Instead, the association between vessel distances and cognitive performance differed between CSVD patients and controls, as indicated by the interaction effect. This indicates smaller vessel distance metrics as a factor of resilience , i.e. a smaller distance of the hippocampus to its surrounding vessels only seems to become beneficial in the context of disease. For the MoCA score, there was even a statistical trend towards an association of higher vessel distances (gVD and CoMD) with better cognitive performance across the whole sample (no association for ADAS-cog scores), which was driven by the surplus of controls as compared to the CSVD patients (26 versus 15). In controls only, greater CoMD values were even statistically significantly related

to better MoCA scores. Even in controls the apparent association between better cognitive performance and greater mean distances of the hippocampus from its surrounding vessels is unexpected. While the reason for this is unclear, it suggests that gVD and CoMD might be dependent on other factors than just vessel densities and the vascular pattern (speculations follow in chapters 3.4 and 5.4).

Our study also has several limitations. Since the data is purely cross-sectional, it does not allow any inference about time courses or causality. Although our hypotheses and models imply a clear directionality (HVP affects structure, which affects cognition), we cannot exclude reverse causality, meaning that a larger brain structure simply requires a greater blood supply. Given the limited statistical power and unbalanced design (32 augmented-supply versus 11 basic-supply subjects), one should be careful with over-interpretations.

Moreover, it is conceivable that there was a small degree of under-classification of dual-supply hemispheres due to unidentified uncal branches beyond the detection threshold, as suggested by Wiesmann and de Leeuw [2020]. We note, however, that the proportion of dual-supply hemispheres in our study does not differ significantly from the proportion observed by Erdem et al. [1993] (Fisher's exact test, $p = 0.53$).

One also has to note the primarily qualitative character of this study. The HVP is not a quantitative measure of hippocampal blood supply and it has yet to be examined how the HVP relates to hippocampal perfusion. From a qualitative point of view, we need to gain a better understanding of the contribution of the anterior and posterior circulation to hippocampal vascularization and its role for downstream effects by considering variations in the Circle of Willis. Relevant variants in that context could be a fetal or hypoplastic PCA as well as hypoplasticity or absence of the posterior communicating artery, as also suggested by Gutierrez [2020]. Nonetheless, the strength of the presented classification is its simplicity in the light of its apparent relevance, granting it a translational character.

VDM addresses some of the aforementioned weaknesses of the HVP by providing non-binary measures that are less influenced by potential subjectivity. VD metrics appear suitable as complementary measures reflecting additional vascular aspects like vessel densities, but also vessel patterns to a certain extent (mainly in CoMD). However, VDM has some shortcomings on its own. As of now, it is more labor intensive due to the requirement of manual arterial segmentations. Simultaneously, the manual segmentations represent a potential source of bias due to subjectivity in the segmentation, especially of smaller hippocampal arteries. Prospectively, automatized segmentation, e.g. through deep learning approaches, could solve both issues by providing an automatic and standardized segmentation, making VDM metrics more robust and easily accessible. Other potential sources of bias include the resolution and the variable inflow enhancement. Although the resolution of the ToF sequence at a field strength of 7T was already quite high with 0.28mm, the smallest hippocampal arteries beyond this resolution could not be visualized. Yet, as hippocampal arteries measure from 0.2 to 0.9mm in diameter [Erdem et al., 1993, Marinković et al., 1992], most arteries (but not arterioles or capillaries) should be visualized. Due to the inflow enhancement the ToF sequence is susceptible to blood flow velocity, such that faster blood flow, e.g. as a consequence of caffeine consumption, results in greater signal intensity and thus influences the visibility of the

vessels. Of note, all VD metrics are dependent on the region of interest they are put in context with, here the hippocampus. Consequently, the metrics are conflated with the structure of the hippocampus, such that structural changes of the hippocampus like atrophy would influence the observed VD values. Despite these limitations, the apparent contribution of VD metrics to cognitive resilience to vascular disease suggests them as useful complementary measures of brain vascularization.

The finding that augmented-supply individuals have more preserved regional and total GM volumes than age-matched basic-supply individuals is a first indicator that the HVP might contribute to brain reserve or brain maintenance (as defined by Stern et al. [2020]) in the context of aging. Notably, this evidence requires confirmation from longitudinal studies. If a basic hippocampal supply represents a predictor for cognitive decline later in life, this could have implications for risk modification and preventive therapies, as these individuals might be more vulnerable to develop dementia. Finally, the pattern of hippocampal vascularization might be an important modifier of hippocampal plasticity. We have shown that exercise-related vascular plasticity is highly variable among older adults [Maass et al., 2015], suggesting that other factors, such as the vascularization patterns in the MTL might modify exercise-related benefits.

To summarize, future studies should examine the relationship between the HVP and quantitative perfusion measures in the hippocampus and MTL. Moreover, investigating the relation between the HVP and brain structure in young adults would help to understand its role in brain development and provide further insight into whether vascularization relates to brain reserve or maintenance (see next chapter). Longitudinal data will be required to distinguish higher baseline-levels prior to onset of atrophy from slower rates of structural (and cognitive) decline. Furthermore, investigation of the implications in resistance and resilience against Alzheimer's disease appear very worthwhile given the overlap of the area where tau first accumulates (see Braak and Braak [1995]) with the area that seems to benefit the most from the HVP.

2.5 Contributions

With respect to the first part of the project (hippocampal vascularization patterns [Vockert et al., 2021]) Valentina Perosa and Anastasia Priester contributed to the study by classifying the hippocampal vascularization pattern and originally conceptualizing the pattern classification together with Marco Spallazzi, Stefanie Schreiber and Emrah Düzel. I performed all other data processing steps for the current study and all statistical analyses. I wrote the manuscript, which was edited by Valentina Perosa, Gabriel Ziegler, Frank Schreiber, Marco Spallazzi, Berta Garcia-Garcia, Hendrik Mattern, Emrah Düzel, Stefanie Schreiber and Anne Maass. For the additional analyses involving vessel distance mapping [Garcia-Garcia et al., 2023], Berta Garcia-Garcia performed the arterial segmentations and Hendrik Mattern conceptualized and provided the VDM framework and processing of VD maps. I performed the statistical analyses. Berta Garcia-Garcia and Hendrik Mattern wrote the initial draft of the methodology that the respective methods section is based on. Anne Maass and Stefanie Schreiber supervised the work.

3 Hippocampal structure and cognition in young adults are invariant to natural variations in the hippocampal vascularization

3.1 Introduction

The hippocampal vascularization pattern as distinguished between solely PCA-dependent or AChA-assisted has been associated with better memory and cognitive performance in older adults as shown in the previous chapter of this thesis [Perosa et al., 2020, Vockert et al., 2021]. This relationship was mediated by greater anterior MTL volumes [Vockert et al., 2021], illustrating a potential involvement of the HVP in brain reserve or brain maintenance. Likewise, a previous study has shown that lower CVR in the temporal lobe is associated with higher reaction times in a memory task [Catchlove et al., 2018a]. Moreover, lower hippocampal CVR was specifically associated with worse memory performance in older adults [Catchlove et al., 2018a]. This suggests that vascular responsiveness is linked to cognitive performance also in cognitively normal people. Additionally, microvascular rarefaction in the whole brain and in the hippocampus specifically seem to have detrimental effects on cognition, as illustrated by the lower cognitive performance in older adults with sparser microvascular networks [Brown et al., 2007, Troen et al., 2008]. As the previous chapter illustrated, hippocampal vessel distances, which are related to vessel densities, were associated with cognitive performance in patients with CSVD, suggesting a resilience mechanism against cerebrovascular disease [Garcia-Garcia et al., 2023]. Furthermore, a study by Yin et al. [2024] indicated a potential link between vessel tortuosity and cognitive performance. Specifically, they found that more abnormal tortuosity metrics of the extracranial ICA and vertebral artery were related to worse cognitive performance. An association between tortuosity of the PCA and AChA (vessels potentially involved in the hippocampal blood supply) and PComA (an essential part of the Circle of Willis) with cognitive performance has not been examined yet.

However, variation in all hippocampal vascular parameters described above might only be relevant for cognition in the presence of other age-related changes or even disease and has not been well examined in young adults. One exception is the study with null findings regarding the relationship between hippocampal CVR and memory performance in young adults [Catchlove et al., 2018a]. Yet, in this study CVR was assessed with an ASL sequence at 3T, which has lower SNR in comparison to BOLD fMRI [Liu et al., 2017]. Hence, an assessment of hippocampal CVR via 7T BOLD fMRI with more accurate hippocampal masks owing to a dedicated hippocampus sequence paired with a specific hippocampal segmentation algorithm might allow for a more fine-grained depiction of potential CVR-cognition relationships in young adults.

Hence, the aim of this study was to extensively characterize a cohort of young adults with regard to their hippocampal vascularization encompassing the hippocampal vascularization pattern, hippocampal vessel distances, hippocampal CVR and tortuosity of PCA, AChA and PComA using ultra-high field MRI at 7T. We examined the relationship of this broad set of hippocampal vascular parameters with memory and cognitive performance in order to gain a better understanding of the nature of previously observed effects in older adults (study 1). In this respect, we also studied how these vascular parameters are linked to brain structural measures. If hippocampal vascularization patterns were linked to increased brain volumes in young adults, this would imply an involvement of hippocampal vascularization in brain reserve.

3.2 Methods

3.2.1 Sample

47 young adult participants between 19 and 34 years of age were included in the study between October 2020 and December 2022. Exclusion criteria were indications of any cardiovascular, neurological or psychiatric disease as well as contraindications against 7T MRI. The participants were also required to have a minimum German language proficiency of level C1. Data collection repeatedly had to be stopped due to Covid-19 restrictions. The collected data comprised (f)MRI data and cognitive data from both paper-and-pencil tests and a computerized visuospatial memory task for object location (object location task (OLT)). The OLT consisted of one memory encoding and two memory recall (retrieval) sessions. The encoding session was performed on a computer, approximately one hour before the first recall session, which was carried out inside the MRI scanner. Exactly one week later, the participants had another appointment including the second memory recall session (done on a computer) and additional cognitive testing. 33 participants received a supplementary MRI scan between March and November 2023 (see Fig. 3.1 for an overview over the study timeline). All participants provided written informed consent according to the declaration of Helsinki. The study was approved by the local Ethics Committee (193/19).

Five subjects were excluded from all analyses because large amounts of their MRI and cognitive data were missing or invalid (e.g. because the scan had to be terminated, the

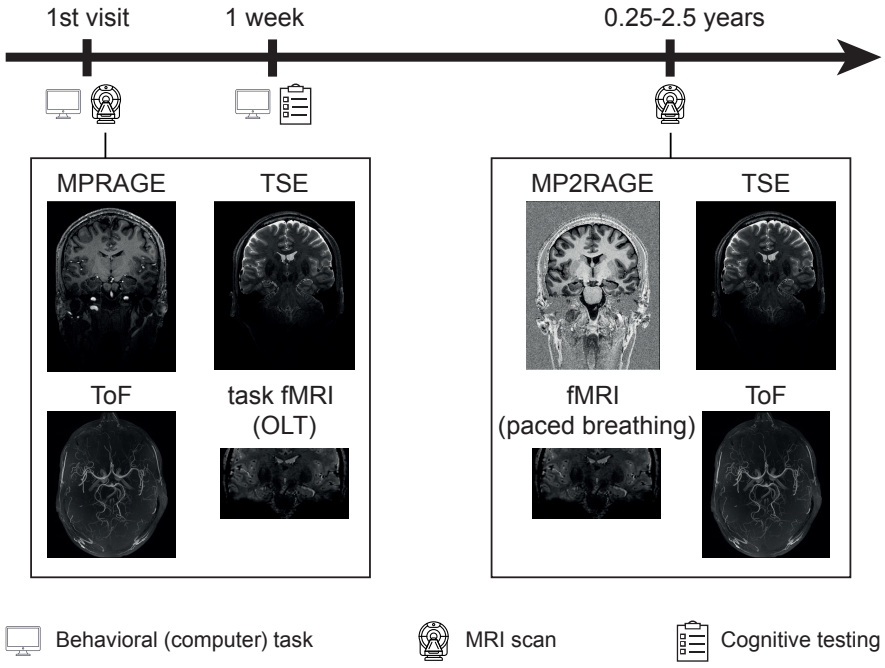

Figure 3.1: **Schematic overview of the timeline of the study.**

slab had the wrong orientation or due to motion artifacts), leaving 42 participants for the analyses. However, it is important to note that sample sizes varied between analyses, as different parts of data were missing for different participants. The maximum sample size in a given analysis was 36.

3.2.2 Cognitive Testing

The first part of cognitive testing was a visuospatial memory task querying the location of objects in a room (OLT) comprising an encoding phase with immediate recall (behavioral), a delayed recall after ca. one hour (fMRI) and another delayed recall after one week (behavioral). During the encoding phase of the task, the participants encountered two types of trials. In the first and more prevalent trial type the participants were presented with a room containing two objects (see Fig. 3.2). They were asked to remember the location of the two objects and imagine themselves in the image, interacting with the objects . On the subsequent screen the same room was shown. It now included a red circle in one of the objects' locations that prompted an immediate recall of the object memory. From a selection of three objects, the participants had to choose the correct one with a button press. The three objects included the correct one, a lure object (the second object that had been in the room) and a third, unrelated (novel) object. Sub-

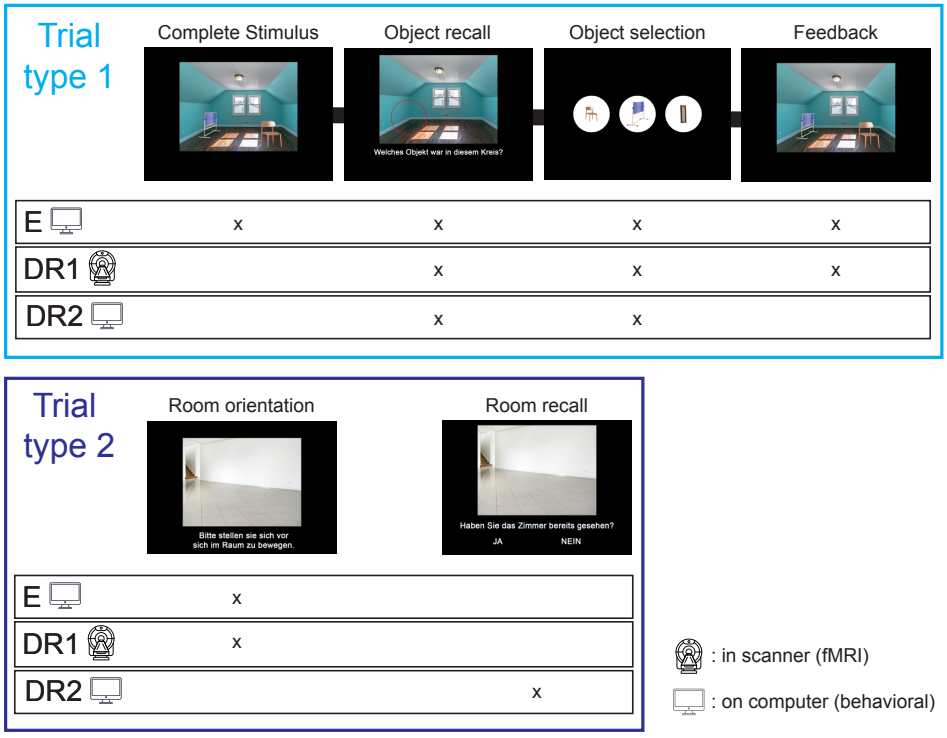

Figure 3.2: **Schematic outline of the object location task.** The 'x' indicates what both types of trials (type 1: objects in room, type 2: room only) looked like in encoding (E), the first delayed recall after about 1 hour (DR1) and the second delayed recall one week later (DR2). The fixation cross that was shown prior to all trials was omitted in the illustration.

sequently, the room including both objects was shown again to provide feedback to the participant. Every object's location was queried once, i.e. every room was shown four times in total (twice as initial presentation, twice for feedback). The locations of both objects in the same room were not queried immediately one after another, but interspersed with other rooms. The second trial type consisted of images with empty rooms, which the participants were asked to move in (see Fig. 3.2). The primary purpose of the second trial type was to serve as a control condition for the fMRI task.

After approximately one hour, the participants performed the delayed memory recall phase in the MRI scanner. The delayed recall for trial type 1 was the same as the immediate recall, where participants had to choose the correct object out of three objects (see Fig. 3.2). Again, feedback was provided in the form of the room containing both objects. For trial type 2, the participants were again presented with empty rooms that they were asked to imagine themselves in. Task activity was analyzed in cooperation with the group of Dorothea Hämmerer. Notably, the task-specific fMRI activity was not further analyzed here and not related to our vascular metrics as there was no significant task-related activity in the hippocampus. Hence, only the behavioral data of the fMRI task was considered in this thesis.

The second delayed memory recall session followed one week later. Again, the participants were asked to select the correct object matching the position in the rooms marked by the red circle. In this recall, participants were additionally presented with empty rooms, for which they had to indicate if they had seen them before (yes/no). The participants' memory performance was evaluated as the accuracy of correctly recalled object locations in the delayed recall sessions 1 and 2, respectively.

As the second part of cognitive testing, a paper-and-pencil cognitive test battery was administered a few minutes after the second recall session of the visuospatial memory task (one week after MRI). It comprised seven paper-based tests: The Rey-Osterrieth Complex Figure Test (ROCFT) [Osterrieth, 1944, Rey and Osterrieth, 1941], Trail Making Test (TMT) [Tombaugh, 2004], Logical Memory from the Wechsler Memory Scale [Wechsler, 1945] (fourth edition), Digit Span (DS) from the Wechsler Adult Intelligence Scale [Wechsler, 1940] (fourth edition), the Color and Word Interference Test after Stroop (SCWT) [Bäumler, 1985], and the Symbol Digits Modalities Test (SDMT) [Smith, 1973]. Scoring of the ROCFT was done after Lezak [2004]. For the recognition part of the ROCFT, a corrected hit rate was calculated as the difference between hits and false positives, divided by the number of true positives.

The cognitive tests were used to obtain a global cognitive factor score as well as a composite memory score. The global cognitive factor was acquired from a principal component (PC) analysis on the following 19 scores: (1) total scores of the immediate recall of the LM, (2) total scores of the delayed recall of the LM, (3) the total recognition score for the LM, (4) immediate recall score for the ROCFT, (5) delayed recall score for the ROCFT, (6) corrected hit rate of the ROCFT recognition trial, (7) DS forward, (8) DS backward and (9) DS sequential, (10) the number of correctly assigned symbols during the 90s of the SDMT, (11) the number of symbols remembered after the SDMT, (12) the number of symbols correctly assigned to its corresponding number after the SDMT (incidental encoding), times for (13) TMT A and (14) TMT B, (15-17) median

times for the three trials of SCWT (read colored words, name colored bars, interference task), and accuracies from (18) retrieval 1 and (19) retrieval 2 of the visuospatial memory task. Times were entered with a negative sign, such that for all 19 variables higher numbers would correspond to better scores in order to simplify interpretability of the factor loadings. The ROCFT copy score was not included in the PC analysis, as there was little variance in the score in this cohort of younger adults and small deviations from the maximum score mostly represented small inaccuracies in drawing.

Five participants had missing values for either the first (N = 2) or second (N = 3) retrieval session of the visuospatial memory task. These values were imputed via a memory-specific PC analysis with the *missMDA* package in R version 4.2.2. The PC analysis included the following five variables: (1) immediate and (2) delayed recall in ROCFT, (3) delayed recall in LM and accuracies from OLT (4) retrieval 1 and (5) retrieval 2. The composite memory score was calculated as the sum of z scores of the same five memory tests: f_mem_z = z(OLT_DR1) + z(OLT_DR2) + z(ROCFT_IR) + z(ROCFT_DR) + 2*z(LM_DR_tot). The delayed recall score from logical memory (verbal memory) was included twice to achieve a more balanced contribution of verbal and non-verbal memory domains.

Composite cognitive scores were available for 41 participants.

3.2.3 MRI acquisition

MRI data was collected from 7T ultra-high field (f)MRI scans using a Siemens MAGNETOM 7T scanner equipped with a Nova Medical 32-channel head-coil. Initially, the participants were scanned once, but a second MRI scan with additional sequences was added later on in order to assess additional parameters (see Fig. 3.1).

The protocol of the first MRI session included a T1-weighted magnetization-prepared gradient echo (MPRAGE; 3D GRAPPA PAT 2, 0.7x0.7x0.7mm^3 isotropic resolution, 256 sagittal slices, TR 2500ms, TE 2.55ms, inversion time 1050ms, FA 5°, echo spacing 6.1ms, RBW 320 Hz/Px, ca. 7 min), a T2-weighted scan (optimized for MTL volumetry, 0.4375x0.4375x1.1mm^3 anisotropic resolution, 50 coronal slices orthogonal to the hippocampal long axis, TR 8000ms, TE 90ms, FA 60°, echo spacing 15ms, RBW 158 Hz/Px, ca. 8 min), a ToF angiography (2D GRAPPA PAT 3, 0.28x0.28x0.28mm^3 isotropic resolution, 192 axial slices parallel to the hippocampal long axis, TR 22ms, TE 4.59ms, FA 19°, RBW 142 Hz/Px, ca. 19 min) and task fMRI scan (2D EPI, GRAPPA PAT 4, multi-band acceleration factor: 2, 1mm^3 isotropic resolution, 80 axial slices aligned perpendicularly to the back of the brainstem, TR 2660ms, TE 24ms, FA 75°, 210 volumes, 4 blocks of ca. 10 mins each).

The protocol of the second MRI session included a Magnetization Prepared 2 Rapid Acquisition Gradient Echo (MP2RAGE; GRAPPA PAT 2, 0.5x0.5x0.5mm^3 isotropic resolution, 352 sagittal slices, TR 4800ms, TE 2.18ms, TI1 900ms, TI2 2750ms, FA1 5°, FA2 3°, echo spacing 6.6ms, RBW 250 Hz/Px, ca. 17 min), a T2-weighted scan that was very similar to the previous one (optimized for MTL volumetry, 0.4375x0.4375x1.1mm^3 anisotropic resolution, 50 coronal slices orthogonal to the hippocampal long axis, TR 8000ms, TE 92ms, FA 60°, echo spacing 13.1ms, RBW 158 Hz/Px, ca. 8 min) and an

fMRI sequence (2D EPI, GRAPPA PAT 4, 0.9x0.9x0.9mm^3 isotropic resolution, 58 axial slices parallel to the hippocampal long axis with interleaved acquisition, TR 2000ms, TE 20ms, FA 80°, 206 volumes, ca. 9 min). During fMRI, the participants performed a paced breathing task as suggested by Liu et al. [2020] in order to assess CVR. It comprised 10 rounds of 12s paced breathing alternated with 30-60s free breathing. The breathing frequency during paced breathing was set to 6s/breath, i.e. 3s breathe in and 3s breathe out, with the goal to introduce variations in the breathing patterns and manipulate arterial CO_2 concentrations. Instructions about breathing were displayed in German ("Einatmen", "Ausatmen","Freies Atmen" ="Breathe in","Breathe out","Breathe freely") in gray font on a black background in order to minimize visual stimulation. Other sequences included in the protocols of the two MRI sessions were not analyzed in this study.

3.2.4 Image processing

The T1-weighted images were segmented into six tissue classes in SPM12 in MATLAB_R2018a. Total gray and white matter volumes were obtained as cumulative sums of the corresponding tissue probabilities. The T2-weighted images were processed with ASHS (ashs-fastashs v2.0.0, `https://www.nitrc.org/frs/?group_id=370&release_id=3852`) with the IKND Magdeburg Young Adult 7T Atlas in order to segment the MTL. The hippocampal borders were manually corrected according to the manual segmentation protocol by Berron et al. [2017]. The hippocampus segmentation was split into an anterior (hippocampal head) and posterior part (hippocampal body and tail) at the end of the uncus, which served as the last slice of the anterior hippocampus. Subsequently, hippocampal volumes were obtained from the segmentations. Of note, the T2-weighted images from the first MRI session of four participants were of insufficient quality due to movement. For these participants, the T2-weighted images from the second MRI session were segmented with ASHS and manually corrected. For all participants, the corrected hippocampus segmentations were extracted as a single label and used as a binary mask for all ROI analyses which included the hippocampus. From the two inversion images of the MP2RAGE a UNI-T1 image was derived by the scanner, which was used for co-registration of the functional images. In order to estimate different vascular parameters, three arteries were manually segmented on the ToF images of 36 participants, namely the PCA, AChA and PComA (see Figs. 1.1C and 1.3). The PCA was segmented from its origin as the terminal branch of the basilar artery until the end of its P3 segment including all branches supplying the temporal lobe. The AChA was segmented from its origin in the ICA along its entire visible trajectory including all branches. The PComA was also segmented along its entire length from its origin in the ICA until its termination in the P2 segment of the PCA. In the case of an FTP, the PCA was segmented as PComA from its P2 segment onwards, as its blood flow is dominated by the ICA (anterior circulation) in this case.

Classification of the HVP

For classification of the HVP, hippocampal masks were extracted from the ASHS segmentation and coregistered with the ToF images. Hemispheres were classified as dual supply when an uncal branch was identified which (i) arose from the AChA, (ii) was in close proximity to the hippocampal mask and (iii) whose trajectory was pointed towards the hippocampal head. Otherwise the hemisphere was classified as a single supply. Classification was performed independently by two raters (BGG and NV) and consensus was reached in cases of disagreement. As in study 1, individuals with two single-supply hemispheres were classified as basic supply individuals. In contrast, individuals with at least one dual-supply hemisphere were classified as having an augmented supply. The HVP was classified successfully in 76 out of 84 hemispheres, allowing a classification of the HVP in 37 out of 42 individuals. In the remaining cases classification was ambiguous, e.g. due to extremely faint uncal branches or unclear origin of a visible branch.

Classification of fetal-type PCAs

Fetal-type PCAs (FTPs) were rated on the ToF images. They were defined as the PComA having a greater diameter than the P1 segment of the ipsilateral PCA or with an absent P1 segment [Altinbas et al., 2014, Waaijer et al., 2007]. Transitional configurations with roughly equal diameters of the PCA and PComA were not considered FTPs. Eight of the 42 participants had FTPs, four in the left hemisphere and four in the right hemisphere.

Tortuosity

The start and end coordinates of the PCA, AChA and PComA were determined on the segmented ToF images as the origins of the arteries and the end of the segmented arteries' main trunks, respectively. The *Dijkstra* algorithm (MATLAB implementation by Aryo [2024]) was used to calculate the length of the vessels based on the coordinates and the segmentations. The TI was calculated as the quotient of the vessel length and the Euclidian distance between vessel start and end. TI of the AChA was calculated for all 36 participants with artery segmentations. However TI of the AChA in one hemisphere was excluded due to its very high value (outlier). TI of the PCA was not determined for FTPs, leaving 29 participants with bilateral TI of the PCA and 7 with unilateral values. TI for the PComA could not be calculated for absent PComAs and was not calculated for PComAs ipsilateral to an FTP. 24 participants had bilateral values for TI of the PComA, 11 unilateral values (totalling 59 unilateral values) and one participant had no TI values for the PComA.

Vessel distance mapping

According to the methodology of the first study, gVD (as a general measure of arterial distance/density) and CoMD (as a measure more closely related to the vessel pattern) of the hippocampus were calculated (see Fig. 3.3). vsVD as a very similar measure was not

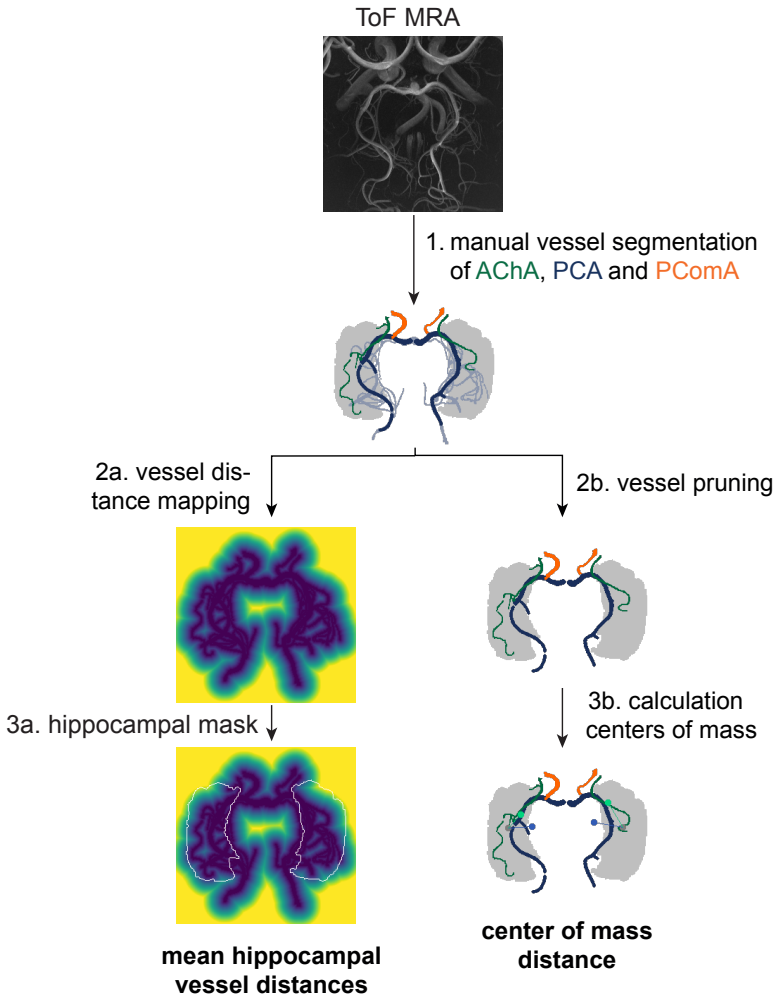

Figure 3.3: **Calculation of vessel distance metrics.** Illustration how the raw vessel distance metrics were obtained. For the calculation of the corresponding metrics in MNI space the vessel distance map/pruned vessel segmentation was transformed into MNI space prior to step 3. Please note that the original images are three-dimensional and the displayed images are maximum intensity projections in 2D for illustration purposes. The grey outline in the image after step 3a denotes the outlines of the hippocampus.

considered additionally in order to reduce the number of analyses (that would require a greater potential correction for multiple comparisons). For calculation of gVD, the distance of every voxel in the ToF image to its closest segmented artery was calculated in a first step. After co-registration of the T2-weighted image with the ToF via the MPRAGE, the hippocampal mask was transformed into the space of the ToF image in order to extract the mean gVD values within the hippocampus. Additionally, a normalized version of gVD was created in order to account for differences in hippocampal size (see results). For this purpose, the gVD maps were transformed to MNI space. A generic hippocampus mask that had been obtained by Freesurfer segmentation of the MNI template was used as ROI in this case. Hence, gVD in MNI space could be seen

as a representation of gVD under the assumption that every participant had the same brain and hippocampus structure and size, but the vascular structure differed.

For CoMD, the centers of mass of the PCA, AChA and hippocampus were determined and combined in a root mean square. Like gVD, CoMD was additionally calculated in MNI space after transformation of the ToF image and the arterial segmentation to MNI space in order to account for differences in hippocampus size. ComD was not calculated for participants with an FTP because in these participants the PCA's role was taken by the PComA, whose center of mass would not have been directly comparable to the PCA's. Since it was also unclear if vessel distances in participants with an FTP are comparable to those of participants with an adult PCA, additional sensitivity analyses were performed in a subsample containing solely participants with adult PCAs.

One participant was excluded from all analyses involving gVD and CoMD (raw values, but not MNI), as the mean bilateral hippocampal vessel distance in native space was an extreme outlier ($>$ 3*IQR above the 3rd quartile), leaving 35 and 28 participants for the analysis on the whole sample and the subsample (excluding FTPs), respectively.

CVR calculation

fMRI data processing and analysis were performed using SPM12 and Matlab_R2018a. The image preprocessing pipeline comprised the following standard steps: (1) slice time correction, (2) calculation of a voxel-displacement map with the *fieldmap* toolbox in SPM12, (3) motion and distortion correction via SPM's realign & unwarp and (4) coregistration to the (structural) MP2RAGE-derived UNI-T1 image.

Multiple CVR metrics were calculated based on the preprocessed functional data (see Fig. 3.4 for an overview of the calculation workflow). In the case of rs-CVR, after additional processing steps explained below the voxelwise BOLD signal was regressed on the respiratory trace [Zvolanek et al., 2023]. This respiratory regressor originated from the breathing belt data collected during the fMRI measurement at a rate of 200Hz. Recording was started during the preceding MRI sequence, at least 50s before the fMRI measurement with the paced breathing paradigm. In order to convert the raw respiratory signal into the respiratory regressor, a series of steps was required. First, the recording was truncated to the time of the fMRI scan, including 50s prior to the fMRI scan, and z normalized. Next, the z-normalized respiratory trace was smoothed with a moving average with span 10. Subsequently, a peak detection algorithm was run to identify local maxima and minima (peaks and troughs) of the trace. The peaks, troughs and breathing period were then interpolated to the 256 time points corresponding to the fMRI volumes. The respiration volume per time (RVT) was calculated as the breathing volume (difference between peak and trough) divided by the breathing period. Last, the RVT trace was convolved with the respiratory response function (RRF) after Birn et al. [2008], which required data from at least 50s before the fMRI scan. After convolution the preceding 50 seconds were discarded. The z-normalized version of the truncated trace served as the final respiratory regressor.

Before voxel-wise regression of the BOLD time course on the respiratory regressor, the fMRI data was further processed using the *seeVR* toolbox in MATLAB [Bhogal,

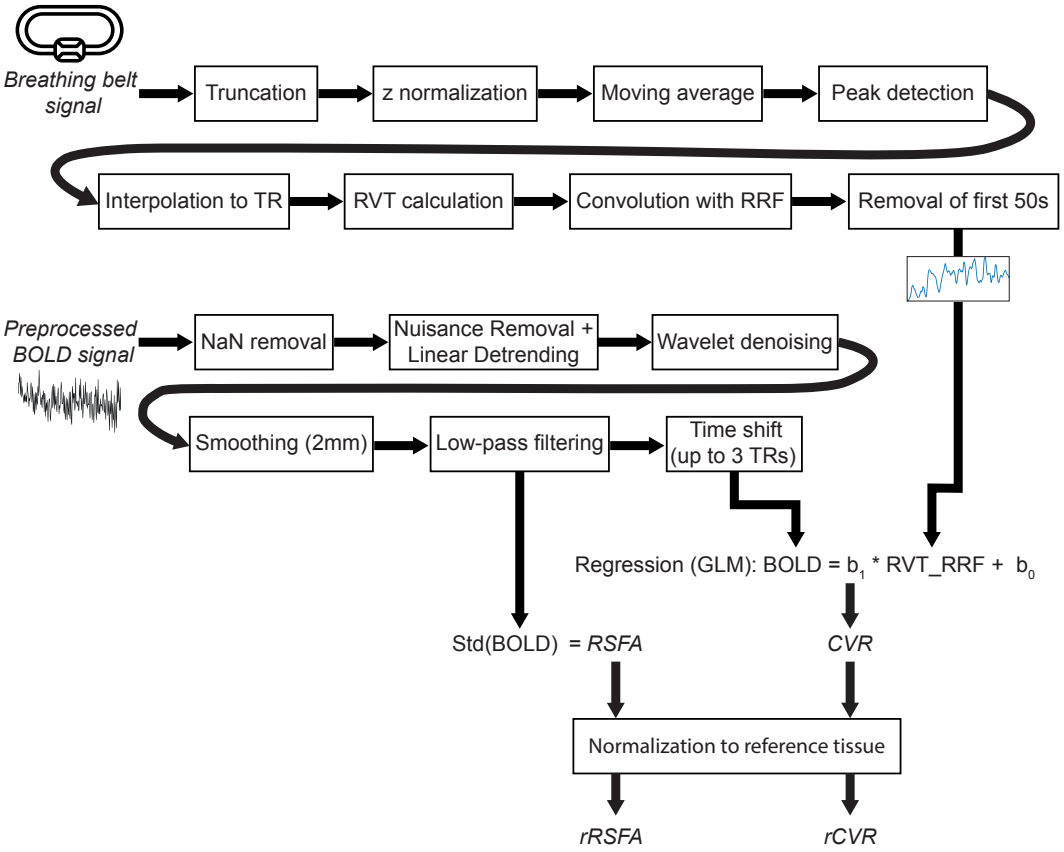

Figure 3.4: **Workflow for calculation of the voxelwise CVR metrics.** Std refers to the temporal standard deviation for each voxel, respectively. The reference tissue was the combined gray and white matter. RVT_RRF = final respiratory regressor.

2021]. Time points with NaN values in the respiratory regressor (due to missing maxima/minima at the border of the breathing signal time series) were removed from the time series. A nuisance regressor was assembled from the six motion parameters (from SPM realignment), their temporal derivatives, squares and the Legendre polynomial of degree 1 (for linear detrending). In order to avoid discarding meaningful variations in the BOLD signal correlated with minimal movement, nuisance regressors with a maximum value below 0.001 were discarded, leaving a maximum of 19 regressors. These nuisance regressors were regressed out of the BOLD signal within the mask. Subsequently, the cleaned BOLD data underwent wavelet denoising, smoothing with a 2mm FWHM Gaussian kernel and low-pass filtering of the data to frequencies between 0.01 and 0.08 Hz. Last, the respiratory regressor was time-shifted by 0 to 3 TRs in order to account for potential time lags between the vascular signal in different regions. The optimal time shift was determined based on the maximal correlation of processed mean BOLD signal in the GM (without contributions of large vessels) with a time-shifted version of the respiratory regressor. Theoretically, the time shift could be performed voxelwise for maximum accuracy. However, this estimation was not equally stable across all voxels, making a

time shift by the optimal lag time of the average BOLD time course preferrable. Subsequently, a voxelwise regression of the BOLD signal on the respiratory regressor was performed, yielding one value per voxel in the mask. In simple words, this value represents how strong the BOLD response is in reference to the expected BOLD response due to the recorded breathing fluctuations. As the breathing is supposed to reflect the arterial CO_2 concentration, it is similar to the classic CVR definition of $\frac{\Delta BOLD}{\Delta EtCO_2}$.

As a second metric the resting state fluctuation amplitude (RSFA) was calculated, which is simply the temporal standard deviation of the BOLD signal. After suitable bandpass filtering as described above RSFA is thought to represent rather the vascular than neural component of the BOLD signal according to Tsvetanov et al. [2021a]. Unfortunately, both RSFA and rs-CVR are not measured in standard, normalized units, which would be recommended for comparisons of CVR across individuals [Pinto et al., 2021, Zvolanek et al., 2023]. Thus, relative versions of both metrics were obtained by normalization with their respective mean value in the gray and white matter, termed rRSFA and rCVR.

Mean values for the hippocampus were extracted for rCVR and rRSFA using the previously obtained hippocampal mask. Due to signal dropout in air-bordering regions like the MTL in fMRI some voxels had to be excluded from the respective masks. Apart from handling signal dropout via the previously mentioned unwarping using the acquired fieldmap, it was further dealt with by excluding voxels with a temporal signal-to-noise ratio (tSNR) below 5 from the calculation of the average hippocampal CVR metrics.

31 participants had fMRI data from the paced breathing task and thus have values for the CVR metrics.

3.2.5 Statistical analysis

The associations between the continuous vascular metrics (TI, gVD, CoMD, rCVR and rRSFA) and cognitive as well as global structural outcome measures (TGM, TWM) were tested in linear models. The vascular metrics were bilaterally averaged in these models. ANCOVAs were used to compare the cognitive and global structural measures between individuals with an augmented and a basic supply. Sex and years of education were included as covariates in all models. Age was not included as a covariate, as age-dependent changes in the young adult age range were not expected and age was strongly correlated with years of education ($r = 0.825$). The models with structural outcomes additionally contained TIV as a covariate. The associations between the vascular metrics (including the HVP) and local structural measures such as whole and anterior hippocampus volume were tested in LMEs, as all measures were defined on a hemisphere-basis. The model included a random intercept for every participant as well as years of education, sex, TIV and hemisphere as covariates. The statistical results have not been corrected for multiple comparisons.

3.3 Results

The sample of 42 participants included 50% females, was on average 24.4±3.3 years old and highly educated with 17.1±2.5 years of education. Only 6 individuals had a basic supply, whereas 31 had an augmented supply. The remaining five participants could not be classified in terms of their subject-level HVP, but two of their ten hemispheres could be classified as single supply and entered the hemisphere-level analyses.

An example for a single- and a dual-supply hemisphere are shown in Fig. 3.5A-D. As observed on the MRA images, the trajectories of the hippocampal vessels as visualized with a 7T ToF sequence with 0.28mm isotropic resolution show the following approximate patterns, which can partially be seen in 3.5A-D: The AChA originates in the ICA

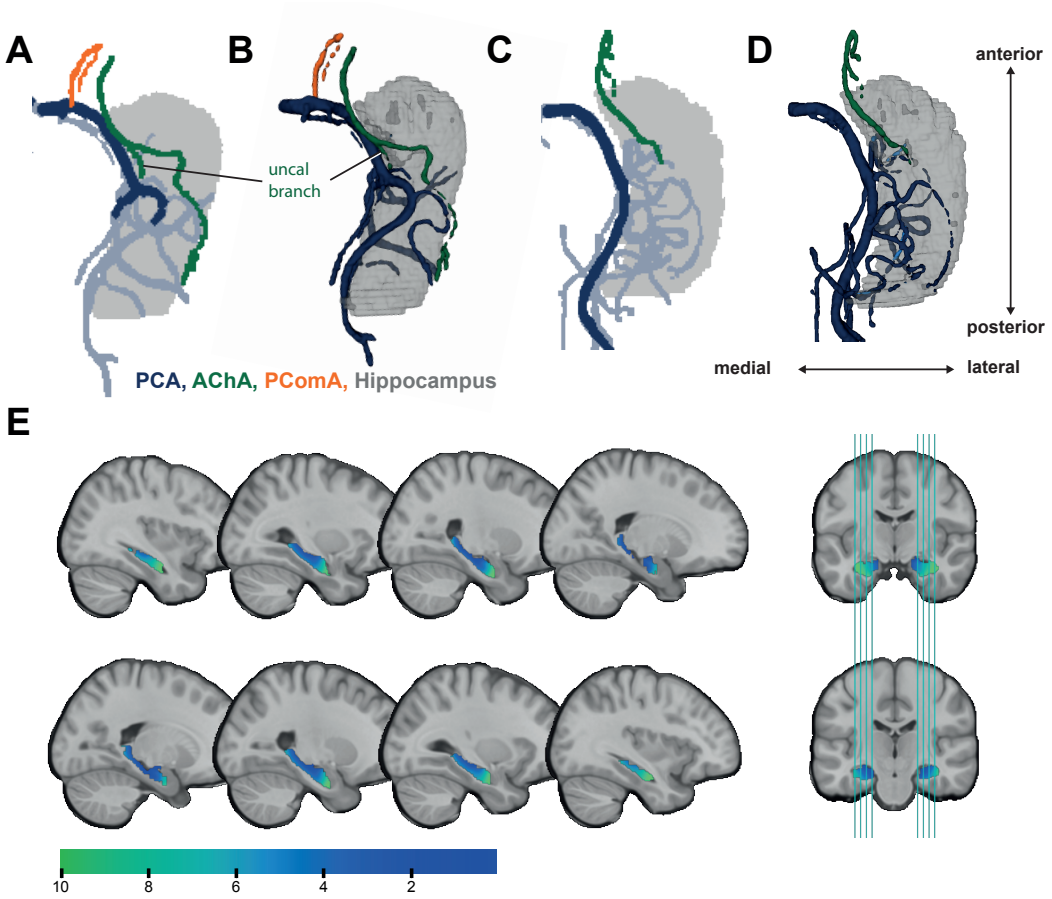

Figure 3.5: **Hippocampal vascularization and vessels distances.** (A) Exemplary image of a right hemisphere with a dual supply through an uncal branch of the AChA. (B) 3D rendering of the segmentation shown in A. (C) Exemplary image of a right hemisphere with a single supply. Note that the PComA is missing in this hemisphere. (D) 3D rendering of the segmentation shown in C. PCA branches can be observed to run both superior (in the front) and inferior (behind) to the hippocampal body and tail in panels B and D. PCA branches that were pruned are displayed as transparent in panels A and C. (E) Mean voxel-wise vessel distances of all participants in MNI space. Scale is in mm.

(not shown), from where it starts its course from anterior to posterior. It is first located medially to the hippocampus and then runs superolaterally until it has passed about half of hippocampus' extent from medial to lateral, sometimes sending off branches towards the hippocampal head on its way. Approximately upon reaching the hippocampal body on its anterior-posterior course, the AChA often fell below the resolution limits of the ToF sequence. If visible, one could see it continuing posteriorly along the hippocampus without forming additional hippocampal branches. The main trunk of the PCA is also located medially to the hippocampus and runs roughly parallel to its long axis. It sends off branches that run infero- and superolaterally along the hippocampal body and tail. The hippocampal head was always rather spared from vessels within our resolution limit. Hence, the hippocampus is not surrounded by supplying vessels from all directions, but mainly from the medial side along the body and tail. These observations are reflected in a mean vessel distance map of all participants (Fig. 3.5E), which demonstrates particularly high distances to the closest vessel in the hippocampal head and in lateral parts of the hippocampus across all participants.

3.3.1 Composite scores capture global cognitive and memory performance

A principal component analysis on 19 scores from different cognitive tests spanning the domains of attention, executive function, language, memory and visuospatial abilities was used to obtain a single score representing overall cognition (see section 3.2.2). The first PC explained 35.03% of the variance in the 19 scores. The first PC of a PC analysis on only 5 memory scores explained 54.63% of the variance in these. The factor loadings of the scores to the first PC of both PC analyses are illustrated in Fig. 3.6.

As shown in Fig. 3.6A, the loadings are all positive. There is no clear dominance of one cognitive domain over another, suggesting the factor score as a reasonable representation of overall cognitive abilities. The strongest loadings seem to come from tests of executive function and visuospatial memory tests. Tests with lower loadings tend to be the easiest ones that exhibit a low amount of variance between participants, for example reading color names (Stroop) or recalling symbols from the SDMT. As shown in Fig. 3.6B, the visuospatial tests have strong loadings on the memory factor, whereas the verbal memory test has a comparably low loading. In contrast, the composite memory score attempts to rebalance the lack of verbal memory influence by including the LM score twice. The correlation between the memory factor score and the memory (z score) composite was very high ($r = 0.937$), and thus the composite memory score was used in further analyses because it represented a better balance between the different memory domains.

3.3.2 Young augmented-supply adults do not have greater brain structure nor cognition

In young adults there was no evidence for a benefit of an augmented hippocampal vascular supply with regard to brain volume or cognitive performance as compared to a basic supply. Unlike in older adults, augmented supply individuals did not have greater brain structure globally than individuals with a basic supply represented by

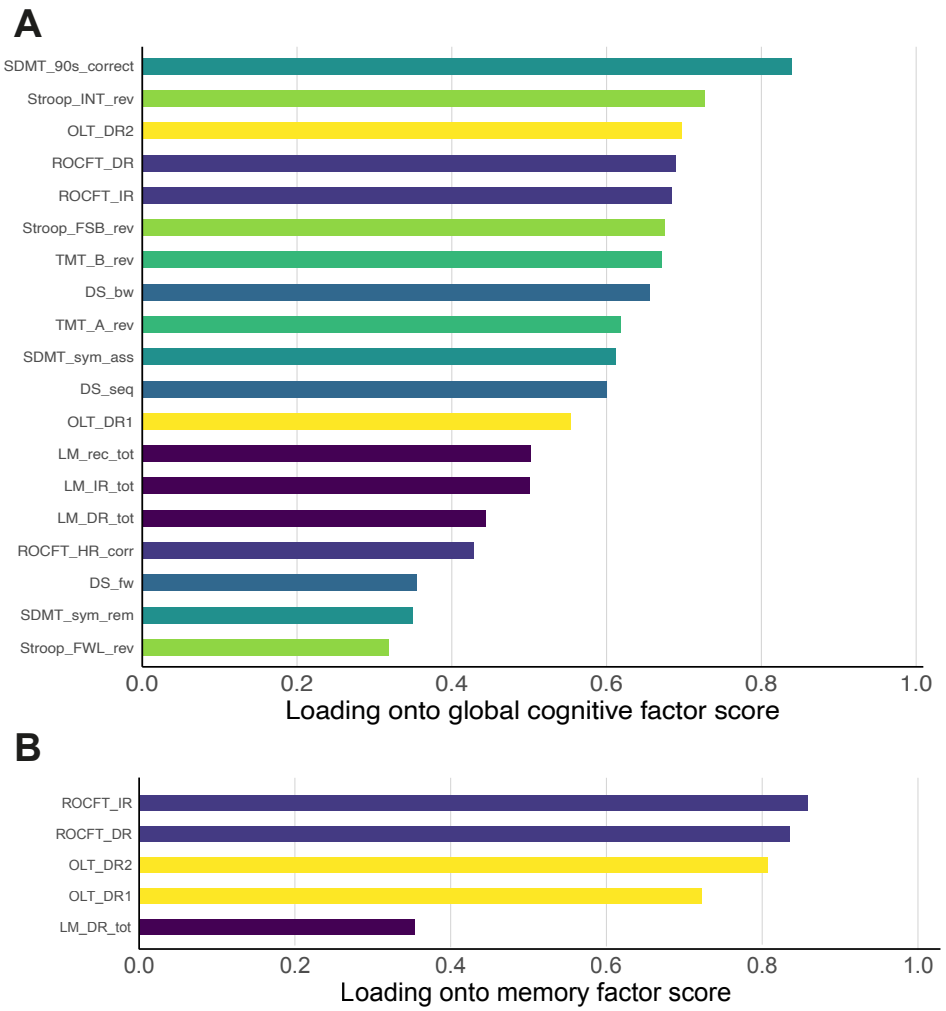

Figure 3.6: **Loadings of cognitive test scores onto factor scores.** (A) Loadings to global cognitive factor score. (B) Loadings to memory factor score. Colors indicate which test the scores belong to. DR = delayed recall, IR = immediate recall, HR = hit rate, rev = reversed, tot = total; DS: fw = forward, bw = backward, seq = sequential; SDMT: 90s_correct = correctly assigned symbols in 90s, sym_ass = symbols correctly assigned to number after SDMT (max. 9), sym_rem = symbols correctly recalled after SDMT (max. 9); Stroop: FWL = read color words ("Farbwörter lesen"), FSB = name color bars ("Farbstriche benennen"), INT = interference condition.

their total gray matter volumes (t(32) = 0.727, p = 0.47, β = 0.092). Hemispheres with a dual supply also did not contain greater MTL structures locally, neither in the anterior hippocampus (t(40.7) = -0.985, p = 0.33, β = -0.052; see Fig. 3.7A) nor whole hippocampus (t(38.6) = -0.224, p = 0.82, β = -0.010) and also not in the entorhinal cortex (t(46.48) = -0.866, p = 0.39, β = -0.072). Individuals with an augmented supply further did not show better memory performance (t(33) = 0.546, p = 0.59, β = 0.093; see Fig. 3.7B) nor general cognitive performance (t(33) = 0.721, p = 0.48, β = 0.126).

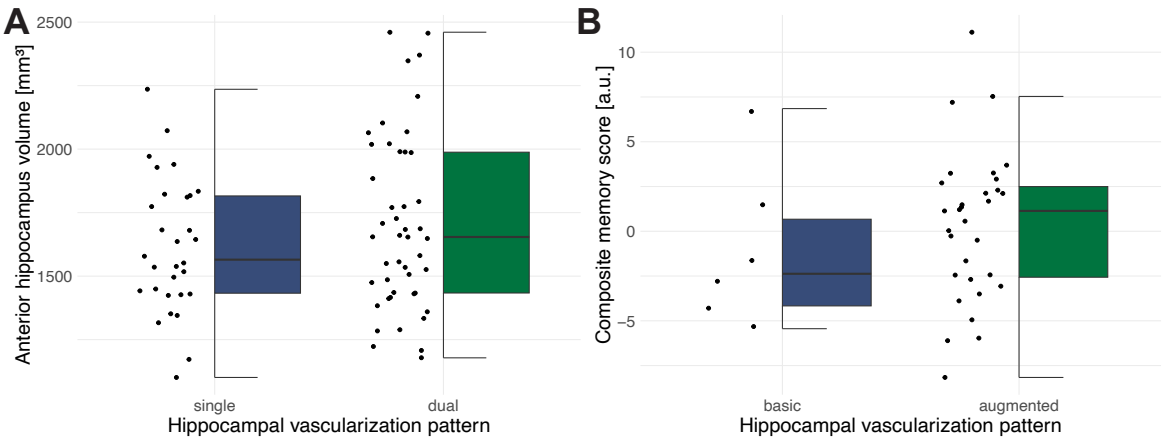

Figure 3.7: **HVP shows no significant associations with memory nor anterior hippocampus volume.** (A) Association between hemisphere-level HVP and unilateral anterior hippocampus volumes. Please note that after correction for hemispheric effects dual-supply hemispheres contained (statistically non-significant) smaller aHC volumes, in alignment with the results presented in the main text. (B) Association between the subject-level hippocampal vascularization pattern and the composite memory score.

3.3.3 Vessel distance metrics are not associated with brain structure nor cognition

Analyses of vessel distance metrics and hippocampal volumes were performed i) in subject space (raw gVD and CoMD) and ii) in a common template (MNI) space after warping of VD maps and with usage of a common template hippocampal mask. In subject space, hippocampal volumes were (unexpectedly) positively correlated with gVD ($r = 0.294$, $p = 0.012$; see Fig. 3.8). After correcting for covariates including TIV there was no statistically significant relationship between raw hippocampal gVD and whole

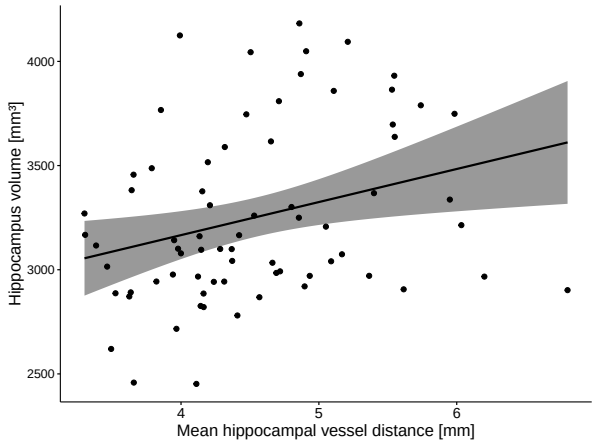

Figure 3.8: **Hippocampal volume and mean hippocampal vessel distance (in subject space) are significantly correlated.** Shaded area denotes 95% confidence intervals.

Table 3.1: **Relationship of vessel distances with brain structure and cognition.** The results in the table denote t values (degrees of freedom in parentheses) from the linear models or LMEs adjusted for covariates. In the columns 'no fetals' the results of models without individuals with FTPs are reported. Please note that CoMD was not calculated for individuals with FTPs (see methods). 'All' means all available individuals were included in the model. 'Raw' represents raw measures based on a subject-specific hippocampus mask in ToF space. 'MNI' denotes that VD and CoMD were calculated in MNI space with a generic hippocampus mask. '+' denotes p values < 0.1. P values were not corrected for multiple comparisons.

	All		No fetals			
	gVD		gVD		CoMD	
	Raw	MNI	Raw	MNI	Raw	MNI
Memory composite	$1.906^{+}(31)$	0.657(32)	1.588(24)	0.356(25)	1.112(24)	0.694(25)
Global cogn. factor	1.490(31)	0.586(32)	1.066(24)	0.313(25)	1.089(24)	1.062(25)
wHC vol	0.466(39.6)	-1.354(38.4)	0.028(30.4)	$-1.736^{+}(30.0)$	0.862(32.7)	0.345(35.5)
aHC vol	0.405(43.5)	-1.324(41.0)	-0.424(31.4)	$-1.844^{+}(31.0)$	0.454(34.9)	-0.054(37.8)
TGM	0.640(30)	0.447(31)	1.560(23)	1.100(24)	-0.721(23)	-0.779(24)
TWM	0.911(30)	1.099(31)	0.430(23)	0.933(24)	0.392(23)	0.604(24)

hippocampus volumes anymore in the whole sample (t(39.6) = 0.466, p = 0.643, β = 0.027; see Tab. 3.1)

When considering mean hippocampal gVD in MNI space, the relationship with the volume of the anterior and whole hippocampus was negative, although this association was not statistically significant (t(41.0) = -1.324, p = 0.186 and t(38.4) = -1.354, p = 0.176, respectively). In the subsample of participants without FTPs the associations were stronger (see Fig. 3.9A). Here, smaller distances of the hippocampus to its surrounding arteries (in MNI space) tended to be associated with greater hippocampal

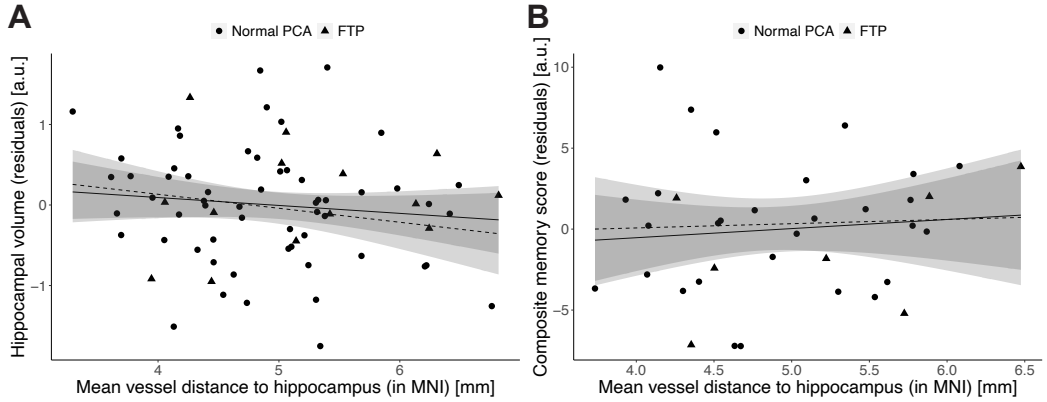

Figure 3.9: **Non-significant association of gVD with (whole) hippocampus volume and memory.** (A) Association between unilateral mean hippocampal vessel distances and ipsilateral volumes of the whole hippocampus. (B) Association between bilaterally averaged mean hippocampal vessel distances and the composite memory score. The regression lines refer to the whole sample (solid line) and sample without individuals with FTP (dashed line), respectively. Shaded areas denote 95% confidence intervals.

volumes (t(31.0) = -1.844, p = 0.075, β = -0.127 for the anterior hippocampus and t(30.0) = -1.736, p = 0.093, β = -0.109 for the whole hippocampus, respectively). In terms of cognitive performance, raw hippocampal vessel distances showed a trend towards a statistically significant positive association with the composite memory score in the whole sample (t(31) = 1.906, p = 0.066, β = 2.050), but not the subsample without FTPs (t(24) = 1.588, p = 0.125, β = 2.011; see Fig. 3.9B). This association was also diminished in the whole sample when considering gVD values in MNI space. There were no statistically significant associations of gVD with global structural measures. Likewise, the CoMD metric did not exhibit any statistically significant relation with brain structure nor cognitive performance. In summary, we found no significant associations between vessel distance metrics and hippocampal volume or cognition (when adjusting for covariates) in young adults (only statistical trends without correction for multiple comparisons).

3.3.4 Tortuosity index is not associated with brain structure nor cognition

The tortuosity of the PCA, AChA and PComA was assessed in the form of the tortuosity index. Although most associations between TI and cognitive as well as structural measures were negative as expected, no association reached statistical significance (see Tab. 3.2).

3.3.5 Relative CVR metrics are partially weakly associated with brain structure or cognition

Cerebrovascular reactivity was assessed by rRSFA and rCVR, averaged over the whole hippocampus. Lower rCVR in the hippocampus was found to be related to better cognitive performance when not considering correction for multiple comparisons (t(24) = -2.212, p = 0.037, β = -1.524; Fig. 3.10A). Lower hippocampal rRSFA values were related to greater volumes of the hippocampus, with a trend towards statistical significance (t(33.3) = 1.969 p = 0.057, β = -0.110,; Fig. 3.10B). Otherwise, no statistically significant relationships were observed (see Tab. 3.3). For absolute CVR and RSFA there

Table 3.2: **Relationship of tortuosity with brain structure and cognition.** The results in the table denote t values (degrees of freedom in parentheses) from the linear models or LMEs adjusted for covariates. No associations were statistically significant.

	TI_{PCA}	TI_{AChA}	TI_{PComA}
Memory composite	-1.201(25)	-0.667(31)	0.113(20)
Global cogn. factor	-1.091(25)	-0.570(31)	-0.927(20)
wHC vol	-1.106(41.9)	-0.465(39.9)	-0.112(33.1)
aHC vol	-0.953(45.8)	-0.382(43.9)	0.800(34.8)
TGM	-0.828(24)	-0.647(30)	-1.207(19)
TWM	-0.106(24)	-0.903(30	0.209(19)

Table 3.3: **Relationship of CVR with brain structure and cognition.** The results in the table denote t values (degrees of freedom in parentheses) from the linear models or LMEs adjusted for covariates. All values for the CVR metrics represent mean values in the hippocampus. '+' denotes p values < 0.1, '$*$' denotes $p < 0.05$. P values were not corrected for multiple comparisons.

	rCVR	rRSFA
Memory composite	-1.345(24)	-1.444(25)
Global cogn. factor	-2.212*(24)	0.101(25)
wHC vol	-0.772(32.7)	-1.969^{+}(33.3)
TGM	-1.371(24)	-1.075(25)
TWM	-0.816(24)	0.576(25)

were also no statistically significant associations with brain structure nor cognition (see Tab. S3).

3.4 Discussion

We were able to thoroughly characterize the cerebral vasculature around the hippocampus in terms of both structural and functional features in a cohort of young adults. The use of ultra-high field MRI enabled us to determine the hippocampal vascularization pattern and aided the quantification of vessel distances with the previously introduced VDM approach as well as of the reactivity of the hippocampal vessels. The latter was assessed utilizing a recently introduced approach that relies on natural variations in the arterial CO_2 concentrations, which were reinforced with an accompanied paced breathing paradigm. Another novel feature of the hippocampal vasculature examined here was the tortuosity of its surrounding arteries. We investigated the relationships of these hip-

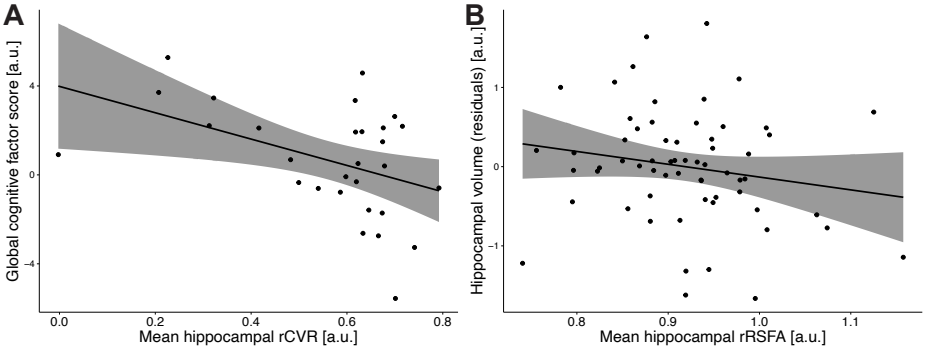

Figure 3.10: **Hippocampal CVR is significantly associated with global cognitive performance and hippocampal volume.** (A) Mean hippocampal rCVR (bilaterally averaged) exhibits a negative relationship with the global cognitive factor score. (B) Mean hippocampal rRSFA is positively related with ipsilateral hippocampal volume. Shaded area denotes 95% confidence intervals.

pocampal vascular metrics with brain structure and cognition, allowing us to gain insight into the role of hippocampal vascularization in brain reserve and brain maintenance.

Overall, very few statistically significant associations of the hippocampal vascular metrics with any of the selected outcome variables were observed (and none would survive a correction for the multitude of comparisons made in this study), providing no support for the idea that better hippocampal vascularization yields structural or cognitive benefits in adults (already) in their early adulthood. If there are any effects in young adults, these are likely small. Thus, hippocampal vascularization as represented by the hippocampal vascularization pattern, vessel distances, tortuosity and CVR does not seem to confer a brain reserve in early life that could protect individuals from cognitive deficits in late life. The observation that the hippocampal vascularization pattern has been linked to greater structural integrity in older adults [Perosa et al., 2020, Vockert et al., 2021], however, indicates structural benefits due to the HVP in late adulthood. In concert, these observations indicate an involvement of the HVP in brain maintenance, although longitudinal data is needed to confirm this hypothesis. Resilience to cognitive decline as suggested for hippocampal vessel distances [Garcia-Garcia et al., 2023] might be driven by other mechanisms than neurobiological substrate alone. For example, the ability to match metabolic demands and avoid accumulation of metabolic waste products through their timely clearance is essential for optimal neuronal functioning. As such, cerebral blood flow, especially in the hippocampus, which all investigated vascular metrics are linked to, could be another determinant for maintaining memory and other cognitive functions in aging and disease [Heo et al., 2009]. Another important factor in this context, which was not examined in this study, is the neuroinflammatory profile [Brosseron et al., 2022, Hayek et al., 2024] that is also closely linked to vascular health.

In our study, the statistically strongest relationship was observed between higher cerebrovascular reactivity within the hippocampus (represented by relative CVR) and worse cognitive scores, refuting our expectations. Likewise, higher reactivity of the hippocampal vessels as represented by rRSFA was related to lower hippocampal volumes (trend-level). Yet, it seems unlikely that a lower vasodilatory ability of the hippocampal vessels is indeed related to worse cognitive performance or smaller hippocampi, since this ability is important for the regulation of cerebral blood flow. Additionally, lower CVR in older adults has been associated with poorer cognitive function [Catchlove et al., 2018b, Kim et al., 2021a, Sur et al., 2020], also longitudinally (change-change relationship) [Peng et al., 2018]. Hence, considering previous findings, the unexpected negative associations of CVR with cognitive function and hippocampal volumes observed here might qualify as coincidence and we note that it would not survive a correction for multiple comparisons. No other association of CVR with other variables was observed, also not with episodic memory. Similarly, a previous study did not find an association between hippocampal CVR and memory performance in young adults, but only in older adults [Catchlove et al., 2018a].

There are also methodological challenges with respect to our CVR assessment that need to be considered. While CVR mapping via a respiratory regressor (through physiological measurement of breathing amplitude with a breathing belt) instead of measurements of $EtCO_2$ has been shown to yield quasi-indistinguishable maps of CVR am-

plitude, it comes with the drawback of yielding a CVR measure with arbitrary units, rendering direct comparisons between participants difficult [Zvolanek et al., 2023]. The same problem applies to RSFA as the temporal standard deviation of the raw BOLD signal. Normalization to a large reference region has been suggested for inter-individual comparisons [Liu et al., 2021]. The reference chosen here was the total gray and white matter. Yet, owing to the high desired resolution, the fMRI coverage was restricted to a slab containing the MTL and parts of the occipital and parietal lobes. Due to differences in individual slab placement, which was planned parallel to the long axis of the hippocampus, slab coverage and thus the reference region slightly varied between participants. Consequently, the heterogeneous normalization procedure might have negatively impacted the comparability of the relative measures of CVR. On top of that, despite the benefits of BOLD fMRI in terms of SNR, imaging the MTL is challenging due to signal dropout. Here, we excluded voxels with a tSNR below 5. Yet, systematic (versus random) missingness of anterior and inferior parts of the hippocampus to different degrees across participants could have led to a bias of the estimated average. In an attempt to take this into account, the regressions were weighted by the percentage of hippocampal voxels included in the calculation of the mean hippocampal CVR metrics, which retained the interpretation of the results (see Tab. S4).

Similar to the absent or weak effects of CVR, there was also very little evidence that lower vessel distances provide a benefit with regard to brain volumes or cognitive performance in young adults. Only when disregarding participants with fetal-type PCAs, a weak association between lower arterial distances in MNI space and hippocampus size was observed. This calls to question the comparability between individuals with fetal-type or adult PCAs. The low number of individuals with FTPs did not allow reliable analyses targeting differences in hippocampal vascularization (or brain volumes/cognitive performance) between PCA variants. Previous studies showed that in individuals with FTPs, reduced blood flow in the BA is compensated by increased blood flow in the ICA [Amin-Hanjani et al., 2015, Hendrikse et al., 2005], illustrating the greater flow demands to and dependence on the anterior circulation. It seems comprehensible that a fetal-type PCA could exhibit reduced blood flow due to the additional demand on the anterior system. Yet, one study examining CBF in cerebral arteries in CoW variations did not find differences in blood flow between FTPs and contralateral adult PCAs in the same participants [Zarrinkoob et al., 2015]. Moreover, the VDM approach is agnostic to the identity of the vessels, as it approximates vessel densities in the form of global vessel distances, which to our knowledge are not dependent on PCA variants. Consequently, the results regarding gVD in the whole sample are likely a more accurate representation of the actual effect than the results for the (smaller) subsample without FTP.

Furthermore, we observed that the raw hippocampal vessel distances in subject space were positively correlated with hippocampus volume (but not when derived from a common MNI space mask). Speculative reasons for this observation could be vessel location/anatomy and resolution bias. More specifically, the hippocampus receives its blood supply exclusively from the medial side [Marinković et al., 1992]. The PCA as the main source of hippocampal blood supply is located medially to the hippocampus and runs

parallel to it, sending off branches that run infero- and superolaterally around the hippocampus (Fig. 3.5). These temporal arteries (or sometimes the main branch of the PCA itself) send feeding arteries, which enter the hippocampus through the uncal sulcus, hippocampal sulcus and fimbriodentate sulcus or by penetrating the dentate gyrus [Erdem et al., 1993]. The AChA runs from the medial towards the superolateral side of the hippocampus, sometimes sending off a branch that runs inferiorly into the uncal sulcus, passing the uncus on the medial side [Erdem et al., 1993]. The hippocampal head is mostly spared from visible vessels (Fig. 3.5). Hippocampi thus have a lot of potential for extension into directions averted from the primary vessels, which could effectively increase the average distance of the hippocampus from those as it grows. Expansion of tissue directly bordering the visible vessels could also lead to further displacement of these visible vessels from the center. In absence of concomitant changes that affect the visibility of the smaller arteries, the average distance would increase. However, in reality, the lateral portion and the center of bigger hippocampi, which are farther away from the visible vessels, might still be well innervated by the arcs of arterioles and ultimately capillaries, whose size is beyond the (already high) resolution of the utilized ToF MRA sequence.

A word of caution should be appreciated regarding the hippocampal vascularization pattern, for which also no association with brain structure or cognition was observed. First, the proportion of participants with a basic supply was very low (N = 6 or 16.2%) due to a high amount of participants with a once augmented hippocampal vascular supply (N = 16 or 43.2%), leading to a very skewed distribution of the HVP and a potentially inaccurate estimation of differences in outcome variables in the subject-wise analyses. In contrast, the distribution of the hemisphere-level HVP was more even (39.4% single versus 60.6 % dual supply), causing no problems in the analyses of local MTL structural integrity. Second, the pattern classification was not always obvious, but is susceptible to the subjectivity of the rater, which we tried to address by having two raters that sought consensus in case of divergent classifications. Third, the identification of an uncal branch does not ensure the irrigation of the hippocampal head through the AChA. In fact, two types of posterior uncal arteries exist: uncal arteries, which supply only the uncus, and unco-hippocampal arteries that additionally supply the hippocampal head [Fernández-Miranda et al., 2010]. Discrimination of both types of uncal arteries on ToF MRA might only be possible with even higher resolution enabling the identification of its trajectory until its destination in either the uncus or the hippocampal head. As a consequence, the HVP might rather represent an assessment of the visibility of uncal branches with reasonable trajectories instead of the certain identification of an AChA-assisted hippocampal supply. However, the bigger diameter or faster blood flow indicated by the visibility of an uncal branch on ToF MRA might in turn be an indication of a bigger perfusion territory and hence be a useful hint for a dual supply. The distribution of single- and dual-supply hemispheres observed in this study (39:61) was at least very close to the distribution observed in the post-mortem study of Erdem et al. [1993] (40:60).

We also studied vessel tortuosity in our sample which did not show any trend for an association with any structural or cognitive outcome measure. Yet, this was to our knowledge the first study that quantified AChA tortuosity directly. Tortuosity of the

PCA and PComA have rarely been assessed and only so in the context of aneurysms [Kim et al., 2021b, Sahni et al., 2007]. Evidence regarding the relationship of cerebral vessel tortuosity with cognitive performance is also quite sparse and mixed [Chen et al., 2022b, Yin et al., 2024], but relationships with ischemic stroke [Cartwright et al., 2006, Martins et al., 2018, Shang et al., 2022] indicate hypoperfusion that could well be severe enough to evoke cognitive deficits depending on the affected artery. The employed tortuosity index is the simplest quantitative measure of tortuosity, which might miss local tortuosity [Bullitt et al., 2003]. The use of more sensitive methods like the sum of angles method might be better suited to investigate relationships with cognition in future studies in both younger and older adults.

The use of composite measures of overall cognitive performance and memory explicitly represents a strength of the study. Instead of relying on a specific domain (e.g. verbal memory), single cognitive tests or even subtests, the calculated composites are a more robust representation of the participants' cognitive performances and are less susceptible to measurement noise. Moreover, the OLT encoding and retrieval 1 sessions that contributed to the factor scores were performed on a separate day than the other cognitive tests, which diminishes the potential effects of participants 'having a bad day'.

In conclusion, hippocampal vascularization does not seem to convey brain reserve in the form of greater neurobiological capital in young adulthood. Instead, considering the current findings and our previous findings in older adults (see study 1), the hippocampal vascularization pattern might rather contribute to brain maintenance in older adults, leading to better preservation of anterior MTL volumes in augmented-supply individuals compared to those with a basic supply. Longitudinal studies are needed to finally determine whether the hippocampal vascularization pattern provides brain maintenance in aging. Other factors of hippocampal vascularization besides the pattern could also be involved in cognitive resilience. Future efforts should be aimed at investigating the relationship between the tortuosity of the PCA, PComA and AChA and cognitive performance in older adults with a sensitive metric like the sum of angles method. Studies using ToF MRA for visualization of hippocampal blood supply should aim for even higher resolution, possibly with the use of compressed sensing to counter long acquisition times [Lakhani et al., 2023]. This would aid both the hippocampal vessel distance metrics and improve the reliability of the classification of the hippocampal vascularization pattern that optimally should be validated ex-vivo. Moreover, further studies should examine the involvement of cerebral blood flow in cognitive resilience by testing if it mediates the (potential) cognitive benefits of CVR, tortuosity and vessel distances/densities.

3.5 Contributions

Yeo-Jin Yi provided the code for the OLT. Lilli Lümkemann performed the segmentation of the arteries on the ToF images and further assisted in determining the arteries' start and end points. Berta Garcia-Garcia and Lilli Lümkemann also helped with judgment of FTPs. Hendrik Mattern provided the methodological VDM framework. I did the

VDM data processing. The script for the conversion of the breathing belt signal to the physiological regressor as well as the CVR script were written by Niklas Behrenbruch. I executed all other image (pre)processing tasks as well as all statistical analyses. I wrote the text of this chapter. Anne Maass supervised the study. Stefanie Schreiber co-supervised the study, which was conducted within the CRC1436 (subproject B04).

4 Cognitive Reserve Against Alzheimer's Pathology Is Linked to Brain Activity During Memory Formation

Substantial parts of this chapter have been published in
"**Vockert, N.**, Machts, J., Kleineidam, L., Nemali, A., Incesoy, E. I., Bernal, J., ... Ziegler, G., Maass, A. & Delcode Study Group. (2024). Cognitive Reserve Against Alzheimer's Pathology Is Linked to Brain Activity During Memory Formation. *Nature Communications*, 15(1), 9815."

4.1 Introduction

The two previous studies of this thesis investigated resilience against cognitive decline primarily from a structural perspective, i.e. via brain reserve and brain maintenance. In contrast, cognitive reserve is conceptualized as a mismatch between an individual's brain pathology burden and level of cognitive performance due to cognitive and functional brain mechanisms, which are not necessarily accompanied by macroscopic structural brain alterations. In alignment with its definition (see chapter 1.2), the most recent research framework operationalizes CR in the form of a moderator variable [Stern et al., 2023]. As such, it states the requirement of three components for CR research. First, it requires a measure of changes in brain status like brain atrophy or pathology. Second, a quantification of longitudinal changes in cognition theoretically associated with brain status is needed. The third component of this moderation approach is a proposed CR measure, which should moderate the relationship between brain status and cognitive changes. The use of functional neuroimaging methods presents a viable avenue to investigating the neural implementation of CR within this framework. For this purpose, the moderator variable can be represented by the expression of brain activity during cognition using fMRI.

Previous studies have only partially been able to address these aspects, even though a wide range of methodologies has been utilized. Most functional neuroimaging studies on CR have identified regions or networks contributing to CR by correlating their expression (activity/connectivity) with a CR proxy like education or IQ instead of investigating their ability to moderate the relationship between aging- or pathology-related brain changes and cognitive performance. For instance, resting-state functional connectivity profiles have been associated with sociobehavioral CR proxies, manifesting at different levels, including ROI-to-ROI [Arenaza-Urquijo et al., 2013a], global connectivity of a seed region [Cole et al., 2012, Franzmeier et al., 2017b], global functional connectivity within a network [Franzmeier et al., 2017a] and employing dimensionality reduction to a ROI-to-ROI connectome [Stern et al., 2021]. Notably, van Loenhoud et al. [2020] recently employed a task potency method, examining the relationship between whole ROI-to-ROI connectomes in the resting and task state and their association with CR proxies.

Several task-based fMRI investigations pertaining to CR have relied on the Reference Ability Neural Networks Study, wherein participants engaged in 12 cognitive tasks during MRI scanning [Habeck et al., 2016, 2018, Stern et al., 2018, van Loenhoud et al., 2020] encompassing three tasks each from the four reference abilities of episodic memory, fluid reasoning, perceptual speed, and vocabulary [Stern et al., 2014]. This comprehensive approach first facilitated the identification of overlapping regions of brain activity across tasks [Habeck et al., 2016, 2018, Stern et al., 2018] and activity patterns exhibiting correlations with IQ [Stern et al., 2018] and education [Habeck et al., 2016]. Moreover, Stern et al. [2008] observed a distinctive spatial pattern of BOLD activity, the expression of which displayed significant correlations with measures of CR as task load increased.

Among the most notable findings, the default mode network (DMN) [Stern et al., 2021, van Loenhoud et al., 2020] emerged as a potential CR-related region, alongside

its individual components such as the left precuneus [Bosch et al., 2010, Stern et al., 2018], left posterior cingulate [Bosch et al., 2010, Stern, 2005], precuneus and cingulate [Stern et al., 2008], and medial frontal gyrus [Stern et al., 2018]. Left prefrontal cortex activity both within and outside of the frontoparietal network [Cole et al., 2012] as well as global connectivity of the left frontal cortex [Franzmeier et al., 2017b] were also related to CR. Additionally, there is some evidence for involvement of the anterior cingulate cortex (ACC) in CR [Arenaza-Urquijo et al., 2019, Stern, 2005, Stern et al., 2018].

However, most previous attempts neglect that a network underpinning CR should be capable of altering the relationship between aging- or pathology-related brain changes and cognitive performance [Stern et al., 2023]. Moreover, functional neuroimaging studies on CR are more prevalent in aging research, whereas very few investigations have explored CR in the context of neurodegeneration and AD [Franzmeier et al., 2017b, Stern et al., 2018]. A major challenge in addressing this gap is to obtain brain activity during cognition in large longitudinal cohorts where AD-related pathological burden is thoroughly quantified.

The primary objective of this study was thus to investigate the neural implementation of CR by identifying task fMRI activity patterns associated with cognitive reserve in a large scale multicentric cohort of nearly 500 older individuals along the AD spectrum with the use of the moderation framework. Notably, the cohort was enriched in individuals who still perform normal but are at increased risk for developing AD. To accomplish this, we employed a task fMRI paradigm on memory formation to explore CR within the context of episodic memory. Given that episodic memory is among the earliest and most frequently affected cognitive faculties in dementias like AD dementia [Morris and Kopelman, 1986, Petersen et al., 1994], memory-related activity patterns hold particular relevance in CR investigations. As the central hub of episodic memory formation and due to its vulnerability in AD, the hippocampus is further of distinct significance for quantification of AD-related neurodegeneration [Frisoni et al., 2010, Henneman et al., 2009, Small et al., 2011]. Our study sought to complement previous approaches by (A) adhering closely to the research framework [Stern et al., 2023] while (B) identifying a memory activity pattern capable of moderating the impact of AD pathology on cognitive performance. Drawing on insights from prior functional neuroimaging studies on CR, we expected that CR-related activity patterns might encompass regions such as the DMN, frontal regions such as the ACC and task-specific regions like the MTL [Soch et al., 2021a]. Our approach takes advantage of a moderation model in a multivariate fashion (utilizing principal component regression) and effectively condensing the multidimensional AD pathological process (reflecting fluid biomarkers and hippocampal atrophy) into a single pathological load (PL) score. We further derived a neuroimaging-based CR score from an individual's expression of the CR-related fMRI activity patterns and show its alignment with educational attainment, a well-established proxy for CR. Finally, we explored the longitudinal implications of the CR index, meticulously examining its potential to modify cognitive trajectories over time.

4.2 Methods

4.2.1 Sample

The sample is part of the DZNE-Longitudinal Cognitive Impairment and Dementia Study (DELCODE) study, a multicentric observational study of the German Center for Neurodegenerative Diseases (DZNE). It focuses on the characterization of subjective cognitive decline (SCD) in patients recruited from memory clinics, but additionally enrolled individuals with amnestic mild cognitive impairment (aMCI), mild AD dementia patients, AD patient first-degree relatives (ADR), and cognitively normal (CN) control subjects. Participants were scheduled for annual follow-up appointments over five years. More detailed information about the study has been provided previously [Jessen et al., 2018]. Our analyses were based solely on the baseline measures of the participants, with the exception of annually acquired cognitive data, which was used to assess cognitive trajectories and how they might be modified depending on an individual's cognitive reserve. The whole baseline sample comprised 1079 participants, of which 558 participants had undergone an MRI session including the fMRI task. 442 participants had cerebrospinal fluid (CSF) data available and could thus be used for creating the PL score. The final fMRI sample used in the subsequent CR analysis consisted of 490 participants after quality control and outlier exclusion, of which 232 had CSF measures and thus a PL score. Of the 490 participants, 152 were CN, 202 had SCD, 64 aMCI and 21 had a clinical diagnosis of AD dementia. The sample also contained 51 first-degree relatives of AD patients.

CN was defined as having memory test performances within 1.5 std of the age-, sex-, and education-adjusted normal performance on all subtests of the CERAD (Consortium to Establish a Registry of AD test battery). ADR had to achieve unimpaired cognitive performance according to the same criteria. SCD was defined as the presence of subjective cognitive decline as expressed to the physician of the memory center and normal cognitive performance as assessed with the CERAD [Jessen et al., 2014]. Participants were classified as aMCI when displaying an age-, sex-, and education-adjusted performance below –1.5 std on the delayed recall trial of the CERAD word-list episodic memory tests. aMCI patients were non-demented and had no impairment in daily functioning. Finally, only participants with a clinical diagnosis of mild AD dementia [McKhann et al., 2011] obtaining ≥ 18 points on the MMSE were included in DELCODE. All participants were 60 years or older, fluent speakers of German and had a relative who completed informant questionnaires. Exclusion criteria are described in Jessen et al. [2018].

The study protocol was approved by Institutional Review Boards of all participating study centers of the DZNE [Jessen et al., 2018]. The process was led and coordinated by the ethical committee of the medical faculty of the University of Bonn (trial registration number 117/13). All relevant ethical regulations were complied with. All participants provided written informed consent.

4.2.2 Cognitive tests

An extensive list of all neuropsychological tests administered in DELCODE is provided elsewhere [Jessen et al., 2018]. In our analysis we use composite scores from those tests, namely the Preclinical Alzheimer's Cognitive Composite 5 (PACC5) [Papp et al., 2017], a neuropsychological composite measure designed to index cognitive changes in the early phase of AD, and a latent memory factor derived from a confirmatory factor analysis (details in Wolfsgruber et al. [2020]). The factor analysis yielded five factors for different cognitive domains: learning and memory, language, visuospatial abilities, executive function and working memory. These were further combined to a domain-general global cognitive factor in the form of their mean value. The PACC5 scores were calculated as a mean of the PACC5's five subitems (see Papp et al. [2017] for a specification of the subtests). Prior to calculation of the PACC5 scores, the five subitems were z-transformed using the mean and standard deviation of the cognitively unimpaired sample consisting of CN, ADR and SCD participants. Nine of the fMRI-participants lacked PACC5 test scores. One of them also had missing factor scores. In terms of the PACC5 score, for most of the subjects data from multiple time points was available (68, 125, 72, 107, 96, 17 participants with 1, 2, 3, 4, 5, 6 time points, respectively) which was used to model the cognitive trajectories longitudinally.

4.2.3 CSF measures

AD biomarkers were determined using commercially available kits according to vendor specifications: V-PLEX $A\beta_{42:40}$ Peptide Panel 1 (6E10) Kit (K15200E) and V-PLEX Human Total Tau Kit (K151LAE) (Mesoscale Diagnostics LLC, Rockville, USA), and Innotest Phospho-Tau(181P) (81581; Fujirebio Germany GmbH, Hannover, Germany). More information on CSF acquisition, processing, and analysis in the DELCODE cohort can be found in a previous publication [Jessen et al., 2018]. Here, we focused on $A\beta_{42:40}$ and phospho-tau181 (p-tau) as CSF measures of amyloid β and tau pathology. Of note, these were used as continuous measures.

4.2.4 MRI acquisition

MRI data was acquired with Siemens scanners (3 TIM Trio systems, 4 Verio systems, one Skyra and one Prisma system) at 10 different scanning sites. The current analysis was performed using T1-weighted images (3D GRAPPA PAT 2, $1mm^3$ isotropic, 256x256 px, 192 sagittal slices, TR 2500ms, TE 4.33ms, TI 1100ms, FA 7°, ca. 5min), T2-weighted images (optimized for medial temporal lobe volumetry, 0.5x0.5x1.5 mm^3, 384x384 px, 64 slices orthogonal to the hippocampal long axis, TR 3500ms, TE 353ms, ca. 12min) and a task fMRI protocol (2D EPI, GRAPPA PAT 2, $3.5mm^3$ isotropic, 64x64 px, 47 slices, oblique axial/AC-PC aligned, TR 2580ms, TE 30ms, FA 80°, 206 volumes, ca. 9 min). For more details see previous publications [Düzel et al., 2018, Jessen et al., 2018]. For task fMRI, all sites used the same 30 inch MR-compatible LCD screen (Medres Optostim) matched for distance, luminance, color and contrast constant across sites, and the same response buttons (CurrentDesign). All participants underwent vision

correction with MR-compatible goggles (MediGlasses, Cambridge Research Systems) according to the same standard operating procedure (SOP). SOPs, quality assurance and assessment were provided and supervised by the DZNE imaging network.

Subjects performed a modified version of an incidental visual encoding task using pictures of indoor and outdoor scenes [Düzel et al., 2010, 2018]. After familiarization with two "Master" scenes (one indoor, one outdoor) outside of the scanner, participants were presented with 44 repetitions of the Master scenes (22/22) and 88 novel scenes (half outdoor, half indoor) in the MRI scanner using the software Presentation (Neurobehavioral Systems Inc.). Participants were instructed to classify each scene as either indoor or outdoor by pressing a button. Each scene presentation lasted 2500ms, with an optimized inter-trial jitter for statistical efficiency. After a retention delay of 60min, memory was tested outside of the scanner with a 5-point recognition-confidence rating for the 88 former novel scenes and 44 new distractor scenes, to assess successful incidental memory encoding. A response of 1 referred to "I am sure I have not seen this picture before", a 5 meant "I have definitely seen this picture before" and 3 referred to "I don't know".

4.2.5 Image processing

FreeSurfer 6.0 (`http://surfer.nmr.mgh.harvard.edu/`) was used to obtain measures for hippocampal volumes by combining T1- and T2-weighted images using a multispectral analysis algorithm [Iglesias et al., 2015]. Mean cortical thickness was also acquired via FreeSurfer 6.0. Total intracranial volumes (TIV) were derived using the CAT12 toolbox (version 12.6) [Gaser et al., 2024] in SPM12 r7771 (Wellcome Center for Human Neuroimaging, University College London, UK). Total gray matter volumes were calculated as cumulative sums of the gray matter probability maps from SPM segmentation (see step 3 of fMRI data processing).

fMRI data processing and analysis were performed using SPM12 and Matlab_R2016b/ Matlab_R2018a. The image preprocessing followed standard procedures: (1) Slice time correction; (2) realignment and unwarping using voxel-displacement maps derived from the fieldmaps; (3) segmentation into gray matter, white matter and CSF; (4) coregistration of functional images to the structural; (5) normalization of the functional images to a population standard space via geodesic shooting non-linear image registration; (6) normalization to MNI space via an affine transformation; (7) spatial smoothing of the functional images with a 6mm isotropic Gaussian kernel.

In this study, we focused on reserve patterns based on the so called subsequent memory effect, also referred to as successful (memory) encoding, which considers the BOLD-activation during encoding of a stimulus as a function of its subsequent remembering. Following previous methodological research, we decided to model the subsequent memory effect parametrically (see Soch et al. [2021b]) as opposed to categorically. Higher β values of the subsequent memory contrast images indicate a stronger modulation of the local voxel-based BOLD signal according to the form of the parametric modulator (here arcsine; see below), i.e. a larger difference in BOLD during encoding of later remembered compared to neutral ("unsure") or later forgotten stimuli.

In the first-level general linear model (GLM), all novel scenes were collected into a

single onset regressor and a parametric modulator with an arcsine-transformation was applied resulting in the subsequent memory regressor $\arcsin(\frac{x-3}{2}) \cdot \frac{2}{\pi}$ for a given confidence rating x. A previous study has revealed evidence that this parametric modulator, which puts higher weights on definitely forgotten (1) or remembered (5) items in comparison to probably forgotten (2) or remembered (4) items, is the best choice for a theoretically derived parametric modulator in the same task-design [Soch et al., 2021b]. The first-level GLM further included the onsets of the Master scenes and covariates including the six motion regressors from the realignment and a CSF-based nuisance regressor. Including nuisance regressors from regions with noise/artifact signal has been shown to increase the sensitivity of BOLD-fMRI studies [Behzadi et al., 2007]. In order to obtain a time series for the CSF nuisance regressor, the first eigenvariate of the BOLD time-series was extracted from an anatomical CSF mask. The CSF mask was obtained by thresholding the MNI shoot template of CSF tissue probabilities with a conservative value of 0.9 and eroding it once.

Additional smoothing with a 6mm Gaussian kernel was applied to the subsequent memory contrast images to improve the signal-to-noise ratio in the heterogeneous large clinical sample. In view of the multivariate setting of our analysis and the required dimensionality reduction of the (high-dimensional) memory contrast images, an inclusion of potential noise components seemed particularly problematic. Hence, we focus on regions with significant subsequent memory contrast activation and deactivation ($p_{FWE} < 0.05$; illustrated in Fig. 4.3A; 13695 voxels) and therefore excluded regions that might reflect more substantial noise. The obtained "task-active mask" was used to restrict all subsequent fMRI-based reserve analyses.

To enhance the signal-to-noise ratio, we opted for stringent outlier exclusion criteria, predicated on behavioral and task-related fMRI metrics. Individuals were excluded if either of the following was true: (1) They made more than 8 errors in their indoor/outdoor judgment. This corresponds to individuals with extreme outliers in the distribution of indoor/outdoor errors and could be related to lack of attention or confusion. (2) Based on response bias in their confidence rating during post-MRI retrieval, represented by the criterion location $c = -\frac{1}{2}(z(HR) + z(FAR))$; z = normal inverse cumulative distribution function, HR = hit rate, FAR = false alarm rate. Individuals with absolute response bias values above 1.5 were excluded, since strong bias could potentially render the parametric modulation invalid for two reasons. First, the response category would likely not correspond to the actual BOLD signal at the time of encoding. Second, a reliable estimation of the subsequent memory regressor does require some variability in the response categories. (3) Framewise displacement (FD) was above 0.5mm in a single EPI or above 0.2mm in more than 2% of the EPIs. This exclusion was supposed to limit motion effects on the data quality. (4) An individual had extreme outliers (1st quartile - 3*IQR or 3rd quartile + 3*IQR) in the β values of more than 10% of the voxels of their (GM-masked) regressor image. This was indicative of inaccurate estimations of the subsequent memory regressor in large parts of the brain and could have skewed the results of subsequent modeling steps. 68 individuals (10.4% of the original sample; 11 CN, 6 ADR, 20 SCD, 19 aMCI, 12 AD dementia) were excluded based on these criteria, leaving an fMRI sample with 490 individuals. We note that the proportion of

excluded participants with aMCI (n = 19; 22.9% of the 83 in the original sample) and Alzheimer's disease dementia (ADD) (n = 12; 36.4% of the 33 in the original sample) was disproportionately higher due to their greater movement during fMRI, response bias etc.

4.2.6 One-dimensional pathological load score

We base our multivariate reserve model of CR on a dimensional approach to individual pathological load. More specifically, we here extend the ATN classification system [Jack et al., 2016] to continuous measures by focusing on joint variation across A, T and N simultaneously. This enables a simplified biological assessment of the individual pathological state, which is likely to be on the continuum from healthy to AD and also avoids difficult a-priori choices for cut-offs. The utilized ATN measures were the following: CSF $A\beta_{42:40}$ ratio (A), CSF p-tau (T) and hippocampal volumes (N). The latter were represented by the sum of their bilateral volumes, divided by the subject's TIV. All three variables were z-normalized with their respective means and standard deviations to ensure similar scaling. Due to the non-linearity of the disease progression trajectory along the AD continuum in 3D ATN space, a non-linear dimensionality reduction method called t-distributed stochastic neighbor embedding (t-SNE) [Van Der Maaten and Hinton, 2008] was employed to reduce the dimension to one, yielding a single PL score per subject. For this purpose, the scikit-learn library 0.23.2 in Python 3.7 was utilized. Broadly speaking, t-SNE converts the Euclidian distances between datapoints in the high-dimensional space into conditional probabilities, which represent similarities. Likewise, conditional probabilities are defined for the low-dimensional counterparts. A perfect representation of the data in a lower-dimensional space would retain the conditional probabilities from the high-dimensional space between all pairs of datapoints. Hence, an optimal solution is sought by minimizing the mismatch between the conditional probabilities in both spaces, which is quantified via the Kullback-Leibler divergence. More details about the method can be found in Van Der Maaten and Hinton [2008]. Assuming that the biomarker progression profile across individuals is homogeneous, t-SNE would be able to extract this progression profile faithfully by retaining the similarities between datapoints from the ATN space as much as possible in the one-dimensional output space.

As the name suggests, t-SNE is a stochastic algorithm. Hence, the random seed was fixed to 617 to ensure reproducibility. The algorithm was applied to all 441 participants with complete ATN data available using a perplexity parameter of 50. One individual was considered an outlier and removed from all analyses, as visual inspection indicated that its assigned PL score was an erroneous representation of its AD biomarker status, as assessed from comparison to all other individuals' PL scores (see Fig. S4 for a plot including the declared outlier). Subsequently, the resulting score was scaled to fall into the range between 0 and 1 by subtracting the minimal value across participants and then dividing it by the maximal value. For reasons of interpretability, the scale was adjusted such that increasing numbers of the PL score refer to increasing amounts of AD pathology.

Moreover, the algorithm was tested with five different choices of the perplexity parameter (10, 25, 30, 50, 100) and the results were correlated with each other to check stability. On average, the correlation was 0.950, indicating that the obtained score does not exhibit substantial dependence on the selected perplexity parameter. Robustness of the PL score was further checked by applying the t-SNE algorithm 1000 times, each time randomly holding out 10% of the data. The mean correlation over 1000 iterations was 0.945, suggesting a high robustness of the proposed PL score based on ATN.

4.2.7 Multivariate reserve model of brain activity patterns

According to the recent consensus definition, a network that underlies CR should moderate the effect of brain pathology on cognitive performance [Stern et al., 2020]. The examination of this moderation effect represents the essence of our multivariate model of CR. More specifically we further study CR in the context of fMRI activity patterns during memory encoding as represented by first level GLM contrast images, one per subject, quantifying their encoding success (for details see section 4.2.5).

First, assuming that (scalar) brain activity in a given region is represented by A and pathological load by PL, a basic linear moderation model for testing a potential CR effect of brain activity on cognitive outcomes y can be formulated as follows:

$$y = b_0 + b_1 \cdot A + f(A) \cdot PL + \epsilon \tag{4.1}$$

where b_0 denotes the intercept, b_1 the main effect of activity, and $f(A)$ is some function of brain activity. For CR to have a beneficial impact on performance, there could be (1) a linear additive effect of activity ($b_1 > 0$ for activations), and/or (2) a non-linear or multiplicative moderation effect, whereby the impact of pathology on cognition depends on the level of activity, i.e. the slope of PL varies as a function of A ($f(A) \neq const$). In principle, this would suggest that regional brain activity could be optimized to enhance cognitive performance and/or reduce the negative effects of pathology, for instance through interventions or individual predispositions. While acknowledging that most biological processes are considerably more complex, for the sake of simplicity we here focus on a case in which above slope is a simple linear function of activity, i.e. $f(A) = b_2 + b_3 \cdot A$, with main effect of pathology b_2 and an interaction/moderation effect b_3. Please note that in what follows PL is just used as a quadratic term, as it has been identified as a better predictor of PACC5 compared to a linear term (see section 4.3.3).

Second, it would be feasible to implement this approach in a mass-univariate (voxel-based) manner that enables testing whether a region in isolation contributes to CR in above described ways (1) and/or (2). However, since the subsequent memory contrast activity is representing spatially correlated patterns in many brain areas reflecting distributed information processing we opt for a multivariate approach, also avoiding multiple testing and increasing sensitivity. We therefore further assume the above activity A that might contribute to CR to be reflected by patterns of voxelwise subsequent memory contrast images (in task-active areas), i.e. $b_3 \cdot A = \sum w_i \beta_i$ with linear group-level weights w_i describing a voxel's potential contribution to CR and its contrast value β_i. Please note that we assumed free weight parameters to be positive or negative enabling

potentially enhanced and reduced activations serving reserve processes. This approach generalizes above ideas of univariate CR as well as brain-based multivariate cognition-prediction models by asking if there is any activity pattern (which a subject could more or less express) that facilitates CR by means of a moderation of pathology effects.

Third, due to the large number of parameters w_i we implement the multivariate reserve model by means of representing the subsequent memory contrast images by projections on P-order principal components basis functions (images) obtained from a PC analysis. This resembles an application of principle components regression with principal components being used for quantification of patterns of (1) main effects as well as (2) the moderation effect representing CR in a narrower sense. The finally applied multivariate reserve model is a prediction model of cognitive performance including main effects of activity patterns and their interactions with pathology:

$$y = b_0 + \sum_{p=1}^{P} b_{1,p} \cdot PC_p + (b_2 + \sum_{p=1}^{P} b_{3,p} \cdot PC_p) \cdot PL^2 + c \cdot COV + \epsilon \tag{4.2}$$

with PACC5 cognitive performance scores y, individual pathological load score PL, component scores PC_p for corresponding (PC) eigenimages p and COV representing the covariates age at baseline, sex, TIV and a binary dummy variable indicating MRI acquisition at a specific site. Since PL scores were dependent on the availability of CSF measures, the model was restricted to a subsample of 232 participants (see Fig. S3). Age and TIV were mean-centered. Education was deliberately not chosen as a covariate in this context due to its role as a CR proxy. PACC5 scores had been transformed with a Box-Cox transformation ($\lambda = 2.8$) in order to achieve a closer approximation of the model's residuals to a normal distribution. The coefficients $b_{3,p}$ represent the moderation effect indicative of CR according to the consensus framework [Stern et al., 2020]. The optimal number of principal components P required to characterize reserve patterns based on subsequent memory contrast images is a free hyperparameter in the multivariate reserve model. It was optimized using a 10-fold cross-validation approach, whose results are shown in Fig. S6. Since not all participants with functional data had CSF measures and thus a PL score, the data was stratified into two groups accordingly. This ensured similar proportions of both groups within each fold, as participants with missing values for any of the variables in the moderation model could still be used for PC analysis. PC analysis was performed separately on the training data in each of the folds after mean-centering the masked functional (training) data. The coefficients of the moderation model from Eq. 4.2 were then determined for different numbers of principal components (1-25) using the least-squares method. With these coefficients the held-out (test) data was predicted. Across the ten folds, all data was predicted once based on the remaining 90% for each number of principal components. The coefficient of determination (R^2) between the true and predicted PACC5 values (Box-Cox transformed) was calculated based on the aggregated data, done once per number of principal components. In order to ensure independence of a particular division into folds, this procedure was repeated 10 times with different partitioning of the data into folds. The optimal number of principal components was identified as the corresponding model with the highest mean R^2 value across the 10 predictions (see Fig. S6).

In the next step, PC analysis was performed on the complete (mean-centered) functional data using the optimized value of P. The multivariate reserve model (Eq. 4.2) with the previously identified optimal number of principal components was estimated on the whole data set, obtaining coefficients for each PC. While the model was not cross-validated during model fitting, validation occurs in later stages in multiple forms (see section 4.2.8). We additionally note that our aim was not to build a predictive (AI) model with primary focus on predictive capabilities for new data, but to build an explanatory model that helps to elucidate the neural underpinnings of cognitive reserve (see Shmueli [2010] for a comparison).

Then, the approach enables us to project the obtained moderation coefficients $b_{3,p}$ for the PCs back into the image space for the purpose of illustration and to determine the net moderation effect $w_i = \sum_{p=1}^{P} b_{3,p} V_{p,i}$ of all voxels i with eigenimages V_p obtained from PC analysis. Therefore, w_i represents how (strong) the local subsequent memory contrast in voxel i, i.e. the activity associated with successful memory encoding, contributes to moderation of the effect that pathology has on cognitive performance differences and thus its potential role for cognitive reserve. Finally, we introduce a useful reserve score as the amount of how an individual's successful encoding activity aligns with the reserve pattern we identified on the group level by aggregating individual contrast images using the reserve weights over all voxels in the mask: $CR_{score} = \sum w_i \beta_i$.

4.2.8 Statistical Analyses

PL score

For validation purposes, the association between the retrieved PL scores and PACC5 cognitive test scores was examined, including education and the covariates age at baseline, sex and site of data acquisition. Both models with PL as a linear and a higher-order quadratic predictor of PACC5 were tested and their performance was compared in terms of their explained variance (R^2 value). The quadratic predictor was tested due to visual indications for a quadratic relationship between PL and PACC5. Furthermore, such quadratic relationships have been observed in similar contexts, for example between age and brain structure (see e.g. Ziegler et al. [2012]). Instead of testing a full quadratic model including a linear term, we restricted ourselves to finding a single predictor of disease severity in order to avoid a further increase in the complexity of the subsequent multivariate reserve model and thus aid its interpretability. Furthermore, inclusion of an additional linear term did not provide substantial increases in explained variance ($\Delta R^2 = 0.014$; in comparison: $\Delta R^2 = 0.040$ between the quadratic-only and linear-only model). An additional model assessed an interaction of the PL score with education as a CR proxy according to the assumption that cognitive reserve moderates the effect that brain pathology (PL) has on cognitive outcomes (PACC5).

Multivariate reserve model - voxel-wise inference

Inference on the voxel-level in the context of the multivariate moderation analysis was performed using a bootstrap procedure. The following steps were done in 5000 iterations

of bootstrapping:

1. Create a bootstrap sample of equal size as the original sample used in the multivariate moderation model by randomly resampling subjects with replacement.
2. Estimate bootstrap coefficients $\hat{b}_{3,p}$ from Eq. 4.2 for the bootstrap sample.
3. Obtain individual voxel bootstrap moderation coefficients $\hat{w}_i$.

For every voxel, the coefficients $\hat{w}_i$ were then sorted in ascending order. 95% confidence intervals were obtained by specifying the lower bound as the 126th value (=2.5th percentile + 1) and the upper bound as the 4875th value (=97.5th percentile). Voxels whose 95% confidence intervals did not contain 0 were then judged as significant. Apart from inferring significance, this allowed us to estimate uncertainty in the voxels' coefficients.

Validation of the CR score

In order to ensure the validity of the CR score (section 4.2.7), its moderating effect between the PL score and cognitive performance was tested in a separate moderation model using different cognitive scores on top of PACC5.

$$Performance = b_0 + b_1 \cdot BAE + b_2 \cdot PL^2 + b_3 \cdot CR_{score} \cdot PL^2 + c \cdot COV + \epsilon \quad (4.3)$$

where CR_{score} represents the subject-level weighted sum of moderation coefficients ($b_{3,p}$). BAE reflects the simpler additive effect of brain activity on performance, i.e. a score calculated analogously to the CR score but aggregating the additive components $b_{1,p}$ from Eq. 4.2 instead. In addition to PACC5 we here used a memory factor and a global cognitive factor score as dependent variables to demonstrate that the main result obtained from learning reserve patterns based on PACC5 generalizes to other cognitive scores. This validation analysis was not possible in the subset of participants without a PL score (due to biomarker unavailablility). We instead performed a similar analysis for these participants in which the PL score (in Eq. 4.3) was replaced solely by 'hippocampal atrophy' (squared). Please note that we (imprecisely) use the term hippocampal atrophy for convenience to denominate a variable that has higher values for lower hippocampal volumes instead of actual longitudinal changes in hippocampal volumes as the name might suggest. Hippocampal atrophy ranged from 0 to 1 like the PL score, with higher values representing smaller volumes, and was obtained by multiplying the TIV-corrected hippocampal volumes with -1 and then re-scaling them. Additionally, the correlation between the CR score and education as a typical CR proxy was assessed across the whole sample.

Since the above model training and analyses were cross-sectional, as a final validation step, we utilized linear mixed-effects modeling (package lme4 in R) to test the moderation effect between pathology and the CR score longitudinally. The model included a subject-specific intercept and slope, as a model comparison had suggested a model with both random intercept and slope as superior compared to one with a random intercept alone. The model examined the three-way interaction effect between the CR score, hippocampal

atrophy (squared) and time between measurements (as a continuous variable). It also included the corresponding two-way interactions. Hippocampal atrophy was used to maximize sample size for the longitudinal analysis. Age at baseline, sex, site of data acquisition, BAE and a BAE by time interaction were included as covariates. One individual was considered an extreme outlier based on their CR score (> Q3 + 3*IQR) and was thus excluded from analyses involving the CR score.

4.3 Results

4.3.1 Demographics

Our reserve analysis focused on a sample of 490 older participants of cognitively normal (including first degree relatives of AD patients and individuals with subjective cognitive decline) and cognitively impaired individuals (with aMCI or ADD) who performed task fMRI. Their demographics are presented in Tab. 4.1. The sample was on average 69.7(±5.6) years old, included slightly more females (53%) than males and was comparably well educated (14.6±2.9 years of education). The sample's mean pathological load (PL) was 0.42±0.3. PL was significantly higher in patients with ADD and aMCI compared to other groups, suggesting its validity with respect to clinical diagnosis.

Table 4.1: **Demographics of the final fMRI sample**. Values represent the mean(standard deviation). *9 participants did not have PACC5 scores. **258 participants did not have PL scores due to missing CSF data. CN = cognitively normal, SCD = subjective cognitive decline, aMCI = amnestic mild cognitive impairment, ADD = mild Alzheimer's disease dementia, ADR = AD patient first-degree relatives.

	N	Age [years]	Sex [% female]	Education [years]	PACC5	PL
CN	152	68.89(5.1)	63.2	14.57(2.7)	0.21(0.5)	0.33(0.2)
ADR	51	66(4.7)	56.9	14.49(2.8)	0.14(0.7)	0.3(0.2)
SCD	202	70.01(5.9)	44.6	15.2(2.9)	-0.04(0.7)	0.4(0.3)
aMCI	64	72.62(4.8)	53.1	13.44(2.8)	-1.22(0.8)	0.58(0.3)
ADD	21	73.36(5.4)	66.7	13.71(2.8)	-2.97(1.2)	0.84(0.2)
all	490	69.73(5.6)	53.7	14.64(2.9)	-0.19(1.0)*	0.42 (0.3)**

4.3.2 Construction of a continuous one-dimensional pathological load score

Based on the ATN framework that represents a biological characterization of AD [Jack et al., 2016], a novel data-driven index for disease severity along the AD continuum was constructed combining CSF and MRI biomarkers of ATN in a one-dimensional score. The score ranges from 0 to 1, where 0 represents minimal AD pathology and 1 means maximal AD pathology in reference to the underlying sample. As demonstrated in Fig. 4.1, the underlying continuum follows a non-linear pattern capturing dependencies across all three ATN biomarkers. More specifically, low $A\beta_{42:40}$ ratios (A), high p-tau measures

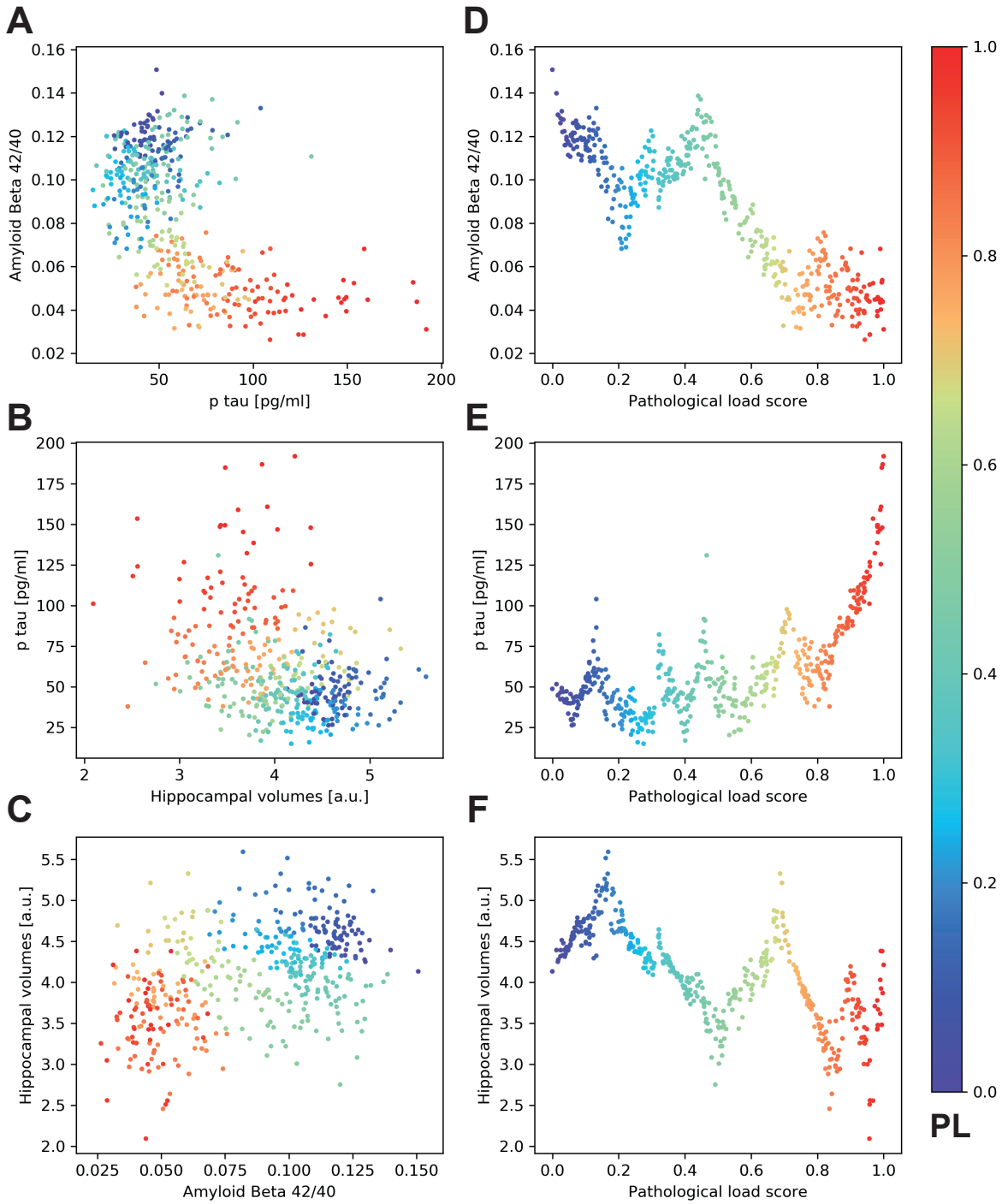

Figure 4.1: **Relationship between ATN biomarkers and data-driven PL score.** (A-C) All three possible combinations of pairs of biomarkers are shown. The points are color-coded based on the corresponding pathological load score. (D-F) Biomarkers plotted against the PL score. Hippocampal volumes refer to bilateral hippocampal volumes corrected for TIV. Please note that coloring of data points is redundant in panels D-F and was only done for illustrative purposes. Figure copied from Vockert et al. [2024] with permission.

(T), and small hippocampal volumes (N) result in high PL scores. Figs. 4.1A and C suggest that $A\beta_{42:40}$ is generally the strongest contributor to the PL score.

In the lowest range of PL scores from 0 to about 0.2, lower $A\beta_{42:40}$ ratios seem to be the main determinant of the PL score, which is thought to represent (biological) disease severity (Fig. 4.1). From roughly 0.2 until 0.5, higher values of the PL score are mainly characterized by lower hippocampal volumes (Fig. 4.1F). From there until PL scores of ca. 0.75 it is again primarily lower $A\beta_{42:40}$ ratios that contribute to a higher PL score. On the upper end of the PL score above 0.8, p-tau is the main dimension of variance (Fig. 4.1E).

Additionally, the correlation between the PL score and its single components was tested, to examine which dimension is (linearly) most strongly related to the PL score. The cross-correlations were -0.862 for $A\beta_{42:40}$, 0.670 for p-tau and -0.684 for the TIV-corrected hippocampal volumes. This confirmed the impression that the A dimension had the biggest influence on the construction of the PL score. P-tau and the hippocampal volumes are reflected in the PL score to a similar extent, with different signs. This matches the observation that AD severity is associated with higher p-tau measures and lower hippocampal volumes.

In summary, the substantial correlations of the PL score with the ATN measures suggest shared variance and hence a meaningful reduction of the AD continuum to a single dimension for our purpose.

4.3.3 Pathological load is associated with cognitive performance

As a robust marker for disease severity along the AD continuum, the PL score exhibited substantial associations with cognitive measures derived from neuropsychological testing. Notably, empirical findings indicated a non-linear relationship (Fig. 4.2), prompting a comparison of models with linear and quadratic terms for PL. Both models demonstrated a strong link between PL and PACC5, a composite measure of cognitive performance in the memory domain. The model incorporating a quadratic term displayed a superior fit ($t(400) = -11.864$, $p = 5.03 \cdot 10^{-28}$, $\beta = -0.516$, $R^2 = 0.385$) to the model with a linear term ($t(400) = -10.356$, $p = 2.00 \cdot 10^{-22}$, $\beta = -0.469$, $R^2 = 0.345$).

Since this work focuses on reserve as moderation in terms of interactions with PL, we next tested whether education as a well-established CR proxy moderated the impact of PL on cognitive performance ($t(398) = 3.914$, $p = 0.0001$, $\beta = 0.752$), which suggested the pivotal role of education in promoting factors that might contribute to the relationship between AD pathology and cognitive abilities (Fig. 4.2B). Additionally, in the interaction model, a main effect of the (quadratic) PL score was evident ($t = -6.467$, $p = 2.94 \cdot 10^{-4}$, $\beta = -1.223$), while no further independent main effect of education was observed ($t = 0.561$, $p = 0.575$, $\beta = 0.033$). The moderation model demonstrated an R^2 value of 0.441, further affirming its predictive capability.

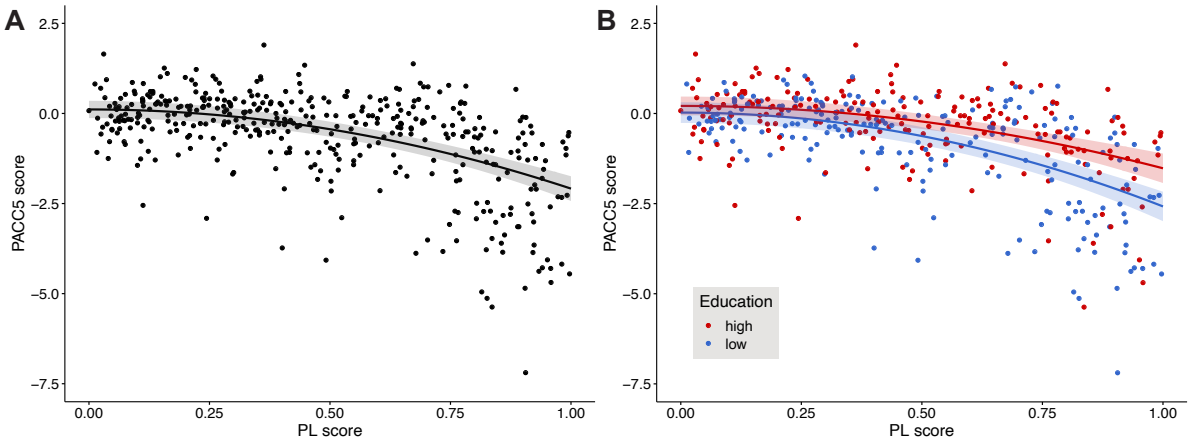

Figure 4.2: **Cognitive performance declines with higher AD pathological load.** Cognitive performance is represented by the baseline PACC5 score, which was normalized to the unimpaired sample (CN, SCD, ADR). (A) Quadratic model: $PACC5 = b_0 + b_1 \cdot PL^2 + c \cdot COV$. The black line depicts a regression model (with 95% confidence intervals) with a quadratic effect of PL. (B) Same model as in (A), but with additional terms for years of education and its interaction with the quadratic PL score. Red and blue dots refer to individuals with high and low education, respectively, as obtained by a median split. Red and blue lines are regression models for an individual with average covariate values and 17 (median of the high education group) or 12 years of education (median of the low education group), respectively. Shaded areas refer to the respective 95% confidence intervals. Figure copied from Vockert et al. [2024] with permission.

4.3.4 Identification of a CR-related activity pattern

Fig. 4.3A illustrates brain regions exhibiting heightened activity during encoding for subsequently remembered scenes (warm colors) or later forgotten ones (cool colors). In exploring cognitive reserve, we aimed to identify those spatial patterns (in terms of local voxel-level weights) from the parametric activity contrast that might moderate the impact of a subject's AD pathological load on cognitive performance using a multivariate moderation approach that predicts performance. Through cross-validation, we determined that the optimal number of PCs for the model was 7, yielding a mean cross-validation $R^2 = 0.3436$ (see Fig. S6 for cross-validation results).

Our investigation unveiled patterns of brain regions contributing both positively (depicted in Fig. 4.3B, warm colors) or negatively (cool colors) to the moderation of the relationship between AD pathology and cognitive performance. The former indicates that greater memory-related encoding activity (more positive or less negative) is linked to superior cognitive performance despite the presence of pathology. Conversely, in regions contributing negatively to the moderation patterns, more negative or less positive activity aligns with better cognitive performance amidst increased pathological burden. In other words, individuals with elevated pathology demonstrated better-than-expected cognitive performance when their BOLD signal differences between subsequently remembered and forgotten stimuli were substantial within regions bearing corresponding colors in Figs. 4.3A and B. These findings highlight the complex interplay between

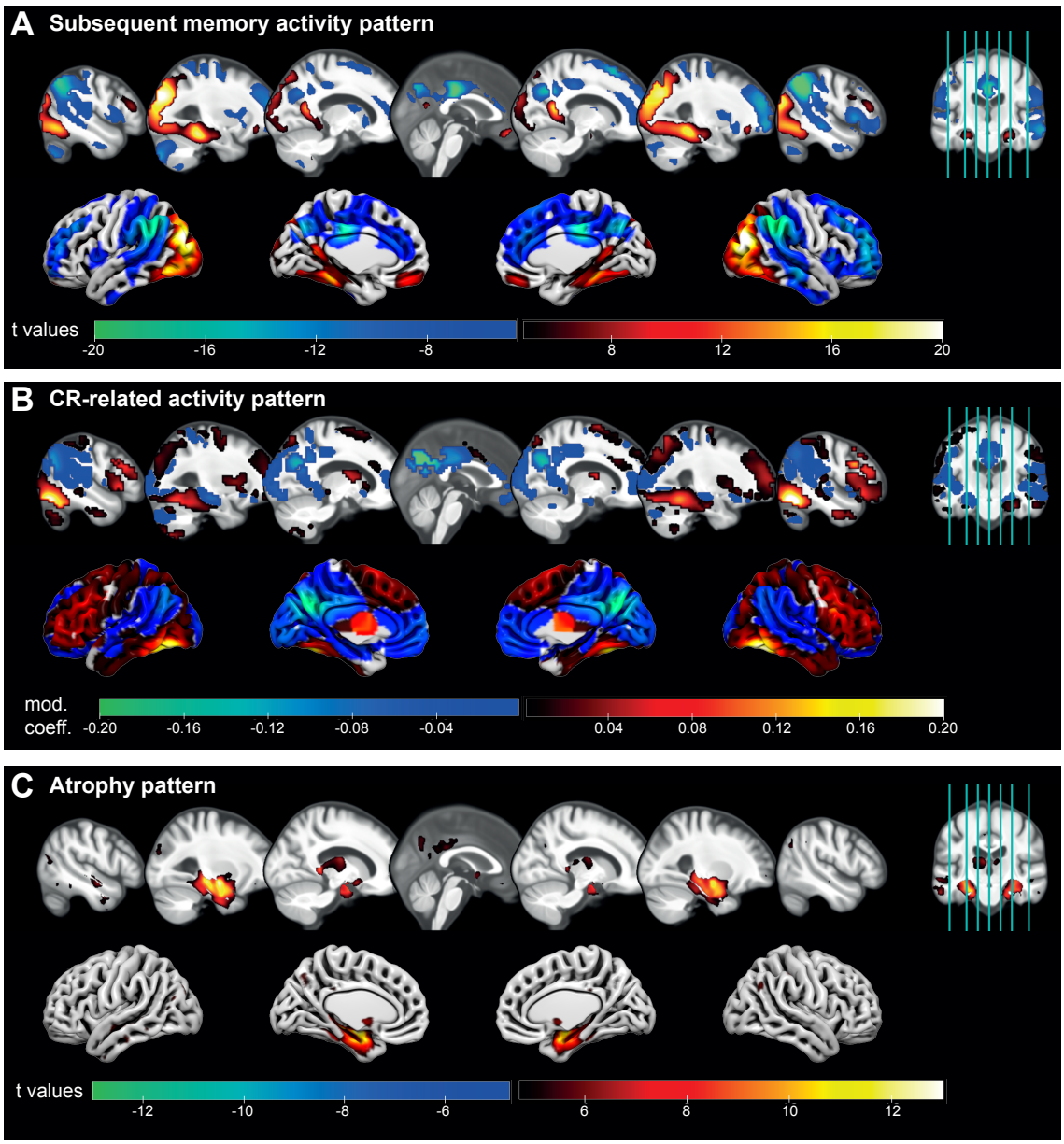

Figure 4.3: **Illustration of the CR-related activity pattern that moderates effects of pathology**. (A) Activation (hot colors) and deactivation (cool colors) during encoding of subsequently remembered compared to subsequently forgotten stimuli as identified by t-contrasts of the subsequent memory regressor in the whole fMRI sample. T values of voxels with $p_{FWE} < 0.05$ are shown. (B) Group-level CR-related activity pattern that when expressed minimizes effects of AD pathology on cognitive performance as identified via a multivariate approach. The net contribution (moderation coefficient; positive/hot colors and negative/cool colors) of every voxel to the CR-pattern is displayed (unthresholded). (C) Atrophy pattern in the whole baseline DELCODE sample as obtained by a VBM GM analysis of CN vs ADD patients. T values of voxels with $p_{FWE} < 0.05$ are shown. Figure copied from Vockert et al. [2024] with permission.

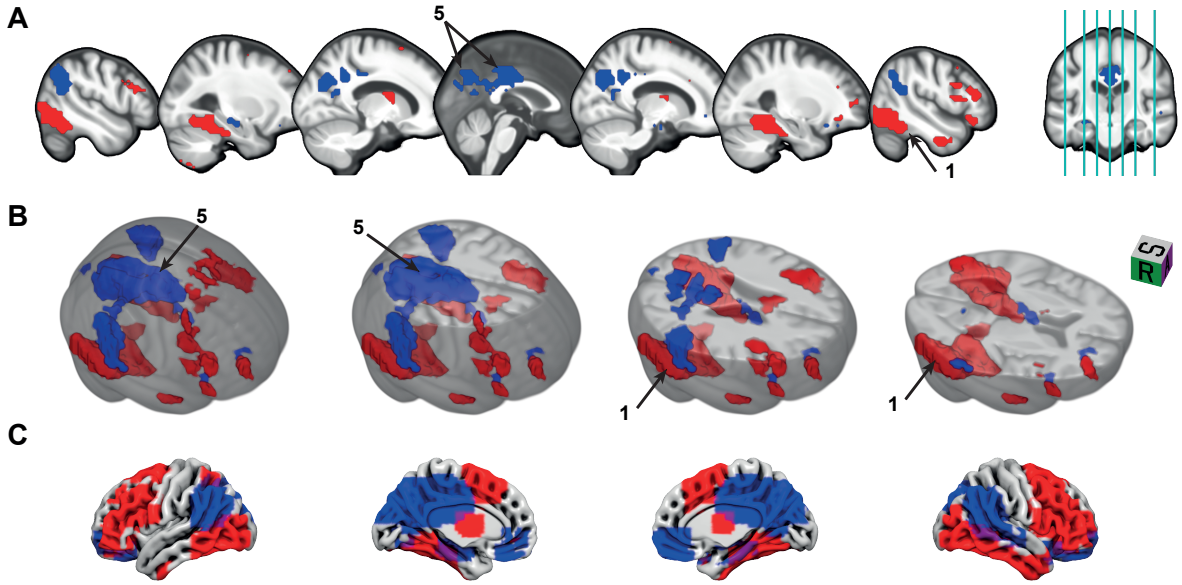

Figure 4.4: **Significant regions in the CR-related activity pattern.** Several clusters of voxels were determined via bootstrapping whose contribution to the CR pattern (w_i) was found to be significant ($p < 0.05$, see methods section 4.2.8). Displayed numbers refer to the clusters described in Tab. 4.2 with peaks in the following brain structures. 1: right inferior temporal cortex, 5: left precuneus. In panel B, small clusters have been removed for illustrative purposes. It is important to note that the CR pattern is multivariate in nature, interpretable as a whole and cluster descriptives are reported for transparency of obtained non-negligible coefficients contributing to the pattern. Figure copied from Vockert et al. [2024] with permission.

neural activation patterns and cognitive resilience.

To validate and explore the obtained CR-related activity pattern we then identified clusters with significant contributions (to moderation of the relationship between pathology and cognitive performance) using bootstrapping (Fig. 4.4 and Tab. 4.2). Brain regions with the most positive moderation effects were located bilaterally in the inferior temporal and inferior occipital cortices including the fusiform gyri and small parts of right parahippocampal cortex (clusters 1&2). To a weaker extent, parts of the frontal cortex also contributed positively to CR, especially bilateral inferior frontal gyri including opercular, triangular and orbital parts (clusters 3&4) as well as parts of right PFC (cluster 8 in Tab. S5). The strongest negative contribution to moderation were observed in bilateral precuneus, cuneus, posterior cingulate cortex (PCC; cluster 5). Slightly weaker coefficients were found in bilateral inferior parietal cortex around the angular gyrus (clusters 6&7).

Interestingly, CR-related activity patterns did not predominantly reflect regions showing atrophy in the DELCODE cohort (mostly found in the hippocampus and medial temporal lobe, Fig. 4.3C), with minor overlaps in left hippocampus, precuneus and PCC. Overall, this lack of overlap between identified CR-related regions and regions of strongest atrophy was supported by a low correlation of their coefficients of -0.102 (Figs.

Table 4.2: **Significant clusters in CR-related activity pattern.** Structures and peak voxels were identified in MRIcroGL, using the AAL (Automated Anatomical Labeling) atlas [Tzourio-Mazoyer et al., 2002]. 'w_i' refers to the CR coefficient of a voxel i. '% concordant' refers to the proportion of voxels in the cluster that have the same valence (sign) for the CR coefficient and the parametric subsequent memory contrast coefficient as shown in Fig. 4.5. A concordant region is one where a higher/lower activity reduces effects of pathology and which is typically activated/deactivated during the task. Clusters smaller than 50 voxels (voxel size: 3.5x3.5x3.5mm) have been omitted. It is important to note that the CR pattern is multivariate in nature, interpretable as a whole and cluster descriptives are reported for transparency of obtained non-negligible coefficients contributing to the pattern.

#	**Mean w_i**	**Size [voxels]**	**% concordant**	**Peak[x,y,z]**	**Peak Structure**
1	0.100	623	100	49,-63,-17	Temporal_Inf_R
2	0.085	594	100	-49,-66,-17	Occipital_Inf_L
3	0.055	149	79.19	49, 14, 28	Frontal_Inf_Oper_R
4	0.075	119	93.28	-49, 25, 24	Frontal_Inf_Tri_L
5	-0.105	873	90.38	0,-60, 32	Precuneus_L
6	-0.067	235	97.45	-45,-63, 35	Angular_L
7	-0.048	213	100	52,-56, 39	Parietal_Inf_R

4.3B and C).

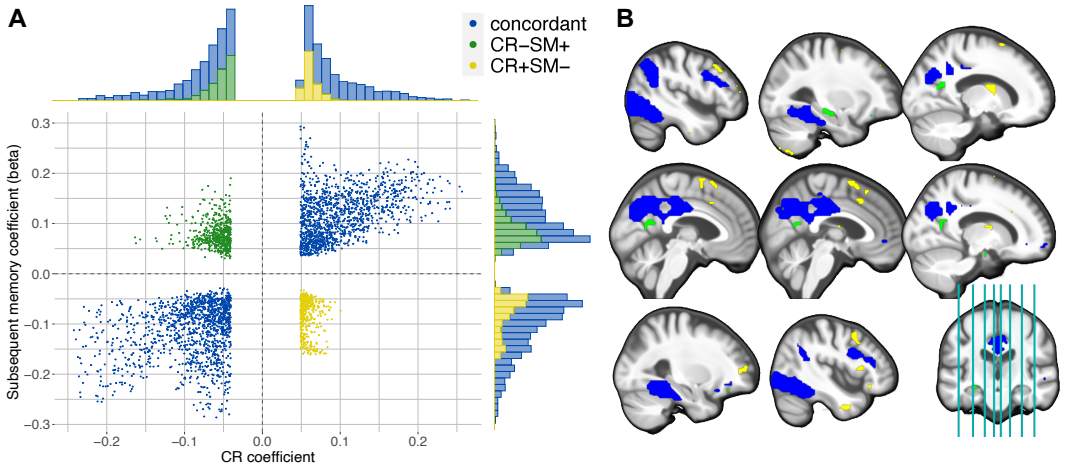

Figure 4.5: **CR pattern and the subsequent memory contrast predominantly align.** (A) The scatter plot displays the CR coefficients w_i and subsequent memory contrast coefficients (beta) for every voxel with significant contribution to CR. They form three groups: 1. Concordant voxels, in which both coefficients have the same sign (blue); 2. positive CR coefficient, but negative subsequent memory beta (CR+SM-; yellow); 3. negative CR coefficient, but positive subsequent memory beta (CR-SM+; green). The histograms display the frequency of the voxels in the corresponding groups. The gray dashed line separates the four quadrants. (B) The CR-related activity pattern is shown color-coded corresponding to the colors in panel A. It is important to note that the CR pattern is multivariate in nature, interpretable as a whole and cluster descriptives are reported for transparency of obtained non-negligible coefficients contributing to the pattern. Figure copied from Vockert et al. [2024] with permission.

To delve deeper into our comprehension of the identified pattern, we conducted an examination of the overlap between the CR-related activity pattern and the generic subsequent memory activity pattern (illustrated in Fig. 4.3A). A substantial concurrence between these patterns was observed in the most extensive clusters of CR-related deactivations, notably in regions such as the precuneus, posterior cingulate cortex (PCC), angular gyrus and ACC, and activations, particularly in inferior temporal areas (Fig. 4.5, blue). Within those regions a higher reserve is reflected by an increase in the 'amplitude' of the task-related activation/deactivation. However, it was also apparent that reserve is not uniformly contributing across this task-active network and that certain regions exhibiting significant (de)activation during successful memory encoding did not substantially contribute to cognitive reserve at all (such as portions of the parietal, frontal, temporal, particularly occipital cortex, as well as the cerebellum and basal ganglia).

Moreover, a striking observation emerged in a few brain regions where the valence of the coefficients did not align, a phenomenon we term "discordant" (Tab. 4.2, Fig. 4.5). For instance, voxels surrounding the calcarine sulci (parts of the bigger cluster 5), bordering the cuneus and precuneus, displayed activation during successful encoding but exhibited a negative contribution to CR (CR-SM+, green in Fig. 4.5). This trend was also observed in the left hippocampus and medial orbitofrontal regions. Conversely, positive contributions to CR were evident in certain right frontal areas, such as the insula and mid/superior orbitofrontal cortex (e.g. parts of clusters 3&4; CR+SM-, yellow in Fig. 4.5), despite subsequent memory-related deactivation. Taken together, the correlation between the voxelwise CR coefficients and SM contrast values were found to be 0.384. This suggests that predominantly showing activation patterns closer to the typical activation/deactivation might support cognitive functioning. On the other hand, more complex region-specific multifaceted relationships between these neural signatures and cognitive reserve might exist, indicated e.g. by discordant voxels.

Next, we exemplify how subsequent memory-related activity moderates the detrimental effect of pathology (PL score) on cognitive performance in two brain regions located in right inferior temporal cortex (Fig. 4.6A) and around bilateral cuneus/precuneus/PCC (Fig. 4.6B), respectively (taking clusters 1 and 5 from Fig. 4.4 and Tab. 4.2). The moderation effect has unveiled a notable phenomenon: as levels of pathological load (PL) rise, the disparities in cognitive performance between individuals with high and low levels of (de)activation become increasingly apparent. Among individuals with high PL, those with high SM contrast values have cognitive ability at the level of individuals with low PL.

4.3.5 CR score moderates effects of pathology on cognitive performance, also longitudinally

Utilizing the CR-related activity pattern that we identified above, we next derived individualized CR scores. To ascertain its validity as an indicator of cognitive reserve, we expected it to (i) moderate the effect that pathology has on independent cognitive performance measures; (ii) moderate longitudinal cognitive decline; and (iii) be correlated with sociobehavioral proxies of CR according to the consensus research criteria [Stern

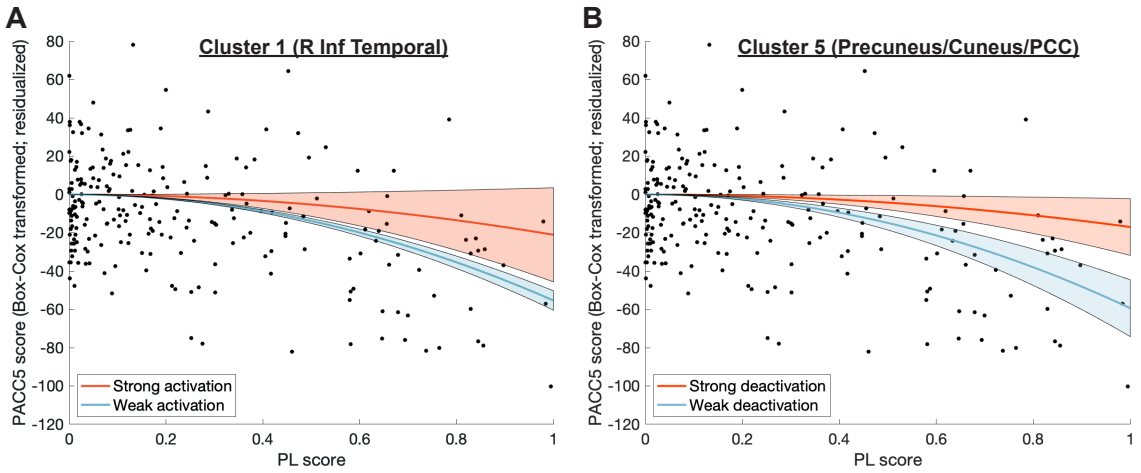

Figure 4.6: **Subsequent memory-related activity moderates relationship between PL and PACC5.** The relationship between the PL score and the PACC5 score (Box-Cox transformed and residualized for covariates) is moderated depending on the subsequent memory-related activity in two previously identified clusters (see Tab. 4.2 or Fig. 4.4). (A) Moderation effect of activation in cluster 1 located around the inferior temporal cortex including fusiform gyrus (positive moderation coefficients). (B) Moderation effect of deactivation in cluster 5 including bilateral cuneus and precuneus as well as posterior cingulate (negative moderation coefficients). The red lines in both panels depict the predicted PACC5 score for a hypothetical individual with an activation 1 std above the mean, the blue lines for an activation 1 std below the mean in the respective cluster. The shaded areas represent the 95% confidence intervals. Black dots represent the individual subjects' values for PL and (transformed + residualized) PACC5. Figure copied from Vockert et al. [2024] with permission.

et al., 2020].

Our results affirmed the first criterion, demonstrating a moderation effect of the CR score on the relationship between the (quadratic) PL score and cognitive performance across various cognitive tests (Fig. 4.7A). This moderation effect was evident for the latent memory factor ($t(218) = 7.224$, $p = 8.38 \cdot 10^{-12}$, $\beta = 0.381$), the domain-general factor ($t(218) = 5.814$, $p = 2.15 \cdot 10^{-8}$, $\beta = 0.325$) and the PACC5 score ($t(214) = 8.338$, $p = 9.15 \cdot 10^{-15}$, $\beta = 0.447$), which was originally used in identifying the CR-related activity pattern. Importantly, this moderating effect was not only observed in individuals with cognitive impairment, i.e. aMCI and AD patients, but also when analyzing the same models only in cognitively unimpaired individuals (memory factor: $t(171) = 4.223$, $p = 3.91 \cdot 10^{-5}$, $\beta = 0.273$; domain-general factor: $t(171) = 3.358$, $p = 0.0010$, $\beta = 0.220$; PACC5: $t(170) = 4.781$, $p = 3.77 \cdot 10^{-6}$, $\beta = 0.301$). This emphasizes that the fMRI activity patterns associated with CR might benefit a broad spectrum of cognitive abilities.

Furthermore, in the remaining sample without a PL score (due to missing CSF data) the same CR score exhibited a weaker yet significant moderation effect on the association between AD pathology and cognitive performance (see Fig. 4.7B) for the latent memory factor ($t(244) = 3.697$, $p = 1.17 \cdot 10^{-6}$, $\beta = 0.202$), domain-general factor ($t(244) = 2.346$,

p = 0.020, β = 0.138) and PACC5 score (t(240) = 4.958, p = $1.35 \cdot 10^{-6}$, β = 0.271). Here, the PL score was replaced by hippocampal atrophy (squared, as the PL score).

In a longitudinal context, lower hippocampal volumes at baseline worsened cognitive

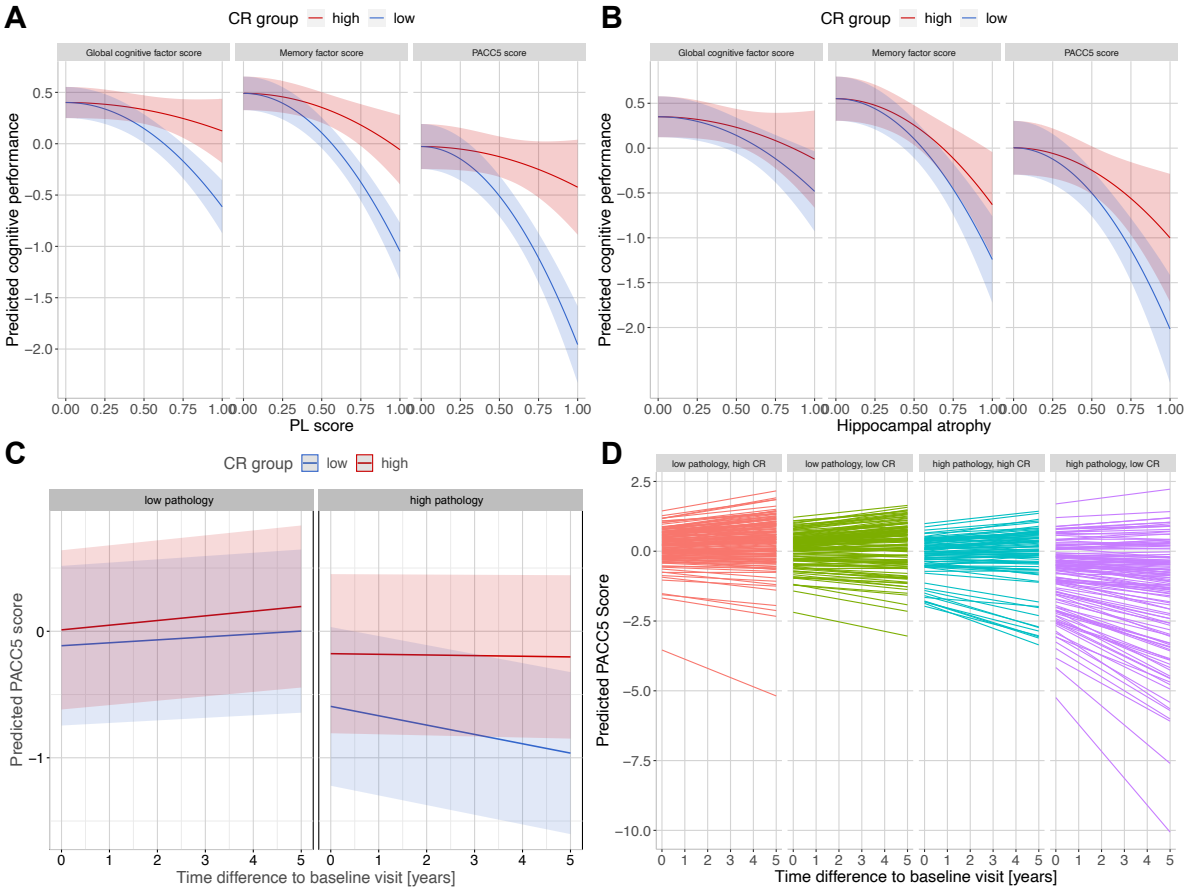

Figure 4.7: **CR score is linked to cognitive performance cross-sectionally and longitudinally.** (A) The relationship between the PL score and cognitive performance at baseline is moderated by the CR score. Cognitive performance is represented by three different scores: a global cognitive factor score, a memory factor score and the PACC5 score (previously used for identification of the CR-related activity pattern). Cognitive performance was predicted using the respective regression model for an average individual with high (above median; red curve) or low (below median; blue curve) CR score. (B) In the sample without PL score, the CR score moderates the relationship between smaller hippocampal volumes and cognitive performance. (C) The pathology-dependent differences in longitudinal trajectories of cognitive performance are ameliorated by the baseline CR score. The PACC5 scores at 5-year follow-up were predicted using the previously described LME (see methods section) fitted on the original longitudinal data for an average individual with high (above median; red line) or low (below median; blue line) CR score and high or low pathology (here represented by high and low hippocampal atrophy corresponding to the 25th and 75th percentile). (D) Predictions of all individual cognitive trajectories. Individuals were categorized as high/low CR based on their above/below average CR scores and as low/high pathology based on their below/above average hippocampal atrophy. Shaded areas in panels A-C denote 95% confidence intervals. Figure copied from Vockert et al. [2024] with permission.

decline rates in the PACC5 score (t(158.6) = -5.717, p = $5.24 \cdot 10^{-8}$, β = -0.140) in the whole sample. The CR score attenuated this relationship (three-way interaction of CR score, atrophy and time; t(124.5) = 3.974, p = $1.19 \cdot 10^{-4}$, β = 0.118), suggesting that activity patterns during memory encoding hold the potential to influence cognitive trajectories in the face of pathology (Fig. 4.7C and D). There was also an interaction of the CR score with hippocampal atrophy (t(487.6)= 6.790, p = $3.28 \cdot 10^{-11}$, β = 0.338) as in the cross-sectional models. Moreover, the CR score exhibited a positive correlation with education across the entire sample (r = 0.114, p = 0.012).Collectively, these findings robustly support the contention that the obtained CR score is intimately associated with cognitive reserve, both in cross-sectional and longitudinal assessments.

4.4 Discussion

In this study, we combined multiple ideas to investigate the neural implementation of cognitive reserve utilizing task fMRI data from a substantial sample comprising 490 participants. First, we employed the most contemporary research criteria governing CR assessment via functional neuroimaging [Stern et al., 2020, 2023]. Second, in order to enable this moderation approach we reduced the dimensionality of AD biomarkers in a non-linear fashion, introducing a novel data-driven index quantifying Alzheimer's disease-related pathological load. Third, we pioneered a novel multivariate approach to modeling reserve, which uncovered a task-related functional activity pattern capable of moderating the impact of brain pathology on cognitive performance. Fourth, we provided both cross-sectional and longitudinal validation of the proposed activity pattern of cognitive reserve. Our findings illuminate a compelling connection: older individuals whose brain responses during successful memory encoding more closely align with this identified pattern exhibit diminished cognitive deficits when faced with AD pathology. Moreover, a more pronounced expression of this activity pattern was associated with a slower rate of cognitive decline over longitudinal follow-ups and especially attenuated the detrimental effect of pathology on cognitive trajectories.

In healthy young individuals and older adults, episodic memory encoding is associated with a highly replicated "canonical" pattern of brain activation in some regions and deactivation in other regions [Kim, 2011, Soch et al., 2021a]. We found that a more pronounced expression of this canonical activation/deactivation pattern was associated with higher cognitive reserve. CR was especially characterized by a stronger activation during memory encoding in inferior occipital and inferior temporal areas including the fusiform gyrus, i.e. parts of the ventral visual stream. Some frontal areas showed a similar contribution to CR, though to a smaller extent. CR was further characterized by stronger deactivation in the posterior cingulate cortex, precuneus, cuneus and lateral parietal cortex including angular gyrus, regions that are considered to be part of the DMN [Buckner et al., 2008]. This combined pattern of inferior temporal activations and DMN deactivations has previously been associated with better memory performance in older adults [Maillet and Rajah, 2014, Richter et al., 2023, Soch et al., 2021a] and, more recently, with severity across the Alzheimer's risk spectrum [Soch et al., 2024].

These findings shed new light on the neural implementation of CR. As the majority of brain regions showed concordant activity for CR and successful memory encoding, cognitive reserve primarily seems to be associated with continued recruitment of core cognitive circuits. This indicates that some individuals are able to maintain functional integrity in parts of the core cognitive circuitry despite the presence of AD pathology. Generally, significant decreases in fMRI activity in regions of the DMN have been shown to co-occur with amyloid deposition in older adults [Buckner et al., 2005, Sperling et al., 2009]. Furthermore, AD has been characterized with impairment of regional cerebral blood flow and regional glucose metabolism during resting-state, predominantly in temporo-parietal regions [Frackowiak et al., 1981, Silverman et al., 2001]. Hence, the ability to maintain core functional circuits might represent resilience against pathological changes like neurodegeneration and Aβ accumulation, possibly accompanied by conservation of glucose metabolism. Our findings suggest that this ability is central to CR. The neural mechanisms underlying this ability are still unclear. An attempt to identify additional factors related to the CR score (seeFig. S9) did not reveal associations with resting-state functional connectivity within the DMN or other large-scale networks nor mean task signal, although a partial moderation of the DMN BOLD signal by resting-state fluctuation amplitude cannot be excluded [Kizilirmak et al., 2023]. One possibility is that pathology within core circuitry can be counteracted by non-affected neural populations. The weak, yet significant relationship between the CR score and GM volumes in CR-related regions indeed suggests it as a small contribution (Fig. S9). This possibility is further supported by the pattern of spread of tau-pathology within brain tissue where selective cellular vulnerability leads to dysfunction in specific neuronal subpopulations [Chen et al., 2022a, Delpech et al., 2021]. Another possibility is that there are individual differences in pathology that were not quantified in the PL score. These include inflammation, vascular supply and clearance [Bernal et al., 2023, Brosseron et al., 2022, Dörner et al., 2024, Hayek et al., 2024]. It is possible that individuals who are capable of maintaining function in core circuitry despite of tau, amyloid and hippocampal neurodegeneration have less expression of these additional pathologies. A weak negative correlation between white matter hyperintensity volumes and the CR score supports this hypothesis (see also Fig. S9). In conclusion, our findings primarily support the notion that some CR factors might operate within core circuits themselves above compensatory activity discordant with successful encoding activity.

Some brain regions within the canonical episodic memory activity network were not associated with CR. Visual areas showed strong activation in the subsequent memory contrast due to the visual nature of the memory task, but did not contribute substantially to cognitive reserve. These regions have not been discussed much in the context of CR, although there has been scattered evidence for a contribution of inferior and middle occipital regions [Habeck et al., 2018].

Encoding-related activity in the hippocampus was discordant with cognitive reserve. Thus, although the hippocampus is well-known to be activated during successful memory encoding, weaker left hippocampal activity during encoding was associated with better cognitive performance in the presence of AD pathology. This aligns with observations regarding hyperactivity of the hippocampus in an Aβ- and especially tau-dependent

manner that is not related to better cognitive performance [Huijbers et al., 2019, Maass et al., 2019, Sperling et al., 2009]. An absence of pathology-related over-activation in the hippocampus might actually be beneficial for cognitive performance and clinical progression. The calcarine sulci (part of cluster 5) and right medial orbitofrontal regions show the same kind of discordant activity for successful memory encoding versus CR. Some frontal regions including the insula and mid/superior orbitofrontal cortex were deactivated during successful memory encoding and have positive moderation coefficients, indicating better cognitive performance with weaker deactivation. Yet, it is also conceivable that decreased activity in these regions itself is not actually beneficial for cognitive performance, but systematically co-occurs with beneficial activity changes in other regions. Similar to our findings regarding discordant regions, previous reports have identified comparable phenomena. For instance, Elman et al. [2014] discovered a cluster in medial parietal cortex in which deactivation was parametrically modulated by the level of memory encoding detail across the entire sample of young and older adults with and without Aβ. In this cluster, greater deactivation was associated with higher detail recall. However, young adults exhibited no such deactivation, resembling our observations of discordant regions.

Generally, the strongest negative contributions to CR were observed in the cuneus, angular gyri, PCC and particularly the precuneus. This is in line with a large body of evidence highlighting the role of the DMN in cognitive reserve. For instance, deactivations of the left precuneus [Bosch et al., 2010, Stern et al., 2018] and posterior cingulate [Bosch et al., 2010] were associated with CR in previous studies. Moreover, the precuneus together with the cingulate gyrus contributed negatively to some aspects of a CR-related fMRI pattern [Stern et al., 2008]. Connectivity-based methods provide additional evidence for DMN contribution. For instance, using a task-potency method, which captures a brain region's functional connectivity during task performance after adjusting for its resting-state baseline, the DMN has been found to be the predominant contributor to a task-invariant CR network [van Loenhoud et al., 2020]. Furthermore, inhibitory information flow from inferior temporal cortex, which showed a positive contribution to CR in this study, to the precuneus has been associated with better memory performance in an independent cohort of older adults, using the same encoding task [Schott et al., 2023]. Additionally, Stern et al. [2021] suggested that connections involving the DMN might be weaker at rest in individuals with higher IQ. Our findings provide further evidence that stronger deactivation of some DMN regions is related to CR.

The ACC has also previously been identified in the context of cognitive reserve, e.g. as part of the task-invariant CR pattern of [Stern et al., 2018]. Moreover, greater volume and metabolism in the ACC were found to be related to higher levels of education [Arenaza-Urquijo et al., 2013a]. It was further identified as part of a 'resilience signature' whose metabolism was associated with global cognitive performance in cognitively stable individuals older than 80 years [Arenaza-Urquijo et al., 2019]. Here, we only observed a few significant voxels around the ACC with negative contributions to CR, providing weak additional evidence for an involvement of the ACC in cognitive reserve.

The strongest positive contributions to CR were observed in the fusiform gyri and surrounding temporal to inferior occipital regions. With respect to the fusiform gyrus,

there has been both evidence for negative as well as positive contributions to CR [Habeck et al., 2018, Stern et al., 2008]. Further, some frontal regions have been proposed to play a role in cognitive reserve. For instance, Franzmeier et al. [2017b] discovered that global connectivity of the left frontal cortex attenuated the relationship of precuneus FDG-PET hypometabolism (as proxy for AD severity) on lower memory performance in amyloid-positive individuals with aMCI. The left frontal cortex also showed positive contributions to CR in our study (cluster 4 in Tab 4.2; see also Fig. 4.4). Likewise, left prefrontal cortex connectivity both within and outside the frontoparietal network has been found to correlate with fluid intelligence as a proxy of CR [Cole et al., 2012].

The expression of this CR activity pattern in an individual, as represented by the task-derived CR score, further fulfills the latest research criteria on CR. First, the CR score moderates the effect of pathological load on cognitive performance. Hence, individuals with lower cognitive reserve scores show a stronger non-linear decline in their cognitive abilities with increasing pathological burden compared to individuals with higher levels of cognitive reserve. The CR score retains its disease-moderating characteristic in the context of multiple different cognitive scores like an independent composite memory measure as well as a very broad measure of cognitive abilities spanning learning and memory, language, visuospatial abilities, executive function and working memory. This reveals a certain robustness of the moderating effect of the CR score and supports its validity. Importantly, the CR score ameliorated the negative influence that baseline pathology had on cognitive trajectories over longitudinal follow-ups, stressing its significance not only for present cognitive abilities, but also for their development over time. Furthermore, the CR score was related to education, even though the correlation was found to be rather low to moderate. On the one hand, this could mean that our CR score might capture cognitive reserve incompletely due to the apparent task-dependency. On the other hand, the correlation should not be close to 1 either, since education itself is only a proxy of CR. Thus, education and CR as identified via functional neuroimaging approaches do share parts of their variance, but are also partially independent.

Taken together, the moderating effect of the obtained CR score and its relation to another sociobehavioral CR proxy suggest it as a valid, even though incomplete representation of overall cognitive reserve. It also provides evidence that the underlying network indeed contributes to CR, at least in context of the incidental encoding task at hand.

This study has a number of limitations. The approach was enabled by dimensionality reduction of ATN via the t-SNE method, which provided us with a useful tool for quantifying pathological load. Yet, the PL score is a purely cross-sectional construct that is agnostic for the order of events along the disease progression towards Alzheimer's disease and cannot be interpreted as a sequence of events. In fact, according to the prevailing model of the Alzheimer's pathological cascade, abnormal levels of Aβ are the initiating event in AD [Jack et al., 2010], followed by abnormal tau levels and neurodegeneration. However, we found that hippocampal volumes already showed a strong contribution to increasing PL scores at its lower levels, which would indicate atrophy as an early pathological change. It may further be an oversimplification to represent the ATN system of AD biomarkers by a single variable. Likewise, while hippocampal atrophy is a

key feature of AD, it is an oversimplification to represent neurodegeneration solely by hippocampal measures.

The challenges for a dimensionality reduction method in this context are manyfold. t-SNE tries to maintain neighborhood relationships between data points in lower-dimensional spaces. As one could theoretically find four mutually equidistant data points in a three-dimensional space, there is no way to accurately retain these distances in a one-dimensional space. This is part of a challenge known as the "crowding problem" [Van Der Maaten and Hinton, 2008]. Since space in one dimension is comparably limited, data points that are farther removed from the majority of data points in the original space will be pushed closer together in the lower-dimensional space. As a consequence, the distribution of PL scores appears rather uniform (see Fig. 4.1 and Fig. S5). Given the composition of the sample, which has an over-representation of individuals devoid of even early clinical symptoms, more severe AD biomarker profiles might not be represented faithfully in the PL score, as the algorithm tries to the preserve the distances between the many less progressive AD biomarker profiles. On the other side, also age-related and non-AD related pathological changes (e.g. of vascular origin) might contribute to hippocampal atrophy and cognitive decline in our sample. This might be responsible for the stronger contribution of hippocampal volumes to lower PL scores. Furthermore, the influence of uncaptured covariates should not be underestimated. However, even if the sample uniformly represented individuals across different stages of the AD continuum, recent evidence for distinguishable AD subtypes (see e.g. Vogel et al. [2021]) indicate the potential presence of multiple differential biomarker trajectories. In concert, these challenges might explain the unexpected pattern of trajectory reversals of the biomarkers with increasing PL scores that can be observed in Fig. 4.1.

Strong associations with the three biomarkers as well as with cognitive performance nevertheless suggest the PL score as a meaningful index of overall disease severity (rather than disease progression) for the purpose of this study. In fact, usage of three alternative methods (PC analysis, spectral embedding, diffusion pseudotime [Haghverdi et al., 2016]) produced highly correlated PL scores that in turn yielded very similar CR coefficients (see Figs. S13-S15), indicating that, within reason, the method for obtaining a PL score has only a minor influence on the results. Regional quantification of tau pathology using tau-PET, rather than the regionally agnostic fluid biomarker-based tau measurement here, could in future help to determine to what extent the recruitment of the CR regions depends on the absence of tau pathology in those regions. Despite its limitations, t-SNE or other non-linear dimensionality reduction tools like spectral embedding and Laplacian Eigenmaps among many others (see e.g. Van Der Maaten et al. [2009] for an overview) or even trajectory inference methods like diffusion pseudotime (see e.g. Saelens et al. [2019]) might be useful in many other studies investigating multidimensional disease-related phenomena.

Furthermore, our multivariate regression approach relied on reducing the complexity of fMRI data via PC analysis. As a consequence the moderation analysis might represent an incomplete characterization of CR in the context of successful memory encoding. As the difference in mean cross-validation R^2 was small in comparison to its variability, other choices for the number of principal components (from 2-9) also appear reasonable.

Consequently, we would like to note that this model hyperparameter is a non-negligible determinant of the results, susceptible to the bias-variance tradeoff. In particular, a model with only two PCs (shown in Fig. S12) was found to be too restrictive considering the obtained worse model generalization (in cross-validation) and further validation analysis results (not shown). To support the confidence in the presented results, we provide an illustration of the overlap of CR regions in dependence of the number of PCs and a comparison of models with different numbers of PCs in Fig. S10.

The approach was applied under the simple working assumption that pathology is the initial driver of cognitive decline, and that individual variations of task-related activity potentially affect this relationship. However, since the proposed main approach using cross-sectional data exploits simple correlations and symmetric interaction terms, it does allow for several alternative causal interpretations with inter-changed roles of key variables. Future longitudinal studies might focus deeper on the empirical plausibility of these alternative patterns of interplay.

Moreover, one might consider learning the moderating function of brain activity $f(A)$ and its interactions with pathology (see methods Eq. 4.1) more directly using neuronal nets and other data-driven approaches [Murphy, 2018]. Additionally, CR is treated as a static measure in this study, contrasting with CR's conceptualization as a dynamic entity, susceptible to variation over time [Bettcher et al., 2019, Lenehan et al., 2016]. However, our approach theoretically allows to represent CR in a dynamic manner by incorporating longitudinal fMRI data. Furthermore, the current study focuses on an approach that assumes sample-level identification of reserve patterns, while ignoring the possibility that CR might actually be implemented differently across different subpopulations or disease stages. For instance, CR-related activity patterns might differ between early and late disease stages [Billette et al., 2022] or males and females (see Figs. S16 and S17). Our search (or model input-) space was limited to the widespread successful encoding network, restricting our ability to identify regions that show compensatory activity to these areas. An analysis extending this search space to all gray matter indicated CR regions essentially as a resemblance of the successful encoding network (Fig. S11). However, we also advise against overinterpretation of these findings, since we cannot exclude the possibility of compensatory activity in other tasks or fMRI contrasts. Last, we remark the dependency of the CR-related activity pattern on the task and contrast at hand. We recognize the efforts of task-invariant approaches to identify an underlying pattern of CR that is task-independent and note that the presented multivariate model could be extended to accommodate multi-task data, memory-independent contrasts, other indicators of pathology, or other forms of reserve-related imaging features such as resting-state fMRI as well. Nonetheless, apart from task-specific components the presented CR activity pattern most likely also contains task-invariant components, e.g. the DMN and ACC. Furthermore, since our contrast probes memory, which is the earliest and most strongly affected faculty in AD, our specific CR-related activity pattern is of great significance in the context of (AD) dementia.

In summary, using a multivariate approach to modeling CR we have identified a memory encoding-based activity pattern of cognitive reserve in the context of successful memory encoding according to the latest research definitions. We provide further evi-

dence for the hypothesis of a generic role of the DMN and potentially ACC in cognitive reserve. Additionally, we identified regions less commonly associated with cognitive reserve like the fusiform gyrus and some frontal regions. Overall, our findings suggest an enhanced maintenance of core cognitive circuits as the primary neural implementation of cognitive reserve. Consequently, interventional efforts should incorporate methods to maintain the functionality of core cognitive circuitry, for instance through direct brain stimulation, in order to ameliorate future cognitive decline. However, adequate judgment about compensation in the context of cognitive reserve should be based on further studies specifically designed for its investigation, involving multi-task and -contrast information as well as manipulation of task demand. Ultimately, more longitudinal studies are necessary to assess the degree of dynamics of CR over time and its ability to modulate trajectories of cognitive decline. Furthermore, CR patterns have only been assessed on the group-level, assuming CR works similarly across all individuals. Upcoming approaches should account for individual differences in functional (re)organisation, considering individual-level expressions of cognitive reserve.

4.5 Contributions

The study was done in a huge collaborative effort with the DELCODE study group from multiple DZNE sites. Overall design, implementation and collection of data for the DELCODE study at the different study sites was provided by Enise I. Incesoy, Hartmut Schütze, Oliver Peters, Daria Gref, Luisa S. Schneider, Lukas Preis, Josef Priller, Eike J. Spruth, Slawek Altenstein, Anja Schneider, Klaus Fliessbach, Jens Wiltfang, Ayda Rostamzadeh, Wenzel Glanz, Stefan Teipel, Ingo Kilimann, Doreen Goerss, Christoph Laske, Matthias H. Munk, Peter Dechent, Stefan Hetzer, Klaus Scheffler, Björn H. Schott, Frank Jessen and Emrah Düzel. Luca Kleineidam, Enise I. Incesoy, Jose Bernal, Renat Yakupov, Annika Spottke, Nina Roy, Michael T. Heneka, Frederic Brosseron, Michael Wagner, Steffen Wolfsgruber, Laura Dobisch and Emrah Düzel provided core methodological data. I conceptualized the present data analysis together with Anne Maass and Gabriel Ziegler. Judith Machts, Enise I. Incesoy, Jose Bernal, Renat Yakupov, Peter Zeidman, Gabriel Ziegler and I preprocessed the MRI data. I performed the statistical analyses, the present methodology (PL score, multivariate moderation model including cross-validation and principal component analysis, CR score) and visualizations. I wrote the initial draft of the manuscript, which was reviewed and edited by Judith Machts, Luca Kleineidam, Aditya Nemali, Enise I. Incesoy, Renat Yakupov, Michael Wagner, Peter Zeidman, Yaakov Stern, Björn H. Schott, Emrah Düzel, Anne Maass and Gabriel Ziegler. Anne Maass and Gabriel Ziegler supervised the present project equally.

5 General Discussion

5.1 Summary

The work presented in this thesis aids the understanding of different mechanisms of resilience to aging and disease. In the first two studies, structural and functional aspects of hippocampal vascularization were investigated with ultra-high field MRI at 7T. This enabled the visualization of small hippocampal branches that allowed for the classification of the HVP and the usage of VDM of the hippocampus in relation to its surrounding arteries. The first study expanded on recent observations of an involvement of the HVP in resilience [Perosa et al., 2020]. It linked an augmented hippocampal vascular supply to global cognitive performance via higher total gray matter volumes in the form of a mediation analysis. This indicates that the HVP exerts its cognitive benefits via structural correlates, i.e. the resilience mechanism that the HVP seems to boost is either brain reserve or brain maintenance [Stern et al., 2023].

The second study built on the knowledge gained in the first study by examining the relation of hippocampal vascularization with cognition and brain structure in young adults. For this purpose, hippocampal vascularization was characterized more thoroughly, extending the vascular features by tortuosity and cerebrovascular reactivity. The study revealed no compelling associations between hippocampal vascularization and brain structure in young adults, indicating that better hippocampal vascularization does not establish greater neural resources in young adulthood. In reconciliation of the findings from the first two studies, the hippocampal vascularization pattern seems to protect the brain from age- and pathology-related loss of structural integrity and preserve cognitive function in this manner.

The third study took a different approach to resilience, away from factors potentially conveying brain structural benefits. Instead, it provided a functional perspective using fMRI and helped to progress understanding of the neural underpinnings of cognitive reserve. It mainly provided evidence that maintained or reinforced engagement of core cognitive circuits, especially the default mode network and the anterior cingulate cortex, helps to retain cognitive performance in the presence of aging and early Alzheimer's disease pathology.

5.2 Role of hippocampal vascularization in resilience to aging and brain disease

The structure of the hippocampal vasculature in humans has not been an extensive topic of research. Most knowledge is based on post-mortem studies, which meant to inform surgical procedures [Erdem et al., 1993, Fernández-Miranda et al., 2010, Huther

et al., 1998, Marinković et al., 1992]. Advances in ultra-high field MRI over the past couple of years have enabled a fine-grained examination of the hippocampal vasculature in vivo, including the classification of hippocampal vascularization patterns [Spallazzi et al., 2019]. A pattern of hippocampal blood supply with combined contributions of the PCA and AChA has been associated with better cognitive performance in older adults with and without cerebral small vessel disease [Perosa et al., 2020]. The thesis at hand demonstrated greater local volumes of the anterior hippocampus and ERC in augmented supply individuals of the same cohort, matching the perfusion territory of the AChA in dual-supply hemispheres [Erdem et al., 1993, Fernández-Miranda et al., 2010, Huther et al., 1998]. An augmented supply might have benefits for structural integrity beyond the ipsilateral MTL, as shown for the ERC contralateral to a dual-supply hemisphere in this thesis. Such structural covariance between homotopic structures, as also previously observed by Mechelli et al. [2005], might be driven by activity-dependent plasticity through connections between homotopic regions. Benefits of an augmented hippocampal supply seem to reach beyond the MTL to the brain's overall gray matter, whose volume mediated the cognitive benefits of an augmented hippocampal vascular supply, based on the results presented in chapter 2. This suggests that the resilience towards aging and cerebrovascular pathology conveyed by the HVP is mechanistically based on brain reserve or brain maintenance [Stern et al., 2023].

The second study helped to elucidate the resilience mechanism further by showing no association between the HVP and brain structure in young adults, neither globally nor locally. The contrast between structural results in younger and older adults indicates brain maintenance as the mechanism underlying HVP-conveyed resilience to the detrimental changes associated with aging and disease. In other words, an augmented hippocampal vascular supply appears not to lead to a greater build-up of gray matter in the brain, but to provide the ability to better maintain the brain structure in the face of detrimental changes associated with aging and disease. On a more basic level, a dual supply could convey greater blood flow, which in turn could ensure a better supply with oxygen and nutrients as well as better clearance of harmful substances and metabolic by-products. Such greater hippocampal blood flow (at rest) has been positively correlated with spatial memory performance in older adults [Heo et al., 2009].

The introduced measure of mean hippocampal vessel distances, which approximates vessel densities in the presence of sparse vascular maps, shows a different relation to cognitive performance than the HVP. Here, hippocampal vessel distances especially showed distinct relations with cognitive performance between controls and CSVD patients, suggesting that smaller vessel distances convey resilience to cerebrovascular pathology, but not aging in general. In contrast, findings in mice suggest that hippocampal microvascular rarefaction in the hippocampus is generally related with worse cognitive performance, not only in the presence of disease [Troen et al., 2008, Tucsek et al., 2014]. However, parts of the mice had diet-induced hyperhomocysteinemia [Troen et al., 2008] or obesity [Tucsek et al., 2014] and group-differences in the density-cognition relationship have not been examined. The results regarding VDM presented in chapters 2 and 3 suggest no such general association between smaller mean hippocampal vessel distances and better cognitive performance in young nor healthy older adults, but only a resilience against

cerebrovascular pathology. Yet, vessel distance metrics also capture other aspects than plain vascular density (see section 5.4).

According to the presented results, tortuosity of the AChA, PCA and PComA, i.e. arteries surrounding the hippocampus and partially involved in its blood supply, was not related to better cognitive performance in young adults. There has been no previous study examining tortuosity of these arteries in reference to cognitive performance, neither in young nor old adults. Limited recent evidence indicates a positive relationship of the extracranial ICA and VA with MoCA scores [Yin et al., 2024], but another study found no statistically significant relationship between whole brain arterial tortuosity and MoCA scores [Chen et al., 2022b]. The association between tortuosity of the arteries surrounding the hippocampus and cognitive performance thus remains elusive. Mechanistically, the increased resistance to blood flow in tortuous vessels [Schep et al., 2002] might have the potential to impair cerebral blood flow and cause cognitive deficits.

From a functional vascular perspective, vascular reactivity of the hippocampal vessels as measured with fMRI at 7T in a intermittent breathing paradigm was not related to better cognitive performance in young adults in this thesis. This replicates results that have been observed in the context of CVR induced by a hypercapnic CO_2 stimulus and measured with 3T fMRI [Catchlove et al., 2018a]. In contrast, older adults showed an association between hippocampal CVR and memory reaction times in the same study [Catchlove et al., 2018a]. While not all studies show a relationship between CVR and cognitive performance, the overall impression is that impairment of cognitive performance and CVR (in various brain regions) appear to be linked [Catchlove et al., 2018b].

Across the bank all examined hippocampal vascular metrics failed to reveal associations with brain structure in young adults in this study. Hence, none of these appears to convey a brain reserve that is built in early adulthood. Instead, they might contribute to brain maintenance (especially the pattern of hippocampal vascularization), i.e. help to preserve brain structure throughout the lifetime and in the face of pathology. Alternatively, they might promote cognitive functioning in older age in a structure-independent manner via the mechanism of cerebrovascular reserve [Davenport et al., 2012, Novak, 2012], ensuring sufficient blood supply to match local demands in nutrients and oxygen and thus facilitating neuronal functioning.

5.3 Neural implementation of cognitive reserve

As opposed to identifying mere sociobehavioral proxies, neuroimaging methods are uniquely suited to examine the neural implementation of cognitive reserve, providing more insight into its underlying mechanisms [Stern et al., 2023]. Many studies have used fMRI, both resting-state and task, in the pursuit of CR, but few have followed the recently devised operational consensus definition [Stern et al., 2023] as done in this thesis. According to the results presented here, cognitive reserve in the context of an fMRI task of successful memory encoding task is primarily characterized by a more pronounced expression of the activation/deactivation pattern characteristic for episodic

memory encoding [Kim, 2011, Soch et al., 2021a]. Activation during memory encoding in inferior occipital, inferior temporal regions including the fusiform gyrus, and some frontal regions supports cognitive reserve in the context of AD pathology. In contrast, encoding-related deactivation of the precuneus, cuneus, angular gyrus and posterior cingulate cortex, i.e. of regions that are considered part of the DMN, contribute to cognitive reserve. Such a pattern of DMN deactivation combined with inferior temporal activations has previously been associated with better memory performance in older adults [Maillet and Rajah, 2014, Richter et al., 2023, Soch et al., 2021a]. In alignment with CR involvement of frontal regions presented here, global connectivity of left frontal cortex and the left prefrontal cortex have also been associated with cognitive reserve [Cole et al., 2012, Franzmeier et al., 2017b]. Notably, Franzmeier et al. [2017b] had employed a dedicated moderation approach to the relationship between AD severity represented by precuneus hypometabolism and memory performance in amyloid-positive aMCI participants, in concordance with the consensus framework [Stern et al., 2023]. Evidence regarding the fusiform gyrus in CR has been mixed. It has both been shown to contribute positively and negatively to CR [Habeck et al., 2018, Stern et al., 2008]. There has also been convincing evidence for an involvement of the ACC in cognitive reserve, e.g. via simple correlation with education as a popular CR proxy [Arenaza-Urquijo et al., 2013b]. The ACC was also part of a metabolic 'resilience signature' that was related to cognitive performance in individuals over 80 years who had remained cognitively unimpaired [Arenaza-Urquijo et al., 2019]. Finally, the ACC has been reported as part of a task-independent CR pattern [Stern et al., 2018]. Small parts of ACC also negatively contributed to CR in the third study of this thesis.

Cognitive reserve encompasses the two complementary processes of neural reserve and neural compensation [Stern, 2009]. In concordance with neural reserve, Düzel et al. [2010] and Soch et al. [2021a] found that greater deviation in successful memory encoding-related brain activity patterns from young adults was associated with greater memory impairment. Other studies have observed that older adults recruit brain regions which are typically not used by young adults in the same task and that this activity pattern has beneficial consequences for their cognitive performance or is related to cognitive reserve proxies (e.g. Cabeza et al. [2002], Elman et al. [2014], Stern [2005]), in alignment with the idea of neural compensation. The results from chapter 4 preferentially support the idea of neural reserve, as cognitive reserve was largely characterized by a more pronounced expression of the subsequent memory network that is commonly activated in the task in healthy adults. While the approach was not directed at identifying compensatory activity outside of the task-active network, a supplementary analysis revealed essentially no evidence towards such compensatory activity in brain regions not involved in successful memory encoding in healthy older adults. Interestingly, our study revealed certain regions within the task-related network in which CR-related activity was not aligned with the direction (sign) of activity related to successful memory encoding, i.e. less of the normally observed (de)activation was associated with better cognitive performance in the presence of AD pathology. Besides the calcarine sulci, right medial orbitofrontal cortex, insula and superior orbitofrontal cortex, the hippocampus was one of such regions, in concordance with previous reports about non-beneficial hippocampal

hyperactivity in the presence of Aβ and tau [Huijbers et al., 2019, Maass et al., 2019, Sperling et al., 2009]. In summary, it is possible that neural reserve and neural compensation act in tandem to form cognitive reserve. Yet, the variety of results across studies suggest that the expression of cognitive reserve might depend on additional factors like sex or disease stage. Specifically in AD, it might also be a consequence of heterogeneous spatial patterns of Aβ and tau spread [Franzmeier et al., 2020, Vogel et al., 2021].

As the BOLD signal intertwines neural and vascular components, it is possible that cognitive reserve is in parts based on cerebrovascular reserve, i.e. the ability of the cerebral vasculature to match local metabolic demands [Davenport et al., 2012, Novak, 2012]. An inability to match the demands could be explained by an inadequate blood flow or blood volume, which would affect the BOLD response to neuronal activation [Kim and Ogawa, 2012], even in the absence of changes in neuronal activation. Cerebral blood flow or volume in turn could be impaired by the vascular factors investigated in the context of the hippocampus in this thesis, i.e. arterial tortuosity, vascular rarefaction, a basic vascular supply (specifically in the hippocampus) or diminished cerebrovascular reactivity. Other possible mechanisms could be neuroinflammation [Brosseron et al., 2022, Hayek et al., 2024], neuronal/synaptic signaling or neuronal metabolism.

5.4 Limitations

The studies presented in this thesis had some shortcomings. First, the advantage of the high resolution offered by the 7T MRI utilized in the first two studies came at the cost of limited sample sizes of around 40-50 participants, restricting the statistical power. With regard to estimations of an effect of the HVP the statistical power was further limited by the unequal sample sizes (i.e. augmented versus basic supply), particularly in the second study.

Despite the high resolution of the ToF MRA, which enabled the classification of the HVP and contributed positively to the reliability of the VDM measures, these measures should not be trusted blindfully. As mentioned by Wiesmann and de Leeuw [2020] there might be uncal branches beyond the detection threshold. Other times, uncal branches might be wrongly classified as contributing to the hippocampal head, when in reality supplying merely the uncus. Even though only arteries implicated in hippocampal blood supply were segmented, a big proportion of these represented merely parental vessels as opposed to arteries that penetrated the hippocampus, let alone arterioles or capillaries, which were beyond the detection limit with diameters below 100µm and 10µm, respectively [Pappano and Gil Wier, 2013]. This biases vessel distance estimates of the hippocampus towards parts of vessels which are not directly involved in hippocampal blood supply. The vessel parts might not even be involved in hippocampal blood supply, but potentially in supply of adjacent regions, e.g. the parahippocampal gyrus in the case of PCA branches running inferior to the hippocampus. Hence, the accuracy of vessel distance estimates as representations of vascular densities might be strongly dependent on the resolution, which should be sufficiently high in order to provide meaningful estimates of these. Such a bias might also explain the dependence of the presented mean

hippocampal vessel distance estimates on hippocampal volume.

In terms of CoMD, a cautionary note should also be made. CoMD was conceptualized as the vessel distance metric most closely approximating the vascular pattern. However, the fact that CoMD values were only slightly smaller in dual- compared to single-supply hemispheres (see Fig. S19) indicates that the potential uncal branches of the AChA, which are rather faint and not particularly long, might not influence CoMD greatly. In contrast, other factors might contribute more strongly to CoMD. For instance, an AChA that can be visually traced and thus segmented longer extends further posterior and will have its center of mass closer to the middle of the hippocampus (in terms of the anterior-posterior axis; see Fig. 3.5A-D and note that the presence of an uncal branch and the long segmentation are not mutually dependent), which might lead to a smaller CoMD value. Therefore, smaller CoMD values might be driven more strongly by factors affecting visibility of the AChA, e.g. greater blood flow or greater diameter. This might explain the positive relationship observed between CoMD and MoCA scores in the first study (Fig. 2.8C). Nevertheless, the potential involvement in resilience against cerebrovascular pathology according to the results of study 1 suggests CoMD as a meaningful metric independent of its exact representation.

Possible implications of variations in the Circle of Willis like fetal-type PCAs for the examined vascular parameters have not been further investigated here due to their low prevalence. Particularly, increased flow demands to the ICA in individuals with an FTP [Amin-Hanjani et al., 2015, Hendrikse et al., 2005] might cause greater ICA tortuosity. Increased dependence on the ICA could also alter individuals more susceptible to hippocampal ischemia following ICA stenosis. Another particularly interesting group of individuals would be those with a single hippocampal vascular supply and an absent or severely hypoplastic PComA, as in these individuals hippocampal blood flow would be solely dependent on the posterior circulation, potentially rendering the hippocampus more susceptible to ischemia following stenosis of the vertebrobasilar arteries.

In terms of cerebrovascular reactivity, the usage of a respiratory regressor instead of $EtCO_2$ had the disadvantage of yielding a CVR measure in non-standard units that could not easily be compared between participants. Further, the alternative solution of normalizing the obtained metrics to a reference region was problematic, as there was some heterogeneity in the reference region and hence in the normalization. Additionally, this rendered the measure relative to the reference region rather than absolute, potentially occluding higher hippocampal CVR values in the presence of higher global (whole-brain) CVR.

Even though most fMRI studies on cognitive reserve including the one presented in chapter 4 aimed to investigate its underpinnings from a neural perspective, the measured BOLD signal is also dependent on the vascular response through neurovascular coupling [Iadecola, 2017]. Considering the multitude of changes in the cerebral vasculature in aging and disease (see chapter 1.5), neurocognitive aging should not be considered a separate entity from neurovascular aging in the context of fMRI [Tsvetanov et al., 2021b]. As such, vascular aspects examined in this thesis could contribute to cognitive reserve. Consequently, fMRI studies on neurocognitive aging including cognitive reserve should account for underlying differences in cerebral vasculature, e.g. via normalization to base-

line CBF or baseline CVR, or with the usage of calibrated fMRI techniques [Tsvetanov et al., 2021b].

Since the search space of the multivariate moderation model was restricted to the task-active regions in successful memory encoding, it did not allow for an investigation of compensatory activity outside of these regions. A supplementary analysis with an extended search space including all gray matter basically identified a pattern reminiscent of the successful encoding network (Fig. S11). However, the approach was not well suited to investigate cognitive reserve outside the task-active regions due to the increased amount of noise in the contrast in these regions compared to within the task-active regions.

The neural implementation of cognitive reserve as investigated with fMRI might depend on multiple factors, which might explain the vast heterogeneity observed across studies of CR. For instance, investigations employing fMRI are dependent on the utilized task and contrast. In this context, task-invariant fMRI approaches aim at elucidating CR independent of a specific task [Stern et al., 2018, van Loenhoud et al., 2020]. However, given the early and strong impairment of memory function in most dementias, the identified pattern has great significance for CR in the realm of (AD) dementia. Besides, the identified activity pattern of cognitive reserve likely represents a mixture of task-invariant components like the DMN and ACC as well as more specific components like the fusiform gyrus. Another factor affecting results regarding CR might be a distinct expression of CR between diseases, sexes or early and late disease stages [Billette et al., 2022].

5.5 Conclusions and Outlook

Despite the central role of the hippocampus in memory functioning, its early deterioration in AD and its vulnerability to hypoxia, the vasculature of the hippocampus and its role in successful cognitive aging are still underexamined. Consequently, there are many intriguing open questions. For instance, the role of tortuosity of arteries relevant for hippocampal perfusion in cognitive functioning of older adults remains yet to be examined. With regards to the hippocampal vascularization pattern, ultra-high field MRI studies employing even higher resolutions, possibly via the use of a compressed sensing sequence, could help to solve the problem of missed uncal branches and to resolve the identity of uncal branches as a mere supply of the uncus or as uncohippocampal branches. Additionally, a validation with post-mortem data could provide confidence in the equality of in-vivo versus ex-vivo classifications. Likewise, the estimation of hippocampal vessel densities from vessel distances could benefit tremendously from even higher resolutions. A comparison between hippocampal vessel distances at different resolutions could shine light on the severity of the resolution bias (see also previous chapter). Additionally, variants of the Circle of Willis should be taken into account, as the vascular redundancy in a full CoW presumably protects the brain from ischemia. The combined classification of CoW variants and the HVP could be used to compare three groups with different susceptibility to hippocampal ischemia: (a) an anterior-based hippocampal supply via

the ICA (e.g. FTP with or without dual supply), (b) a posterior-based supply via the PCA alone or (c) a mixed supply (no FTP and dual supply). The third group would presumably exhibit the highest resilience in the context of cerebrovascular disease and possibly aging. Variants of the Circle of Willis should also be considered with respect to ICA tortuosity and hippocampal blood flow. Ultimately, all structural vascular features should be mapped to functional features of the hippocampal vasculature, such as CBF and CVR. This way, a link between the hippocampal vascularization pattern and an actual better vascular supply (e.g. higher perfusion) could to be established.

Future efforts examining cognitive reserve should be aimed at identifying task-invariant components. Dedicated studies should employ the moderation approach from the consensus framework to examine neural compensation as a potential complementary mechanism of cognitive reserve. Further, normalization and calibration methods could help to elucidate the actual neural implementation of cognitive reserve independent of vascular influences. On the other hand, this could help to elucidate the significance of the 'cerebrovascular reserve' for cognitive reserve.

Ultimately, longitudinal studies with large sample sizes will be required to make adequate judgements about the involvement of hippocampal vascularization and Circle of Willis variants in brain maintenance and cognitive reserve. Such a design could also illuminate the modifiability of the hippocampal vascularization pattern. In any case, the hippocampal vascularization pattern could serve to identify individuals at increased risk for cognitive decline. Interventional efforts to prevent or at least delay cognitive impairment should be aimed at enhancing brain activity in core cognitive circuits. For instance, low-intensity focused transcranial ultrasound enables the modulation of neural activity, also of deep brain structures, and increases cerebral perfusion locally [Kuhn et al., 2023]. Other promising venues for intervention based on this thesis could be factors promoting angiogenesis including focused ultrasound [McMahon et al., 2018] and (e.g. hypoxia-induced) expression of VEGF [Boero et al., 1999, Chavez et al., 2000, Rosenstein et al., 1998, Warrington et al., 2012] or modulation of (cerebro)vascular reactivity, e.g. via heat exposure [Brunt and Minson, 2021], apart from physical activity and management of cardiovascular risk factors.

Bibliography

G. K. Aguirre, J. A. Detre, D. C. Alsop, and M. D'Esposito. The Parahippocampus Subserves Topographical Learning in Man. *Cerebral Cortex*, 6(6):823–829, 1996.

I. Allaman and P. Magistretti. *Fundamental Neuroscience: Fourth Edition*, chapter Brain Energy Metabolism, pages 261–284. Elsevier Inc., 2012.

A. Altinbas et al. Ipsilateral foetal-type posterior cerebral artery is associated with cognitive decline after carotid revascularisation. *BMC Neurology*, 14(1):1–7, 2014.

G. Alvares Pereira, M. V. Silva Nunes, P. Alzola, and I. Contador. Cognitive reserve and brain maintenance in aging and dementia: An integrative review. *Applied Neuropsychology: Adult*, 29(6):1615–1625, 2022.

AlzForum Foundation Inc. Revised Again: Alzheimer's Diagnostic Criteria Get Another Makeover. `https://www.alzforum.org/news/conference-coverage/revised-again-alzheimers-diagnostic-criteria-get-another-makeover`, 2023. Last accessed: 27.05.2024.

AlzForum Foundation Inc. Donanemab Approved in the U.S. `https://www.alzforum.org/news/community-news/donanemab-approved-us`, 2024. Last accessed: 04.09.2024.

Alzheimer Forschung Initiative e.V. Alzheimer-Wirkstoff Donanemab (Kisunla): Der aktuelle Stand. `https://www.alzheimer-forschung.de/forschung/aktuell/donanemab/`, 2024. Last accessed: 04.09.2024.

S. Amin-Hanjani et al. Effect of age and vascular anatomy on blood flow in major cerebral vessels. *Journal of Cerebral Blood Flow and Metabolism*, 35(2):312–318, 2015.

E. M. Arenaza-Urquijo and P. Vemuri. Resistance vs resilience to Alzheimer disease. *Neurology*, 90(15):695–703, 2018.

E. M. Arenaza-Urquijo et al. Relationships between years of education and gray matter volume, metabolism and functional connectivity in healthy elders. *NeuroImage*, 83: 450–457, 2013a.

E. M. Arenaza-Urquijo et al. Cognitive reserve proxies relate to gray matter loss in cognitively healthy elderly with abnormal cerebrospinal fluid amyloid-β levels. *Journal of Alzheimer's Disease*, 35(4):715–726, 2013b.

E. M. Arenaza-Urquijo, M. Wirth, and G. Chételat. Cognitive reserve and lifestyle: Moving towards preclinical Alzheimer's disease. *Frontiers in Aging Neuroscience*, 7: 134, 2015.

E. M. Arenaza-Urquijo et al. The metabolic brain signature of cognitive resilience in the 80+: beyond Alzheimer pathologies. *Brain*, 142(4):1134–1147, 2019.

S. Arvind Gunnal, M. S. Farooqui, and R. N. Wabale. Anatomical Variability of the Posterior Communicating Artery. *Asian Journal of Neurosurgery*, 13, 2018.

D. Aryo. Dijkstra Algorithm. `https://www.mathworks.com/matlabcentral/fileexchange/36140-dijkstra-algorithm`, 2024. Last accessed: 10.04.2024.

J. Attems et al. Cause of death in demented and non-demented elderly inpatients; an autopsy study of 308 cases. *Journal of Alzheimer's Disease*, 8(1):57–62, 2005.

D. Attwell et al. Glial and neuronal control of brain blood flow. *Nature*, 468(7321): 232–243, 2010.

F. C. Barone et al. Mouse Strain Differences in Susceptibility to Cerebral Ischemia are Related to Cerebral Vascular Anatomy. *Journal of Cerebral Blood Flow and Metabolism*, 13:683–692, 1993.

D. Bates. Mixed models in R using the lme4 package Part 3: Inference based on profiled deviance. `http://lme4.r-forge.r-project.org/slides/2011-01-11-Madison/3Profiling.pdf`, 2011. Last accessed: 02.09.2024.

D. Bates, M. Mächler, B. M. Bolker, and S. C. Walker. Fitting Linear Mixed-Effects Models Using lme4. *Journal of Statistical Software*, 2015.

G. Bäumler. *Farbe-Wort-Interferenztest (FWIT) nach JR Stroop*. Verlag für Psychologie Dr. CJ Hogrefe, 1985.

A. E. Beaudin et al. Cerebrovascular Reactivity Across the Entire Brain in Cerebral Amyloid Angiopathy. *Neurology*, 98(17):E1716–E1728, 2022.

Y. Behzadi, K. Restom, J. Liau, and T. T. Liu. A component based noise correction method (CompCor) for BOLD and perfusion based fMRI. *NeuroImage*, 37(1):90–101, 2007.

R. Beigelman et al. Are kinking and coiling of carotid artery congenital or acquired? *Angiology*, 61(1):107–112, 2010.

M. A. Bell and M. J. Ball. Morphometric comparison of hippocampal microvasculature in ageing and demented people: Diameters and densities. *Acta Neuropathologica*, 53 (4):299–318, 1981.

J. Bernal et al. Arterial hypertension and β-amyloid accumulation have spatially overlapping effects on posterior white matter hyperintensity volume: a cross-sectional study. *Alzheimer's Research and Therapy*, 15(1):1–13, 2023.

M. Bernier, S. C. Cunnane, and K. Whittingstall. The morphology of the human cerebrovascular system. *Human Brain Mapping*, 39(12):4962–4975, 2018.

D. Berron et al. A protocol for manual segmentation of medial temporal lobe subregions in 7 Tesla MRI. *NeuroImage: Clinical*, 15:466–482, 2017.

R. A. Bethlehem et al. Brain charts for the human lifespan. *Nature*, 604(7906):525–533, apr 2022.

B. M. Bettcher et al. Dynamic change of cognitive reserve: associations with changes in brain, cognition, and diagnosis. *Neurobiology of Aging*, 83:95–104, 2019.

A. A. Bhogal. Medullary vein architecture modulates the white matter BOLD cerebrovascular reactivity signal response to CO2: Observations from high-resolution T2* weighted imaging at 7T. *NeuroImage*, 245:118771, 2021.

O. V. Billette et al. Novelty-Related fMRI Responses of Precuneus and Medial Temporal Regions in Individuals at Risk for Alzheimer Disease. *Neurology*, 99(8):E775–E788, 2022.

Biogen Inc. FDA Grants Traditional Approval for LEQEMBI® (lecanemab-irmb) for the Treatment of Alzheimer's Disease. `https://investors.biogen.com/news-releases/news-release-details/fda-grants-traditional-approval-leqembir-lecanemab-irmb`, 2023. Last accessed: 29.07.2024.

Biogen Inc. Biogen to Realign Resources for Alzheimer's Disease Franchise. `https://investors.biogen.com/news-releases/news-release-details/biogen-realign-resources-alzheimers-disease-franchise`, 2024. Last accessed: 29.07.2024.

T. D. Bird. Alzheimer disease overview. *GeneReviews®[Internet]*, 2018.

R. M. Birn, M. A. Smith, T. B. Jones, and P. A. Bandettini. The respiration response function: The temporal dynamics of fMRI signal fluctuations related to changes in respiration. *NeuroImage*, 40(2):644–654, 2008.

G. W. Blair et al. Intracranial hemodynamic relationships in patients with cerebral small vessel disease. *Neurology*, 94(21):E2258–E2269, 2020.

K. Blennow, M. J. de Leon, and H. Zetterberg. Alzheimer's disease. *The Lancet*, 368 (9533):387–403, 2006.

M. Boccardi et al. Delphi definition of the EADC-ADNI Harmonized Protocol for hippocampal segmentation on magnetic resonance. *Alzheimer's and Dementia*, 11(2): 126–138, 2015.

J. A. Boero et al. Increased brain capillaries in chronic hypoxia. *Journal of Applied Physiology*, 86(4):1211–1219, 1999.

B. Bosch et al. Cognitive reserve modulates task-induced activations and deactivations in healthy elders, amnestic mild cognitive impairment and mild Alzheimer's disease. *Cortex*, 46(4):451–461, 2010.

H. Braak and E. Braak. Staging of Alzheimer's disease-related neurofibrillary changes. *Neurobiology of Aging*, 16(3):271–278, 1995.

H. Braak and E. Braak. Frequency of Stages of Alzheimer-Related Lesions in Different Age Categories. *Neurobiology of Aging*, 18(4):351–357, 1997.

M. G. Bright and K. Murphy. Reliable quantification of BOLD fMRI cerebrovascular reactivity despite poor breath-hold performance. *NeuroImage*, 83:559–568, 2013.

T. L. Brink et al. Screening Tests for Geriatric Depression. *Clinical Gerontologist*, 1(1): 37–43, 1982.

F. Brosseron et al. Soluble TAM receptors sAXL and sTyro3 predict structural and functional protection in Alzheimer's disease. *Neuron*, 110(6):1009–1022.e4, 2022.

W. R. Brown and C. R. Thore. Review: Cerebral microvascular pathology in ageing and neurodegeneration. *Neuropathology and Applied Neurobiology*, 37(1):56–74, 2011.

W. R. Brown et al. Capillary loss precedes the cognitive impairment induced by fractionated whole-brain irradiation: A potential rat model of vascular dementia. *Journal of the Neurological Sciences*, 257:67–71, 2007.

H. R. Brunnström and E. M. Englund. Cause of death in patients with dementia disorders. *European Journal of Neurology*, 16(4):488–492, 2009.

V. E. Brunt and C. T. Minson. Heat therapy: mechanistic underpinnings and applications to cardiovascular health. *Journal of Applied Physiology*, 130(6):1684–1704, 2021.

R. L. Buckner et al. Molecular, Structural, and Functional Characterization of Alzheimer's Disease: Evidence for a Relationship between Default Activity, Amyloid, and Memory. *Journal of Neuroscience*, 25(34):7709–7717, 2005.

R. L. Buckner, J. R. Andrews-Hanna, and D. L. Schacter. The brain's default network: Anatomy, function, and relevance to disease. *Annals of the New York Academy of Sciences*, 1124:1–38, 2008.

E. Bullitt et al. Measuring Tortuosity of the Intracerebral Vasculature from MRA Images. *IEEE Transactions on Medical Imaging*, 22(9):1163–1171, 2003.

R. Cabeza, N. D. Anderson, J. K. Locantore, and A. R. Mcintosh. Aging Gracefully: Compensatory Brain Activity in High-Performing Older Adults. *NeuroImage*, 17: 1394–1402, 2002.

S. Cantin et al. Impaired cerebral vasoreactivity to CO2 in Alzheimer's disease using BOLD fMRI. *NeuroImage*, 58(2):579–587, 2011.

M. S. Cartwright, W. H. Hickling, and E. S. Roach. Ischemic stroke in an adolescent with arterial tortuosity syndrome. *Neurology*, 67(2):360–361, 2006.

S. J. Catchlove et al. Regional Cerebrovascular Reactivity and Cognitive Performance in Healthy Aging. *Journal of Experimental Neuroscience*, 12, 2018a.

S. J. Catchlove, A. Pipingas, M. E. Hughes, and H. Macpherson. Magnetic resonance imaging for assessment of cerebrovascular reactivity and its relationship to cognition: A systematic review. *BMC Neuroscience*, 19(1):1–15, 2018b.

M. Cavaglia et al. Regional variation in brain capillary density and vascular response to ischemia. *Brain Research*, 910(1-2):81–93, 2001.

A. Charidimou et al. Total Magnetic Resonance Imaging Burden of Small Vessel Disease in Cerebral Amyloid Angiopathy: An Imaging-Pathologic Study of Concept Validation. *JAMA Neurology*, 73(8):994–1001, 2016.

J. C. Chavez, F. Agani, P. Pichiule, and J. C. LaManna. Expression of hypoxia-inducible factor-1α in the brain of rats during chronic hypoxia. *Journal of Applied Physiology*, 89(5):1937–1942, 2000.

S. Chen et al. Wolframin is a novel regulator of tau pathology and neurodegeneration. *Acta Neuropathologica*, 143(5):547–569, 2022a.

Z. Chen et al. Associations of intracranial artery length and branch number on non-contrast enhanced MRA with cognitive impairment in individuals with carotid atherosclerosis. *Scientific Reports*, 12(1):1–9, 2022b.

K. Cilliers and B. J. Page. Variation and Anomalies of the Posterior Cerebral Artery: Review and Pilot Study. *Turkish Neurosurgery*, 29(1):1–8, 2019.

S. Ciurică et al. Arterial Tortuosity - Novel Implications for an Old Phenotype. *Hypertension*, 13(2):67–70, 2019.

N. J. Cohen and L. R. Squire. Preserved learning and retention of pattern-analyzing skill in amnesia: Dissociation of knowing how and knowing that. *Science*, 210(4466): 207–210, 1980.

M. W. Cole et al. Global connectivity of prefrontal cortex predicts cognitive control and intelligence. *Journal of Neuroscience*, 32(26):8988–8999, 2012.

F. Cormack et al. Extra-hippocampal grey matter density abnormalities in paediatric mesial temporal sclerosis. *NeuroImage*, 27(3):635–643, 2005.

J. Cummings et al. Aducanumab produced a clinically meaningful benefit in association with amyloid lowering. *Alzheimer's Research and Therapy*, 13(1):1–3, 2021.

M. H. Davenport et al. Cerebrovascular reserve: The link between fitness and cognitive function? *Exercise and Sport Sciences Reviews*, 40(3):153–158, 2012.

R. de Flores et al. Characterization of hippocampal subfields using ex vivo MRI and histology data: Lessons for in vivo segmentation. *Hippocampus*, 30(6):545–564, 2020.

C. M. De Frias, M. Lövdén, U. Lindenberger, and L.-G. Nilsson. Revisiting the dedifferentiation hypothesis with longitudinal multi-cohort data. *Intelligence*, 35:381–392, 2006.

I. J. Deary et al. The Impact of Childhood Intelligence on Later Life: Following Up the Scottish Mental Surveys of 1932 and 1947. *Journal of Personality and Social Psychology*, 86(1):130–147, 2004.

L. Del Corso et al. Tortuosity, Kinking, and Coiling of the Carotid Artery: Expression of Atherosclerosis or Aging? *Angiology*, 49(5):361–371, 1998.

D. C. Delis, J. H. Kramer, E. Kaplan, and B. A. Ober. *California Verbal Learning Test*. Pearson, London, 2 edition, 2000.

J. C. Delpech et al. Wolframin-1-expressing neurons in the entorhinal cortex propagate tau to CA1 neurons and impair hippocampal memory in mice. *Science Translational Medicine*, 13(611):8455, 2021.

S. Dhillon. Aducanumab: First Approval. *Drugs*, 81(12):1437–1443, 2021.

X. Di and B. B. Biswal. Metabolic Brain Covariant Networks as Revealed by FDG-PET with Reference to Resting-State fMRI Networks. *Brain Connectivity*, 2(5):275–283, 2012.

M. J. Donahue et al. Vascular space occupancy (VASO) cerebral blood volume-weighted MRI identifies hemodynamic impairment in patients with carotid artery disease. *Journal of Magnetic Resonance Imaging*, 29(3):718–724, 2009.

M. Dörner et al. Inferior Frontal Sulcal Hyperintensities on Brain MRI Are Associated with Amyloid Positivity beyond Age—Results from the Multicentre Observational DELCODE Study. *Diagnostics*, 14(9):940, 2024.

A. T. Du et al. Higher atrophy rate of entorhinal cortex than hippocampus in AD. *Neurology*, 62(3):422–427, 2004.

J. B. Du Prel, G. Hommel, B. Röhrig, and M. Blettner. Confidence Interval or P-Value? *Deutsches Ärzteblatt*, 106(19):335–339, 2009.

M. Duering et al. Neuroimaging standards for research into small vessel disease-advances since 2013. *The Lancet. Neurology*, 22(7):602–618, 2023.

O. M. Dumitrascu et al. Retinal venular tortuosity jointly with retinal amyloid burden correlates with verbal memory loss: A pilot study. *Cells*, 10(11):2926, 2021.

H. M. Duvernoy et al. *The human hippocampus: Functional anatomy, vascularization and serial sections with MRI, fourth edition*. Springer, 2013.

E. Düzel et al. Hippocampal atrophy in temporal lobe epilepsy is correlated with limbic systems atrophy. *Journal of Neurology*, 253(3):294–300, 2006.

E. Düzel, H. Schütze, A. P. Yonelinas, and H.-J. Heinze. Functional phenotyping of successful aging in long-term memory: Preserved performance in the absence of neural compensation. *Hippocampus*, 21(8):803–814, 2010.

E. Düzel, H. Van Praag, and M. Sendtner. Can physical exercise in old age improve memory and hippocampal function? *Brain*, 139(3):662–673, 2016.

E. Düzel et al. CSF total tau levels are associated with hippocampal novelty irrespective of hippocampal volume. *Alzheimer's and Dementia: Diagnosis, Assessment and Disease Monitoring*, 10:782–790, 2018.

A. Eid, I. Mhatre, and J. R. Richardson. Gene-environment interactions in Alzheimer's Disease: A potential path to precision medicine. *Pharmacology & therapeutics*, 199: 173, jul 2019.

A. D. Ekstrom et al. Cellular networks underlying human spatial navigation. *Nature*, 425(6954):184–188, 2003.

F. M. Elahi, M. M. Wang, and J. F. Meschia. Cerebral Small Vessel Disease–Related Dementia: More Questions Than Answers. *Stroke*, 54(3):648–660, 2023.

J. A. Elman et al. Neural compensation in older people with brain amyloid-β deposition. *Nature neuroscience*, 17(10):1316–1318, 2014.

J. A. Elman et al. Issues and recommendations for the residual approach to quantifying cognitive resilience and reserve. *Alzheimer's Research and Therapy*, 14(1), 2022.

A. Erdem, M. G. Yaşargil, and P. Roth. Microsurgical anatomy of the hippocampal arteries. *Journal of Neurosurgery*, 79(2):256–265, 1993.

M. Y. Eun et al. Global intracranial arterial tortuosity is associated with intracranial atherosclerotic burden. *Scientific Reports*, 14(1):1–9, 2024.

European Medicines Agency. Aduhelm. `https://www.ema.europa.eu/en/medicines/human/EPAR/aduhelm`, 2024a. Last accessed: 04.09.2024.

European Medicines Agency. Leqembi. https://www.ema.europa.eu/en/medicines/human/EPAR/leqembi, 2024b. Last accessed: 04.09.2024.

M. S. Fanselow and H.-W. Dong. Are the Dorsal and Ventral Hippocampus Functionally Distinct Structures? *Neuron*, 65:7–19, 2010.

L. A. Farrer et al. Effects of Age, Sex, and Ethnicity on the Association Between Apolipoprotein E Genotype and Alzheimer Disease: A Meta-analysis. *JAMA*, 278 (16):1349–1356, 1997.

F. Fazekas et al. MR Signal Abnormalities at 1.5 T in Alzheimer's Dementia and Normal Aging. *American Journal of Roentgenology*, 149(2):351–356, 1987.

F. Fernández-Klett et al. Pericytes in capillaries are contractile in vivo, but arterioles mediate functional hyperemia in the mouse brain. *Proceedings of the National Academy of Sciences of the United States of America*, 107(51):22290–22295, 2010.

J. C. Fernández-Miranda et al. Microvascular anatomy of the medial temporal region: Part 1: Its application to arteriovenous malformation surgery. *Neurosurgery*, 67: ons237–ons276, 2010.

A. M. Fjell et al. Critical ages in the life course of the adult brain: nonlinear subcortical aging. *Neurobiology of Aging*, 34:2239–2247, 2013.

M. F. Folstein, S. E. Folstein, and P. R. Mchugh. "Mini-Mental State" A Practical Method for Grading the Cognitive State of Patients for the Clinician. *Journal of Psychiatric Research*, 12:189–198, 1975.

R. S. Frackowiak et al. Regional cerebral oxygen supply and utilization in dementia. A clinical and physiological study with oxygen-15 and positron tomography. *Brain*, 104: 753–778, 1981.

N. Franzmeier et al. Resting-state global functional connectivity as a biomarker of cognitive reserve in mild cognitive impairment. *Brain Imaging and Behavior*, 11(2): 368–382, 2017a.

N. Franzmeier et al. Left frontal cortex connectivity underlies cognitive reserve in prodromal Alzheimer disease. *Neurology*, 88(11):1054–1061, 2017b.

N. Franzmeier et al. Patient-centered connectivity-based prediction of tau pathology spread in Alzheimer's disease. *Science Advances*, 6(48):eabd1327, 2020.

M. A. Fraser, M. E. Shaw, and N. Cherbuin. A systematic review and meta-analysis of longitudinal hippocampal atrophy in healthy human ageing. *NeuroImage*, 112: 364–374, 2015.

G. B. Frisoni et al. The clinical use of structural MRI in Alzheimer disease. *Nature Reviews Neurology*, 6(2):67–77, 2010.

G. B. Frisoni et al. The EADC-ADNI Harmonized Protocol for manual hippocampal segmentation on magnetic resonance: Evidence of validity. *Alzheimer's & Dementia*, 11(2):111–125, 2015.

J. Frossard and O. Renaud. Permutation Tests for Regression, ANOVA, and Comparison of Signals: The permuco Package. *Journal of Statistical Software*, 99(15):1–32, 2021.

B. Garcia-Garcia et al. Vessel distance mapping: A novel methodology for assessing vascular-induced cognitive resilience. *NeuroImage*, 274:120094, 2023.

A. Garnier-Crussard, F. Cotton, P. Krolak-Salmon, and G. Chételat. White matter hyperintensities in Alzheimer's disease: Beyond vascular contribution. *Alzheimer's & Dementia*, 19(8):3738–3748, aug 2023.

C. Gaser et al. CAT: a computational anatomy toolbox for the analysis of structural MRI data. *GigaScience*, 13:1–13, 2024.

T. Gorbach et al. Longitudinal association between hippocampus atrophy and episodic-memory decline. *Neurobiology of Aging*, 51:167–176, 2017.

P. B. Gorelick et al. Vascular Contributions to Cognitive Impairment and Dementia: A Statement for Healthcare Professionals from the American Heart Association/American Stroke Association. *Stroke*, 42(9):2672–2713, 2011.

C. L. Grady. Meta-analytic and functional connectivity evidence from functional magnetic resonance imaging for an anterior to posterior gradient of function along the hippocampal axis. *Hippocampus*, 30(5):456–471, 2020.

Y. Gürsoy Özdemir, H. Bolay, E. Erdem, and T. Dalkara. Occlusion of the MCA by an intraluminal filament may cause disturbances in the hippocampal blood flow due to anomalies of circle of Willis and filament thickness. *Brain Research*, 822(1-2):260–264, 1999.

J. Gutierrez. Heterogeneity of the circle of Willis and its implication in hippocampal perfusion. *Brain*, 143(7):e58–e58, 2020.

J. Gutierrez et al. Circle of Willis Configuration as a Determinant of Intracranial Dolichoectasia. *Cerebrovascular Diseases*, 36(5-6):446–453, 2013.

R. A. Haast et al. Effects of MP2RAGE B1+ sensitivity on inter-site T1 reproducibility and hippocampal morphometry at 7T. *NeuroImage*, 224, 2021.

C. Habeck et al. The Reference Ability Neural Network Study: Life-time stability of reference-ability neural networks derived from task maps of young adults. *NeuroImage*, 125:693–704, 2016.

C. Habeck et al. Reference ability neural networks and behavioral performance across the adult life span. *NeuroImage*, 172:51–63, 2018.

R. Habib, L. Nyberg, and L. G. Nilsson. Cognitive and Non-Cognitive Factors Contributing to the Longitudinal Identification of Successful Older Adults in the Betula Study. *Aging, Neuropsychology, and Cognition*, 14(3):257–273, 2007.

C. Haffner, R. Malik, and M. Dichgans. Genetic factors in cerebral small vessel disease and their impact on stroke and dementia. *Journal of Cerebral Blood Flow and Metabolism*, 36(1):158–71, 2016.

T. Hafting et al. Microstructure of a spatial map in the entorhinal cortex. *Nature*, 436 (7052):801–806, 2005.

L. Haghverdi et al. Diffusion pseudotime robustly reconstruct lineage branching. *Nature Methods*, 13(10):845–850, 2016.

C. N. Hall et al. Capillary pericytes regulate cerebral blood flow in health and disease. *Nature*, 508(7494):55–60, 2014.

H. C. Han. Twisted Blood Vessels: Symptoms, Etiology and Biomechanical Mechanisms. *Journal of Vascular Research*, 49(3):185–197, 2012.

O. Hansson, K. Blennow, H. Zetterberg, and J. Dage. Blood biomarkers for Alzheimer's disease in clinical practice and trials. *Nature Aging*, 3(5):506–519, 2023.

J. A. Hardy and G. A. Higgins. Alzheimer's disease: The amyloid cascade hypothesis. *Science*, 256(5054):184–185, 1992.

D. Hayek et al. Different inflammatory signatures based on CSF biomarkers relate to preserved or diminished brain structure and cognition. *Molecular Psychiatry*, 29:992–1004, 2024.

M. Hecht et al. Capillary cerebral amyloid angiopathy in Alzheimer's disease: association with allocortical/hippocampal microinfarcts and cognitive decline. *Acta Neuropathologica*, 135(5):681–694, 2018.

T. Hedden and J. D. Gabrieli. Insights into the ageing mind: A view from cognitive neuroscience. *Nature Reviews Neuroscience*, 5(2):87–96, 2004.

A. M. Hedman et al. Human brain changes across the life span: A review of 56 longitudinal magnetic resonance imaging studies. *Human Brain Mapping*, 33(8):1987–2002, 2012.

D. J. Heeger and D. Ress. What does fMRI tell us about neuronal activity? *Nature Reviews Neuroscience*, 3(2):142–151, 2002.

J. Hendrikse et al. Distribution of Cerebral Blood Flow in the Circle of Willis. *Radiology*, 235(1):184–189, 2005.

W. J. Henneman et al. Hippocampal atrophy rates in Alzheimer disease. *Neurology*, 72 (11):999–1007, 2009.

S. Heo et al. Resting hippocampal blood flow, spatial memory and aging. *Brain Research*, 1315:119–127, 2009.

R. A. Hill et al. Regional Blood Flow in the Normal and Ischemic Brain Is Controlled by Arteriolar Smooth Muscle Cell Contractility and Not by Capillary Pericytes. *Neuron*, 87:95–110, 2015.

S. M. Hoy. Lecanemab: First Approval. *Drugs*, 83(4):359–365, 2023.

X. Hu and E. Yacoub. The story of the initial dip in fMRI. *NeuroImage*, 62:1103–1108, 2012.

H. Huang et al. Age and duration of hypertension are associated with carotid artery tortuosity. *Frontiers in Neurology*, 15:1307984, 2024.

J. Huck et al. High resolution atlas of the venous brain vasculature from 7 T quantitative susceptibility maps. *Brain Structure and Function*, 224(7):2467–2485, 2019.

C. P. Hughes et al. A new clinical scale for the staging of dementia. *British Journal of Psychiatry*, 140(6):566–572, 1982.

X. W. Huijbers et al. Tau accumulation in clinically normal older adults is associated with hippocampal hyperactivity. *Journal of Neuroscience*, 39(3):548–556, 2019.

M. Hund-Georgiadis et al. Determination of Cerebrovascular Reactivity by Means of fMRI Signal Changes in Cerebral Microangiopathy: A Correlation with Morphological Abnormalities. *Cerebrovascular Diseases*, 16(2):158–165, 2003.

G. Huther, J. Dörfl, H. Van der Loos, and D. Jeanmonod. Microanatomic and Vascular Aspects of the Temporomesial Region. *Neurosurgery*, 43(5):1118–1136, 1998.

C. Iadecola. The Neurovascular Unit Coming of Age: A Journey through Neurovascular Coupling in Health and Disease. *Neuron*, 96(1):17–42, 2017.

C. Iadecola et al. Vascular Cognitive Impairment and Dementia: JACC Scientific Expert Panel. *Journal of the American College of Cardiology*, 73(25):3326–3344, 2019.

J. E. Iglesias et al. A computational atlas of the hippocampal formation using ex vivo, ultra-high resolution MRI: Application to adaptive segmentation of in vivo MRI. *NeuroImage*, 115:117–137, 2015.

J. P. Ingraham, M. E. Forbes, D. R. Riddle, and W. E. Sonntag. Aging Reduces Hypoxia-Induced Microvascular Growth in the Rodent Hippocampus. *The Journals of Gerontology: Series A*, 63(1):12–20, 2008.

G. R. Isolan et al. Hippocampal vascularization: Proposal for a new classification. *Surgical Neurology International*, 11(378), 2020.

C. R. Jack et al. Rate of medial temporal lobe atrophy in typical aging and Alzheimer's disease. *Neurology*, 51(4):993–999, 1998.

C. R. Jack et al. Serial PIB and MRI in normal, mild cognitive impairment and Alzheimer's disease: implications for sequence of pathological events in Alzheimer's disease. *Brain*, 132(5):1355–1365, 2009.

C. R. Jack et al. Hypothetical model of dynamic biomarkers of the Alzheimer's pathological cascade. *The Lancet Neurology*, 9(1):119–128, 2010.

C. R. Jack et al. A/T/N: An unbiased descriptive classification scheme for Alzheimer disease biomarkers. *Neurology*, 87:539–547, 2016.

C. R. Jack et al. NIA-AA Research Framework: Toward a biological definition of Alzheimer's disease. *Alzheimer's and Dementia*, 14(4):535–562, 2018.

H. Jahanian et al. Measuring vascular reactivity with resting-state blood oxygenation level-dependent (BOLD) signal fluctuations: A potential alternative to the breath-holding challenge? *Journal of Cerebral Blood Flow and Metabolism*, 37(7):2526–2538, 2017.

K. Javed, V. Reddy, and J. M. Das. Neuroanatomy, Posterior Cerebral Arteries. *StatPearls*, 2023.

T. L. Jernigan et al. Effects of age on tissues and regions of the cerebrum and cerebellum. *Neurobiology of Aging*, 22:581–594, 2001.

F. Jessen et al. A conceptual framework for research on subjective cognitive decline in preclinical Alzheimer's disease. *Alzheimer's and Dementia*, 10(6):844–852, 2014.

F. Jessen et al. Design and first baseline data of the DZNE multicenter observational study on predementia Alzheimer's disease (DELCODE). *Alzheimer's Research and Therapy*, 10(1), 2018.

X. Ji et al. Brain microvasculature has a common topology with local differences in geometry that match metabolic load. *Neuron*, 109(7):1168–1187.e13, 2021.

A. C. Johnson. Hippocampal Vascular Supply and Its Role in Vascular Cognitive Impairment. *Stroke*, 54(3):673–685, 2023.

M. J. Johnson and G. Dougherty. Robust measures of three-dimensional vascular tortuosity based on the minimum curvature of approximating polynomial spline fits to the vessel mid-line. *Medical Engineering & Physics*, 29:677–690, 2007.

M. Josefsson et al. Genetic and Lifestyle Predictors of 15-Year Longitudinal Change in Episodic Memory. *Journal of the American Geriatrics Society*, 60(12):2308–2312, 2012.

S. S. Kannurpatti and B. B. Biswal. Detection and scaling of task-induced fMRI-BOLD response using resting state fluctuations. *NeuroImage*, 40(4):1567–1574, 2008.

A. Kapasi, C. DeCarli, and J. A. Schneider. Impact of multiple pathologies on the threshold for clinically overt dementia. *Acta Neuropathologica 2017 134:2*, 134(2): 171–186, 2017.

A. Kapoor et al. Older adults with perivascular spaces exhibit cerebrovascular reactivity deficits. *NeuroImage*, 264:119746, 2022.

K. Kapoor, B. Singh, and L. I. J. Dewan. Variations in the configuration of the circle of Willis. *Anatomical Science International*, 83(2):96–106, 2008.

A. Kastrup, G. Krüger, T. Neumann-Haefelin, and M. E. Moseley. Assessment of cerebrovascular reactivity with functional magnetic resonance imaging: comparison of CO 2 and breath holding. *Magnetic Resonance Imaging*, 19:13–20, 2001.

R. Katzman. Education and the prevalence of dementia and Alzheimer's disease. *Neurology*, 43:13–20, 1993.

R. Katzman et al. Clinical, pathological, and neurochemical changes in dementia: A subgroup with preserved mental status and numerous neocortical plaques. *Annals of Neurology*, 23(2):138–144, 1988.

M. Kawashima et al. Microsurgical anatomy of cerebral revascularization. Part II: Posterior circulation. *Journal of Neurosurgery*, 102(1):132–147, 2005.

S. M. Kazan et al. Vascular autorescaling of fMRI (VasA fMRI) improves sensitivity of population studies: A pilot study. *NeuroImage*, 124:794–805, 2016.

J. A. Kiernan. Anatomy of the Temporal Lobe. *Epilepsy Research and Treatment*, 2012: 12, 2012.

R. J. Killiany et al. MRI measures of entorhinal cortex vs hippocampus in preclinical AD. *Neurology*, 58(8):1188–1196, 2002.

D. Kim et al. Relationship Between Cerebrovascular Reactivity and Cognition Among People With Risk of Cognitive Decline. *Frontiers in Physiology*, 12:645342, 2021a.

H. Kim. Neural activity that predicts subsequent memory and forgetting: A meta-analysis of 74 fMRI studies. *NeuroImage*, 54:2446–2461, 2011.

H. Kim. Encoding and retrieval along the long axis of the hippocampus and their relationships with dorsal attention and default mode networks: The HERNET model. *Hippocampus*, 25(4):500–510, 2015.

H. J. Kim et al. How Cerebral Vessel Tortuosity Affects Development and Recurrence of Aneurysm: Outer Curvature versus Bifurcation Type. *Journal of Stroke*, 23(2):213, 2021b.

S. G. Kim and S. Ogawa. Biophysical and physiological origins of blood oxygenation level-dependent fMRI signals. *Journal of Cerebral Blood Flow and Metabolism*, 32(7): 1188–1206, 2012.

C. Kirst et al. Mapping the Fine-Scale Organization and Plasticity of the Brain Vasculature. *Cell*, 180(4):780–795.e25, 2020.

C. B. Kirwan and C. E. Stark. Overcoming interference: An fMRI investigation of pattern separation in the medial temporal lobe. *Learning & Memory*, 14(9):625, 2007.

K. Kitagawa et al. Cerebral ischemia after bilateral carotid artery occlusion and intraluminal suture occlusion in mice: Evaluation of the patency of the posterior communicating artery. *Journal of Cerebral Blood Flow and Metabolism*, 18(5):570–579, 1998.

J. M. Kizilirmak et al. The relationship between resting-state amplitude fluctuations and memory-related deactivations of the default mode network in young and older adults. *Human Brain Mapping*, 44(9):3586–3609, 2023.

K. B. Kjelstrup et al. Finite scale of spatial representation in the hippocampus. *Science*, 321(5885):140–143, 2008.

M. J. Krabbe-Hartkamp et al. Circle of Willis: morphologic variation on three-dimensional time-of-flight MR angiograms. *Radiology*, 207:103–111, 1998.

J. J. Kril, S. Patel, A. J. Harding, and G. M. Halliday. Patients with vascular dementia due to microvascular pathology have significant hippocampal neuronal loss. *Journal of Neurology Neurosurgery and Psychiatry*, 72(6):747–751, 2002.

T. Kuhn et al. Transcranial focused ultrasound selectively increases perfusion and modulates functional connectivity of deep brain regions in humans. *Frontiers in Neural Circuits*, 17:1120410, 2023.

D. A. Lakhani et al. Clinical application of ultra-high resolution compressed sensing time-of-flight MR angiography at 7T to detect small vessel pathology. *Neuroradiology Journal*, 36(3):335–340, 2023.

A. C. Lee, L. K. Yeung, and M. D. Barense. The hippocampus and visual perception. *Frontiers in Human Neuroscience*, 6(APRIL 2012):17414, 2012.

D. H. Lee et al. Neural substrates of cognitive reserve in Alzheimer's disease spectrum and normal aging. *NeuroImage*, 186:690–702, 2019.

H. Lee, D. GoodSmith, and J. J. Knierim. Parallel processing streams in the hippocampus. *Current Opinion in Neurobiology*, 64:127–134, 2020.

M. E. Lenehan et al. Sending Your Grandparents to University Increases Cognitive Reserve: The Tasmanian Healthy Brain Project. *Neuropsychology*, 30(5):525–531, 2016.

M. Lepage, R. Habib, and E. Tulving. Hippocampal PET Activations of Memory Encoding and Retrieval: The HIPER Model. *Hippocampus*, 8(4):313–322, 1998.

M. D. Lezak. *Neuropsychological assessment*. Oxford University Press, USA, 2004.

Q. Li et al. Cerebral Small Vessel Disease. *Cell Transplantation*, 27(12):1711–1722, 2018.

X. Li et al. Hippocampal subfield volumetry in patients with subcortical vascular mild cognitive impairment. *Scientific Reports*, 6(1):1–8, 2016.

E. Lin and A. Alessio. What are the basic concepts of temporal, contrast, and spatial resolution in cardiac CT? *Journal of Cardiovascular Computed Tomography*, 3(6): 403–408, 2009.

J. Linn et al. Prevalence of superficial siderosis in patients with cerebral amyloid angiopathy. *Neurology*, 74(17):1346–1350, 2010.

P. Liu et al. Cerebrovascular reactivity mapping without gas challenges. *NeuroImage*, 146:320–326, 2017.

P. Liu, J. B. De Vis, and H. Lu. Cerebrovascular reactivity (CVR) MRI with CO2 challenge: A technical review. *NeuroImage*, 187:104–115, 2019.

P. Liu et al. Cerebrovascular reactivity mapping using intermittent breath modulation. *NeuroImage*, 215:116787, 2020.

P. Liu et al. Cerebrovascular Reactivity Mapping Using Resting-State BOLD functional MRI in Healthy Adults and Patients with Moyamoya Disease. *Radiology*, 299(2): 419–425, 2021.

G. Livingston et al. Dementia prevention, intervention, and care: 2020 report of the Lancet Commission. *The Lancet*, 396:413–46, 2020.

G. Livingston et al. Dementia prevention, intervention, and care: 2024 report of the Lancet standing Commission. *The Lancet*, 404:572–628, 2024.

S. Long, C. Benoist, and W. Weidner. World Alzheimer Report 2023 Reducing dementia risk: never too early, never too late. *Alzheimer's Disease International*, 2023.

A. Maass et al. Vascular hippocampal plasticity after aerobic exercise in older adults. *Molecular Psychiatry*, 20(5):585–593, 2015.

A. Maass et al. Entorhinal tau pathology, episodic memory decline, and neurodegeneration in aging. *Journal of Neuroscience*, 38(3):530–543, 2018.

A. Maass et al. Alzheimer's pathology targets distinct memory networks in the ageing brain. *Brain*, 142(8):2492–2509, 2019.

E. A. Maguire and D. Hassabis. Role of the hippocampus in imagination and future thinking. *Proceedings of the National Academy of Sciences*, 108(11):E39–E39, 2011.

D. Maillet and M. N. Rajah. Age-related differences in brain activity in the subsequent memory paradigm: a meta-analysis. *Neuroscience and biobehavioral reviews*, 45:246–257, 2014.

J. R. Manns, R. O. Hopkins, and L. R. Squire. Semantic Memory and the Human Hippocampus. *Neuron*, 38:127–133, 2003.

S. Marinković, M. Milisavljević, and L. Puškaš. Microvascular anatomy of the hippocampal formation. *Surgical Neurology*, 37(5):339–349, 1992.

D. Marr, D. Willshaw, and B. McNaughton. *Simple memory: a theory for archicortex*. Springer, 1991.

C. B. Martin and M. D. Barense. Perception and Memory in the Ventral Visual Stream and Medial Temporal Lobe. *Annual Review of Vision Science*, 9(Volume 9, 2023): 409–434, 2023.

H. F. Martins et al. Morphological changes of the internal carotid artery: prevalence and characteristics. A clinical and ultrasonographic study in a series of 19 804 patients over 25 years old. *European Journal of Neurology*, 25(1):171–177, 2018.

H. Mattern and O. Speck. Vessel distance mapping. In *36th Annual Scientific Meeting of European Society for Magnetic Resonance in Medicine and Biology. ESMRMB September, Online*, volume 10, 2020.

H. Mattern et al. Prospective motion correction enables highest resolution time-of-flight angiography at 7T. *Magnetic Resonance in Medicine*, 80(1):248–258, 2018.

G. M. McKhann et al. The diagnosis of dementia due to Alzheimer's disease: Recommendations from the National Institute on Aging-Alzheimer's Association workgroups on diagnostic guidelines for Alzheimer's disease. *Alzheimer's and Dementia*, 7(3):263–269, 2011.

D. McMahon, E. Mah, and K. Hynynen. Angiogenic response of rat hippocampal vasculature to focused ultrasound-mediated increases in blood-brain barrier permeability. *Scientific Reports*, 8(1):1–12, 2018.

A. Mechelli, K. J. Friston, R. S. Frackowiak, and C. J. Price. Structural covariance in the human cortex. *Journal of Neuroscience*, 25(36):8303–8310, 2005.

A. S. Meel-van den Abeelen, J. Lagro, A. H. van Beek, and J. A. Claassen. Impaired Cerebral Autoregulation and Vasomotor Reactivity in Sporadic Alzheimer's Disease. *Current Alzheimer Research*, 11(1):11–17, 2014.

X. Meng and C. D'Arcy. Education and Dementia in the Context of the Cognitive Reserve Hypothesis: A Systematic Review with Meta-Analyses and Qualitative Analyses. *PLoS ONE*, 7(6):e38268, 2012.

H. Metz et al. KINKING OF THE INTERNAL CAROTID ARTERY in Relation to Cerebrovascular Disease. *The Lancet*, 277(7174):424–426, 1961.

A. Mishra et al. Astrocytes mediate neurovascular signaling to capillary pericytes but not to arterioles. *Nature Neuroscience*, 19(12):1619–1627, 2016.

H. J. Möller and M. B. Graeber. The case described by Alois Alzheimer in 1911. Historical and conceptual perspectives based on the clinical record and neurohistological sections. *European Archives of Psychiatry and Clinical Neuroscience*, 248(3):111–122, 1998.

R. G. Morris and M. D. Kopelman. The Memory Deficits in Alzheimer-type Dementia: A Review. *The Quarterly Journal of Experimental Psychology*, 38(4A):575–602, 1986.

J. A. Mortimer, A. R. Borenstein, K. M. Gosche, and D. A. Snowdon. Very early detection of Alzheimer neuropathology and the role of brain reserve in modifying its clinical expression. *Journal of Geriatric Psychiatry and Neurology*, 18(4):218–223, 2005.

K. Murphy, A. D. Harris, and R. G. Wise. Robustly measuring vascular reactivity differences with breath-hold: Normalising stimulus-evoked and resting state BOLD fMRI data. *NeuroImage*, 54:369–379, 2010.

K. P. Murphy. Machine learning: A probabilistic perspective (adaptive computation and machine learning series). *The MIT Press: London, UK*, 2018.

S. Naganawa, D. G. Norris, S. Zysset, and T. Mildner. Regional differences of fMR signal changes induced by hyperventilation: Comparison between SE-EPI and GE-EPI at 3-T. *Journal of Magnetic Resonance Imaging*, 15(1):23–30, 2002.

Z. S. Nasreddine et al. The Montreal Cognitive Assessment, MoCA: A Brief Screening Tool For Mild Cognitive Impairment. *Journal of the American Geriatrics Society*, 53 (4):695–699, 2005.

S. C. Neu et al. Apolipoprotein E Genotype and Sex Risk Factors for Alzheimer Disease: A Meta-analysis. *JAMA Neurology*, 74(10):1178–1189, 2017.

A. G. Nikonenko, L. Radenovic, P. R. Andjus, and G. G. Skibo. Structural features of ischemic damage in the hippocampus. *Anatomical Record*, 292(12):1914–1921, 2009.

J. Nogueira et al. The Assessment of Cognitive Reserve: A Systematic Review of the Most Used Quantitative Measurement Methods of Cognitive Reserve for Aging. *Frontiers in Psychology*, 13:671, 2022.

U. Nöth et al. Cerebral vascular response to hypercapnia: Determination with perfusion MRI at 1.5 and 3.0 Tesla using a pulsed arterial spin labeling technique. *Journal of Magnetic Resonance Imaging*, 24(6):1229–1235, 2006.

V. Novak. Cognition and Hemodynamics. *Current Cardiovascular Risk Reports*, 6(5): 380–396, 2012.

L. Nyberg et al. Selective adult age differences in an age-invariant multifactor model of declarative memory. *Psychology and Aging*, 18(1):149–160, 2003.

J. O'Keefe and J. Dostrovsky. The hippocampus as a spatial map. Preliminary evidence from unit activity in the freely-moving rat. *Brain Research*, 34(1):171–175, 1971.

P. A. Osterrieth. Le test de copie d'une figure complexe; contribution a l'etude de la perception et de la memoire. *Archives de psychologie*, 1944.

K. V. Papp et al. Optimizing the preclinical Alzheimer's cognitive composite with semantic processing: The PACC5. *Alzheimer's & Dementia: Translational Research & Clinical Interventions*, 3(4):668–677, 2017.

A. J. Pappano and W. Gil Wier. *Cardiovascular Physiology (Tenth Edition)*, chapter 8 - The Microcirculation and Lymphatics, pages 153–170. Elsevier, 2013.

O. Paulsen and E. I. Moser. A model of hippocampal memory encoding and retrieval: GABAergic control of synaptic plasticity. *Trends Neurosci.*, 21:273–278, 1998.

L. Pellegrino, G. Prencipe, and F. Vairo. Dolicho-arteriopathies (kinking, coiling, tortuoosity) of the carotid arteries: study by color Doppler ultrasonography. *Minerva Cardioangiologica*, 46(3):69–76, 1998.

S. L. Peng et al. Age-related changes in cerebrovascular reactivity and their relationship to cognition: A four-year longitudinal study. *NeuroImage*, 174:257–262, 2018.

C. M. Peppiatt, C. Howarth, P. Mobbs, and D. Attwell. Bidirectional control of CNS capillary diameter by pericytes. *Nature*, 443(7112):700–704, 2006.

R. Peres, F. De Guio, H. Chabriat, and E. Jouvent. Alterations of the cerebral cortex in sporadic small vessel disease: A systematic review of in vivo MRI data. *Journal of Cerebral Blood Flow and Metabolism*, 36(4):681–695, 2016.

V. Perosa et al. Hippocampal vascular reserve associated with cognitive performance and hippocampal volume. *Brain*, 143(2):622–634, 2020.

J. Persson et al. Longitudinal Structure–Function Correlates in Elderly Reveal MTL Dysfunction with Cognitive Decline. *Cerebral Cortex*, 22(10):2297–2304, 2012.

N. Peters et al. The pattern of cognitive performance in CADASIL: A monogenic condition leading to subcortical ischemic vascular dementia. *American Journal of Psychiatry*, 162(11):2078–2085, 2005.

R. C. Petersen. Mild cognitive impairment as a diagnostic entity. *Journal of Internal Medicine*, 256(3):183–194, 2004.

R. C. Petersen et al. Memory function in very early Alzheimer's disease. *Neurology*, 44 (5):867–867, 1994.

H. Petrovitch et al. AD lesions and infarcts in demented and non-demented Japanese-American men. *Annals of Neurology*, 57(1):98–103, 2005.

J. Pinto, M. G. Bright, D. P. Bulte, and P. Figueiredo. Cerebrovascular Reactivity Mapping Without Gas Challenges: A Methodological Guide. *Frontiers in Physiology*, 11:608475, 2021.

R. A. Poldrack, J. A. Mumford, and T. E. Nichols. *Handbook of functional MRI data analysis*. Cambridge University Press, 2011.

J. Poppenk, H. R. Evensmoen, M. Moscovitch, and L. Nadel. Long-axis specialization of the human hippocampus. *Cell*, 17(7):230–240, 2013.

G. M. Potter, F. M. Chappell, Z. Morris, and J. M. Wardlaw. Cerebral Perivascular Spaces Visible on Magnetic Resonance Imaging: Development of a Qualitative Rating Scale and its Observer Reliability. *Cerebrovascular Diseases*, 39(3-4):224–231, 2015.

K. J. Preacher and A. F. Hayes. SPSS and SAS procedures for estimating indirect effects in simple mediation models. *Behavior Research Methods, Instruments, and Computers*, 36(4):717–731, 2004.

K. J. Preacher and A. F. Hayes. Asymptotic and resampling strategies for assessing and comparing indirect effects in multiple mediator models. *Behavior Research Methods*, 40(3):879–891, 2008.

C. Qiu, M. Kivipelto, and E. Von Strauss. Epidemiology of Alzheimer's disease: Occurrence, determinants, and strategies toward intervention. *Dialogues in Clinical Neuroscience*, 11(2):111–128, 2009.

M. E. Raichle and M. A. Mintun. Brain work and brain imaging. *Annual Review of Neuroscience*, 29(Volume 29, 2006):449–476, 2006.

P. M. Rasmussen et al. APOE gene-dependent BOLD responses to a breath-hold across the adult lifespan. *NeuroImage: Clinical*, 24:101955, 2019.

N. Raz et al. Aging, sexual dimorphism, and hemispheric asymmetry of the cerebral cortex: Replicability of regional differences in volume. *Neurobiology of Aging*, 25(3): 377–396, 2004.

N. Raz et al. Regional Brain Changes in Aging Healthy Adults: General Trends, Individual Differences and Modifiers. *Cerebral Cortex*, 15(11):1676–1689, 2005.

N. Raz et al. Volume of the hippocampal subfields in healthy adults: differential associations with age and a pro-inflammatory genetic variant. *Brain Structure and Function*, 220(5):2663–2674, 2015.

B. R. Reed et al. Measuring cognitive reserve based on the decomposition of episodic memory variance. *Brain*, 133(8):2196–2209, 2010.

A. Rey and P. A. Osterrieth. Rey-osterrieth complex figure copying test. *Psychological Assessment*, 1941.

M. Richardson et al. *Capnography for monitoring end-tidal CO2 in hospital and prehospital settings: A health technology assessment*. Canadian Agency for Drugs and Technologies in Health, 2016.

A. Richter et al. Single-value scores of memory-related brain activity reflect dissociable neuropsychological and anatomical signatures of neurocognitive aging. *Human Brain Mapping*, 44(8):3283–3301, 2023.

D. R. Riddle, W. E. Sonntag, and R. J. Lichtenwalner. Microvascular plasticity in aging. *Ageing Research Reviews*, 2:149–168, 2003.

F. Riederer. Donanemab in early Alzheimer's Disease. *Journal fur Neurologie, Neurochirurgie und Psychiatrie*, 22(3):142–143, 2021.

E. J. Rogalski et al. Youthful Memory Capacity in Old Brains: Anatomic and Genetic Clues from the Northwestern SuperAging Project. *Journal of Cognitive Neuroscience*, 25(1):29–36, 2013.

M. Rönnlund, L. Nyberg, L. Bäckman, and L. G. Nilsson. Stability, growth, and decline in adult life span development of declarative memory: Cross-sectional and longitudinal data from a population-based study. *Psychology and Aging*, 20(1):3–18, 2005.

E. Rose et al. Classification and Endovascular Treatment Aneurysms of the Posterior Cerebral Artery: Aneurysms of the Posterior Cerebral Artery: Classification and Endovascular Treatment. *American Journal of Neuroradiology*, 22:27–34, 2001.

W. G. Rosen, R. C. Mohs, and K. L. Davis. A new rating scale for Alzheimer's disease. *American Journal of Psychiatry*, 141(11 (1356-1364),), 1984.

J. M. Rosenstein, N. Mani, W. F. Silverman, and J. M. Krum. Patterns of brain angiogenesis after vascular endothelial growth factor administration in vitro and in vivo. *Proceedings of the National Academy of Sciences*, 95(12):7086–7091, 1998.

E. Rostrup et al. Regional Differences in the CBF and BOLD Responses to Hypercapnia: A Combined PET and fMRI Study. *NeuroImage*, 11:87–97, 2000.

J. W. Rowe and R. L. Kahn. Human Aging: Usual and Successful. *Science*, 237(4811): 143–149, 1987.

D. C. Ryman et al. Symptom onset in autosomal dominant Alzheimer disease: A systematic review and meta-analysis. *Neurology*, 83(3):253–260, 2014.

L. Saba et al. Association between internal carotid artery dissection and arterial tortuosity. *Neuroradiology*, 57(2):149–153, 2015.

W. Saelens, R. Cannoodt, H. Todorov, and Y. Saeys. A comparison of single-cell trajectory inference methods. *Nature Biotechnology*, 37(5):547–554, 2019.

D. Sahni, I. Jit, and V. Lal. Variations and anomalies of the posterior communicating artery in northwest Indian brains. *Surgical Neurology*, 68:449–453, 2007.

T. A. Salthouse. Localizing age-related individual differences in a hierarchical structure. *Intelligence*, 32:541–561, 2004.

G. Salvadó et al. Specific associations between plasma biomarkers and postmortem amyloid plaque and tau tangle loads. *EMBO Molecular Medicine*, 15(5), 2023.

K. Sam et al. Impaired dynamic cerebrovascular response to hypercapnia predicts development of white matter hyperintensities. *Neuroimage:*, 11:796–801, 2016a.

K. Sam et al. Development of White Matter Hyperintensity Is Preceded by Reduced Cerebrovascular Reactivity. *Annals of Neurology*, 80(2):277–285, 2016b.

M. Samuraki et al. Cerebral Amyloid Angiopathy-Related Microbleeds Correlate with Glucose Metabolism and Brain Volume in Alzheimer's Disease. *Journal of Alzheimer's Disease*, 48(2):517–528, 2015.

P. Satz. Brain Reserve Capacity on Symptom Onset After Brain Injury: A Formulation and Review of Evidence for Threshold Theory. *Neuropsychology*, 7(3):273–295, 1993.

A. M. Saunders et al. Association of apolipoprotein E allele 4 with late-onset familial and sporadic alzheimer's disease. *Neurology*, 43(8):1467–1472, 1993.

D. L. Schacter et al. The Future of Memory: Remembering, Imagining, and the Brain. *Neuron*, 76:677–694, 2012.

E. Scharrer. Vascularization and vulnerability of the cornu ammonis in the opossum. *Archives of Neurology And Psychiatry*, 44(3):483–506, 1940.

G. Schep et al. Detection and treatment of claudication due to functional iliac obstruction in top endurance athletes: A prospective study. *Lancet*, 359(9305):466–473, 2002.

P. Schmidt. *Bayesian inference for structured additive regression models for large-scale problems with applications to medical imaging*. PhD Thesis, Ludwig-Maximilians-Universität München, 2017.

R. Schmidt-Kastner and T. F. Freund. Selective vulnerability of the hippocampus in brain ischemia. *Neuroscience*, 40(3):599–636, 1991.

J. A. Schneider, Z. Arvanitakis, W. Bang, and D. A. Bennett. Mixed brain pathologies account for most dementia cases in community-dwelling older persons. *Neurology*, 69 (24):2197–2204, 2007.

B. H. Schott et al. Inhibitory temporo-parietal effective connectivity is associated with explicit memory performance in older adults. *iScience*, 26(10), 2023.

S. Schreiber et al. Impact of lifestyle dimensions on brain pathology and cognition. *Neurobiology of Aging*, 40:164–172, 2016.

S. Schreiber et al. Invited Review: The spectrum of age-related small vessel diseases: potential overlap and interactions of amyloid and nonamyloid vasculopathies. *Neuropathology and Applied Neurobiology*, 2019.

M. Schünke et al. *Prometheus: Kopf, Hals und Neuroanatomie*. Thieme, 2009.

K. Shang et al. Arterial Tortuosity and Its Correlation with White Matter Hyperintensities in Acute Ischemic Stroke. *Neural Plasticity*, 2022.

M. Shapiro and E. Raz. *Cerebrovascular Development and Evolution*, pages 1–30. Springer New York, New York, NY, 2014.

K. Shaw et al. Neurovascular coupling and oxygenation are decreased in hippocampus compared to neocortex because of microvascular differences. *Nature Communications*, 12(1):1–16, 2021.

G. Shmueli. To Explain or to Predict? *Statistical Science*, 25(3):289–310, 2010.

D. H. Silverman et al. Positron Emission Tomography in Evaluation of Dementia: Regional Brain Metabolism and Long-term Outcome. *JAMA*, 286(17):2120–2127, 2001.

J. R. Sims et al. Donanemab in Early Symptomatic Alzheimer Disease: The TRAILBLAZER-ALZ 2 Randomized Clinical Trial. *JAMA*, 330(6):512–527, 2023.

O. A. Skrobot et al. Progress toward standardized diagnosis of vascular cognitive impairment: Guidelines from the Vascular Impairment of Cognition Classification Consensus Study. *Alzheimer's & Dementia*, 14(3):280–292, 2018.

E. Sleight et al. Cerebrovascular Reactivity Measurement Using Magnetic Resonance Imaging: A Systematic Review. *Frontiers in Physiology*, 12:643468, 2021.

S. A. Small et al. A pathophysiological framework of hippocampal dysfunction in ageing and disease. *Nature Reviews Neuroscience*, 12(10):585–601, 2011.

A. Smith. Symbol Digit Modalities Test. *The Clinical Neuropsychologist*, 1973.

D. A. Snowdon. Aging and Alzheimer's Disease: Lessons From the Nun Study. *The Gerontologist*, 37(2):150–156, 1997.

J. Soch et al. A comprehensive score reflecting memory-related fMRI activations and deactivations as potential biomarker for neurocognitive aging. *Human Brain Mapping*, 42(14):4478–4496, 2021a.

J. Soch et al. Bayesian model selection favors parametric over categorical fMRI subsequent memory models in young and older adults. *NeuroImage*, 230, 2021b.

J. Soch et al. Single-value brain activity scores reflect both severity and risk across the Alzheimer's continuum. *Brain*, 2024.

M. Spallazzi et al. Hippocampal vascularization patterns: A high-resolution 7 Tesla time-of-flight magnetic resonance angiography study. *NeuroImage: Clinical*, 21, 2019.

J. Spaniol et al. Event-related fMRI studies of episodic encoding and retrieval: Meta-analyses using activation likelihood estimation. *Neuropsychologia*, 47:1765–1779, 2009.

R. A. Sperling et al. Amyloid Deposition Is Associated with Impaired Default Network Function in Older Persons without Dementia. *Neuron*, 63(2):178–188, 2009.

W. Spielmeyer. Zur Pathogenese örtlich elektiver Gehirnveränderungen. *Zeitschrift für die gesamte Neurologie und Psychiatrie*, 99(1):756–776, 1925.

L. R. Squire. Memory systems of the brain: A brief history and current perspective. *Neurobiology of Learning and Memory*, 82:171–177, 2004.

L. R. Squire, C. E. Stark, and R. E. Clark. The Medial Temporal Lobe. *Annual Review of Neuroscience*, 27:279–306, 2004.

J. Staals et al. Total MRI load of cerebral small vessel disease and cognitive ability in older people. *Neurobiology of Aging*, 36(10):2806–2811, 2015.

S. M. Stark, A. Frithsen, and C. E. Stark. Age-related alterations in functional connectivity along the longitudinal axis of the hippocampus and its subfields. *Hippocampus*, pages 1–17, 2020.

Y. Stern. What is cognitive reserve? Theory and research application of the reserve concept. *Journal of the International Neuropsychological Society*, 8(3):448–460, 2002.

Y. Stern. Brain Networks Associated with Cognitive Reserve in Healthy Young and Old Adults. *Cerebral Cortex*, 15(4):394–402, 2005.

Y. Stern. Cognitive reserve. *Neuropsychologia*, 47(10):2015–2028, 2009.

Y. Stern et al. A Common Neural Network for Cognitive Reserve in Verbal and Object Working Memory in Young but not Old. *Cerebral Cortex*, 18(4):959–967, 2008.

Y. Stern et al. The Reference Ability Neural Network Study: Motivation, design, and initial feasibility analyses. *NeuroImage*, 103:139–151, 2014.

Y. Stern et al. A task-invariant cognitive reserve network. *NeuroImage*, 178:36–45, 2018.

Y. Stern et al. Whitepaper: Defining and investigating cognitive reserve, brain reserve, and brain maintenance. *Alzheimer's & Dementia*, 16(9):1305–1311, 2020.

Y. Stern, E. Varangis, and C. Habeck. A framework for identification of a resting-bold connectome associated with cognitive reserve. *NeuroImage*, 232:117875, 2021.

Y. Stern et al. A framework for concepts of reserve and resilience in aging. *Neurobiology of Aging*, 124:100–103, 2023.

B. A. Strange, M. P. Witter, E. S. Lein, and E. I. Moser. Functional organization of the hippocampal longitudinal axis. *Nature Reviews Neuroscience*, 15(10):655–669, 2014.

T. Sugawara et al. Effects of global ischemia duration on neuronal, astroglial, oligodendroglial, and microglial reactions in the vulnerable hippocampal CA1 subregion in rats. *Journal of Neurotrauma*, 19(1):85–98, 2002.

M. K. Suh, H. Kim, and D. L. Na. Dysphagia in patients with dementia: Alzheimer versus vascular. *Alzheimer Disease and Associated Disorders*, 23(2):178–184, 2009.

Z. Sun et al. Age-Related Tortuosity of Carotid and Vertebral Arteries: Quantitative Evaluation With MR Angiography. *Frontiers in Neurology*, 13:858805, 2022.

S. Sur et al. Association of cerebrovascular reactivity and Alzheimer pathologic markers with cognitive performance. *Neurology*, 95(8):E962–E972, 2020.

S. Suri et al. Reduced cerebrovascular reactivity in young adults carrying the APOE $\varepsilon 4$ allele. *Alzheimer's & Dementia*, 11(6):648–657.e1, 2015.

M. D. Sweeney et al. The role of brain vasculature in neurodegenerative disorders. *Nature Neuroscience*, 21(10):1318–1331, 2018.

K. Taneja et al. Evaluation of cerebrovascular reserve in patients with cerebrovascular diseases using resting-state MRI: A feasibility study. *Magnetic Resonance Imaging*, 59:46–52, 2019.

C. R. Thore et al. Morphometric Analysis of Arteriolar Tortuosity in Human Cerebral White Matter of Preterm, Young, and Aged Subjects. *J Neuropathol Exp Neurol*, 66 (5):337–345, 2007.

D. Tingley et al. Mediation: R package for Causal Mediation Analysis. *Journal of Statistical Software*, 59(5), 2014.

C. Togay-Isikay et al. Carotid artery tortuosity, kinking, coiling: stroke risk factor, marker, or curiosity? *Acta Neurologica Belgica*, 105(2):68–72, 2005.

T. N. Tombaugh. Trail Making Test A and B: Normative data stratified by age and education. *Archives of Clinical Neuropsychology*, 19(2):203–214, 2004.

A. M. Troen et al. B-vitamin deficiency causes hyperhomocysteinemia and vascular cognitive impairment in mice. *Proceedings of the National Academy of Sciences*, 105 (34):12474–12479, 2008.

K. A. Tsvetanov et al. The effects of age on resting-state BOLD signal variability is explained by cardiovascular and cerebrovascular factors. *Psychophysiology*, 58(7): e13714, 2021a.

K. A. Tsvetanov, R. N. Henson, and J. B. Rowe. Separating vascular and neuronal effects of age on fMRI BOLD signals: Neurovascular ageing. *Philosophical Transactions of the Royal Society*, 376(1815):20190631, 2021b.

Z. Tucsek et al. Aging Exacerbates Obesity-induced Cerebromicrovascular Rarefaction, Neurovascular Uncoupling, and Cognitive Decline in Mice. *The Journals of Gerontology: Biological Sciences*, 69(11):1339–1352, 2014.

N. Tzourio-Mazoyer et al. Automated anatomical labeling of activations in SPM using a macroscopic anatomical parcellation of the MNI MRI single-subject brain. *NeuroImage*, 15(1):273–289, 2002.

J. Uchimura. Über die Gefäßversorgung des Ammonshornes. *Zeitschrift für die gesamte Neurologie und Psychiatrie*, 112(1):1–19, 1928.

A. Uz. The segmentation of the posterior cerebral artery: a microsurgical anatomic study. *Neurosurgical Review*, 42(1):155–161, 2019.

A. S. Vagal, J. L. Leach, M. Fernandez-Ulloa, and M. Zuccarello. The Acetazolamide Challenge: Techniques and Applications in the Evaluation of Chronic Cerebral Ischemia. *AJNR*, 30:876–884, 2009.

J. M. Valdueza et al. Changes in blood flow velocity and diameter of the middle cerebral artery during hyperventilation: assessment with MR and transcranial Doppler sonography. *American Journal of Neuroradiology*, 18(10), 1997.

M. J. Valenzuela and P. Sachdev. Brain reserve and dementia: A systematic review. *Psychological Medicine*, 36(4):441–454, 2006.

L. Van Der Maaten and G. Hinton. Visualizing Data using t-SNE. *Journal of Machine Learning Research*, 9:2579–2605, 2008.

L. J. P. Van Der Maaten, E. O. Postma, and H. J. Van Den Herik. Dimensionality Reduction: A Comparative Review. *Journal of Machine Learning Research*, 10, 2009.

A. C. van Loenhoud et al. A neuroimaging approach to capture cognitive reserve: Application to Alzheimer's disease. *Human Brain Mapping*, 38(9):4703–4715, 2017.

A. C. van Loenhoud et al. Identifying a task-invariant cognitive reserve network using task potency. *NeuroImage*, 210, 2020.

A. F. van Raamt, W. P. Mali, P. J. van Laar, and Y. van der Graaf. The Fetal Variant of the Circle of Willis and Its Influence on the Cerebral Collateral Circulation. *Cerebrovascular Diseases*, 22(4):217–224, 2006.

N. Vockert et al. Hippocampal vascularization patterns exert local and distant effects on brain structure but not vascular pathology in old age. *Brain Communications*, 3 (3), 2021.

N. Vockert et al. Cognitive Reserve Against Alzheimer's Pathology Is Linked to Brain Activity During Memory Formation. *bioRxiv*, 2023.

N. Vockert et al. Cognitive Reserve Against Alzheimer's Pathology is Linked to Brain Activity During Memory Formation. *Nature Communications*, 15(1):1–16, 2024.

J. W. Vogel et al. Four distinct trajectories of tau deposition identified in Alzheimer's disease. *Nature Medicine*, pages 1–11, 2021.

A. Waaijer et al. Anatomic Variations in the Circle of Willis in Patients with Symptomatic Carotid Artery Stenosis Assessed with Multidetector Row CT Angiography. *Cerebrovascular Diseases*, 23(4):267–274, 2007.

K. B. Walhovd et al. Consistent neuroanatomical age-related volume differences across multiple samples. *Neurobiology of Aging*, 32:916–932, 2011.

C. Wang et al. A systematic review of the association between dementia risk factors and cerebrovascular reactivity. *Neuroscience & Biobehavioral Reviews*, 148, 2023.

H. F. Wang et al. Extracranial internal carotid artery tortuosity and body mass index. *Frontiers in Neurology*, 8(SEP):289121, 2017.

J. M. Wardlaw, C. Smith, and M. Dichgans. Mechanisms of sporadic cerebral small vessel disease: Insights from neuroimaging. *The Lancet Neurology*, 12(5):483–497, 2013a.

J. M. Wardlaw et al. Neuroimaging standards for research into small vessel disease and its contribution to ageing and neurodegeneration. *The Lancet Neurology*, 12(8): 822–838, 2013b.

J. P. Warrington et al. Cerebral microvascular rarefaction induced by whole brain radiation is reversible by systemic hypoxia in mice. *American Journal of Physiology - Heart and Circulatory Physiology*, 300:736–744, 2011.

J. P. Warrington et al. Whole Brain Radiation-Induced Impairments in Learning and Memory Are Time-Sensitive and Reversible by Systemic Hypoxia. *PLOS ONE*, 7(1): e30444, 2012.

D. Wechsler. The measurement of adult intelligence. *The Journal of Nervous and Mental Disease*, 91(4):548, 1940.

D. Wechsler. *Wechsler memory scale.* Psychological corporation, 1945.

H. S. Wei et al. Erythrocytes Are Oxygen-Sensing Regulators of the Cerebral Microcirculation. *Neuron*, 91(4):851–862, 2016.

J. Weibel and W. S. Fields. Tortuosity, coiling, and kinking of the internal carotid artery: II. Relationship of morphological variation to cerebrovascular insufficiency. *Neurology*, 15(5):462–468, 1965.

D. G. Welsh and S. S. Segal. Endothelial and smooth muscle cell conduction in arterioles controlling blood flow. *American Journal of Physiology*, 274(1 PART 2), 1998.

WHO. Dementia - Facts in pictures. `https://www.who.int/news-room/facts-in-pictures/detail/dementia`, 2021. Last accessed: 24.04.2024.

WHO. Ageing and health fact sheet. `https://www.who.int/news-room/fact-sheets/detail/ageing-and-health`, 2022. Last accessed: 25.04.2024.

WHO. Dementia fact sheet. `https://www.who.int/news-room/fact-sheets/detail/dementia`, 2023. Last accessed: 25.04.2024.

M. Wiesmann and F.-E. de Leeuw. Vascular reserve in brain resilience: pipes or perfusion? *Brain*, 143(2):390–392, 2020.

L. E. M. Wisse et al. Hippocampal subfield volumetry from structural isotropic 1 mm^3 MRI scans: A note of caution. *Human Brain Mapping*, 42(2):539–550, 2021.

S. Wolfsgruber et al. Minor neuropsychological deficits in patients with subjective cognitive decline. *Neurology*, 95(9):e1134–e1143, 2020.

L. Xie et al. Multi-template analysis of human perirhinal cortex in brain MRI: Explicitly accounting for anatomical variability. *NeuroImage*, 144:183–202, 2017.

L. Xie et al. Automated segmentation of medial temporal lobe subregions on in vivo T1-weighted MRI in early stages of Alzheimer's disease. *Human Brain Mapping*, 40 (12):3431–3451, 2019.

D. A. Yablonskiy, J. J. Ackerman, and M. E. Raichle. Coupling between changes in human brain temperature and oxidative metabolism during prolonged visual stimulation. *Proceedings of the National Academy of Sciences*, 97(13):7603–7608, 2000.

K. Yaffe et al. Predictors of maintaining cognitive function in older adults: The Health ABC Study. *Neurology*, 72(23):2029–2035, 2009.

Y. Yamazaki et al. Apolipoprotein E and Alzheimer disease: pathobiology and targeting strategies. *Nature Reviews Neurology*, 15(9):501–518, 2019.

J. Yang et al. Voxelwise meta-analysis of gray matter anomalies in Alzheimer's disease and mild cognitive impairment using anatomic likelihood estimation. *Journal of Neurological Sciences*, 316:21–29, 2012.

M. A. Yassa and C. E. Stark. Pattern separation in the hippocampus. *Trends in Neurosciences*, 34(10):515–525, 2011.

U. S. Yezhuvath et al. Forebrain-dominant deficit in cerebrovascular reactivity in Alzheimer's disease. *Neurobiology of Aging*, 33:75–82, 2012.

L. Yin et al. Analysis of the correlations between the extracranial internal carotid artery and extracranial vertebral artery and mild cognitive impairment. *Technology and Health Care*, 32(1):467–479, 2024.

P. A. Yushkevich et al. Automated Volumetry and Regional Thickness Analysis of Hippocampal Subfields and Medial Temporal Cortical Structures in Mild Cognitive Impairment. *Human brain mapping*, 36(1):258, 2015.

L. B. Zahodne et al. Quantifying cognitive reserve in older adults by decomposing episodic memory variance: Replication and extension. *Journal of the International Neuropsychological Society*, 19(8):854–862, 2013.

F. H. Zande, P. A. Hofman, and W. H. Backes. Mapping hypercapnia-induced cerebrovascular reactivity using BOLD MRI. *Neuroradiology*, 47(2):114–120, 2005.

L. Zarrinkoob et al. Blood flow distribution in cerebral arteries. *Journal of Cerebral Blood Flow and Metabolism*, 35:648–654, 2015.

X. Zhang et al. High-resolution mapping of brain vasculature and its impairment in the hippocampus of Alzheimer's disease mice. *National Science Review*, 6(6):1223–1238, 2019.

M. Zhu, J. J. Ackerman, A. L. Sukstanskii, and D. A. Yablonskiy. How the body controls brain temperature: The temperature shielding effect of cerebral blood flow. *Journal of Applied Physiology*, 101(5):1481–1488, 2006.

G. Ziegler, R. Dahnke, and C. Gaser. Models of the aging brain structure and individual decline. *Frontiers in Neuroinformatics*, 6(MARCH):3, 2012.

M. Zijlmans et al. The contribution of posterior circulation to memory function during the intracarotid amobarbital procedure. *Journal of Neurology*, 259(8):1632–1638, 2012.

B. Zimmerman, B. Rypma, G. Gratton, and M. Fabiani. Age-related changes in cerebrovascular health and their effects on neural function and cognition: A comprehensive review. *Psychophysiology*, 58(7):e13796, 2021.

K. M. Zvolanek et al. Comparing end-tidal CO 2 , respiration volume per time (RVT), and average gray matter signal for mapping cerebrovascular reactivity amplitude and delay with breath-hold task BOLD fMRI. *NeuroImage*, 272:120038, 2023.

List of Figures

List of Tables

Appendix

Supplementary Figures

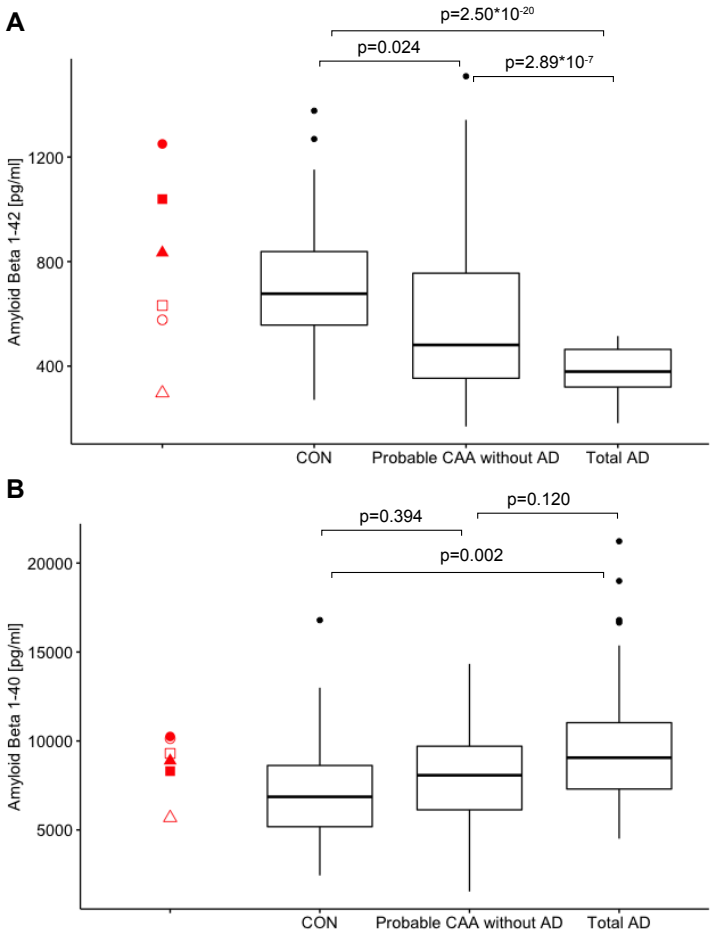

Figure S1: **Boxplots of CSF (A) Aβ_{42} and (B) Aβ_{40} concentrations across different clinical groups of a large cohort of older adults.** Probable CAA diagnosis was based on the modified Boston criteria (n = 60) [Linn et al., 2010]. CON includes HA patients, whose diagnosis was based on the existence of deep microhemorrhages, and controls, who did not reveal any CSVD according to STRIVE and were negative for AD based on the combination of Aβ_{42} and p-tau in CSF (n = 48) [Wardlaw et al., 2013a]. AD diagnosis was based on the NINCDS-ADRDA criteria and the ATN classification with concurrent Aβ_{42} and p-tau positivity (n = 91) [Jack et al., 2018]. The red symbols distinctly represent the six CAA patients in the current study. Group comparisons were conducted using an ANCOVA adjusting for age and sex. Figure copied from Vockert et al. [2021] with permission.

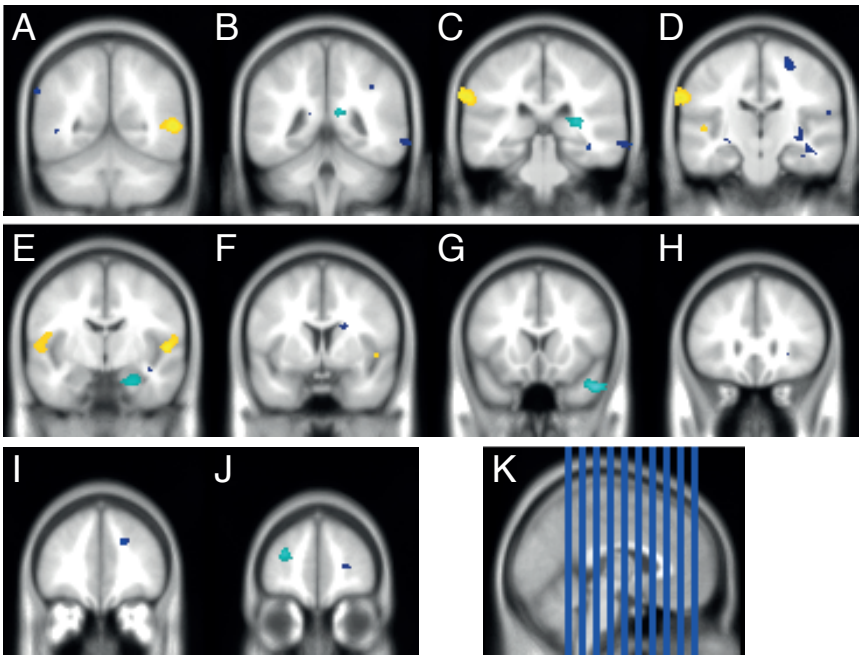

L **Statistics:** *p-values adjusted for search volume*

set-level		cluster-level				peak-level						
p	c	$p_{FWE\text{-}corr}$	$q_{FDR\text{-}corr}$	k_E	p_{uncorr}	$p_{FWE\text{-}corr}$	$q_{FDR\text{-}corr}$	T	$(Z_=)$	p_{uncorr}	mm	mm	mm
0.000	8	0.117	0.051	1530	0.001	**0.914**	**1.000**	**4.62**	**4.08**	**0.000**	**54**	**22**	**-34**
						0.928	1.000	4.60	4.06	0.000	50	16	-30
						1.000	1.000	3.01	2.83	0.002	58	16	-28
		0.007	0.007	2591	0.000	**0.919**	**1.000**	**4.62**	**4.08**	**0.000**	**66**	**-66**	**4**
						0.998	1.000	4.23	3.79	0.000	56	-58	4
						1.000	1.000	3.00	2.82	0.002	42	-54	6
		0.152	0.056	1436	0.001	**0.946**	**1.000**	**4.55**	**4.03**	**0.000**	**-28**	**46**	**12**
		0.000	0.001	3942	0.000	**0.976**	**1.000**	**4.45**	**3.96**	**0.000**	**-70**	**-20**	**30**
						0.999	1.000	4.20	3.77	0.000	-64	-28	30
						1.000	1.000	4.01	3.63	0.000	-70	-32	34
		0.205	0.067	1328	0.002	**1.000**	**1.000**	**4.14**	**3.73**	**0.000**	**12**	**-40**	**16**
						1.000	1.000	3.86	3.52	0.000	30	-32	8
						1.000	1.000	3.40	3.15	0.001	24	-40	12
		0.017	0.012	2237	0.000	**1.000**	**1.000**	**4.00**	**3.62**	**0.000**	**54**	**-14**	**4**
						1.000	1.000	3.35	3.11	0.001	70	-0	10
						1.000	1.000	3.18	2.97	0.001	46	2	-4
		0.305	0.094	1183	0.003	**1.000**	**1.000**	**3.46**	**3.20**	**0.001**	**26**	**-10**	**-26**
		0.069	0.037	1716	0.001	**1.000**	**1.000**	**3.36**	**3.12**	**0.001**	**-48**	**-10**	**14**
						1.000	1.000	3.34	3.10	0.001	-52	-12	4
						1.000	1.000	3.19	2.98	0.001	-46	-20	2

Figure S2: **Results of the exploratory VBM.** (A-J) Regions where subjects with an augmented vascular supply of the hippocampus exhibit greater GM volume than subjects with a basic supply ($p_{voxel} < 0.005$; uncorrected). Blue color indicates clusters with at least 20 voxels, cyan shows clusters which contain at least 1000 voxels, yellow represents clusters with $p < 0.05$ after FDR-cluster correction. (K) Sagittal location of coronal slices A-J. (L) Clusters with at least 1000 voxels with $p_{uncorrected}$ as identified in the VBM analysis. FWE = family-wise error, FDR = false discovery rate, k = cluster size. Figure adapted from Vockert et al. [2021] with permission.

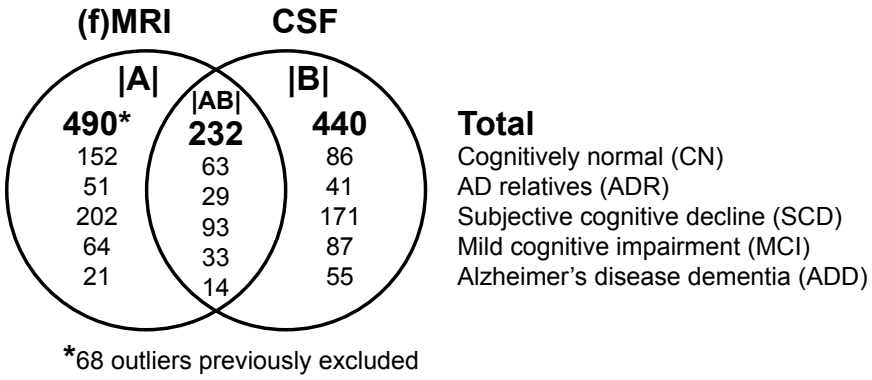

Figure S3: **Venn diagram of the subsamples.** Subsample |A| refers to the participants with fMRI data and was used to derive eigen-images of the subsequent memory contrast images via PCA. Subsample |B| refers to the participants with CSF data, which was used for creating the PL score. Subsample |AB| is the union of both, i.e., the participants with both fMRI and CSF data. Subsample |AB| was used to derive the CR-related activity patterns. The remaining participants of subsample |B| that were not part of |AB| were used for further validation of the CR score by determining its ability to moderate the effect of neurodegeneration on individual measures of cognitive performance. Figure copied from Vockert et al. [2024] with permission.

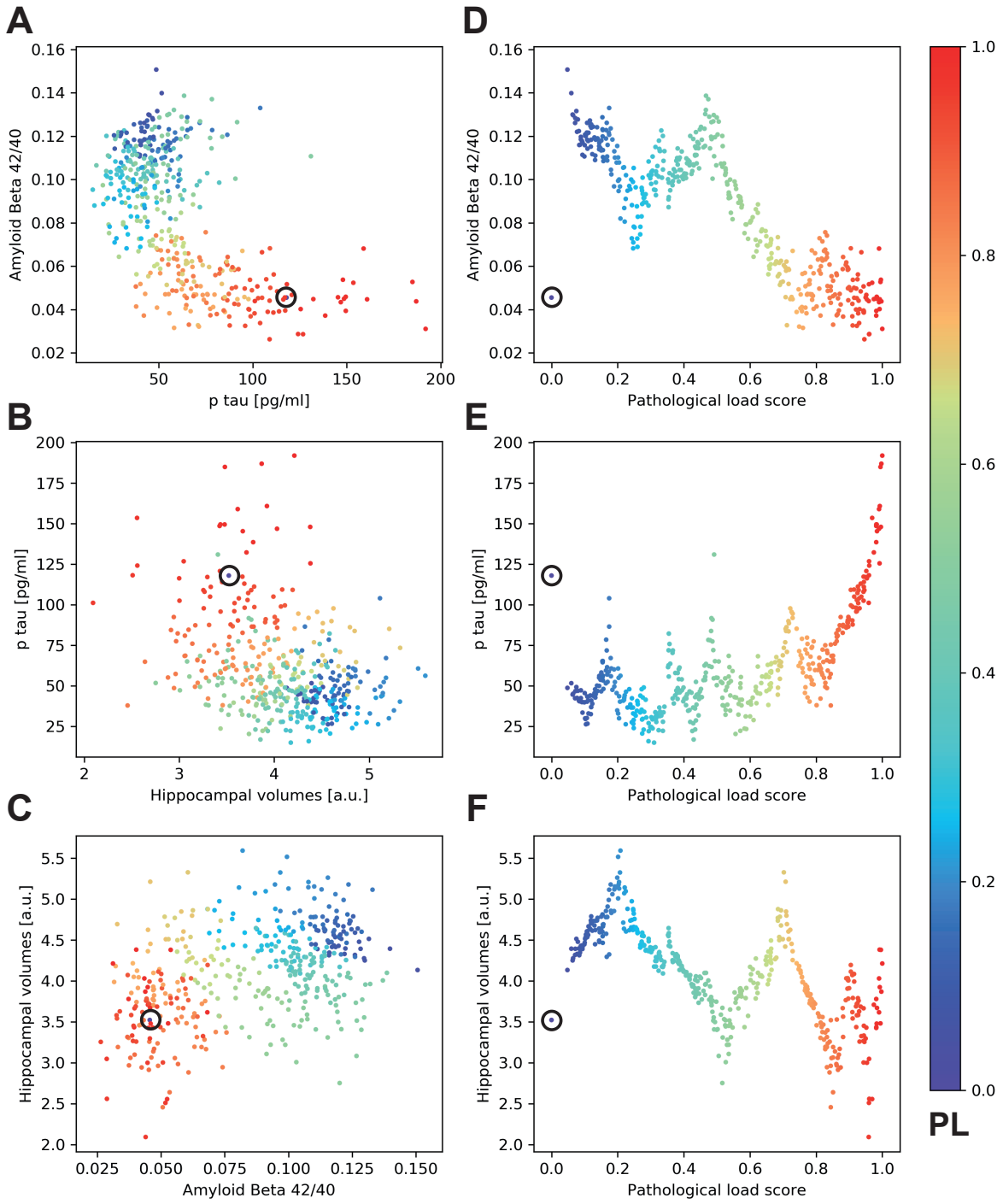

Figure S4: **Relationship between ATN biomarkers and data-driven PL score.** Same as Fig. 4.1, with the exception that one additional subject was included in the derivation of the PL score, which was deemed an outlier and excluded from all analyses. It is marked with a black circle and has a PL score of 0 despite its very low $A\beta_{42:40}$ ratio of 0.46, rather high p-tau levels of 118 pg/ml and TIV-corrected hippocampal volumes of 3.52. Figure copied from Vockert et al. [2024] with permission.

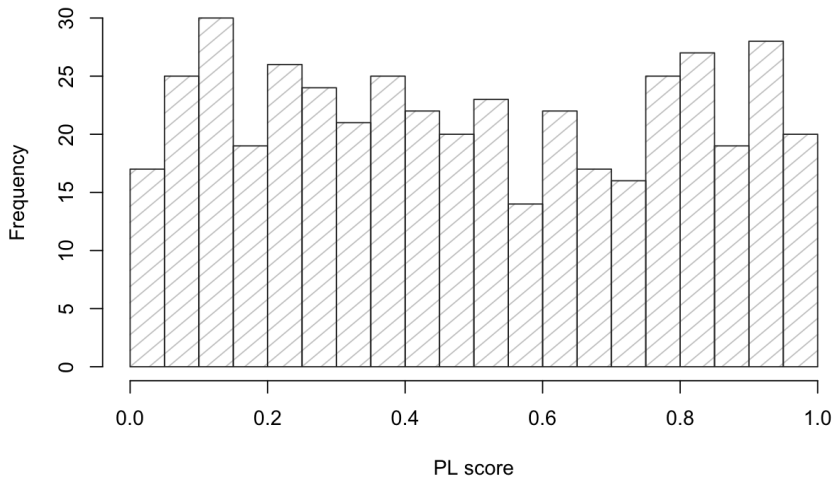

Figure S5: **Distribution of PL score.** The displayed sample is the full CSF sample (|B| in Fig. S3). Figure copied from Vockert et al. [2024] with permission.

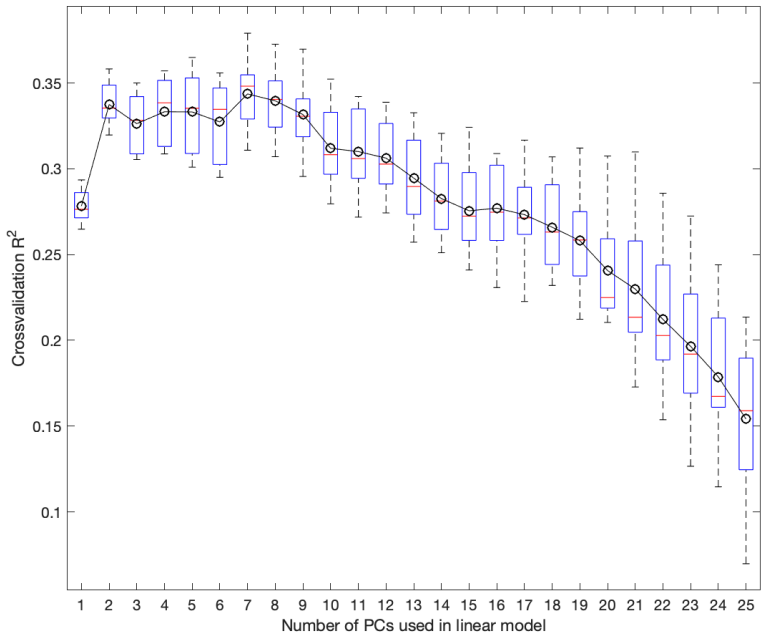

Figure S6: **Cross-validation results for the multivariate moderation model.** According to Eq. 4.2, PACC5 was predicted by varying numbers of principal components (eigen-images) in a 10-fold cross-validation procedure that was repeated 10 times with different partitioning of the data (see section 4.2.7 for details). The boxplots refer to the cross-validation R^2 (coefficient of determination) in PACC5 scores (Box-Cox transformed) in the 10 independent test set predictions. The black line denotes the mean value across the 10 predictions. 7 principal components achieved the best cross-validation results. Figure copied from Vockert et al. [2023] with permission.

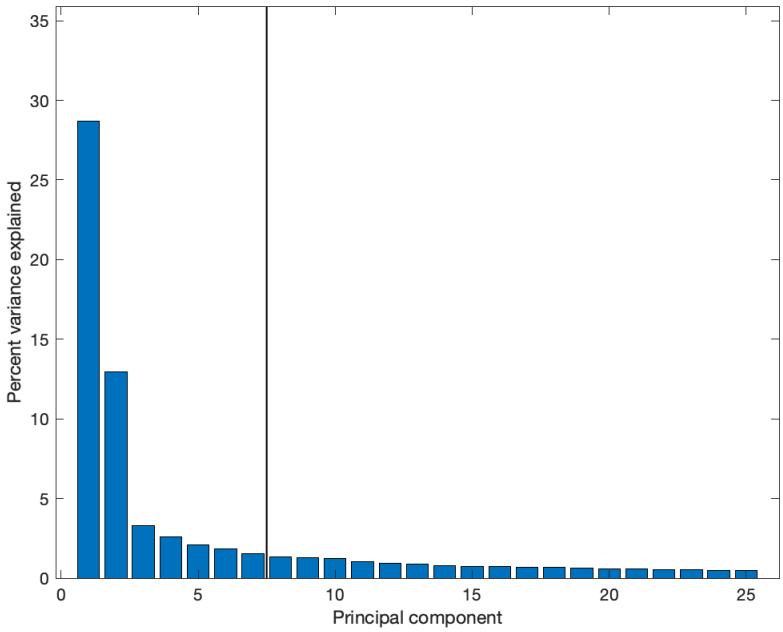

Figure S7: **Amount of variance explained by PCs.** Shown is the amount of variance in the original subsequent memory regressor images that the individual principal components explain as assessed via their eigenvalues. The black line symbolizes the optimal number of PCs determined via a 10-fold cross-validation procedure. Figure copied from Vockert et al. [2024] with permission.

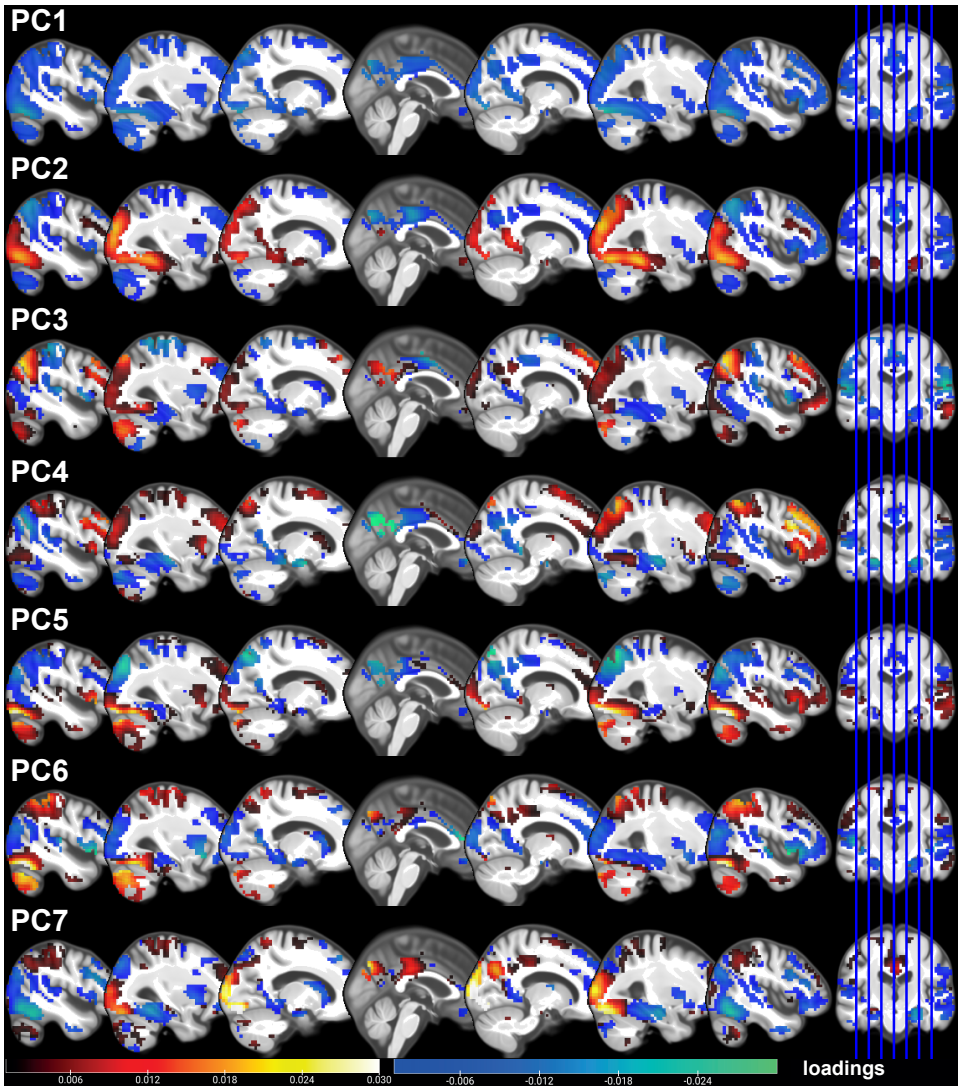

Figure S8: **Principal components of subsequent memory regressor images.** Shown are the loadings of each voxel onto each of the seven principal components (PC1-7) of the regressor images of subsequent memory. Please note that the PCA has been restricted to regions with a significant subsequent memory effect in the baseline sample (compare Fig. 4.3A) and hence does not include regions outside of those 13695 voxels. Figure copied from Vockert et al. [2024] with permission.

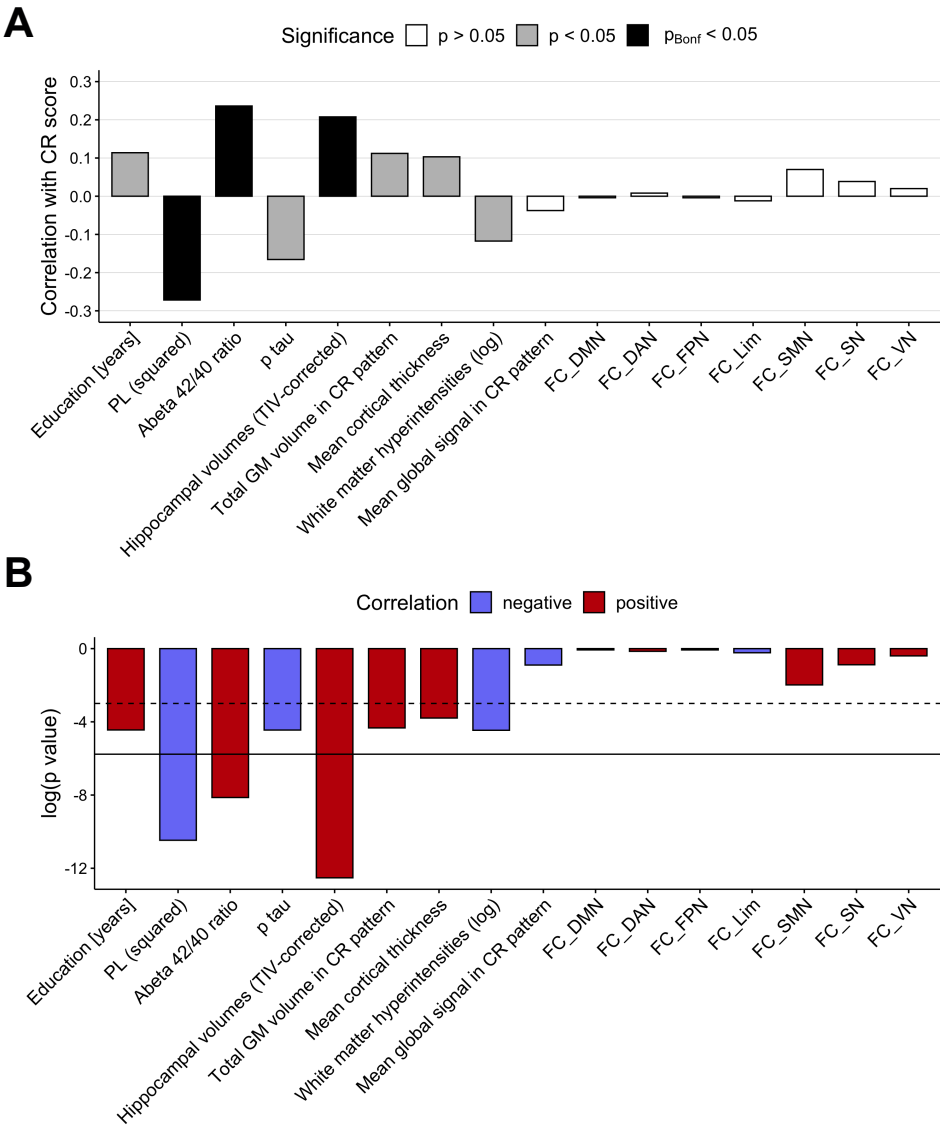

Figure S9: **Correlation of CR score with other variables.** (A) Pearson correlation coefficients between the CR score and the other variables. (B) P values for the corresponding correlations of panel A, illustrated on a logarithmic scale. Bars below the dashed line have $p < 0.05$, below the solid line a Bonferroni-corrected $p < 0.05$. Functional connectivity (FC) measures came from resting-state data. Mean global signal refers to task fMRI. Please note that the sample sizes differed between comparisons: N = 231 for CSF(-related) measures, 452 for all FC measures, 462 for WMH, 489 for the other variables. DMN = default mode network; DAN = dorsal attention network; FPN = fronto-parietal network; Lim = limbic network; SMN = somatomotor network; SN = salience network, VN = visual network. Figure copied from Vockert et al. [2024] with permission.

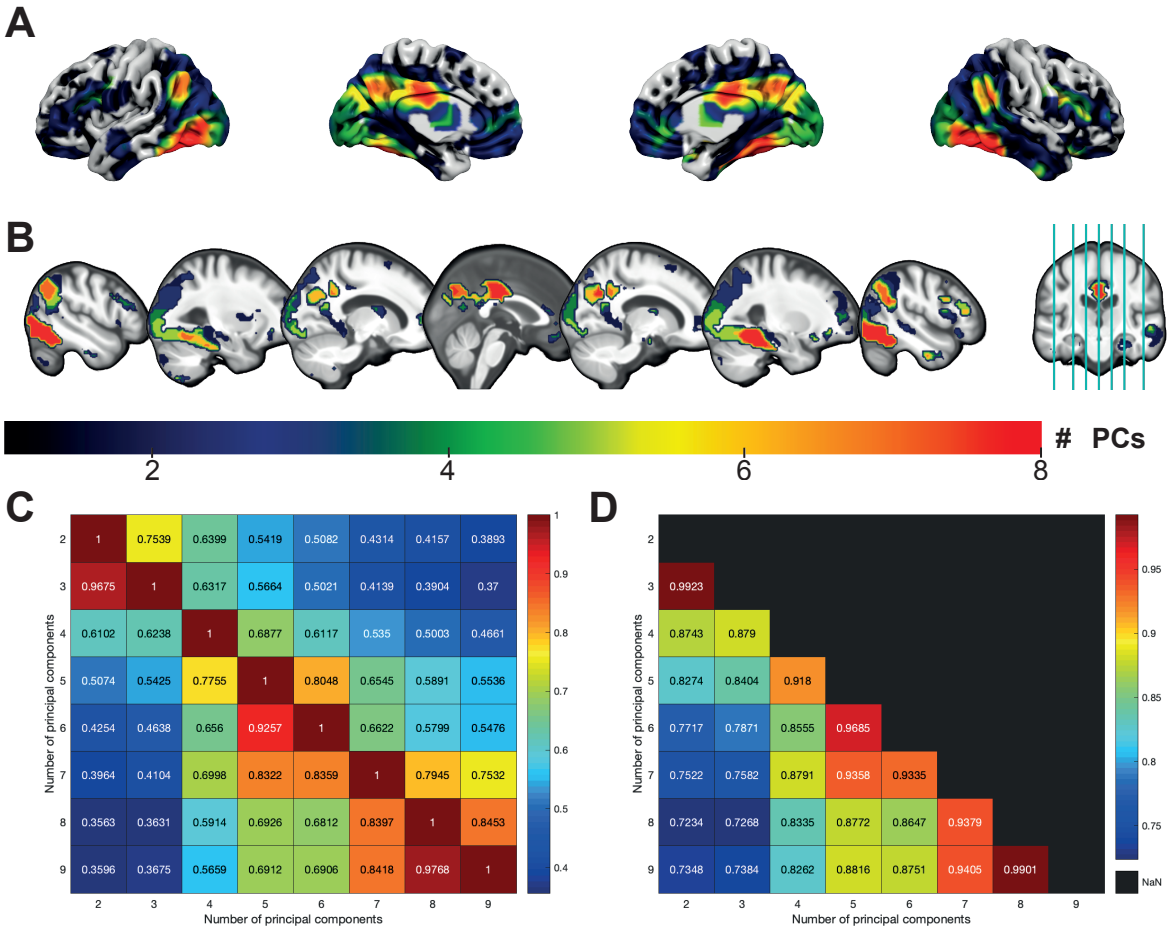

Figure S10: **Significant CR regions across different numbers of principal components.** Like in the cross-validation procedure (Fig. S6), the multivariate model has been fitted on the whole dataset using different amounts of principal components, ranging from 2 to 9. Subsequently, the corresponding voxelwise moderation effects (CR weights), voxels with significant CR weights and individual CR scores have been determined. (A) Surface plot of significant regions. (B) Same as A, but as slice views. Color bar indicates how many of the 8 analyses determined a certain voxel as significant contributor to CR. (C) Heat maps comparing the results in dependence of the number of principal components used in the multivariate model based on the correlation of the voxelwise CR weights (lower triangular part) and Sørensen-Dice coefficient (upper triangular part). (D) Same as C, but for individual CR scores obtained from CR weights and subsequent memory coefficients. It is important to note that the CR pattern is multivariate in nature, interpretable as a whole and cluster descriptives are reported for transparency of obtained non-negligible coefficients contributing to the pattern. Figure copied from Vockert et al. [2024] with permission.

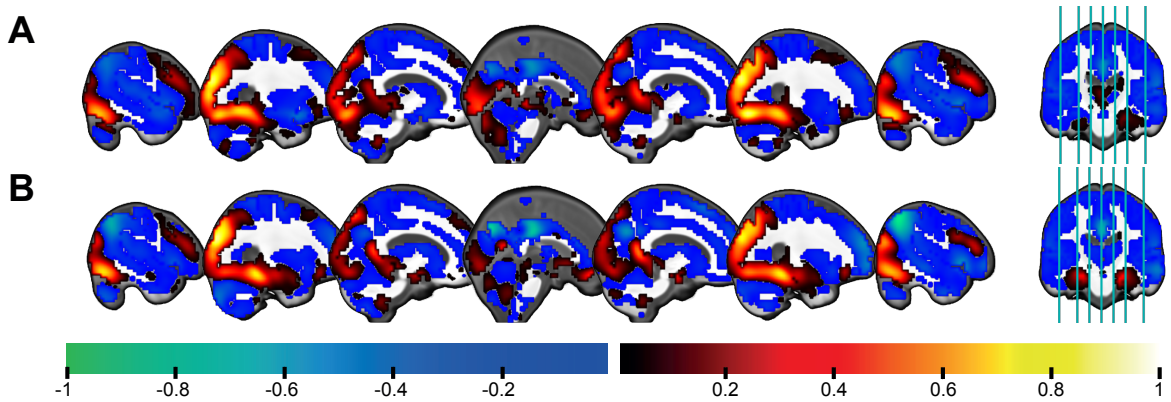

Figure S11: **CR coefficients in whole gray matter.** (A) Results of the same multivariate model when extending the search space to all gray matter instead of only regions contributing to successful memory encoding. (B) Mean beta values of the parametric successful memory contrast. The correlation between A and B is 0.942. All values have been normalized by the highest absolute value of the respective image. Figure copied from Vockert et al. [2024] with permission.

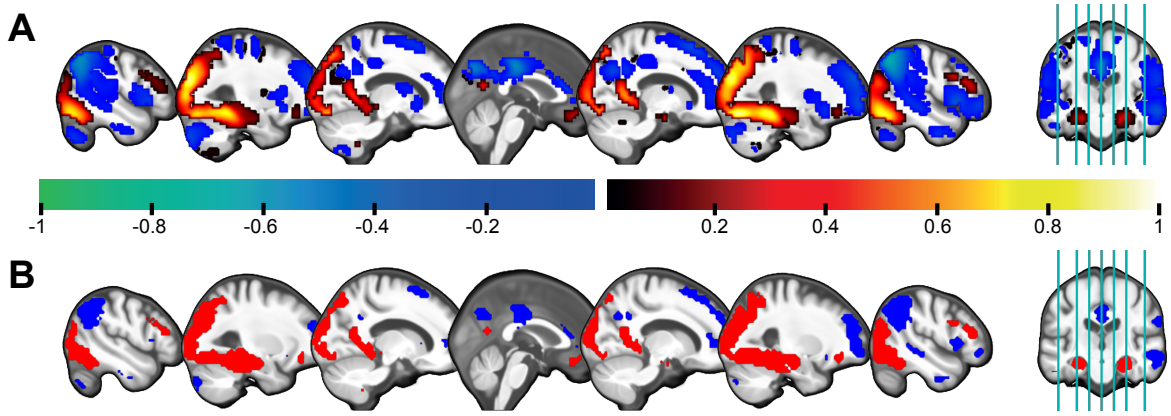

Figure S12: **CR pattern from multivariate model with only 2 principal components.** Results of the same multivariate model using 2 instead of 7 PCs. (A) Voxelwise moderation coefficients (CR), normalized by the highest absolute coefficient. (B) Regions with significant CR coefficients as indicated by bootstrapping. It is important to note that the CR pattern is multivariate in nature, interpretable as a whole and cluster descriptives are reported for transparency of obtained non-negligible coefficients contributing to the pattern. Figure copied from Vockert et al. [2024] with permission.

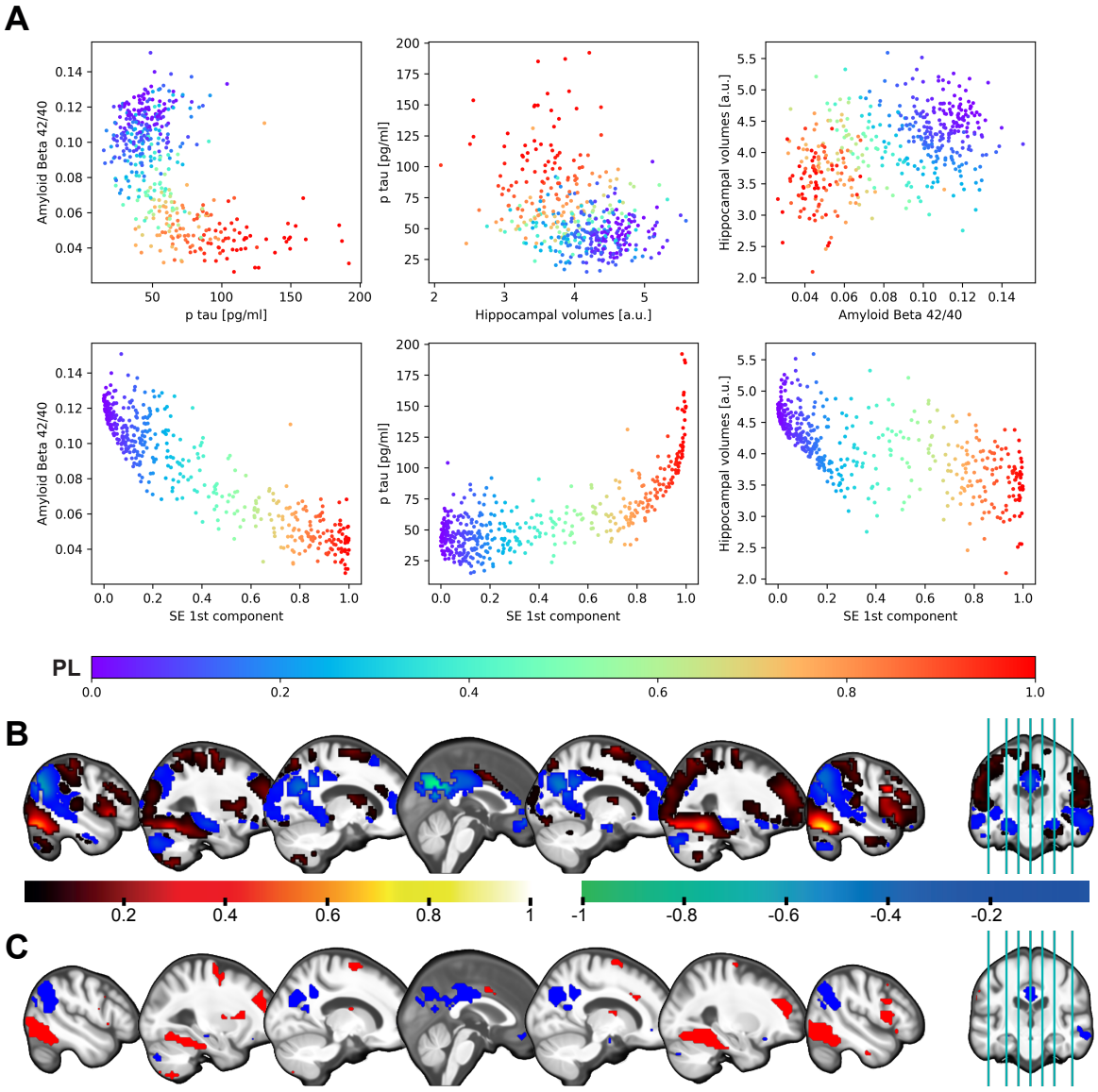

Figure S13: **Spectal embedding-based PL score.** Alternative PL score (r = 0.951 with t-SNE-based PL score) obtained as the first component a non-linear dimensionality reduction method called spectral embedding on $A\beta_{42:40}$, p-tau and TIV-corrected bilateral hippocampal volumes. (A) Relationship of the SE-based PL score to AD biomarkers. (B) Voxelwise moderation coefficients (CR) for multivariate model with SE-based PL score (r = 0.878 with CR coefficients in main text), normalized by the highest absolute coefficient. (C) Regions with significant positive (red) and negative (blue) CR coefficients for multivariate model with SE-based PL score. It is important to note that the CR pattern is multivariate in nature, interpretable as a whole and cluster descriptives are reported for transparency of obtained non-negligible coefficients contributing to the pattern. Figure copied from Vockert et al. [2024] with permission.

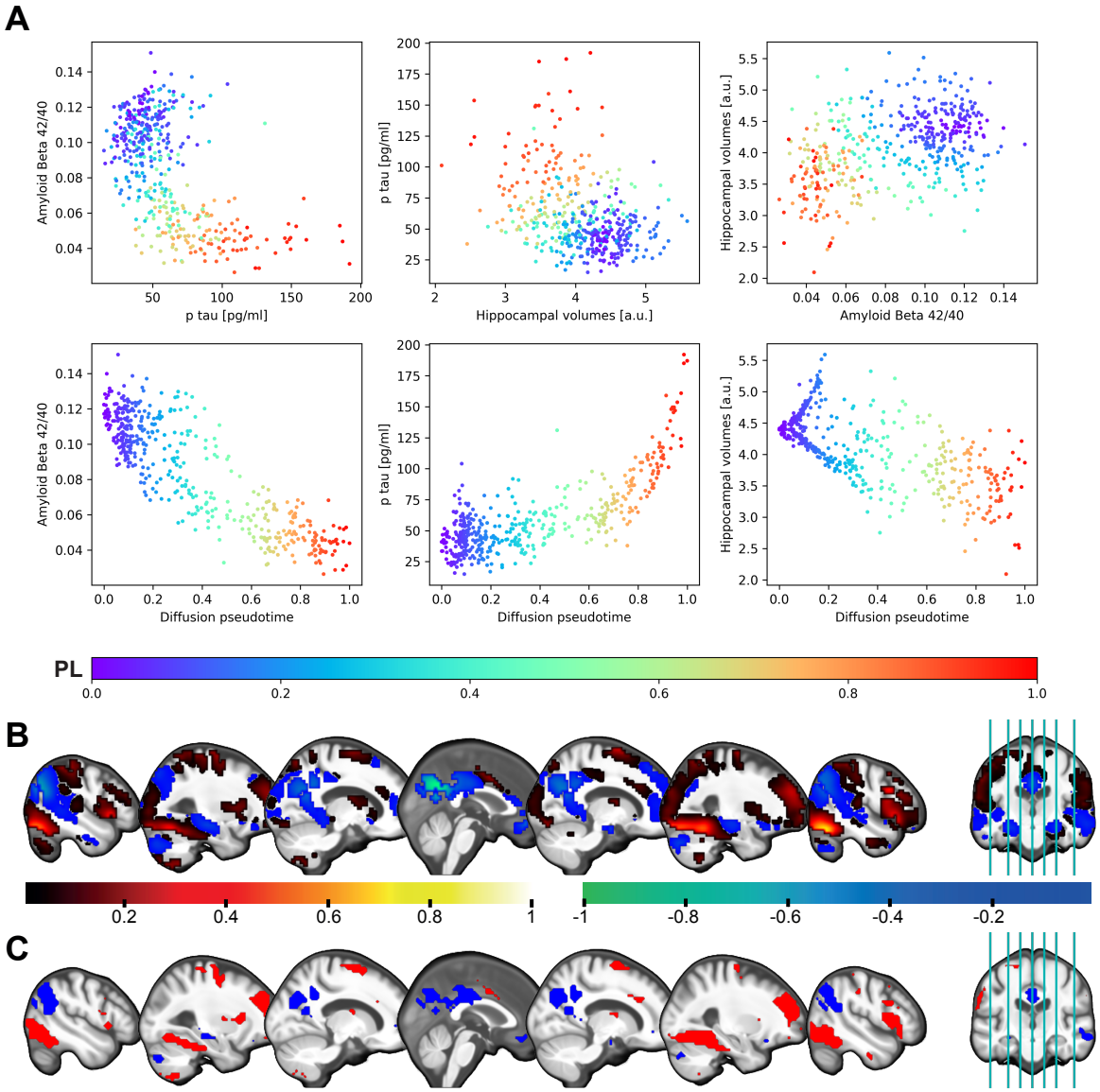

Figure S14: **Diffusion pseudotime-based PL score.** Alternative PL score (r = 0.940 with t-SNE-based PL score) obtained by a diffusion pseudotime (DPT) [Haghverdi et al., 2016] analysis on $A\beta_{42:40}$, p-tau and TIV-corrected bilateral hippocampal volumes. AD biomarkers of the 26 most pathology-free participants with $A\beta_{42:40} > 0.12$ and p-tau < 50 have been averaged and defined as the "root cell" required by the algorithm. (A) Relationship of the DPT-based PL score to AD biomarkers. (B) Voxelwise moderation coefficients (CR) for multivariate model with DPT-based PL score (r = 0.909 with CR coefficients in main text), normalized by the highest absolute coefficient. (C) Regions with significant positive (red) and negative (blue) CR coefficients for multivariate model with DPT-based PL score. It is important to note that the CR pattern is multivariate in nature, interpretable as a whole and cluster descriptives are reported for transparency of obtained non-negligible coefficients contributing to the pattern. Figure copied from Vockert et al. [2024] with permission.

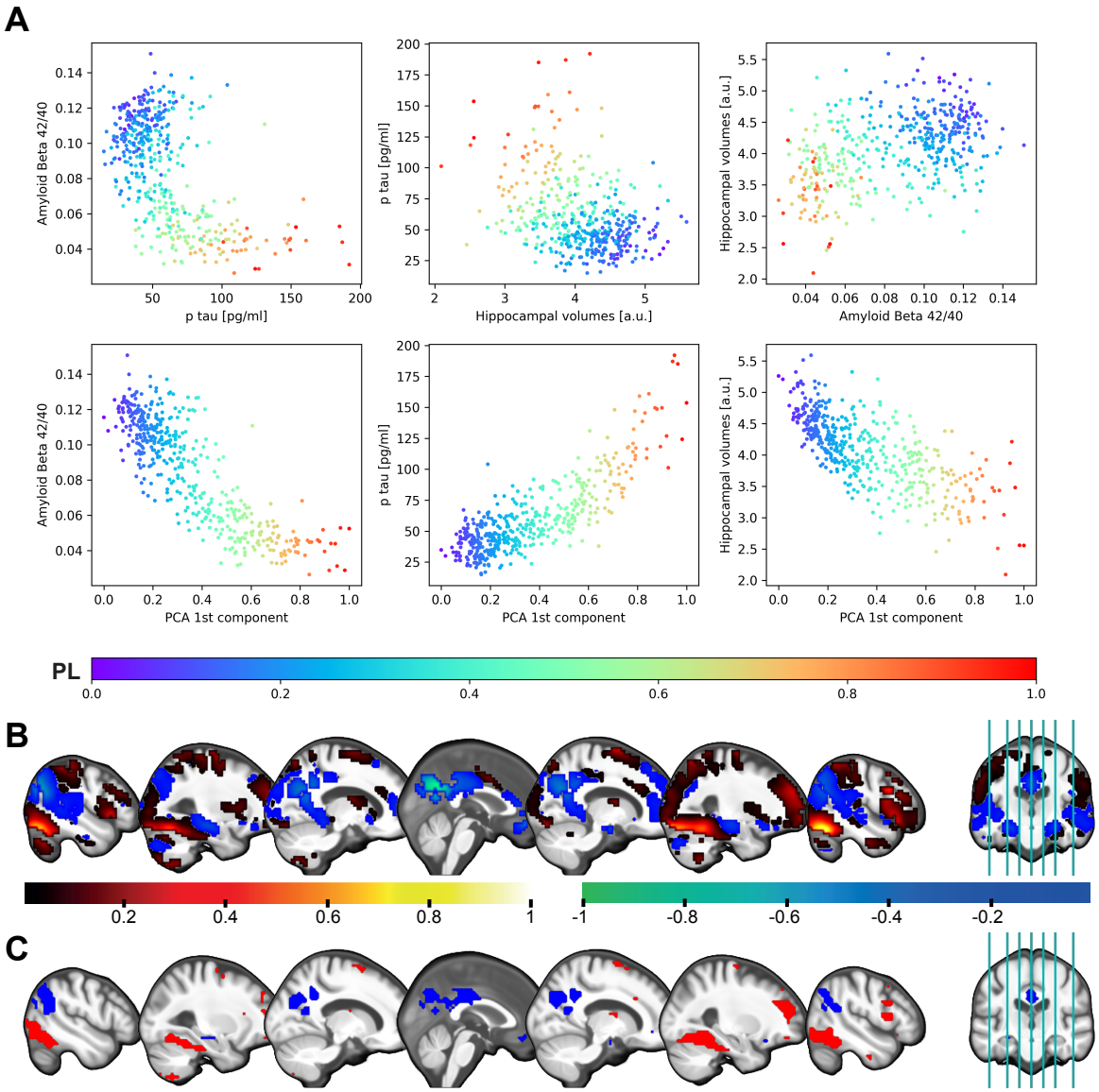

Figure S15: **PC analysis-based PL score.** Alternative PL score (r = 0.930 with t-SNE-based PL score) represented by the first component of a principal component analysis on $A\beta_{42:40}$, p-tau and TIV-corrected bilateral hippocampal volumes. (A) Relationship of the PCA-based PL score to AD biomarkers. (B) Voxelwise moderation coefficients (CR) for multivariate model with PC analysis-based PL score (r = 0.907 with CR coefficients in main text), normalized by the highest absolute coefficient. (C) Regions with significant positive (red) and negative (blue) CR coefficients for multivariate model with PC analysis-based PL score. It is important to note that the CR pattern is multivariate in nature, interpretable as a whole and cluster descriptives are reported for transparency of obtained non-negligible coefficients contributing to the pattern. Figure copied from Vockert et al. [2024] with permission.

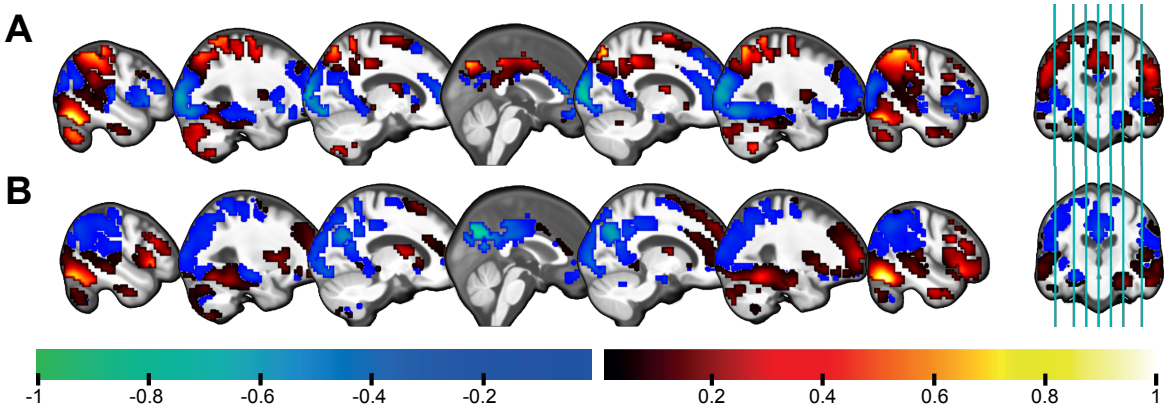

Figure S16: **Separate CR coefficients for CIs and CUs.** (A) Results of the multivariate model when applied only to cognitively impaired people (aMCI, ADD; N = 44; r = 0.150 with CR coefficients in main text). (B) Results of the multivariate model when applying it to only cognitively unimpaired people (HC, ADR, SCD; N = 184; r = 0.891 with CR coefficients in main text). Please note the substantial difference in sample sizes and many variables between the two groups. The CIs are older (72.52 vs 68.95 years, $p = 2.30 \cdot 10^{-5}$), have higher PL scores (0.637 vs 0.359, $p = 2.52 \cdot 10^{-8}$), lower PACC5 scores (-1.76 vs -0.02, $p = 2.40 \cdot 10^{-12}$) and are less educated (13.36 vs 14.82 years, $p = 5.02 \cdot 10^{-4}$). The latter might be another indication that CR not only may work differently in CIs, but CIs might also simply have lower CR that made them more susceptible to cognitive deficits in the first place. In consequence, they might not be a good model for examining CR. Dedicated samples of cognitively impaired participants might be better suited to examine the neural mechanisms of CR in this special subgroup. CR coefficients were normalized by the highest absolute coefficient, respectively. Figure copied from Vockert et al. [2024] with permission.

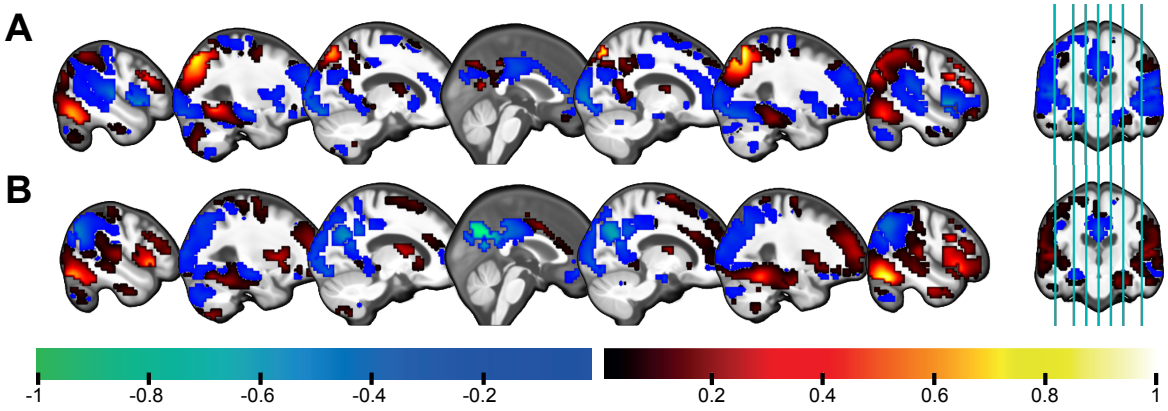

Figure S17: **Separate CR coefficients for females and males.** (A) Results of the multivariate model when applying it to only female participants (N = 114; r = 0.282 with CR coefficients in main text). (B) Results of the multivariate model when applying it to male participants (N = 114; r = 0.879 with CR coefficients in the main text). CR coefficients were normalized by the highest absolute coefficient, respectively. Figure copied from Vockert et al. [2024] with permission.

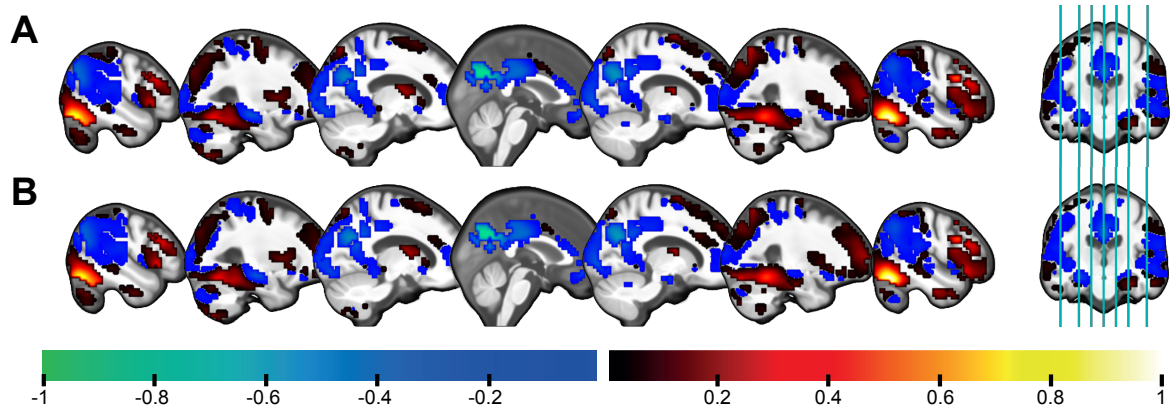

Figure S18: **Normalized CR coefficients when accounting for morphometric covariates.** (A) Results of the multivariate model when including mean cortical thickness (from Freesurfer) as an additional covariate (r = 0.999 with CR coefficients in main text). (B) Results of the multivariate model when including mean GM volumes (from SPM segmentation) of the voxels with significant CR contributions (according to the main model) as an additional covariate (r = 0.995 with CR coefficients in the main text). CR coefficients were normalized by the highest absolute coefficient, respectively. Figure copied from Vockert et al. [2024] with permission.

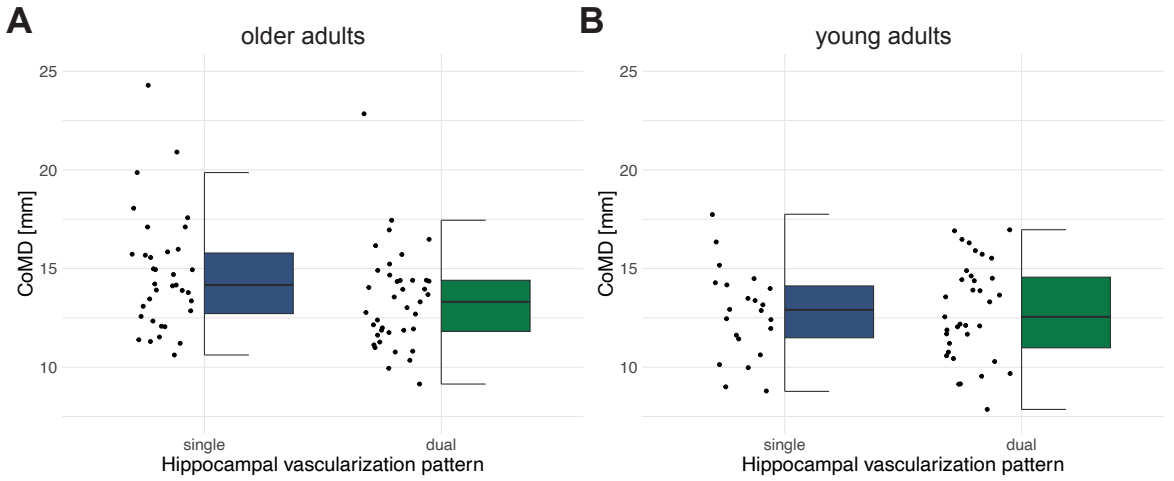

Figure S19: **Boxplots of CoMD by hippocampal vascularization pattern.** (A) Cohort of older adults (from chapter 2). (B) Cohort of young adults (from chapter 3).

Supplementary Tables

Table S1: **Results of permutation ANCOVAs**. Shown are the F values (p values in brackets). Rows contain the independent variables, columns the dependent variables.

	aHC	ERC	PRC	TGM	TWM
HVP	3.94(0.053)	**10.22(0.003)**	0.844(0.364)	**6.58(0.014)**	2.37(0.132)
CSVD	1.57(0.22)	0.11(0.74)	0.12(0.73)	**5.57(0.024)**	2.44(0.127)

Table S2: **Estimated effects of CSVD and the ipsi- and contralateral HVP on aHC and ERC volumes as shown in Table 2.2**. P values from likelihood ratio tests are indicated in round brackets. Significant results shown in bold. ':' symbolises an interaction between two factors.

	ΔaHC [mm^3]	ΔERC [mm^3]
CSVD	-88.79 (0.464)	-1.18 (0.973)
$\text{Dual}_{\text{ipsi}}$	**147.37 (0.037)**	**54.18 (0.014)**
$\text{Dual}_{\text{contra}}$	84.54 (0.227)	**50.22 (0.022)**
$\text{CSVD:Dual}_{\text{ipsi}}$	-117.09 (0.288)	-23.42 (0.502)
$\text{CSVD:Dual}_{\text{contra}}$	75.19 (0.494)	-20.47 (0.557)

Table S3: **Relationship of absolute CVR metrics with brain structure and cognition**. The results in the table denote t values (degrees of freedom in parentheses) from the linear models or LMEs adjusted for covariates. All values for the (absolute) CVR metrics represent mean values in the hippocampus. '+' denotes p values < 0.1, '$*$' denotes $p < 0.05$. No associations were statistically significant.

	CVR	RSFA
Memory composite	-0.129(25)	-1.051(25)
Global cogn. factor	-0.869(25)	-0.906(25)
wHC vol	-0.696(54.9)	-1.130(41.8)
TGM	0.470(25)	0.025(25)
TWM	-0.116(25)	0.265(25)

Table S4: **Relationship of all CVR metrics with brain structure and cognition (weighted regression)**. The results in the table denote t values (degrees of freedom in parenthesis) from the linear models or LMEs adjusted for covariates and weighted for the percentage of hippocampus voxels (i.e. voxels with tSNR > 5) included in the calculation of the mean CVR values. All values for the CVR metrics represent mean values in the hippocampus. '+' symbolizes p values < 0.1, '∗' symbolises p < 0.05. P values were not corrected for multiple comparisons.

	CVR	RSFA	rCVR	rRSFA
Memory composite	-0.089(25)	-1.046(25)	-1.406(24)	-1.453(25)
Global cogn. factor	-0.840(25)	-0.920(25)	-2.261*(24)	0.090(25)
wHC vol	-0.693(54.9)	-1.125(41.7)	-0.764(32.8)	-1.961^{+}(33.3)
TGM	0.470(25)	0.000(25)	-1.422(24)	-1.151(25)
TWM	-0.115(25)	0.235(25)	-0.816(24)	0.539(25)

Table S5: **Significant clusters in CR-related activity pattern**. Same as Tab. 4.2, but includes smaller clusters with sizes between 30 and 50 voxels (all discordant). In two instances, the peak voxel was not contained in the AAL and is thus marked with a '?'.

#	**Mean w_i**	**Size [voxels]**	**% concordant**	**Peak[x,y,z]**	**Peak Structure**
8	0.056	48	0	35, 59, 7	Frontal_Mid_R
9	0.044	45	0	-4, 7, 70	Supp_Motor_Area_L
10	0.053	42	0	42, 14, 39	Frontal_Inf_Oper_R
11	0.058	42	0	7, 3, 73	Supp_Motor_Area_R
12	0.051	37	0	49,14,14	Frontal_Inf_Oper_R
13	0.05	36	0	-11,0,10	? (Caudate_L/Thalamus_L)
14	0.045	34	0	-35,-66,-59	? (near Cerebellum_L)
15	0.043	30	0	49,-7,-32	Temporal_Inf_R
16	-0.068	30	0	-28,-21,-14	Hippocampus_L

Table S6: **Correlation between different PL scores**. All PL scores exhibit very high correlations with each other, but show subtle differences in their patterns of non-linearity (see Figs. S13, S14, S15). t-SNE = t-stochastic neighbor embedding, PCA = principal component analysis, DPT = diffusion pseudotime, SE = spectral embedding.

	t-SNE	PCA	DPT	SE
t-SNE	1.000	0.930	0.940	0.951
PCA	0.930	1.000	0.965	0.963
DPT	0.940	0.965	1.000	0.983
SE	0.951	0.963	0.983	1.000

Table S7: **Subsample characteristics of study 3**. Means ± standard deviations are illustrated. P values were obtained from two-sample t-test or Chi-square test. The group contingency of the five diagnostic groups was not significantly different between both subsamples (p = 0.103). Four participants of the CSF subsample and five participants of the MRI-only subsample had no PACC5 scores.

	CSF subsample	**MRI-only subsample**	**p value**
N	232	258	
Age at baseline	69.6±5.4	69.8±5.9	0.713
Sex [% female]	50.0	57.0	0.146
Education years	14.6±2.7	14.7±3.0	0.573
Hippocampal volumes [a.u.]	4.21±0.53	4.25±0.47	0.304
PACC5 scores [a.u.]	-0.36±1.05	-0.05±0.87	$5.67 \cdot 10^{-4}$

Declaration of Honor

"I hereby declare that I prepared this thesis without the impermissible help of third parties and that none other than the aids indicated have been used; all sources of information are clearly marked, including my own publications.

In particular I have not consciously:

- fabricated data or rejected undesirable results,
- misused statistical methods with the aim of drawing other conclusions than those warranted by the available data,
- plagiarized external data or publications,
- presented the results of other researchers in a distorted way.

I am aware that violations of copyright may lead to injunction and damage claims by the author and also to prosecution by the law enforcement authorities. I hereby agree that the thesis may be electronically reviewed with the aim of identifying plagiarism.

This work has not yet been submitted as a doctoral thesis in the same or a similar form in Germany, nor in any other country. It has not yet been published as a whole."

Magdeburg, 11.09.2024

(Niklas Vockert)